RECENT 3D TUMOR MODELS FOR TESTING IMMUNE-MEDIATED THERAPIES

EDITED BY: Silvia Scaglione, Roberta Castriconi and Jacques Zimmer
PUBLISHED IN: Frontiers in Immunology and Frontiers in Oncology

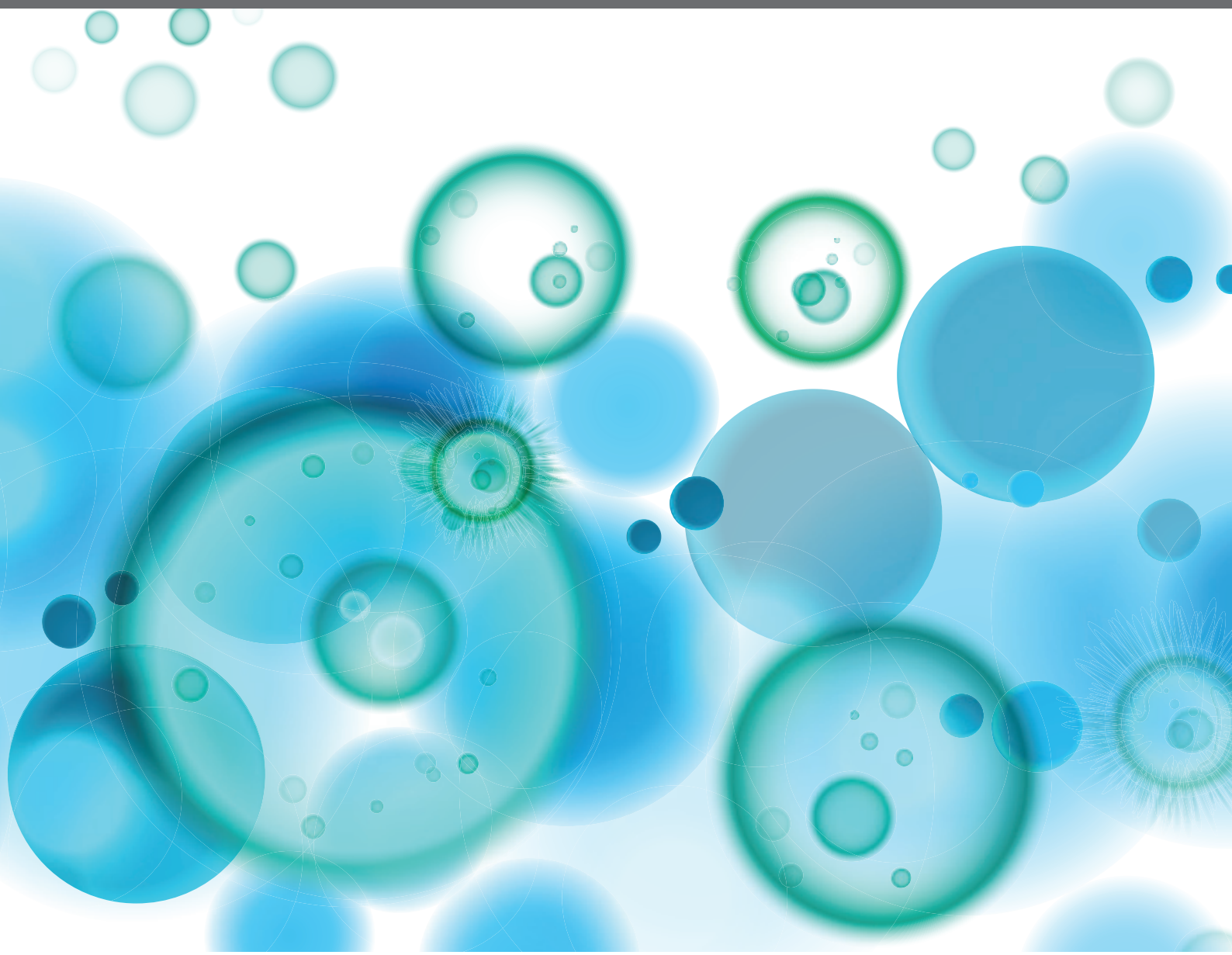

frontiers Research Topics

ISSN 1664-8714
ISBN 978-2-88974-015-4
DOI 10.3389/978-2-88974-015-4

About Frontiers

Frontiers is more than just an open-access publisher of scholarly articles: it is a pioneering approach to the world of academia, radically improving the way scholarly research is managed. The grand vision of Frontiers is a world where all people have an equal opportunity to seek, share and generate knowledge. Frontiers provides immediate and permanent online open access to all its publications, but this alone is not enough to realize our grand goals.

Frontiers Journal Series

The Frontiers Journal Series is a multi-tier and interdisciplinary set of open-access, online journals, promising a paradigm shift from the current review, selection and dissemination processes in academic publishing. All Frontiers journals are driven by researchers for researchers; therefore, they constitute a service to the scholarly community. At the same time, the Frontiers Journal Series operates on a revolutionary invention, the tiered publishing system, initially addressing specific communities of scholars, and gradually climbing up to broader public understanding, thus serving the interests of the lay society, too.

Dedication to Quality

Each Frontiers article is a landmark of the highest quality, thanks to genuinely collaborative interactions between authors and review editors, who include some of the world's best academicians. Research must be certified by peers before entering a stream of knowledge that may eventually reach the public - and shape society; therefore, Frontiers only applies the most rigorous and unbiased reviews.
Frontiers revolutionizes research publishing by freely delivering the most outstanding research, evaluated with no bias from both the academic and social point of view. By applying the most advanced information technologies, Frontiers is catapulting scholarly publishing into a new generation.

What are Frontiers Research Topics?

Frontiers Research Topics are very popular trademarks of the Frontiers Journals Series: they are collections of at least ten articles, all centered on a particular subject. With their unique mix of varied contributions from Original Research to Review Articles, Frontiers Research Topics unify the most influential researchers, the latest key findings and historical advances in a hot research area! Find out more on how to host your own Frontiers Research Topic or contribute to one as an author by contacting the Frontiers Editorial Office: frontiersin.org/about/contact

RECENT 3D TUMOR MODELS FOR TESTING IMMUNE-MEDIATED THERAPIES

Topic Editors:
Silvia Scaglione, National Research Council (CNR), Italy
Roberta Castriconi, Università di Genova, Italy
Jacques Zimmer, Luxembourg Institute of Health, Luxembourg

Citation: Scaglione, S., Castriconi, R., Zimmer, J., eds. (2021). Recent 3D Tumor Models for Testing Immune-Mediated Therapies. Lausanne: Frontiers Media SA. doi: 10.3389/978-2-88974-015-4

Table of Contents

04 ***Editorial: Recent 3D Tumor Models for Testing Immune-Mediated Therapies***
Jacques ZimmerS, Roberta Castriconi and Silvia Scaglione

07 ***Emerging Neuroblastoma 3D* In Vitro *Models for Pre-Clinical Assessments***
Diana Corallo, Stella Frabetti, Olivia Candini, Elisa Gregianin, Massimo Dominici, Horst Fischer and Sanja Aveic

19 ***Glioblastoma Organoids: Pre-Clinical Applications and Challenges in the Context of Immunotherapy***
Eliane Klein, Ann-Christin Hau, Anaïs Oudin, Anna Golebiewska and Simone P. Niclou

37 ***3D Tumor Models and Their Use for the Testing of Immunotherapies***
Nicolas Boucherit, Laurent Gorvel and Daniel Olive

47 ***Physical Characterization of Colorectal Cancer Spheroids and Evaluation of NK Cell Infiltration Through a Flow-Based Analysis***
Azzurra Sargenti, Francesco Musmeci, Francesco Bacchi, Cecilia Delprete, Domenico Andrea Cristaldi, Federica Cannas, Simone Bonetti, Simone Pasqua, Daniele Gazzola, Delfina Costa, Federico Villa, Maria Raffaella Zocchi and Alessandro Poggi

60 ***3D Bioprinting Allows the Establishment of Long-Term 3D Culture Model for Chronic Lymphocytic Leukemia Cells***
Francesca Vittoria Sbrana, Riccardo Pinos, Federica Barbaglio, Davide Ribezzi, Fiorella Scagnoli, Lydia Scarfò, Itedale Namro Redwan, Hector Martinez, Silvia Farè, Paolo Ghia and Cristina Scielzo

75 ***A Reproducible Bioprinted 3D Tumor Model Serves as a Preselection Tool for CAR T Cell Therapy Optimization***
Laura Grunewald, Tobias Lam, Lena Andersch, Anika Klaus, Silke Schwiebert, Annika Winkler, Anton Gauert, Anja I. Heeren-Hagemann, Kathy Astrahantseff, Filippos Klironomos, Alexander Thomas, Hedwig E. Deubzer, Anton G. Henssen, Angelika Eggert, Johannes H. Schulte, Kathleen Anders, Lutz Kloke and Annette Künkele

frontiers in Immunology

EDITORIAL
published: 18 November 2021
doi: 10.3389/fimmu.2021.798493

Editorial: Recent 3D Tumor Models for Testing Immune-Mediated Therapies

Jacques Zimmer[1], *Roberta Castriconi*[2] *and Silvia Scaglione*[3,4]*

[1] Department of Infection and Immunity, Luxembourg Institute of Health, Esch-sur-Alzette, Luxembourg, [2] Department of Experimental Medicine, University of Genova, Genova, Italy, [3] IEIIT Institute, National Research Council (CNR), Roma, Italy, [4] Department R&D, React4life s.r.l., Milan, Italy

Keywords: 3D tumor models, microfluidics, organ-on-chip, bioprinting, colon cancer, neuroblastoma, glioblastoma, CAR-T cells

Editorial on the Research Topic

Recent 3D Tumor Models for Testing Immune-Mediated Therapies

For a long time, cancer research was based on the culture of cell lines and primary tumor cells grown in 2 dimensions (2D), as well as on animal models mainly based on the use of rodents such as mice and rats. However, *in vitro* 2D conventional cell cultures fail to accurately predict the drug responses in humans, as they do not properly resemble the spatial complexity of the human tissue microenvironment; on the other side, research on living animals did not completely meet the public agreement, pointing out ethical questions which have been addressed and regulated by the European Community. In addition to the ethical issues, the heterogeneity of housing conditions, of microbiota and chow compositions and the inability to reproduce the complex interplay between tumor cells and human microenvironment represent additional weaknesses of the most utilized *in vivo* models (1). Therefore, the progressive switch to 3D experimental material is accompanied by several advantages converging in a better reproducibility of the results among different labs.

Current 3D cultures are based on the establishment of different models including tumor organoids. These are derived from epithelial cells of many organs and can be ideally established from each patient, with the possibility to comparatively analyze tumor and normal tissue from the same individual, in the context of personalized medicine (2). As they originate from stem cells, they have the capacity to self-organize and self-renew (2). There are also several possibilities to mimic the tumor microenvironment (TME) in 3D structures. This TME contains various organic and inorganic molecules belonging to extracellular matrix and several non-cancerous cell types that nevertheless create a strongly immunosuppressive environment rendering the cancer resistant to many treatment options (3). The 3D models likewise allow to evaluate treatment efficiency for the individual patient, for example the response to checkpoint inhibitors, correlated with clinical responses (4). Experimental treatments and therapeutic combinations can be tested in 3D tumor spheroid microarrays bringing together NK92-CD16 cells and tumor cell lines with anti-tumor antibodies triggering antibody-dependent cellular cytotoxicity by the natural killer (NK) cell line (5). However, the current 3D models still have some unmet challenges, such as the absence of vascularization in the organoids, or the organ-organ cross-talk, that might be circumvented by the use of organs-on-chip technologies (6).

OPEN ACCESS

Edited and reviewed by:
Catherine Sautes-Fridman, U1138 Centre de Recherche des Cordeliers (CRC) (INSERM), France

***Correspondence:**
Silvia Scaglione
s.scaglione@react4life.com

Specialty section:
This article was submitted to Cancer Immunity and Immunotherapy, a section of the journal Frontiers in Immunology

Received: *20 October 2021*
Accepted: *01 November 2021*
Published: *18 November 2021*

Citation:
Zimmer J, Castriconi R and Scaglione S (2021) Editorial: Recent 3D Tumor Models for Testing Immune-Mediated Therapies. Front. Immunol. 12:798493. doi: 10.3389/fimmu.2021.798493

This Research Topic is dedicated to some recent aspects of the 3D "revolution", describing or reviewing in details the different models. The articles likewise critically discuss the most relevant weaknesses of the 3D models, also suggesting possible methodological approaches to address and resolve them.

Thus, in the first paper, Sargenti et al. report on the relative heterogeneity of weight and size of spheroids derived from four different colon cancer cell lines, which might of course influence the data and the conclusions obtained. With the aim to *in vitro* combine 3D cancer models and fluid dynamic conditions (7), the authors describe a flow-based method focused on a quantitative analysis of weight, size and mass density of cancer spheroids, as well as a measurement of cell infiltration. They use their system to test the cytotoxic effect of NK cells on the tumor spheroids, appreciated through measurements of weight loss and size reduction. The latter are cell line-dependent and thus most likely reflect the patient-specific behavior of primary spheroids and the suitability of the model for personalized medicine and testing of immunotherapeutic modalities.

In the second manuscript, Corallo et al. review emerging 3D technologies to preclinically study neuroblastoma, an aggressive pediatric neuroectodermal tumor with a current unmet therapeutic need (8). Due to the high heterogeneity of this cancer, the development of standardized 3D systems represents a real challenge. However, some 3D models are in development or already available, thus allowing preclinical drug and immunotherapy testing similar to other types of cancer. The paper also widely discusses various properties of extracellular matrix (ECM) components (e.g. scaffolds) mostly used in 3D models and crucial for recapitulating the *in vivo* tumor microenvironment.

Boucherit et al. contributed with a general but comprehensive overview of the most utilized 3D tumor models, comparing cell lines-based structures with patient-derived cultures, 3D bioprinting and organs-on-chip approaches. In each case, advantages and potential pitfalls are discussed.

In the next manuscript, Klein et al. from the Niclou group provide a specialized critical and exhaustive review about glioblastoma (GBM) organoids. In contrast to most other tumors that are at least possible to treat, GBM almost always relapses and the patient survival (median) is less than two years even after the currently available optimized treatment (surgery, radiotherapy, temozolomide) (9). The authors suggest that most clinical trials in GBM fail due to the lack of appropriate preclinical studies mostly neglecting the *in vivo* TME and its properties. The article contains a full table indicating advantages and disadvantages of cell-based models and organoids even genetically-engineered.

Sbrana et al. focused their contribution on chronic lymphocytic leukemia (CLL) which represents the most frequent and still uncurable adult type of leukemia (10). With a 3D-bioprinting method, they achieve to develop a long-term CLL culture model able to assess growth characteristics, functional behavior of the leukemic cells and their sensitivity to potential innovative treatments.

Finally, Grunewald et al. describe another 3D-bioprinting system used to investigate chimeric antigen receptor (CAR)-T cells targeting neuroblastoma *via* the adhesion molecule L1CAM. The cell culture system was viable over time and the CAR-T cells infiltrated the 3D-bioprint, delivering a kind of proof-of-concept about the appropriateness of this preclinical model, mimicking the patient's TME, to test the anti-tumor efficacy of a given CAR construct.

In conclusion, the Research Topic provides a complete and critic overview of the most used and reliable 3D tumor models that represent crucial tools of future cancer research whose optimization will go hand-in-hand with the increasing development of anti-tumor immunotherapeutic strategies.

AUTHOR CONTRIBUTIONS

JZ, RC, and SS wrote the editorial and invited authors to participate in the collection. All authors contributed to the article and approved the submitted version.

FUNDING

This work was supported by the European Union's Horizon 2020 research and innovation programme under grant agreement No 801159.

REFERENCES

1. Leystra AA, Clapper ML. Gut Microbiota Influences Experimental Outcomes in Mouse Models of Colorectal Cancer. *Genes (Basel)* (2019) 10:900. doi: 10.3390/genes10110900
2. Veninga V, Voest E. Tumor Organoids: Opportunities and Challenges to Guide Precision Medicine. *Cancer Cell* (2021) 39:1190–201. doi: 10.1016/j.ccell.2021.07.020
3. Carter EP, Roozitalab R, Gibson SV, Grose RP. Tumour-Microenvironment 3D-Modelling: Simplicity to Complexity and Back Again. *Trends Cancer* (2021) 7(11):1033–46. doi: 10.1016/j.trecan.2021.06.009. S2405-8033(21)00141-2.
4. Bozkus CC, Bhardwaj N. Tumor-Organoid-Originated Biomarkers Predict Immune Responses to PD-1 Blockade. *Cancer Cell* (2021) 39:1187–9. doi: 10.1016/j.ccell.2021.08.003
5. Ghopal S, Kwon SJ, Ku B, Lee DW, Kim J, Dordick JS. 3D Tumor Spheroid Microarray for High-Throughput, High-Content Natural Killer Cell-Mediated Cytotoxicity. *Commun Biol* (2021) 4:893. doi: 10.1038/s42003-021-02417-2
6. Haque MR, Rempert TH, Al-Hilal TA, Wang C, Bhushan A, Bishehsari F. Organ-Chip Models: Opportunities for Precision Medicine in Pancreatic Cancer. *Cancers (Basel)* (2021) 13:4487. doi: 10.3390/cancers13174487
7. Li XJ, Valadez AV, Zuo P, Nie Z. Microfluidic 3D Cell Culture: Potential Application for Tissue-Based Bioassays. *Bioanalysis* (2012) 4:1509–25. doi: 10.4155/bio.12.133
8. Mallepalli S, Gupta MK, Vadde R. Neuroblastoma: An Updated Review on Biology and Treatment. *Curr Drug Metab* (2019) 20:1014–22. doi: 10.2174/1389200221666191226102231
9. Tan AC, Ashley DM, López GY, Malinzak M, Friedman HS, Khasraw M. Management of Glioblastoma: State of the Art and Future Directions. *CA Cancer J Clin* (2020) 70:299–312. doi: 10.3322/caac.21613

10. Hallek M. Chronic Lymphocytic Leukemia: 2020 Update on Diagnosis, Risk Stratification and Treatment. *Am J Hematol* (2019) 94:1266–87. doi: 10.1002/ajh.25595

Conflict of Interest: Author SS is employed by React4life s.r.l.

The remaining authors declare that the research was conducted in the absence of any commercial or financial relationships that could be construed as a potential conflict of interest.

Publisher's Note: All claims expressed in this article are solely those of the authors and do not necessarily represent those of their affiliated organizations, or those of the publisher, the editors and the reviewers. Any product that may be evaluated in this article, or claim that may be made by its manufacturer, is not guaranteed or endorsed by the publisher.

frontiers in Immunology

REVIEW
published: 26 November 2020
doi: 10.3389/fimmu.2020.584214

Emerging Neuroblastoma 3D *In Vitro* Models for Pre-Clinical Assessments

Diana Corallo[1†], *Stella Frabetti*[2†], *Olivia Candini*[2], *Elisa Gregianin*[2], *Massimo Dominici*[2,3], *Horst Fischer*[4] *and Sanja Aveic*[1,4*]

[1] Neuroblastoma Laboratory, Istituto di Ricerca Pediatrica Fondazione Città della Speranza, Padova, Italy, [2] Rigenerand srl, Modena, Italy, [3] Division of Oncology, Department of Medical and Surgical Sciences for Children & Adults, University-Hospital of Modena and Reggio Emilia, Modena, Italy, [4] Department of Dental Materials and Biomaterials Research, RWTH Aachen University Hospital, Aachen, Germany

The potential of tumor three-dimensional (3D) *in vitro* models for the validation of existing or novel anti-cancer therapies has been largely recognized. During the last decade, diverse *in vitro* 3D cell systems have been proposed as a bridging link between two-dimensional (2D) cell cultures and *in vivo* animal models, both considered gold standards in pre-clinical settings. The latest awareness about the power of tailored therapies and cell-based therapies in eradicating tumor cells raises the need for versatile 3D cell culture systems through which we might rapidly understand the specificity of promising anti-cancer approaches. Yet, a faithful reproduction of the complex tumor microenvironment is demanding as it implies a suitable organization of several cell types and extracellular matrix components. The proposed 3D tumor models discussed here are expected to offer the required structural complexity while also assuring cost-effectiveness during pre-selection of the most promising therapies. As neuroblastoma is an extremely heterogenous extracranial solid tumor, translation from 2D cultures into innovative 3D *in vitro* systems is particularly challenging. In recent years, the number of 3D *in vitro* models mimicking native neuroblastoma tumors has been rapidly increasing. However, *in vitro* platforms that efficiently sustain patient-derived tumor cell growth, thus allowing comprehensive drug discovery studies on tailored therapies, are still lacking. In this review, the latest neuroblastoma 3D *in vitro* models are presented and their applicability for a more accurate prediction of therapy outcomes is discussed.

Keywords: 3D *in vitro* models, neuroblastoma, pediatric oncology, immunotherapy, drug screening, extracellular matrix

OPEN ACCESS

Edited by:
Silvia Scaglione,
National Research Council (CNR), Italy

Reviewed by:
Guilan Shi,
University of South Florida, United States
Sabine Taschner-Mandl,
St. Anna Children's Cancer Research Institute (CCRI), Austria
Rosa Noguera,
University of Valencia, Spain

***Correspondence:**
Sanja Aveic
s.aveic@irpcds.org

[†]These authors have contributed equally to this work

Specialty section:
This article was submitted to Cancer Immunity and Immunotherapy, a section of the journal Frontiers in Immunology

Received: *16 July 2020*
Accepted: *02 November 2020*
Published: *26 November 2020*

Citation:
Corallo D, Frabetti S, Candini O, Gregianin E, Dominici M, Fischer H and Aveic S (2020) Emerging Neuroblastoma 3D In Vitro Models for Pre-Clinical Assessments. Front. Immunol. 11:584214. doi: 10.3389/fimmu.2020.584214

INTRODUCTION

The turn of the 20th century was crucial for the development of the basic principles for *in vitro* cell growth enabled substantial biological discoveries. Over time, the complexity of *in vitro* systems has increased according to the needs of various branches of life science. The enhancement of *in vitro* techniques applicable in these two-dimensional (2D) systems greatly changed the perception of cell-related processes and allowed more accurate deciphering of the fundamental biomolecular and biophysical mechanisms active in both, physiological conditions and disease (1). The 21st Century brought great progress in the development of the existing *in vitro* models for the study of more

complex three-dimensional (3D) multicellular entities, while approaching as much as possible *in vivo* situations (2). A major tendency toward replacing, reducing, and refining (3R) animal use took place, supporting the application of the 3R principle for *in vivo* experimentation and energizing the development of diverse 3D cell culture technologies (3). This development represents the achievements of a breakthrough in the field of tissue engineering and regenerative biomedicine. Other disciplines of life science adopted the advances of available 3D models for addressing specific challenges and pitfalls encountered in the use of 2D systems, while also outlining novel considerations of cell and tissue-related questions.

In oncology, the introduction of 3D models for investigating tumor biology and cancer cells behavior is rapidly increasing. However, the standard procedures in this research still mainly follow a conventional route of initial testing in a Petri dish (2D) followed by *in vivo* validations in zebrafish, mice, or other small laboratory animals (4). The highly standardized protocols, well-established experimental approaches, and low costs of 2D tumor models explain the high rate of their application regardless of limited accuracy in representing native neoplastic tissues and predicting physiological values. The major obstacle to a straightforward translation of *in vitro* biological process analyzed in 2D conditions into an *in vivo* response is the lack of multicellular systems that are in direct contact with the cell-extracellular matrix (ECM) components (5). The tumor microenvironment (TME) is formed of several different cell types and non-cellular components (ECM). TME allows malignant cells to grow in 3D conditions, making the system extremely dynamic and complex. Yet, the proper architecture, tumor stiffness and relaxation behavior are not adequately considered in 2D *in vitro* studies, leading to limited information about the realistic changes in signaling pathways, metabolic activities, and genetic/epigenetic backgrounds of tumor and stromal cells (6, 7). The transition from 2D to *in vivo* pharmacological testing during the early stages of drug examination is therefore often critical but without the desired level of success (8). Many efforts are currently attempting to bridge the gap between 2D and *in vivo* systems by proposing different 3D *in vitro* models in which cell line and primary cells can be grown in either static or dynamic conditions.

Even though 3D cell culture techniques can minimize these limitations, their widespread use is still limited due to the relatively high costs, complexity of preparation, and lack of standardized protocols that can guarantee high reproducibility and unequivocal data interpretation (9). Unsurprisingly, 2D cell cultures and *in vivo* animal models are still considered the gold standards in pre-clinical settings in oncology. However, the traditional means of drug efficacy evaluation faces serious limitations, since many compounds that show good anti-cancer effects in murine models fail to provide meaningful clinical benefits for humans (10). Therefore, this scenario is changing in the direction of 3D models more often being built of primary cells as the protagonist of anti-neoplastic drug screening. This trend is also supported by important innovations in live cell *in vitro* imaging techniques that accelerate drug discovery (11). Still, most of these proposals come from cancers developing in adults, whereas there is a clear deficit of a pre-clinical 3D model providing analysis of drug response in pediatric tumors. This is particularly evident for neuroblastoma, for which a vast majority of scientific questions are still answered by using either 2D studies or the transgenic and xenograft zebrafish and murine models (12–14).

Neuroblastoma is an embryonal malignancy of the sympathetic nervous system with very heterogeneous biologic, morphologic, genetic, and clinical characteristics. It is classified as a neuroblastic tumor but in contrast to ganglioneuroblastoma and ganglioneuroma, neuroblastoma is more aggressive (15).

Based on several clinical and molecular risk factors each patient is stratified in one of the following risk groups: very-low, low, intermediate or high-risk (16). Such a pre-treatment risk group assignment facilitates treatment modalities as well (17). In high-risk patients, the aggressive course of the malignancy manifests as a disseminated disease (stage 4) with metastatic processes in the liver, bone marrow and bone, skin and several other organs (18). The treatment of these patients represents one of the most urgent challenges for oncologists. Despite intensive multimodal therapy, in more than 50% of high-risk patients, the disease progresses during the course of therapy leading to a fatal outcome (19).

Recent studies have shed light on the biology of neuroblastoma allowing a more accurate stratification of patients into risk groups, resulting in a reduction of treatment cytotoxicity without affecting the outcome of low and intermediate-risk patients (20, 21). However, the mortality rate of children in high-risk group is still high, and the development of more valuable therapeutic strategies remains urgent. During the last few years, different approaches such as transcriptomics analyses and genome-wide association studies have listed the genes associated with neuroblastoma susceptibility, aggressiveness, and progression (22, 23). The identification of such genes has raised the possibility of developing novel targeted therapies or reconsidering already existing drugs by the repositioning of FDA-approved drugs.

In this review, the latest *in vitro* 3D models suitable for assessing drug-specific responses in neuroblastoma will be addressed. We will discuss their implications in pre-clinical testing and applicability for a more accurate prediction of therapy outcomes. Finally, the possibilities of introducing already available bioengineered platforms and devices for the generation of predictive neuroblastoma models will be explored. We will assess current possibilities for a more accurate *in vitro* investigation of the pharmacotherapeutic cues in this tumor to justify clinical trials.

NEUROBLASTOMA *IN VITRO* 3D MODELS

The lack of reliable *in vitro* tumor platforms for rapid and highly reproducible studies in cancer biology has driven the development of new tumor models by applying various bioengineering methodologies. Although these models share a common 3D conformation, each displays its own intrinsic

property. In addition, the 3D models indicate unambiguously that the proliferation of tumor cells is significantly less when compared with 2D growth conditions (12, 24). In the following paragraphs, we will address the current applications of 3D *in vitro* culture systems in the neuroblastoma research field.

Multicellular Tumor Spheroids (MCTSs)

MCTS is the most well-characterized 3D model for cancer research obtained by growing cancer cell lines under low adherent conditions (25). MCTSs can have different configurations depending on the specific aim of the study: they can be composed of a single or multiple cell types, generated either through the aggregation and compaction of multiple cells in suspension, or by establishing cell masses from a single cell *via* consecutive cell doublings. In either of these cases biomimetic ECM support, playing the role of a scaffold, may or may not be applied (12, 26).

MCTSs obtained by the aggregation of neuroblastoma cell lines represent an attractive tool to reproduce *in vitro* the *in vivo* characteristics of tumor cells with respect to the production of ECM, cell–cell interactions, growth kinetics, cellular heterogeneity, signal pathway activity, and gene expression (13, 25). Given the importance of the cell-ECM interaction in a 3D extent, among the most studied behaviors in the neuroblastoma field are the migratory and invasive potentials of cancer cells. For example, the analysis of different neuroblastoma cell lines embedded in 3D collagen gels revealed the relationship between cellular morphology (elongated/mesenchymal versus amoeboid/rounded cells) and their invasive capability through a surrounding environment (27). The main difference between the cells grown in 2D and 3D collagen structures is recognized in the Rac signaling pathway, which is differently expressed in these structures. It is a crucial regulator of cell invasion from the spheroid body through the surrounding matrix (27). These results highlight that biochemical signals in the neuroblastoma cells may change dramatically in response to changes in their spatio-temporal distribution. Moreover, they strengthen the case for using 3D systems to select the compounds able to counteract invasion of neuroblastoma cells. In addition to single chemical testing, neuroblastoma spheroids are also suitable for investigating the role of specific proteins on neuroblastoma outgrowth. For example, high levels of Stathmin (a Tubulin binding protein) are associated with tumor aggression and the appearance of metastatic disease. This protein has been selected by analyzing cell line-derived MCTSs where it contributes to a higher invasive motility of the cells (28). Besides Stathmin, SNAI2 is also a crucial molecular determinant of invasive tumor strands. This protein defines the border regularity of the MCTSs and promotes local 3D invasion and dissemination of neuroblastoma cells (29).

However, some critical issues related to cell line-derived MCTSs need to be considered. The variability in spheroid size and their inhomogeneous density profoundly affect the response to drug treatments. As a consequence, this feature negatively impacts the reproducibility and reliability of the obtained results (26). In addition, long-term *in vitro* culture of cell line-derived MCTSs is very challenging since these structures lack a stem cell population able to self-renew the spheroid necrotic core. Moreover, this model is not able to faithfully approximate/simulate the complexity of neuroblastoma genetics and the tumor microenvironment found in humans.

Tissue-Derived Tumor Spheres (TDTSs)

TDTSs are obtained by tumor tissue mechanical dissociation (26). Due to the origin of primary cells, this *in vitro* model system more closely reflects the genetic and clonal heterogeneity of the native tumor, thus providing a more accurate pre-clinical platform (30). Despite the fact that these tailored models can lead to an improved level of prediction, their development and application are still a challenge as sample collection and size, protocol standardization and data reproducibility are critical issues for neuroblastoma. More easily established are neuroblastoma-derived spheroids generated from the bone marrow aspirates of patients diagnosed with stage 4 metastatic disease (30). In some cases, surgically removed tumor resections also allow *in vitro* reproduction of neuroblastoma. However, at the moment it is hard to predict which clinico-biological criterion is a determining factor in enabling the successful *in vitro* growth of a single specimen (31). In fact, a success rate of 55% has been reported for neurosphere maintenance *in vitro*. Also, the expansion of neurospheres cannot be linearly predicted from patient clinic data such as age, stage, *MYCN* amplification and the presence of segmental chromosomal aberrations (31). While the characterization of the resulting neurospheres is currently limited to the expression of CD56 and GD2 neuroblastoma markers, their importance relies on the presentation of reproducible protocols for the *in vitro* expansion of often limited amounts of tumor tissue specimens. Screening for additional antigens specific for neuroblastoma is, however, necessary for more accurate selection of tumor cells with stem features that are often responsible for drug resistance development and disease recurrence. Another TDTS model resembling neuroblastoma intratumoral heterogeneity has been reported by Thole and colleagues (30). The primary neuroblastoma TDTSs culture derived from a bone marrow aspirate with 80% tumor cell infiltration can be cultured in Matrigel. Neuroblastoma cells grown as 3D spheroids maintain the tumorigenic capability in a xenotransplantation mouse model through five passages. Importantly, these TDTSs model systems partly reflect the genetic and clonal heterogeneity of the initial biopsy (30). Altogether, the reported neuroblastoma TDTSs represent essential initial steps toward more sophisticated 3D neuroblastoma modeling suitable for pre-clinical testing.

Patient-Derived Tumor Organoids (PDTOs)

Organoids are *in vitro* derived 3D cell aggregates that are capable of self-renewal and self-organization, while exhibiting expected organ functionality. Organoids are usually generated from either embryonic stem cells (ECS) or induced pluripotent stem cells (iPSC) (32). To date, several organoids have been established for many cancer types (reviewed in ref. (33)).

PDTOs cultures show strong phenotypical and genetic similarities to the original tumor, enabling their use across a wide spectrum of applications. PDTOs allow long-term culture and cryopreservation for the generation of patient-derived tumor organoid biobanks (34). However, most of the patient-derived cancer organoids have an epithelial origin. The generation of

organoid cultures from primary neuroblastoma samples, as well from other non-epithelial cancers, remains today a major challenge in organoid technology.

MOVING FROM 2D TOWARD 3D PRE-CLINICAL SETTINGS

In general, we are currently faced with an extremely low efficacy of pre-clinical studies. In oncology, less than 10% of drugs successfully conclude clinical trials (35), resulting in significant time and economic loss. The introduction of high-throughput drug screening (HTS) speeds up target identification and lead compound selection, increasing the number of anti-neoplastic compounds that potentially reach clinical trial (36). As stated above, the majority of HTS studies are based on the use of tumor cell lines grown in 2D conditions. This approach is slowly being reconsidered and comprises the introduction of different 3D cultures in order to increase the likelihood of pre-clinical success (**Figure 1**). In neuroblastoma, the number of studies that have examined 3D spheroids for HTS is relatively low and their introduction is a challenge. This is particularly true for 3D structures containing patient-derived primary cells due to a lack of study material and difficulties to culture and maintain them *in vitro*.

Each tumor can be considered as a heterogeneous structure deriving from the interaction between cancer cells and the surrounding microenvironment, which provides important physical and biochemical signals for its growth. The information coming from the native 3D human cancer structure can affect, for example, the expression of specific genes as well as the diffusion of nutrients and oxygen within the tumor mass. Moreover, this complex network of interactions determines the ability of tumor cells to resist and escape from pharmacological treatments. This diversity could be at the root of treatment failures, which remain a peril in the neuroblastoma field today.

Pioneering 3D Neuroblastoma Models for Drug Screening Studies

In order to address these needs, 3D culture technology has been applied in the testing of the sensitivity of several MCTSs to doxorubicin exposure, confirming the modification in tolerance to this drug when moving from 2D to 3D culture systems (37). Moreover, MCTSs obtained with the SH-SY5Y neuroblastoma cell line shows higher sensitivity to rapamycin and triciribine when compared to the correspondent 2D culture, emphasizing the importance of *in vitro* 3D models as a valid system for initial testing of new anti-cancer agents (38). In a recent work aimed at identifying candidate drugs for repositioning in high-risk patients, HTS of a library of anticancer compounds was tested in neuroblastoma MCTSs (39). This study proposes MCTSs viability validation using a high-content imaging approach as a powerful and reliable 3D platform to predict pre-clinical efficacies and to reproduce drug responses of neuroblastoma tumors.

BIOMIMETIC EXTRACELLULAR MATRIX (ECM) SUPPORTS FOR NEUROBLASTOMA TUMOR MODEL FABRICATION

The ECM represents a dynamic and versatile network of secreted proteins and polysaccharides assembled together in an organized

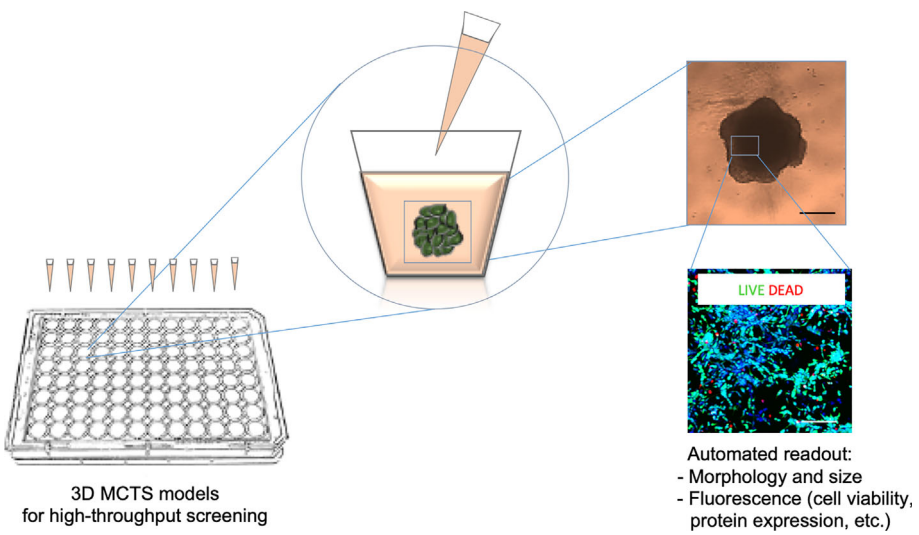

FIGURE 1 | Scheme of the HTS (high throughput drug screening) method. HTS is used to evaluate multiple morphological and cellular parameters in a high number of MCTSs (multicellular tumor spheroids) grown and treated inside microplates. The drug treatment is combined with an optical (upper image) and fluorescence (lower image) microscopy systems for automated image acquisition and coupled analyses through specific software pipelines. These platforms make suitable automatic quantitative analyses of the 3D culture systems in response to drug administration.

network and having distinct roles in cell biology and tissue homeostasis (40). The ECM provides structural support to all organs and provides a substrate upon which cells can migrate. Moreover, the interaction between cells and the ECM macromolecules plays an essential role in tuning the behavior of many cell types in a physiological context. Indeed, during embryonic development the ECM provides essential extrinsic signals for the correct migration of neural crest cells, the pluripotent stem cell population from which neuroblastoma may arise (41).

Role of ECM in Neuroblastoma

The ECM has a complex and tissue-specific molecular composition. The dynamic remodeling of the ECM is of outmost importance in order to determine the specificity of its biological functions during organogenesis and to guarantee a proper tissue homeostasis. As a consequence, the disruption of such mechanisms disorganizes the extracellular niche, leading to abnormal behaviors of resident cells and the failure of tissue homeostasis. Indeed, dysregulation of ECM composition, architecture and stiffness leads toward development or worsening of several diseases, including fibrosis and cancer (42). A large body of experimental evidence emphasizes how ECM proteins promote tumor metastasis and modulate the maintenance and expansion of several cancer cell types and metastatic niches (reviewed in ref. (43–45)).

In neuroblastoma, the presence of a stromal component positively correlates with tumor maturation and favorable prognosis (46). In addition, the deposition of specific ECM components defines an ultra-high risk group of patients affected by neuroblastoma, suggesting that the quantification of tumor stroma components by morphometric techniques could be a valuable tool in improving patients' risk stratification (47). From the molecular perspective, several studies have demonstrated how the cross-talk between neuroblastoma cells and the ECM influences cancer cell differentiation (48). More recently, besides the molecular signaling activated through the cell-ECM interaction, the biomechanical properties of the ECM, such as stiffness and deformability, have also been recognized as mechanical modulators of cancer cell behavior (49). Indeed, dissecting the role of the ECM within the neuroblastoma niche may provide insight into new mechanobiological cues influencing tumor growth and differentiation. This knowledge would provide the basis for future work aimed at the design and exploitation of novel therapeutic strategies against neuroblastoma.

Cast *In Vitro* 3D Models for Studying Neuroblastoma

As mentioned, after important tumor-related knowledge was obtained from 2D cell systems, the importance of introducing ECM component as important determinant of tumor cells behavior pushed the boundaries beyond the second dimension (50). This led to the incorporation of the achievements obtained in the bioengineering field, where different biomimetic matrices have been developed. The full range of available materials, natural, synthetic and semisynthetic (hybrid), have been exploited in the form of hydrogels for their characteristics as a suitable ECM support for tumor cell growth and their autonomous self-assembly in tissue-like structures (**Figure 2**).

The detailed classification of the hydrogels, their applicability and suitable processing approaches have been summarized by Ullah and colleagues (51, 52). The main demands these materials must satisfy are: i) provide proper cell alignment and attachment, ii) sustain cellular metabolic activities, and iii) mimic cell response to mechanical and chemical stimuli as in tissue (53). The cells can be either seeded on the porous scaffold that provides them with 3D support or encapsulated directly within the biomaterials (cell-laden hydrogels) with well-defined stiffness and viscosity. The most commonly used biomaterials for the production of the scaffolds or cell-laden constructs are: collagen, hyaluronic acid (HA), alginate, agarose, gelatin, fibrinogen (natural); poly(lactic-co-glycolide) (PLGA), polyethylene glycol (PEG), poloxamer 407 (Pluronic F127), and polycaprolactone (PCL) (synthetic); and methacrylated gelatin (GelMA) (semisynthetic) (54, 55). The choice is determined by the tumor type and also by specific physical parameters such as elasticity and stiffness (56). In this context, the ways in which biomimetic matrices with different mechanical and biochemical cues can determine the neuroblastoma cell phenotype have been investigated, along with their contribution to the spatio-temporal tumor cell organization or response to drugs. The excellent reproducibility of the *in vivo* data has been demonstrated for the neuroblastoma cell lines Kelly and their cisplatin resilient counterpart (Cis83) when grown on different chemical modifications of collagen, one with glycosaminoglycan (Collagen-GAG) and the other with nanohydroxyapatite (Collagen-nHA) (57). When treated with cisplatin, the cells grown in 3D conditions show similarities with the PDX (patient derived xenograft) treatment, while differing substantially from their 2D control. This finding strengthens the use of 3D models for initial drug evaluations since they more closely approximate the expected response *in vivo*. Bacterial nanocellulose scaffolds coated with collagen is another approach that potentiates SH-SY5Y adhesion in 3D geometric conditions (58). Physical support for neuroblastoma cell growth is also provided by electrospun fibers used as 3D matrices (59). Micro- and nano-fibers created by electrospinning guarantee high porosity of the structures and favor neuroblastoma cell proliferation and adhesion, while promoting neurite out-growth (60). The usefulness of the highly aligned graphene-augmented inorganic nanofiber (GAIN) scaffolds for biomedical cancer research has also been proven for several tumor cell types including neuroblastoma (61). Although they do not allow tumor-like 3D cell organization entirely, these scaffolds open an opportunity for a fast and highly reproducible validation of anti-cancer drugs oriented toward the modulation of cell migration. Another application of graphene is in the fabrication of nanocomposite hydrogel scaffolds in which the magnetic nanoparticle-decorated reduced-graphene oxide (m-rGO) nanosheets lead to a unidirectional orientation of the cells (62). This approach is particularly interesting in the models where both cell orientation and the conductivity of the

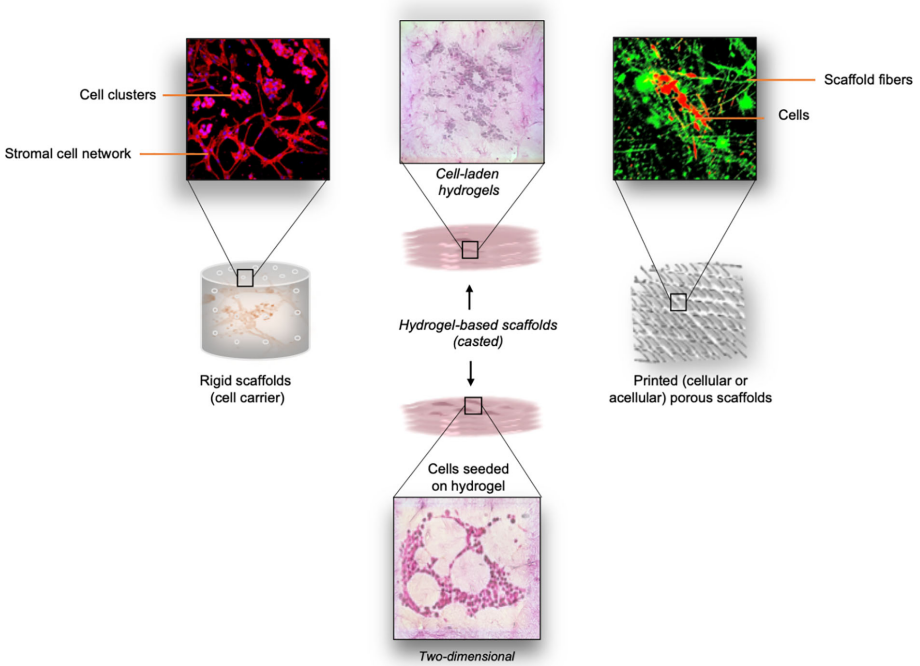

FIGURE 2 | Overview of different types of scaffolds explored for neuroblastoma studies. *Left panel:* Thermal sintering-based approach used for the fabrication of cell-free (rigid) scaffolds with defined geometry. These scaffolds provide mechanical support for cell growth. Cell morphology and cell distribution inside the interconnecting microchannels is directly influenced by the structure of the scaffold. *Middle panel:* Cast cell-laden hydrogels are used as the biomimetic ECM support for the embedded cells. As an option, cells can be seeded on top of the pre-made hydrogel structure. *Right panel:* Printing (e.g. microextrusion, drop-on-demand, laser-based printing) of various bioinks can be adopted for the scaffolding process. Both cellular and acellular approaches can be adopted for the generation of porous scaffolds with defined spatial distribution of the bioink.

biomaterials are required (63). On the other hand, the possibility of growing neuroblastoma cells in collagen-based hydrogels opens another prospect for achieving the 3D structures of neuroblastoma for pre-clinical examinations. Collagen-based structures also allow the reproduction of a 3D microenvironment suitable for better comprehension of pro-migratory pathways activated in neuroblastoma cells (27). Moreover, collagen-based scaffolds offer possibilities for examination of the efficacy of a new class of drugs known as migrastatics (64).

Neuroblastoma cells with different molecular backgrounds show distinct patterns of growth inside biomimetic 3D structures. Moreover, neuroblastoma cells can also be cultured in a mixture of collagen and agarose that is often proposed in order to modify the mechanical properties of pure collagen (65). The encapsulation of neuroblastoma cells is as well supported by alginate and gelatin (66). Either of the cast 3D platforms mentioned can be downscaled thus opening the possibility of HTS applications. In fact, collagen microencapsulation is a highly controllable approach for obtaining miniaturized neuroblastoma tumors (67). In this nanofibrous collagen meshwork, a reconstruction of the neuroblastoma microenvironment is achieved thanks to the stromal cells' support. This study opens the possibility for using neuroblastoma cell-laden bioinks for the reproduction of miniaturized tumors applying different printing methodologies.

(Bio)Printing Neuroblastoma 3D Models

Various 3D printing techniques have been employed to develop more accurate constructs for cell-growth supports (68). Printing technology is challenging the faithful reproduction of the tissue compartments at the microscale while maintaining their unique spatio-temporal organization (69). A parallel expansion of the array of printable biomaterials compatible for research activities or medical requirements has broadened the possibilities for 3D printing (70). The inclusion of (bio)printing methodologies in the neuroblastoma field has been considered in a few studies thus far (**Figure 3**).

A mix of GelMA and methacrylated alginate (AlgMA) have allowed the optimal mechanical properties and porosity for the growth of neuroblastoma cells (71). Similar to the collagen-based hydrogels, this printable bioink also permits tumor cells to organize and create 3D architectures that very closely mimic human neuroblastoma. An optimal level of stability upon printing is also possible with chitosan-gelatin ink, which shows good biocompatibility and allows the proper adhesion of neuroblastoma cells. It is also easily manageable without the need for additional processing post-printing, which makes it a good candidate for high rate production of cell-laden hydrogels (72).

Different neuroblastoma cell lines have been explored using the freeform reversible embedding of suspended hydrogel (FRESH)

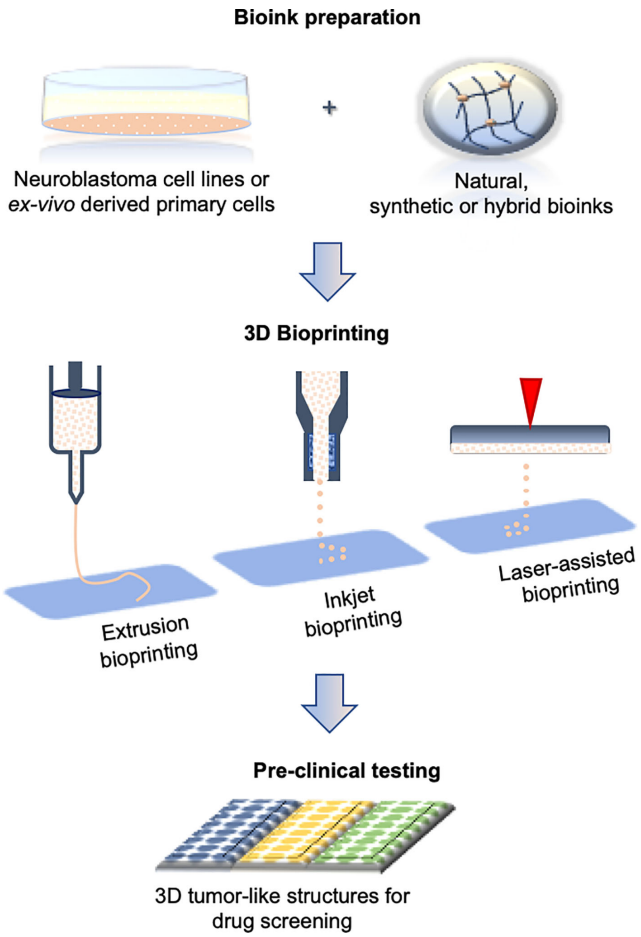

FIGURE 3 | Bioprinting process during *in vitro* 3D model generation. The steps include bioink preparation (cells embedded in biocompatible inks), 3D bioprinting (three most commonly used printing techniques are presented), and drug screening. All the steps can be performed in automated manner.

bioprinting method for conductive scaffolds (73). Although the study was designed for neurodegenerative diseases, the approach and experimental design are incredibly attractive for analyzing tumor cells within 3D conductive bioinks. The FRESH method proves that high resolution of neuroblastoma 3D structures can be obtained using low-viscosity liquids in a supporting bath of gelatin. Neuroblastoma cells can be successfully grown in cellulose and alginate-based hydrogels, demonstrating the applicability of FRESH bioprinting for the generation of microsized 3D neuroblastoma tumors (74). The same type of hydrogel has been explored in the immunology field as well showing the changes in immunophenotype profiles in neuroblastoma cells surrounded by biomimetic ECM (75). Beta tricalcium phosphate (β-TCP) scaffolds used as bone mimetic, have been obtained by combining high resolution 3D printing with manually cast slurry (76). They have been proposed as a suitable approach for sustaining neuroblastoma cell growth inside the metastatic niche (24). In this manner, a local microenvironment is guaranteed allowing the quiescence of tumor stem cells. In this model, the stromal support has been confirmed as a substantial factor in tumor cell organization along with the geometry of the scaffolds. Although the model has not yet been exploited for pre-clinical studies, it can be easily adapted for low/medium scale of drug screening. The metabolic activities and cell death ratio can be easily measured, while microscopy would require special adaptation in the case of live-imaging acquisition.

ENGINEERED PLATFORMS FOR STUDYING TUMOR BIOLOGY, IMMUNOLOGY AND DRUG EFFICACY

The aim of engineered disease models is to reproduce *in vitro* the complexity of the pathological environment in order to gain a better understanding of disease etiology and progression (77). The model composition depends on the research objectives: the more complex the phenomenon under investigation, the more elaborate the model must be (78). *In vitro* cell modeling using miniaturized bioreactors shows great advantages since they allow the use of small volumes of reagents and low cell number, the portability, design versatility and integration with existing devices or platforms for HTS (79). To study the effects of a

static magnetic field on SH-SY5Y neuroblastoma cells, a miniaturized optically accessible bioreactor (MOAB) has been developed based on a prototype of Raimondi et al. (80). This bioreactor is composed of three independent and magnetically lockable culture chambers, each containing a polystyrene scaffold assembled on the top surface of a main body structure. The MOAB is provided with two magnets, located in the chambers and in the main body, whose magnetic coupling ensures a hydraulic seal during the perfusion of 3D constructs. This magnetic seal generates a static magnetic field, which influences cell functions including viability, metabolic activity and gene expression. The MOAB device, specifically conceived to study the influence of a static magnetic field on neuroblastoma cell lines, might potentially be used as an *in vitro* model of neurodegeneration to test perfused 3D cell constructs in terms of response to different stimuli.

To reproduce neuroblastoma vasculogenic mimicry, a complex *in vitro* model has been fabricated by culturing pre-vascularized neuroblastoma cell sheets separated by fibrin layers in a perfusion bioreactor. The cell sheets are prepared by co-culturing the neuroblastoma cell line SK-N-BE(2) with human umbilical vein endothelial cells (HUVEC) on temperature-responsive poly(N-isopropylacrylamide) (PIPAAm)-grafted culture plates. A collagen-gel base with microchannels is used as a support for the vascular bed (81). This platform may represent an interesting option for drug testing, especially for drugs exhibiting antiangiogenic features. The fabrication of an intrinsic system of vasculature allows a better mimicking of the native tumor while augmenting predictive power for translation into pre-clinical applications. However, the difficulty of cell-sheet fabrication and stacking, together with the assembly of the collagen-gel base with microchannels for the perfusion, represent a critical obstacle to a large-scale application of this model.

Another step toward a model resembling native neuroblastomas is represented by the 3D tetra-culture brain microphysiological system (BMPS) used to test neurotoxic chemical agents. This system is developed starting from the OrganoPlate (MIMETAS, Netherlands) in which neuroblastoma cells (N2a), astrocytes (C8-D1A) and microglia (BV-2) are cultured in a collagen type I solution to recreate the brain parenchyma. The neurovascular environment is assured by also including endothelial cells (bEnd.3). The entire system requires culturing in perfusion conditions to permit appropriate 3D cell organization. This plate-based microfluidic platform may be applied for automated, high-throughput and high-content imaging with relatively fast readouts (82). Nevertheless, more consistent validations of their use for a routine drug screening are mandatory.

Clinical Needs and Future Perspectives for *In Vitro* Immunotherapy Evaluations

Immunotherapies have recently attracted great interest as a novel approach for cancer treatment, but the lack of adequate *in vitro* models for testing the efficacy of these therapies at a personalized level is still an issue (75, 83). Immunotherapy strategies rely both, on the ability of the immune system to kill malignant cells by recognizing specific tumor antigens and the ability of tumor cells to evade this physiological defense system. Two major strategies can be identified: re-activation of the tumor infiltrating lymphocytes (TILs) through the immune checkpoint inhibitors and chimeric antigen receptor-T (CAR-T) or T cell receptor (TCR) cell therapy.

Checkpoint inhibitors work by blocking the inhibitory binding between T cells' checkpoint proteins (e.g. PD1) and their ligand on tumor cells (e.g. PDL1), allowing the immune system to become able once again to kill cancer (84). The CAR-T/TCR consists of the patient's T-cells genetically modified to express unique tumor antigens that give them the ability to specifically target cancer cells, such as GD2 for neuroblastoma (84, 85).

Currently, several types of immunotherapy are being studied for use against neuroblastoma (86, 87) and complex *in vitro* 3D models that will allow a close relationship between target and effectors as occurs *in vivo* are needed for pre-clinical efficacy evaluation of immunotherapeutics. As shown in **Figure 4**, immunotherapy strategies can be developed and tested directly using patient derived cells as part of a personalized medicine approach.

To test the migratory and lethality of TCR engineered patient-derived T cells toward hepatic tumors, an interesting 3D *in vitro* model has been developed by Pavesi and colleagues (83). This model consists of a 3D microdevice made of a poly (dimethylsiloxane) structure comprising a gel region with media channels separated from the gel channel by trapezoidal posts. Tumor cells are cultured embedded in a type I collagen gel solution that is injected into the predefined gel region of the device. The culture medium channels allow the cell culture perfusion and the free movement of TCR-T cells from the medium channel into the 3D solid collagen region containing target cells. This 3D assay could lead to a better understanding of what is encountered physiologically during adoptive T cell therapy of solid tumors, where the chemotactic characteristics and intrinsic killing of the engineered T cells are key factors in the successful outcome of the therapy. Although this 3D microdevice has been tested with human liver carcinoma cell line as its target, it could be useful to study other solid tumors including neuroblastoma.

For functional *in vitro* prediction of the efficacy of checkpoint inhibitors, a rapid functional test based on the use of the VITVO device (Rigenerand srl, Italy) has been recently proposed. VITVO is a small, portable bioreactor integrating a synthetic and biocompatible fiber-based matrix, and can host several types of cells, also in combination. Using this platform, primary cells harvested from human lung cancer specimens have been evaluated to predict the patient specific anti-tumor immunity of TILs triggered by checkpoint inhibitor Nivolumab (88). The same approach could also be considered to evaluate neuroblastoma responsiveness to immunomodulatory agents. Although these *in vitro* 3D platforms potentially offer innovative tools for the development of fast and reliable personalized assays, further studies are needed to confirm their relevance for clinical use.

CONCLUSIONS

The more effective targeting of malignant cells remains a highly challenging task since the existing therapeutics approaches do not

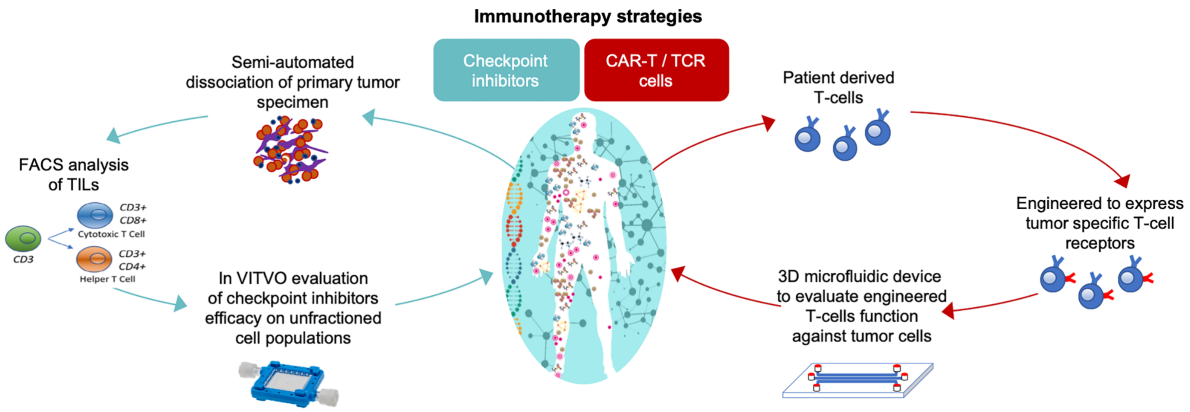

FIGURE 4 | *In vitro* 3D models to test the efficacy of immunotherapeutics in a personalized approach strategy. On the left, the functional assay for cancer responsiveness to checkpoint inhibitors using VITVO bioreactor described by Candini et al. (88); on the right, TCR T-cell activity against tumor using 3D microfluidic device described by Pavesi and colleagues (83).

adequately achieve the same efficacy of *in vitro* determined efficacy when translated to clinical trial. The purpose of including 3D tumor models is therefore to establish a new approach that overcomes the limitations of currently used *in vitro* protocols (**Figure 5**). The 3D *in vitro* models provide a closer reflection of the complexity of malignant tissues by nurturing complex cell-cell and cell-ECM organization. Under these growth modalities, tumor cells more closely approach their native interactions, generating tumor-like structures that strongly define the types of response to toxic drug insults. The number of possibilities for using neuroblastoma 3D models in HTS is increasing thanks to advances in bioengineering field. However, the automation of

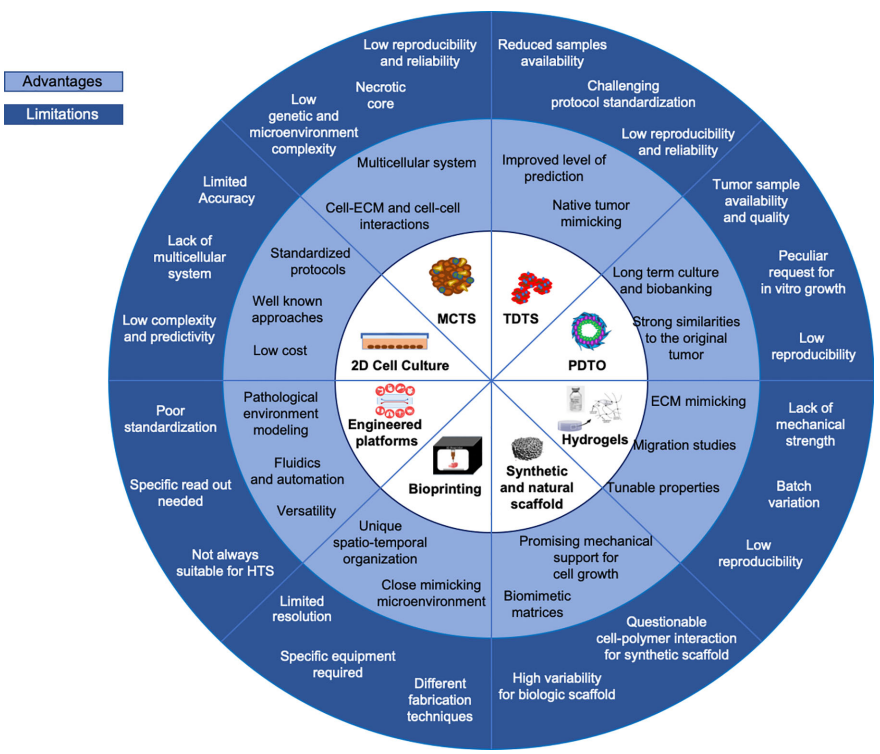

FIGURE 5 | Current *in vitro* models. Advantages and limitations overview of current 3D *in vitro* models versus 2D systems are summarized.

multiparametric data extrapolation in terms of volumetric parameters and cell viability within analyzed 3D structures remains a challenge. The introduction of bioprinting processes in pre-clinical studies is expected to bring to a greater reproducibility of the cell models, as well as higher predictability and controllability of the structures in comparison with the cast approach. The precision and resolution of the cell-laden structure bioprinting are determined by the characteristics of the nozzles, which do not allow the printability of all currently available bioinks. Although very useful, a limitation of using preformed porous scaffolds for sequential cell plating and culturing is the poor reproducibility of the spatio-temporally location of more than one cell type. The combination of (bio)printing and fabrication of microfluidic platforms in the field of neuroblastoma can therefore amplify the possibilities for HTS in 3D conditions. It is particularly intriguing if the described, versatile 3D cell culture systems could advance the pre-clinical evaluation of newly proposed tailored therapies and cell-based therapies that are currently under investigation for defeating neuroblastoma tumor cells.

AUTHOR CONTRIBUTIONS

DC, SA, OC, and SF wrote the manuscript. DC, SF, SA, and OC reviewed the literature and collected available data. CD, SA, OC, EG, and SF designed the figures. HF and MD revised the manuscript. All authors contributed to the article and approved the submitted version.

FUNDING

This work was supported by the Fondazione Italiana per la Lotta al Neuroblastoma (project number 19_20FNBL).

ACKNOWLEDGMENTS

The authors would like to thank Fondazione Italiana per la Lotta al Neuroblastoma, Fondazione Città della Speranza and Fondazione CARIPARO for their support.

REFERENCES

1. Kapałczyńska M, Kolenda T, Przybyła W, Zajączkowska M, Teresiak A, Filas V, et al. 2D and 3D cell cultures – a comparison of different types of cancer cell cultures. *Arch Med Sci* (2016) 14(4):910–9. doi: 10.5114/aoms.2016.63743
2. Mogilner A, Odde D. Modeling cellular processes in 3D. *Trends Cell Biol* (2011) 21:692–700. doi: 10.1016/j.tcb.2011.09.007
3. Graham ML, Prescott MJ. The multifactorial role of the 3Rs in shifting the harm-benefit analysis in animal models of disease. *Eur J Pharmacol* (2015) 759:19–29. doi: 10.1016/j.ejphar.2015.03.040
4. Bart van der Worp H, Howells DW, Sena ES, Porritt MJ, Rewell S, O'Collins V, et al. Can animal models of disease reliably inform human studies? *PLoS Med* (2010) 7:1–8. doi: 10.1371/journal.pmed.1000245
5. Hutchinson L, Kirk R. High drug attrition rates - Where are we going wrong? *Nat Rev Clin Oncol* (2011) 18:189–90. doi: 10.1038/nrclinonc.2011.34
6. Asghar W, El Assal R, Shafiee H, Pitteri S, Paulmurugan R, Demirci U. Engineering cancer microenvironments for in vitro 3-D tumor models. *Mater Today* (2015) 18:539–53. doi: 10.1016/j.mattod.2015.05.002
7. Darnell M, Schreiter T, Zeilinger K, Urbaniak T, Söderdahl T, Rossberg I, et al. Cytochrome P450-Dependent Metabolism in HepaRG Cells Cultured in a Dynamic Three-Dimensional Bioreactor. *Drug Metab Dispos* (2011) 39:1131–8. doi: 10.1124/dmd.110.037721
8. Howes AL, Richardson RD, Finlay D, Vuori K. 3-Dimensional Culture Systems for Anti-Cancer Compound Profiling and High-Throughput Screening Reveal Increases in EGFR Inhibitor-Mediated Cytotoxicity Compared to Monolayer Culture Systems. *PLoS One* (2014) 9:e108283. doi: 10.1371/journal.pone.0108283
9. Graf BW, Boppart SA. (2010) Imaging and Analysis of Three-Dimensional Cell Culture Models. In: Papkovsky D, editor. *Live Cell Imaging. Methods in Molecular Biology (Methods and Protocols), vol 591*. Humana Press. p. 211–27. doi: 10.1007/978-1-60761-404-3_13
10. Klinghoffer RA, Bahrami SB, Hatton BA, Frazier JP, Moreno-Gonzalez A, Strand AD, et al. A technology platform to assess multiple cancer agents simultaneously within a patient's tumor. *Sci Transl Med* (2015) 7:284ra58–284ra58. doi: 10.1126/scitranslmed.aaa7489
11. Isherwood B, Timpson P, McGhee EJ, Anderson KI, Canel M, Serrels A, et al. Live Cell in Vitro and in Vivo Imaging Applications: Accelerating Drug Discovery. *Pharmaceutics* (2011) 3:141–70. doi: 10.3390/pharmaceutics 3020141
12. Nolan JC, Frawley T, Tighe J, Soh H, Curtin C, Piskareva O. Preclinical models for neuroblastoma: Advances and challenges. *Cancer Lett* (2020) 474:53–62. doi: 10.1016/j.canlet.2020.01.015
13. Ornell KJ, Coburn JM. Developing preclinical models of neuroblastoma: driving therapeutic testing. *BMC BioMed Eng* (2019) 1:33. doi: 10.1186/s42490-019-0034-8
14. Corallo D, Candiani S, Ori M, Aveic S, Tonini GP. The zebrafish as a model for studying neuroblastoma. *Cancer Cell Int* (2016) 16:82. doi: 10.1186/s12935-016-0360-z
15. Johnsen JI, Dyberg C, Wickström M. Neuroblastoma—A Neural Crest Derived Embryonal Malignancy. *Front Mol Neurosci* (2019) 12:9. doi: 10.3389/fnmol.2019.00009
16. Matthay KK, Maris JM, Schleiermacher G, Nakagawara A, Mackall CL, Diller L, et al. Neuroblastoma. *Nat Rev Dis Prim* (2016) 2:16078. doi: 10.1038/nrdp.2016.78
17. Cohn SL, Pearson ADJ, London WB, Monclair T, Ambros PF, Brodeur GM, et al. The International Neuroblastoma Risk Group (INRG) Classification System: An INRG Task Force Report. *J Clin Oncol* (2009) 27:289–97. doi: 10.1200/JCO.2008.16.6785
18. Brodeur GM, Bagatell R. Mechanisms of neuroblastoma regression. *Nat Rev Clin Oncol* (2014) 11:704–13. doi: 10.1038/nrclinonc.2014.168
19. Ladenstein R, Pötschger U, Pearson ADJ, Brock P, Luksch R, Castel V, et al. Busulfan and melphalan versus carboplatin, etoposide, and melphalan as high-dose chemotherapy for high-risk neuroblastoma (HR-NBL1/SIOPEN): an international, randomised, multi-arm, open-label, phase 3 trial. *Lancet Oncol* (2017) 18:500–14. doi: 10.1016/S1470-2045(17)30070-0
20. Tolbert VP, Matthay KK. Neuroblastoma: clinical and biological approach to risk stratification and treatment. *Cell Tissue Res* (2018) 372:195–209. doi: 10.1007/s00441-018-2821-2
21. Van Arendonk K, Chung D. Neuroblastoma: Tumor Biology and Its Implications for Staging and Treatment. *Children* (2019) 6:12. doi: 10.3390/children6010012
22. Sridhar S, Al-Moallem B, Kamal H, Terrile M, Stallings RL. New Insights into the Genetics of Neuroblastoma. *Mol Diagn Ther* (2013) 17:63–9. doi: 10.1007/s40291-013-0019-6
23. Bosse KR, Maris JM. Advances in the translational genomics of neuroblastoma: From improving risk stratification and revealing novel biology to identifying actionable genomic alterations. *Cancer* (2016) 122:20–33. doi: 10.1002/cncr.29706
24. Aveic S, Davtalab R, Vogt M, Weber M, Buttler P, Tonini GP, et al. Calcium phosphate scaffolds with defined interconnecting channel structure provide a mimetic 3D niche for bone marrow metastasized tumor cell growth. *Acta Biomater* (2019) 88:527–39. doi: 10.1016/j.actbio.2019.02.030
25. Sutherland RM, Mccredie JA, Inch R. Growth of Multicell Spheroids in Tissue Culture as a Model of Nodular Carcinomas. *J Natl Cancer Inst* (1971) 46 (1):113–20. doi: 10.1093/jnci/46.1.113

26. Nath S, Devi GR. Three-dimensional culture systems in cancer research: Focus on tumor spheroid model. *Pharmacol Ther* (2016) 163:94–108. doi: 10.1016/j.pharmthera.2016.03.013
27. Mitchell CB, O'Neill GM. Rac GTPase regulation of 3D invasion in neuroblastomas lacking MYCN amplification. *Cell Adh Migr* (2017) 11:68–79. doi: 10.1080/19336918.2016.1183868
28. Fife CM, Sagnella SM, Teo WS, Po'uha ST, Byrne FL, Yeap YYC, et al. Stathmin mediates neuroblastoma metastasis in a tubulin-independent manner via RhoA/ROCK signaling and enhanced transendothelial migration. *Oncogene* (2017) 36:501–11. doi: 10.1038/onc.2016.220
29. Vrenken KS, Vervoort BMT, van Ingen Schenau DS, Derks YHW, van Emst L, Grytsenko PG, et al. The transcriptional repressor SNAI2 impairs neuroblastoma differentiation and inhibits response to retinoic acid therapy. *Biochim Biophys Acta Mol Basis Dis* (2020) 1866:165644. doi: 10.1016/j.bbadis.2019.165644
30. Thole TM, Toedling J, Sprüssel A, Pfeil S, Savelyeva L, Capper D, et al. Reflection of neuroblastoma intratumor heterogeneity in the new OHC-NB1 disease model. *Int J Cancer* (2020) 146:1031–41. doi: 10.1002/ijc.32572
31. Barton J, Pacey K, Jain N, Kasia T, Edwards D, Thevanesan C, et al. Establishment and phenotyping of neurosphere cultures from primary neuroblastoma samples. *F1000Research* (2019) 8:823. doi: 10.12688/f1000research.18209.1
32. Clevers H. Modeling Development and Disease with Organoids. *Cell* (2016) 165:1586–97. doi: 10.1016/j.cell.2016.05.082
33. Bleijs M, Wetering M, Clevers H, Drost J. Xenograft and organoid model systems in cancer research. *EMBO J* (2019) 38:e101654. doi: 10.15252/embj.2019101654
34. Sachs N, de Ligt J, Kopper O, Gogola E, Bounova G, Weeber F, et al. A Living Biobank of Breast Cancer Organoids Captures Disease Heterogeneity. *Cell* (2018) 172:373–86. doi: 10.1016/j.cell.2017.11.010
35. Wong CH, Siah KW, Lo AW. Estimation of clinical trial success rates and related parameters. *Biostatistics* (2019) 20:273–86. doi: 10.1093/biostatistics/kxx069
36. Langhans SA. Three-Dimensional in Vitro Cell Culture Models in Drug Discovery and Drug Repositioning. *Front Pharmacol* (2018) 9(6):1. doi: 10.3389/fphar.2018.00006
37. Baek N, Seo OW, Kim M, Hulme J, An SSA. Monitoring the effects of doxorubicin on 3D-spheroid tumor cells in real-time. *Onco Targets Ther* (2016) 9:7207–18. doi: 10.2147/OTT.S112566
38. Bahmad HF, Mouhieddine TH, Chalhoub RM, Assi S, Araji T, Chamaa F, et al. The Akt/mTOR pathway in cancer stem/progenitor cells is a potential therapeutic target for glioblastoma and neuroblastoma. *Oncotarget* (2018) 9:33549–61. doi: 10.18632/oncotarget.26088
39. Sidarovich V, De Mariano M, Aveic S, Pancher M, Adami V, Gatto P, et al. A High-Content Screening of Anticancer Compounds Suggests the Multiple Tyrosine Kinase Inhibitor Ponatinib for Repurposing in Neuroblastoma Therapy. *Mol Cancer Ther* (2018) 17:1405–15. doi: 10.1158/1535-7163.MCT-17-0841
40. Hay ED. Extracellular matrix. *J Cell Biol* (1981) 91:205s–23s. doi: 10.1083/jcb.91.3.205s
41. Perris R, Perissinotto D. Role of the extracellular matrix during neural crest cell migration. *Mech Dev* (2000) 95:3–21. doi: 10.1016/S0925-4773(00)00365-8
42. Frantz C, Stewart KM, Weaver VM. The extracellular matrix at a glance. *J Cell Sci* (2010) 123:4195–200. doi: 10.1242/jcs.023820
43. Hynes RO. The Extracellular Matrix: Not Just Pretty Fibrils. *Sci (80)* (2009) 326:1216–9. doi: 10.1126/science.1176009
44. Lu P, Takai K, Weaver VM, Werb Z. Extracellular Matrix Degradation and Remodeling in Development and Disease. *Cold Spring Harb Perspect Biol* (2011) 3:a005058–a005058. doi: 10.1101/cshperspect.a005058
45. Lu P, Weaver VM, Werb Z. The extracellular matrix: A dynamic niche in cancer progression. *J Cell Biol* (2012) 196:395–406. doi: 10.1083/jcb.201102147
46. Shimada H, Chatten J, Newton WA, Sachs N, Hamoudi AB, Chiba T, et al. Histopathologic Prognostic Factors in Neuroblastic Tumors: Definition of Subtypes of Ganglioneuroblastoma and an Age-Linked Classification of Neuroblastomas. *JNCI J Natl Cancer Inst* (1984) 73:405–16. doi: 10.1093/jnci/73.2.405
47. Tadeo I, Berbegall AP, Castel V, García-Miguel P, Callaghan R, Påhlman S, et al. Extracellular matrix composition defines an ultra-high-risk group of neuroblastoma within the high-risk patient cohort. *Br J Cancer* (2016) 115:480–9. doi: 10.1038/bjc.2016.210
48. Yoon Y-K, Kim H-P, Han S-W, Hur H-S, Oh DY, Im S-A, et al. Combination of EGFR and MEK1/2 inhibitor shows synergistic effects by suppressing EGFR/HER3-dependent AKT activation in human gastric cancer cells. *Mol Cancer Ther* (2009) 8:2526–36. doi: 10.1158/1535-7163.MCT-09-0300
49. Lam WA, Cao L, Umesh V, Keung AJ, Sen S, Kumar S. Extracellular matrix rigidity modulates neuroblastoma cell differentiation and N-myc expression. *Mol Cancer* (2010) 9:35. doi: 10.1186/1476-4598-9-35
50. Tibbitt MW, Anseth KS. Hydrogels as extracellular matrix mimics for 3D cell culture. *Biotechnol Bioeng* (2009) 103:655–63. doi: 10.1002/bit.22361
51. Ullah F, Othman MBH, Javed F, Ahmad Z, Akil HM. Classification, processing and application of hydrogels: A review. *Mater Sci Eng C* (2015) 57:414–33. doi: 10.1016/j.msec.2015.07.053
52. Drury JL, Mooney DJ. Hydrogels for tissue engineering: Scaffold design variables and applications. *Biomaterials* (2003) 24:4337–51. doi: 10.1016/S0142-9612(03)00340-5
53. Haycock JW. 3D Cell Culture: A Review of Current Approaches and Techniques. In: Haycock J, editor. *3D Cell Culture. Methods in Molecular Biology (Methods and Protocols), vol 695*. Humana Press (2010). p. 1–15. doi: 10.1007/978-1-60761-984-0_1
54. Malda J, Visser J, Melchels FP, Jüngst T, Hennink WE, Dhert WJA, et al. 25th Anniversary Article: Engineering Hydrogels for Biofabrication. *Adv Mater* (2013) 25:5011–28. doi: 10.1002/adma.201302042
55. Hutmacher DW. Biomaterials offer cancer research the third dimension. *Nat Mater* (2010) 9:90–3. doi: 10.1038/nmat2619
56. Tilghman RW, Cowan CR, Mih JD, Koryakina Y, Gioeli D, Slack-Davis JK, et al. Matrix Rigidity Regulates Cancer Cell Growth and Cellular Phenotype. *PLoS One* (2010) 5:e12905. doi: 10.1371/journal.pone.0012905
57. Curtin C, Nolan JC, Conlon R, Deneweth L, Gallagher C, Tan YJ, et al. A physiologically relevant 3D collagen-based scaffold–neuroblastoma cell system exhibits chemosensitivity similar to orthotopic xenograft models. *Acta Biomater* (2018) 70:84–97. doi: 10.1016/j.actbio.2018.02.004
58. Innala M, Riebe I, Kuzmenko V, Sundberg J, Gatenholm P, Hanse E, et al. 3D Culturing and differentiation of SH-SY5Y neuroblastoma cells on bacterial nanocellulose scaffolds. *Artif Cells Nanomed Biotechnol* (2014) 42:302–8. doi: 10.3109/21691401.2013.821410
59. Fasolino I, Bonadies I, Ambrosio L, Raucci MG, Carfagna C, Caso FM, et al. Eumelanin Coated PLA Electrospun Micro Fibers as Bioinspired Cradle for SH-SY5Y Neuroblastoma Cells Growth and Maturation. *ACS Appl Mater Interf* (2017) 9:40070–6. doi: 10.1021/acsami.7b13257
60. Doshi J, Reneker DH. Electrospinning process and applications of electrospun fibers. *J Electrostat* (1995) 35:151–60. doi: 10.1016/0304-3886(95)00041-8
61. Kazantseva J, Ivanov R, Gasik M, Neuman T, Hussainova I. Graphene-Augmented Nanofiber Scaffolds Trigger Gene Expression Switching of Four Cancer Cell Types. *ACS Biomater Sci Eng* (2018) 4:1622–9. doi: 10.1021/acsbiomaterials.8b00228
62. Santhosh M, Choi J-WJ-H, Choi J-WJ-H. Magnetic-Assisted Cell Alignment within a Magnetic Nanoparticle-Decorated Reduced Graphene Oxide/Collagen 3D Nanocomposite Hydrogel. *Nanomaterials* (2019) 9:1293. doi: 10.3390/nano9091293
63. Solìs Moré Y, Panella G, Fioravanti G, Perrozzi F, Passacantando M, Giansanti F, et al. Biocompatibility of composites based on chitosan, apatite, and graphene oxide for tissue applications. *J BioMed Mater Res Part A* (2018) 106:1585–94. doi: 10.1002/jbm.a.36361
64. Gandalovičová A, Rosel D, Fernandes M, Veselý P, Heneberg P, Čermák V, et al. Migrastatics—Anti-metastatic and Anti-invasion Drugs: Promises and Challenges. *Trends Cancer* (2017) 3:391–406. doi: 10.1016/j.trecan.2017.04.008
65. Duarte Campos DF, Bonnin Marquez A, O'Seanain C, Fischer H, Blaeser A, Vogt M, et al. Exploring Cancer Cell Behavior In Vitro in Three-Dimensional Multicellular Bioprintable Collagen-Based Hydrogels. *Cancers (Basel)* (2019) 11:180. doi: 10.3390/cancers11020180
66. Fantini V, Bordoni M, Scocozza F, Conti M, Scarian E, Carelli S, et al. Bioink Composition and Printing Parameters for 3D Modeling Neural Tissue. *Cells* (2019) 8:830. doi: 10.3390/cells8080830
67. Yeung P, Sin HS, Chan S, Chan GCF, Chan BP. Microencapsulation of Neuroblastoma Cells and Mesenchymal Stromal Cells in Collagen Microspheres: A 3D Model for Cancer Cell Niche Study. *PLoS One* (2015) 10:e0144139. doi: 10.1371/journal.pone.0144139

68. Park JH, Jang J, Lee J-S, Cho D-W. Three-Dimensional Printing of Tissue/Organ Analogues Containing Living Cells. *Ann BioMed Eng* (2017) 45:180–94. doi: 10.1007/s10439-016-1611-9
69. Hinton TJ, Jallerat Q, Palchesko RN, Park JH, Grodzicki MS, Shue H-J, et al. Three-dimensional printing of complex biological structures by freeform reversible embedding of suspended hydrogels. *Sci Adv* (2015) 1:e1500758. doi: 10.1126/sciadv.1500758
70. Rana Khalid I, Darakhshanda I, Rafi A R. 3D Bioprinting: An attractive alternative to traditional organ transplantation. *Arch BioMed Sci Eng* (2019) 5:007–18. doi: 10.17352/abse.000012
71. Monferrer E, Martín-Vañó S, Carretero A, García-Lizarribar A, Burgos-Panadero R, Navarro S, et al. A three-dimensional bioprinted model to evaluate the effect of stiffness on neuroblastoma cell cluster dynamics and behavior. *Sci Rep* (2020) 10:6370. doi: 10.1038/s41598-020-62986-w
72. Roehm KD, Madihally SV. Bioprinted chitosan-gelatin thermosensitive hydrogels using an inexpensive 3D printer. *Biofabrication* (2017) 10:015002. doi: 10.1088/1758-5090/aa96dd
73. Bordoni M, Karabulut E, Kuzmenko V, Fantini V, Pansarasa O, Cereda C, et al. 3D Printed Conductive Nanocellulose Scaffolds for the Differentiation of Human Neuroblastoma Cells. *Cells* (2020) 9:682. doi: 10.3390/cells9030682
74. Lewicki J, Bergman J, Kerins C, Hermanson O. Optimization of 3D bioprinting of human neuroblastoma cells using sodium alginate hydrogel. *Bioprinting* (2019) 16:e00053. doi: 10.1016/j.bprint.2019.e00053
75. Marrella A, Dondero A, Aiello M, Casu B, Olive D, Regis S, et al. Cell-Laden Hydrogel as a Clinical-Relevant 3D Model for Analyzing Neuroblastoma Growth, Immunophenotype, and Susceptibility to Therapies. *Front Immunol* (2019) 10:1876. doi: 10.3389/fimmu.2019.01876
76. Lindner M, Bergmann C, Telle R, Fischer H. Calcium phosphate scaffolds mimicking the gradient architecture of native long bones. *J BioMed Mater Res Part A* (2014) 102:3677–84. doi: 10.1002/jbm.a.35038
77. Benam KH, Dauth S, Hassell B, Herland A, Jain A, Jang K-J, et al. Engineered In Vitro Disease Models. *Annu Rev Pathol Mech Dis* (2015) 10:195–262. doi: 10.1146/annurev-pathol-012414-040418
78. Katt ME, Placone AL, Wong AD, Xu ZS, Searson PC. In Vitro Tumor Models: Advantages, Disadvantages, Variables, and Selecting the Right Platform. *Front Bioeng Biotechnol* (2016) 4:12. doi: 10.3389/fbioe.2016.00012
79. Izzo L, Tunesi M, Boeri L, Laganà M, Giordano C, Raimondi MT. Influence of the static magnetic field on cell response in a miniaturized optically accessible bioreactor for 3D cell culture. *BioMed Microdev* (2019) 21:29. doi: 10.1007/s10544-019-0387-8
80. Raimondi MT, Eaton SM, Laganà M, Aprile V, Nava MM, Cerullo G, et al. Three-dimensional structural niches engineered via two-photon laser polymerization promote stem cell homing. *Acta Biomater* (2013) 9:4579–84. doi: 10.1016/j.actbio.2012.08.022
81. Villasante A, Sakaguchi K, Kim J, Cheung NK, Nakayama M, Parsa H, et al. Vascularized Tissue-Engineered Model for Studying Drug Resistance in Neuroblastoma. *Theranostics* (2017) 7:4099–117. doi: 10.7150/thno.20730
82. Liu L, Koo Y, Akwitti C, Russell T, Gay E, Laskowitz DT, et al. Three-dimensional (3D) brain microphysiological system for organophosphates and neurochemical agent toxicity screening. *PLoS One* (2019) 14:e0224657. doi: 10.1371/journal.pone.0224657
83. Pavesi A, Tan AT, Chen MB, Adriani G, Bertoletti A, Kamm RD. Using microfluidics to investigate tumor cell extravasation and T-cell immunotherapies. *2015 37th Annu Int Conf IEEE Eng Med Biol Soc (EMBC) (IEEE)* (2015) 1853–6. doi: 10.1109/EMBC.2015.7318742
84. Sanghera C, Sanghera R. Immunotherapy – Strategies for Expanding Its Role in the Treatment of All Major Tumor Sites. *Cureus* (2019) 11(10):e5938. doi: 10.7759/cureus.5938
85. Prapa M, Caldrer S, Spano C, Bestagno M, Golinelli G, Grisendi G, et al. A novel anti-GD2/4-1BB chimeric antigen receptor triggers neuroblastoma cell killing. *Oncotarget* (2015) 6:24884–94. doi: 10.18632/oncotarget.4670
86. Croce M, Corrias MV, Rigo V, Ferrini S. New immunotherapeutic strategies for the treatment of neuroblastoma. *Immunotherapy* (2015) 7:285–300. doi: 10.2217/imt.14.117
87. Sait S, Modak S. Anti-GD2 immunotherapy for neuroblastoma. *Expert Rev Anticancer Ther* (2017) 17:889–904. doi: 10.1080/14737140.2017.1364995
88. Candini O, Grisendi G, Foppiani EM, Brogli M, Aramini B, Masciale V, et al. A Novel 3D In Vitro Platform for Pre-Clinical Investigations in Drug Testing, Gene Therapy, and Immuno-oncology. *Sci Rep* (2019) 9:7154. doi: 10.1038/s41598-019-43613-9

Conflict of Interest: MD is founder and member of the Board of Directors of Rigenerand srl, a University start-up company. MD interests are managed by the University of Modena and Reggio Emilia in accordance with their conflict of interest policies. SF, OC, and EG are currently employed by Rigenerand srl.

The remaining authors declare that the research was conducted in the absence of any commercial or financial relationships that could be construed as a potential conflict of interest.

frontiers in Oncology

REVIEW
published: 08 December 2020
doi: 10.3389/fonc.2020.604121

Glioblastoma Organoids: Pre-Clinical Applications and Challenges in the Context of Immunotherapy

Eliane Klein[1], *Ann-Christin Hau*[1], *Anaïs Oudin*[1], *Anna Golebiewska*[1*†] *and Simone P. Niclou*[1,2*†]

[1] NORLUX Neuro-Oncology Laboratory, Department of Oncology, Luxembourg Institute of Health, Luxembourg, Luxembourg, [2] Department of Biomedicine, University of Bergen, Bergen, Norway

Malignant brain tumors remain uniformly fatal, even with the best-to-date treatment. For Glioblastoma (GBM), the most severe form of brain cancer in adults, the median overall survival is roughly over a year. New therapeutic options are urgently needed, yet recent clinical trials in the field have been largely disappointing. This is partially due to inappropriate preclinical model systems, which do not reflect the complexity of patient tumors. Furthermore, clinically relevant patient-derived models recapitulating the immune compartment are lacking, which represents a bottleneck for adequate immunotherapy testing. Emerging 3D organoid cultures offer innovative possibilities for cancer modeling. Here, we review available GBM organoid models amenable to a large variety of pre-clinical applications including functional bioassays such as proliferation and invasion, drug screening, and the generation of patient-derived orthotopic xenografts (PDOX) for validation of biological responses *in vivo*. We emphasize advantages and technical challenges in establishing immunocompetent *ex vivo* models based on co-cultures of GBM organoids and human immune cells. The latter can be isolated either from the tumor or from patient or donor blood as peripheral blood mononuclear cells (PBMCs). We also discuss the challenges to generate GBM PDOXs based on humanized mouse models to validate efficacy of immunotherapies *in vivo*. A detailed characterization of such models at the cellular and molecular level is needed to understand the potential and limitations for various immune activating strategies. Increasing the availability of immunocompetent GBM models will improve research on emerging immune therapeutic approaches against aggressive brain cancer.

Keywords: brain tumors, glioblastoma, glioma, immunotherapy, preclinical models, organoids, patient-derived xenografts, tumor microenvironment

OPEN ACCESS

Edited by:
Roberta Castriconi, Università di Genova, Italy

Reviewed by:
Janko Kos, University of Ljubljana, Slovenia
Tullio Florio, University of Genoa, Italy

***Correspondence:**
Anna Golebiewska
anna.golebiewska@lih.lu
Simone P. Niclou
simone.niclou@lih.lu

Specialty section:
This article was submitted to Cancer Immunity and Immunotherapy, a section of the journal Frontiers in Oncology

Received: *08 September 2020*
Accepted: *09 November 2020*
Published: *08 December 2020*

Citation:
Klein E, Hau A-C, Oudin A, Golebiewska A and Niclou SP (2020) Glioblastoma Organoids: Pre-Clinical Applications and Challenges in the Context of Immunotherapy. Front. Oncol. 10:604121. doi: 10.3389/fonc.2020.604121

INTRODUCTION

Among primary malignant tumors of the central nervous system (CNS) the most common and aggressive form is glioblastoma (GBM) with a median survival of 12–15 months (1). Standard treatment of care remained unchanged since 2005, consisting of maximal surgical resection followed by concomitant radiotherapy and chemotherapy with the alkylating agent temozolomide (TMZ) (2).

In the last 15 years, novel experimental approaches have shown limited success to improve patient survival and the development of more efficacious therapies remains challenging (3). Several underlying factors, such as aggressive and highly infiltrative growth, inter-patient and intra-tumoral heterogeneity and multiple resistance mechanisms, contribute to the poor outcome (4). More recently, high phenotypic plasticity of GBM has been recognized as an additional hurdle, in particular for precision medicine strategies (5, 6). Improved therapies are desperately needed and novel approaches need to be investigated in adequate preclinical models followed by innovative clinical trials.

Immunotherapy has emerged in recent years as an important success story in oncology, with unprecedented results in various tumor types, e.g., melanoma and breast cancer (7). Rather than targeting tumor cells directly, immunotherapy aims to activate and modulate the immune system in order to stimulate anti-tumor immunity. Currently, numerous clinical trials assess various immunotherapeutic approaches in GBM patients (8). Unfortunately, phase III clinical trials testing immune-checkpoint inhibitors and vaccines have shown so far discouraging results (9, 10). Importantly, GBM is classified as an immunologically 'cold' tumor, with limited lymphocyte infiltration, sequestration within the bone marrow and exhaustion of T lymphocytes (11–13). In parallel, GBM induces a highly immunosuppressive microenvironment and features multidimensional immune escape mechanisms. These include the downregulation of MHC Class I molecules, overexpression of immunosuppressive cytokines, activation and recruitment of immunosuppressive cell types, such as myeloid-derived suppressor cells and regulatory T cells (14–16). Although the exact role of resident microglia and blood-derived monocytes remains elusive, tumor associated microglia/macrophages (TAMs) derived thereof largely present a tumor supportive phenotype, which promotes tumor growth, proliferation, and migration (17). This unique GBM tumor microenvironment (TME) will therefore require tailored immunotherapies targeting the immunosuppressive crosstalk within the brain ecosystem, while at the same time stimulating active immunity (18). Currently, a major limitation for the successful development of immunotherapies in GBM is the lack of appropriate pre-clinical models, which recapitulate an adequate immunocompetent environment, along with the accurate molecular and cellular heterogeneity at the tumor and TME level.

For many years, GBM research relied on conventional *in vitro* cell culture systems based on long-term 2D monolayer cell lines grown in serum-containing medium. However, such cell lines do not reflect the heterogeneity of patient tumors, undergo massive clonal selection and genetic drift, resulting in cells that bear little resemblance with clinical tumors (19–21). Hence, translation of *in vitro* studies into the clinic has been challenging, contributing to the failure of clinical trials (22). The adaptation of patient-derived GBM cultures to 3D spheres grown under serum-free conditions, originally developed for neural stem cells, represented a major step forward. In the literature these cultures are also referred to as GBM neurospheres, brain tumor-initiating cells (BTICs) or glioma stem-like cells (GSCs) (term applied in this review). GSCs were shown to better preserve the genetic background of tumors, to maintain a certain degree of phenotypic heterogeneity and molecular gradients (22–24). When implanted intracranially into immunodeficient rodents, they retain invasive growth patterns *in vivo* (25), a feature lost in conventional cell lines. GSCs do not, however, preserve a complex structural tissue architecture including extracellular matrix (ECM) and TME and can be highly proliferative. Since GSCs are generally maintained as long-term cultures, they also suffer to some extent from clonal selection and genetic drift.

Remodeling of GBM tissue architecture and interactions with TME is possible *in vivo* thanks to patient-derived orthotopic xenografts (PDOXs), where patient tumor cells can grow in the rodent brain (26, 27). These are, however, laborious, time consuming and require the use of immunodeficient strains. Since the TME is of rodent origin, molecular and anatomical inter-species differences need to be taken into account. The recent development of 3D organoid cultures has thus emerged as a promising preclinical tool allowing to model complex tumor architecture *ex vivo* whilst at the same time decreasing the use of animals (28). However preclinical drug testing remains challenging for agents aiming at modulating GBM TME, such as anti-angiogenic compounds or immunotherapeutics. Currently, most immunotherapy approaches against GBM are tested *in vivo* using a single syngeneic immunocompetent mouse model (GL261). This murine model displays a hypermutated genome, develops a 'hot tumor'-like TME and responses to immunotherapies which are of limited clinical value (29–31). In this context tumor organoids integrating immune components along with PDOXs developed in humanized mice emerge as powerful tools for new preclinical studies (32, 33).

In this review we will discuss different protocols for GBM organoid derivation and maintenance, as well as a wide range of organoid-based applications for GBM research and precision oncology. We further review recent attempts in the development of immunocompetent organoids for evaluating immunotherapies and discuss emerging limitations. Finally, we present opportunities and challenges of immunocompetent xenograft models based on orthotopic implantation of GBM organoids in mice with a functional human immune system for studying immunotherapies *in vivo*.

ORGANOID TECHNOLOGY FOR CANCER MODELING

Healthy Tissue Organoids

During the past decade, growing tissue as organoids *in vitro* has been spearheaded in developmental biology and the technology has been further developed to encompass mature organ tissue (34). Organoids are defined as self-organized, three dimensional (3D) organotypic structures, recapitulating the original organ-like composition *in vitro*. Pioneering work by the Clevers lab successfully established intestinal organoids derived from murine Lgr5+ stem cells, which formed 3D crypt villus structures similar to the *in vivo* organ (35). Nowadays, by applying defined developmental signaling programs, organoids of different organs can be developed. Organoids can be initiated from single or multiple organ-restricted adult stem cells but also embryonic stem cells (ESC) and induced pluripotent stem cells (iPSCs). The

denomination of healthy tissue organoids implies several basic features, including the presence of multiple cell types and a morphological organization similar to the parental tissue. They are widely used to model *in vitro* normal organ and disease development, such as infectious, immunological or hereditary disorders (for detailed reviews see (32, 34). Healthy tissue organoids exposed to potential carcinogenic agents, including viral and bacterial infections, are also an excellent model to study early stages of tumorigenesis (36, 37). On the other hand, CRISPR-Cas9 based genetic engineering opened possibilities to assess precise mutational processes at early stages of tumor development (38).

Human cerebral organoids, also called 'mini-brains', were established by Lancaster and Knoblich from pluripotent stem cell-derived embryonic bodies (39). Mini-brains developed in ECM (e.g., matrigel) showed characteristics of human cerebral cortex and recapitulated features of different brain regions. Currently, numerous methods are available for the generation of mini-brains, e.g., from pluripotent stem cells (40), from lineage-restricted neural progenitors (41, 42) or from fetal brain tissue (42). Such organoids can also be established to recapitulate region-specific brain structures such as the midbrain (41, 43). Although the presence of different cell subtypes and the maturation stage of brain organoids are limited, they proved to be instrumental in studies of human development and disease (44). They can also be applied for GBM modeling and GBM co-cultures (reviewed below).

Tumor Organoids

In analogy to healthy tissue organoids, organoid cultures can mimic tumor tissue structure. Several strategies exist to develop tumor organoids: they are generally established directly from resected patient tumors, or can be generated by genetic engineering of stem cells and/or healthy tissue organoids (28). Noteworthy, organoids derived from patient tumor tissue have been used for many years in cancer research and were initially referred to as 'organotypic tumor spheroids' (45). At present, the terminology has been updated and terms such as 'tumor organoids' or 'tumoroids' are in wide use, in analogy to healthy tissue organoids. Instead the term spheroids is now sometimes applied to 3D serum-free sphere cultures, such as GSCs. Protocols and culture conditions for generating patient-derived tumor organoids vary depending on the tumor type. The initial organotypic cultures were derived in serum-containing medium, while more recent protocols apply defined serum-free media similar to healthy organoids. E.g., colon cancer organoids develop in similar conditions as healthy intestinal organoids; however, depletion of Wnt and R-spondins is needed to select for tumor cells (46). Although certain organoids can be developed from single tumor cells after tissue dissociation, the application of intact tumor fragments or multiple cells is recommended to retain genetic and phenotypic heterogeneity. Tumor organoids have been successfully established for many tumor types, including brain (26), breast (47), kidney (48), and liver (49). Interestingly, the success rate of tumor organoid derivation is generally higher than for cell lines and allows to propagate tumors such as prostate cancer (50), less aggressive pancreatic cancer (51) and lower grade gliomas (27), of which cell lines cannot be easily established. This is likely due to minimal clonal selection and a better recapitulation of niche-dependent signals. Compared to previous more simplified *in vitro* models, tumor organoids display a better resemblance with the original patient tumor and retain to a certain extent an *in vivo*-like structural organization (52, 53). If sufficiently proliferative *ex vivo*, organoids can also be successfully expanded into organoid lines with limited clonal evolution, and cryopreserved allowing for efficient and high throughput biobanking (28, 47, 48, 54, 55). This is particularly valuable if combined with corresponding healthy tissue organoids.

GLIOBLASTOMA ORGANOIDS

Generation of GBM organoids can be traced back to the pioneering work of Rolf Bjerkvig and colleagues in the 1980ties, who demonstrated the use of patient-derived GBM tissue obtained from needle biopsies or tumor resections to generate multicellular organoids that could be maintained under specific non-adherent culture conditions (45, 56). Although initially termed 'organotypic tumor spheroids', these cultures fulfill the criteria of self-organizing organoids. In contrast to 2D or 3D cell lines, these organoids have been shown to closely maintain the genomic profile of the parental tumor, conserve the cellular and molecular phenotype of the original tumor and recapitulate inter- and intra-tumoral heterogeneity (19, 45, 56). In recent years, several research groups have directed their efforts in generating GBM organoids and progress has been made in developing different technical approaches. Here we provide an overview of different available methods and discuss relevant advantages and limitations (**Table 1**).

Patient-Based Glioblastoma Organoids

The Bjerkvig method has been optimized and is still used by multiple labs including ours (25, 27, 63–67) (**Figure 1**). Fresh tumor tissue resected during surgery is mechanically cut in small pieces using scalpels to avoid enzymatic digestion. Tumor fragments are cultured in non-adherent conditions in medium supplemented with serum and non-essential amino acids, but without additional growth factors. During the first days of culture, tissue fragments self-organize into 3D organoids while damaged/necrotic cells are dying. This ensures the preservation of healthy tumor cells within a heterogeneous 3D structure including intact cell-cell interactions and ECM components. GBM organoids generally reach a diameter of 300–1000 μm, thereby recapitulating hypoxic gradients and phenotypic heterogeneity. To a certain extent blood vessels and other TME cells are also retained (25, 66). The success rate of GBM organoid derivation is high (approximately 80%), failure is typically due to excessive necrosis or tissue damage during the surgical procedure (27). To avoid selection processes and genetic drift, we avoid long-term expansion and passaging *in vitro*. Instead we use patient-derived organoids for downstream applications within 1–2 weeks of establishment. The same protocol also allows the derivation of organoids from lower grade gliomas (success rate approximately 70%), recurrent gliomas (27), meningiomas (unpublished) and other brain tumors including metastases (68), but not normal adult brain. Over the last decade we have established a living biobank of over 500 successfully generated patient organoids with an effective cryopreservation protocol.

TABLE 1 | Overview and comparison of GBM culture models.

	Culture model	Description	Advantages	Disadvantages	References
Cell lines	2D	Long-term adherent GBM cells cultivated in serum-containing medium	Rapid expansion, low cost, easy maintenance, available for genetic manipulations	Loss of intratumoral heterogeneity, no TME components, clonal selection, genetic drift, *in vivo* phenotype does not reflect human GBM, Low derivation success rate	(20, 21, 24, 57)
	3D	GSC cultures (also termed BTICs), grown as neuropheres in serum-free, growth factor – supplemented conditions	3D growth, moderate expansion, moderate cost, easy maintenance, invasive phenotype *in vivo*, limited recapitulation of molecular gradients, enhanced stem-like features	Clonal selection, some genetic drift, limited intra-tumoral heterogeneity, no TME components, tedious genetic manipulations	(22–24, 58)
Organoids	Patient-derived GBM organoids	Organoids established as primary cultures from resected tumor tissue	High derivation success rate, retention of genetic features and inter- and intra-tumoral heterogeneity, contain some TME components, feasibility of co-culture with autologous immune cells, clinically-relevant drug responses	Costly and labor intensive, lack of vascularization and limited immune component, requires access to fresh patient material and limited by availability of biological material	(25, 27, 59, 60)
	Genetically modified GBM organoids	Gene-edited hESC-derived cerebral organoids initiating tumorigenesis	Recapitulation of early stages of tumorigenesis, defined genetic background, natural development in human brain-like structures, largely recapitulating TME	Time consuming, costly and laborious protocol to generate cerebral organoids, lack of vascularization and immune components	(61, 62)

GSC, glioma stem-like cell; BTIC, brain tumor initiating cell; TME, tumor microenvironment; hESC, human embryonic stem cell.

Our protocol is limited by the availability and the quality of the original patient material, *i.e.*, the resected tumor tissue from surgery or biopsy. Resection of viable tumor tissue followed by fast processing of the sample is essential to maximize viability and to ensure a good organoid quality. GBM organoid growth is limited and variable across patients, where most organoids do not expand beyond the 2-week-culture. They do remain viable for longer time periods and have a tendency to fuse with each other into bigger structures. While for certain patient tumors further expansion and *in vitro* passaging may be possible, we generally do not attempt it in order to limit *in vitro* selection processes. Instead, we apply expansion *in vivo* by implantation of organoids into the brain of immunodeficient rodents. These so called patient-derived orthotopic xenografts (PDOXs, **Figure 1**) enable the propagation of human tumor tissue in a brain microenvironment without relying on *in vitro* expansion. Generally, high quality GBM organoids will efficiently generate tumors in the brain of mice. Serial transplantation, which implies cycles of *in vivo* growth and derivation of organoids from xenotransplanted tumors, allows for extended expansion of patient tumors for large studies, where higher amounts of biological material and/or of xenografted mice are required (27). Similar to patient-derived organoids, organoids derived from PDOXs retain well GBM tissue architecture, ECM and to a certain extent mouse-derived TME (25). We have shown that this procedure preserves genetic and epigenetic profiles of parental tumors, including mutational profiles, copy number aberrations, gene amplifications and DNA ploidy, which are regularly altered in long-term cultures (69). The main challenges to this approach are the costs, the time that is necessary to grow the tumors in the rodent brain and the logistics in planning experiments based on PDOX material. Our model can also be adapted towards growth in serum-free conditions (27, 66) and allows for further derivation of GSC lines. In contrast however to our organoids, we have detected marked changes at different molecular levels during first GSC passages (27).

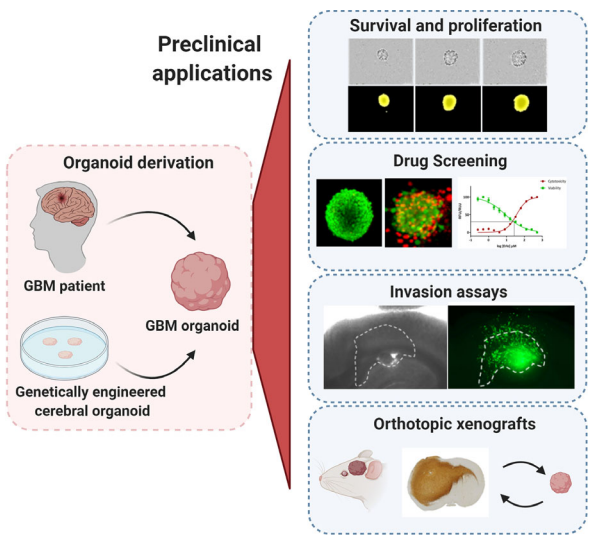

FIGURE 1 | Preclinical applications of GBM organoids. GBM organoids derived from patient tumors or from genetically engineered cerebral organoids can be applied for numerous functional assays such as: tumor cell survival, proliferation and self-renewal, drug screening, *ex vivo* invasion assays, and derivation of orthotopic xenografts. All experimental images were acquired by the authors. Illustration created with Biorender.com.

In recent years, alternative approaches to establish GBM organoids have been published based on serum-free conditions. By combining the protocol of GSC cultures with that used for cerebral organoids, the Jeremy Rich lab successfully established GBM organoids by embedding either dissociated GSCs or intact GSC spheres in ECM (Matrigel) (59). The media composition corresponds to GSC lines and is based on Neurobasal medium supplemented with B27 and the growth factors bFGF and EGF. In contrast to GSC spheres that reach a maximum size of 300 μm after

2 weeks, these organoids can grow up to 3–4 mm in 2 months. Although beyond this point proliferation is limited, organoids remained intact and viable for over one year without passaging. These GBM organoids recapitulated hypoxic gradients, proliferation rates and phenotypic heterogeneity, but do not contain TME components. The organoids give rise to tumors after xenotransplantation, with a longer latency compared to GSCs (59). The protocol can also be applied for fresh mechanically minced tumor tissue or tumors developed in engineered mouse models. No information is available regarding success rate, recapitulation of genetic/epigenetic features of parental tumors and retention of TME when fresh patient material is used.

Another protocol for GBM organoid derivation based on mechanically dissociated GBM tissue was recently reported (60). Small GBM fragments of 0.5–1 mm were cultured in serum-free medium containing mixed Neurobasal/DMEM:F12 supplemented with B27 and N2 and human insulin. Here, growth factors (EGF, bFGF) were not added to the medium. GBM tissue fragments were grown in non-adherent conditions on an orbital shaker without ECM. Under these conditions organoids self-organize within 1–2 weeks and continuously proliferate for over 1 month. To avoid necrosis in the core and to propagate organoids *in vitro*, larger organoids can be regularly cut into small pieces of approximately 0.2–0.5 mm. This allows to preserve cell-cell interactions and natural ECM. These organoids were shown to recapitulate well genetic and molecular traits of original tumors, including inter-patient and intra-tumoral heterogeneity. Phenotypic heterogeneity and a hypoxic gradient were regularly present. Interestingly, despite culture conditions selecting for neural cell lineages, TME components, such as vasculature, TAMs and T cells, were partially preserved within these organoids, at least at early stages. The authors report high success rates of organoid generation from primary GBM (>90%). Recurrent tumors and IDH-mutated astrocytomas also gave rise to organoids, albeit at a slightly lower success rate (75 and 67%, respectively). To create a biobank, primary organoids of approximately 1 month were cut into 100 µm and cryopreserved. Recovered organoids display good viability and continuous growth. These organoids also give rise to tumors upon xenotransplantation with high success rate.

Glioblastoma Organoid Derivation *via* Genetic Engineering of Cerebral Organoids

GBM organoids can also be generated through genetic engineering of healthy tissue stem cells or cerebral organoids to induce tumor formation. Bian et al. developed an efficient system to introduce simultaneously gain and/or loss of function of tumorigenic genes *via* Sleeping Beauty transposon-mediated gene insertion and CRISPR-Cas9–based mutagenesis of tumor suppressor genes respectively (61). The authors modified the protocol of human ESC-based cerebral organoids (39), where a combination of plasmids is introduced *via* electroporation at the neural stem/progenitor cell stage, before full organoid maturation is accomplished in an ECM. By applying combinations of clinically relevant genetic aberrations they identified sets of genetic cooperations leading to the development of tumor organoids, termed neoplastic cerebral organoids or neoCORs, resembling GBMs and pediatric CNS-PNET. CNS-PNET-like tumors were linked to the overexpression of the oncogene *MYC*, whereas GBM-like cells developed from 3 different sets of genotypes: $CDKN2A^{-/-}/CDKN2B^{-/-}/EGFR^{OE}/EGFRvIII^{OE}$, $NF1^{-/-}/PTEN^{-/-}/TP53^{-/-}$, and $EGFRvIII^{OE}/CDKN2A^{-/-}/PTEN^{-/-}$. Emerging GBM-like cells, traced by GFP expression, are proliferative and display classical astrocytic markers. Tumor regions within organoids are visible within one month and show a disorganized structure with marked invasion of GBM-like cells into adjacent normal organoid structures. On the other hand, perivascular palisading necrosis is not present, probably due to the small size and/or the overall lack of vasculature in brain organoids.

Human ESC-derived cerebral organoids were also applied by Ogawa et al. to induce GBM tumors by CRISPR-Cas9–based expression of oncogenic *HRAS* ($HRAS^{G12V}$) with simultaneous disruption of the tumor suppressor *TP53* (62). The authors used mature 4-months-old brain organoids and introduced plasmids *via* electroporation to the cortical structures, close to the surface. At 2 weeks after electroporation, first tdTomato-positive transformed cells were visible. At 8 weeks, GBM-like cells encompassed <5% of the organoid; however, onset of fast proliferation leads to complete take over by GBM-like cells by 16 weeks, with the tumor mass growing beyond the boundaries of the organoids. The developed GBM-like cells can be further cultured as adherent GBM cell lines, GSCs, and also form tumors upon xenotransplantation.

Challenges and Opportunities

Although organoids have gained significant attention in recent years, the technology is still immature. The term 'organoid' is broad and encompasses different biological entities based on different underlying procedures. While patient-derived GBM organoid protocols largely converge, they exhibit significant differences, which carry their own advantages and pitfalls. Organoids derived from mechanically minced tissues preserve best cell-to-cell interactions and TME components, whereas organoids derived from dissociated GBM cells may give higher flexibility and reproducibility. Although serum-containing medium is often criticized for inducing differentiation processes, we have not observed this in our short term organoid cultures. Moreover, while serum is known to cause differentiation in normal stem cells, this differentiation process is incomplete and fully reversible in cancer stem cells (5). GBM organoids exposed to serum retain *in vivo* tumorigenicity and heterogeneous expression of stem cell markers similar to patient tumors (5, 27, 66). Moreover limited *in vitro* expansion reduces clonal selection processes and maintains increased tumor heterogeneity. Serum-containing medium however limits proliferation *in vitro* and requires amplification of the tumor material *in vivo*. On the other hand serum-free conditions supplemented with growth factors allow for faster *in vitro* growth, enabling biobanking without the use of animal components, but risk increased tumor cell selection and adaptation of cultures. In general, serum-containing medium better maintains TME components, including glial and immune cells. However such cells were also detected in organoids grown in serum-free medium adjusted for neural cell cultures. More data is needed to fully comprehend the influence of medium components and passaging on the maintenance of tumor and TME populations in organoid cultures. Importantly, both serum-grown and serum-

free patient-derived GBM organoids were reported to recapitulate well molecular gradients and phenotypic heterogeneity, which represents a major drawback of GBM cell lines (**Table 1**). In addition, patient-derived GBM organoids largely maintain genetic signatures of their parental tumors, including gene amplifications often lost in GBM cell lines. Still, it remains to be seen to what extent long-term culture of organoid lines may lead to adaptation of tumor cells including clonal selection and further genetic drift, as well as loss of patient-specific genetic and phenotypic heterogeneity. To ensure the accuracy and genetic stability of organoids, the genetic status of organoid lines should be regularly verified after a defined number of passages.

Genetically engineered organoids provide excellent and flexible *in vitro* models for the study of early stages of GBM: they allow for the identification of driver mutations and downstream pathways during the onset of GBM. At present however, it remains unclear to what extent the introduced driver mutations recapitulate the complex genetic heterogeneity of human GBM within the organoid. This has limitations in particular for personalized treatment approaches. Cerebral organoids, particularly those derived from pluripotent stem cells, do not reach complete post-mitotic maturity, and thus represent rather a developing fetal structure than an adult brain. Therefore, they may be more valuable to interrogate tumorigenic potential of pediatric tumors, rather than GBM in adults. Another drawback of this approach is the long process for the establishment of cerebral organoids, which takes months and needs a certain expertise along with a high costs.

APPLICATIONS OF GBM ORGANOIDS

The major asset of organoids is the close recapitulation of genetic and phenotypic heterogeneity of the parental tumor. Hence they hold a great potential for a wide range of pre-clinical applications. In comparison to GBM cell lines, the common drawback of organoids is the increased technical effort needed to perform functional assays and drug testing, particularly in a high-throughput manner. In this chapter, we describe fundamental applications established in the field (**Figure 1**) and review the technical requirements that need adaptation for successful application of organoids to preclinical assays.

GBM Survival, Proliferation, and Self-Renewal

Assessing GBM proliferation and survival in organoids is more challenging than with conventional GBM cell lines and GSCs due to a compact growth of GBM cells within complex 3D structures. Direct counting of single GBM cells present within patient-derived GBM organoids or after enzymatic dissociation is usually not precise, thus measurement of growth is more often followed by changes in the diameter of the organoids themselves over time (**Figure 1**). To obtain reproducible results, this growth (proliferation) assay should ideally be performed on smaller organoids of similar size at the early development stage to avoid halted proliferation in organoids at later stages. Two options are possible (i): mechanical cutting followed by manual collection of smaller organoids of similar size (60), or (ii) reformation of organoids from dissociated single cells (59). Although our organoid protocol relies on mechanical dissociation of tumor tissue, we showed that the organoid preparation can be adapted for one-off experiments if size standardization is required (25, 27): Organoids can be recreated from enzymatically dissociated patient or PDOX-derived tumor tissue, where single cells self-assemble back into organoid structures. This protocol allows for purification of subpopulations and/or standardization of organoid size and shape for specific functional studies (25, 27, 69–72). This dissociation step should be avoided for serial transplantations and long-term maintenance and propagation of the patient derived tumor material. Self-renewal can be followed by growth of organoids from single cells or *via* serial dilution assay, but these protocols are applicable mostly to the proliferative organoid models based on GSCs (59). Organoid formation and growth can be monitored during a limited period of time in a live cell analysis system or simply by microscopy. Immunohistochemistry-based antibody stainings, classically applied to tumor tissue sections, are a valuable source of information with regard to organoid structure and phenotypic organization. E.g., Ki67 staining can be used to identify proliferating tumor cells. EdU (5-ethynyl-2-deoxyuridine) or BrdU (bromo-deoxyuridine) based DNA labeling assays can be used for the qualitative and quantitative evaluation of proliferation inside organoids (73, 74). Additionally, the estimation of cell death within the organoid can be performed by fluorescent labeling of the cells with viability and cytotoxicity markers allowing for calculation of the ratio between viable and dead cells (70, 72). Proliferation of tumor cells within genetically engineered organoids is possible by detection and quantification of the fluorescence/bioluminescence signal of the genetically modified GBM-like cells (61, 62). Viral barcoding labeling can further enable tracing of clonal lineages and proliferation capacities (75).

Drug Screening

2D monolayer cell cultures have been widely used for drug screening purposes, mostly because of easy availability and low maintenance costs (76), but unfortunately at the expense of minimal success rates in clinical trials due to lack of efficacy or toxicity. They have been reported to show a disproportionate cellular response to anticancer drugs, partially due to very high proliferation rates and profound phenotypical changes. GSC cultures in combination with novel biological and synthetic scaffolding techniques have shown a better reflection of the patient tumors along with improved drug response when compared to 2D models (22, 77). As these cultures select for proliferative stem-like GBM cells, the drug responses may still be restricted towards these specific phenotypic states. Thus drug responses in heterogeneous organoids may better reflect clinical reality. As all patient-derived GBM organoid models better recapitulate oxygen and nutrient-based heterogeneity, the response to heterogeneous states may be measured simultaneously (27, 59, 60).

Drug responses in GBM organoids can be followed by applying similar technical adaptations as described for proliferation assays, where organoid size and phenotypic/histological changes are measured to determine drug responses. Accurate drug testing requires standardization in terms of size and shape as well as proliferation status. In theory, varying expansion capacities during different stages of organoid development could be exploited to probe drug responses at different proliferation stages of the tumor.

Additional challenges need to be taken into account, while adapting drug testing towards high-throughput screens. Classical microscopy-based evaluation is laborious and time-consuming and measurement of organoid size can be limited due to cellular debris surrounding the organoid. Immunohistochemistry for viability, proliferation (Ki67) and apoptotic markers can give a detailed readout on heterogeneous responses to chemo- and radiotherapy within organoid structures (59, 60), but again is low-throughput. The old-fashioned cell viability tests, such as MTT or WST, are not adapted towards non-adherent organoids because of low cell number. Development of more sensitive assays, such as CellTiter-Glo, combined with growth or organoids in 384-well plate format allows to scale up organoid-based drug screen protocols (78) (**Figure 1**). Using GBM PDOX-derived organoids of standardized size derived from 1000 tumor cells, we have applied a similar medium-throughput protocol and showed patient-specific and clinically relevant responses to TMZ and EGFR inhibitors (27). In accordance with clinical outcome, *MGMT* promoter-methylated GBM organoids showed higher sensitivity to TMZ in comparison to *MGMT* promoter-unmethylated organoids, an effect that is not always recapitulated in GBM cell lines (79). Similarly to short term GBM cultures (80), patient-derived GBM organoids' responses to EGFR inhibitors were linked to EGFR expression and mutations present in individual tumors. These associations cannot be easily assessed in long-term adherent cell lines and GSCs due to the general loss of *EGFR* amplification in these cultures (81). Clinically-relevant heterogeneous responses were also observed in patient-derived organoids cultured in serum-free medium (60), although more models in (epi)genetically-defined groups will be needed for a comprehensive evaluation. We were also able to reconstruct GBM organoids in alginate using cell printing technology. Cell printing combined with automated high content imaging of viable cells allows for a higher throughput automated drug library screening (77, 82). Other detection techniques, such as optical metabolic imaging, not requiring specific dyes for detection also arise as an interesting option (83).

Although the organoid technology is very promising and enables relatively fast drug testing in clinically relevant timing, several challenges should be considered. Similarly to nutrients and growth factors, drugs may not be able to fully penetrate bigger 3D structures, thus organoids of smaller sizes should be applied for drug testing. Both patient-derived organoids and genetically-engineered organoids contain also normal non-malignant cells to various degrees, thus more adequate read-out techniques may be needed to distinguish effects on different cell types. *E.g.*, Brian et al. quantified the ratio between tumor and normal cells *via* flow cytometry (61). Although fluorescence/bioluminescence allows to distinguish GBM-like cells within genetically-modified organoids, high throughput application may require faster detection and precise calculation algorithms. An additional drawback in GBM is the lack of equivalent patient-derived normal brain organoids. This would allow to screen for drugs that selectively kill tumor cells while leaving healthy cells untouched. Although iPSCs could be derived from each GBM patient and used for cerebral organoid development, the technology is still immature and inefficient to be applied for routine testing. This could be partially resolved by applying GBM organoids in co-cultures with cerebral organoids or organotypic brain slices, as described for the invasion assays below (74).

GBM Invasion

Tumor cell invasion is a hallmark of GBM strongly contributing to inevitable regrowth of tumors after surgery (84). Invasion capacities of tumor cells are classically tested *in vitro* with Boyden chambers, where single cells can invade membrane pores covered with different combinations of ECM. Subjecting intact organoids to Boyden chamber assays is not optimal as invasion from a 3D structure through a membrane is irregular and difficult to measure. Although single cells obtained from enzymatically dissociated organoids can be applied (25), this may lead to an additional stress of GBM cells not adjusted to survive as single cells. The sprouting assay represents a more adapted approach as it simply involves embedding organoids directly in the ECM and quantifying cells invading out of the organoid into the matrix (65, 67). A more advanced technique for measuring invasion could take advantage of adult organotypic brain slice cultures of rodent or human origin (**Figure 1**), where organoids encounter the natural brain microenvironment (85, 86). So far this technique was applied to GBM cell lines and GSCs, injection of organoids into the brain slice may be more challenging. Organoids may remain non-attached or only adhere to the surface of the brain slice. Importantly, this technique requires fluorescent labelling of tumor cells for detection and quantification of invasion and single cell velocity by microscopy.

Organotypic brain slice cultures can also be replaced by healthy cerebral organoids. In this case, direct co-culture is possible, where GBM cells can spontaneously fuse with brain organoids to form hybrid organoids. Linkous et al. showed successful interactions between GSCs with human ESC and iPSC-derived brain organoids, creating a so called GLICO (cerebral organoid glioma) model (74). The authors showed that GSCs were able to invade and proliferate within the healthy brain organoid and to form interconnecting microtubes. Another study confirmed that GSCs transcriptionally adapted to mini-brain microenvironment in line with their *in vivo* behavior (87). Although Linkous et al. showed similar invasion of GSCs in cerebral organoids of different age, others reported GBM cell invasion only in early stage cerebral organoids, whereas invasion into fully mature organoids was halted (88). Similar co-cultures of human cerebral organoids could be applied to patient-derived GBM organoids in the future. Of note, the protocol is tedious, as efficient GBM invasion inside the cerebral organoid often requires removal of the ECM embedding (87, 88). If ECM is preserved, GBM cells primarily adhere to the matrix and grow on top of the surface. Injection of GBM organoids inside the cerebral organoids could also be envisaged, although this may destroy the fragile mini-brain structure, particularly if still embedded in the ECM. A similar co-culture approach is also feasible with mini-brains derived from neural progenitors isolated from rat fetal brain (42, 65). Patient-derived GBM organoids and GSCs spontaneously fuse with rat brain organoids and progressively invade the healthy brain tissue. The process is faster and more efficient in comparison to human cerebral organoids, as rat brain organoids are not embedded in ECM. Also other brain tumors were shown to

interact with healthy rat brain organoids, but GBM cells showed most prominent invasion, up to complete destruction of the healthy tissue (89). Although species differences should be considered, rat brain organoids derived from fetal tissue are faster to generate, more reproducible and appear to reach better maturation status compared to human cerebral organoids derived from iPSCs or ESCs. Again, fluorescent or bioluminescent labelling is needed to efficiently measure GBM invasion into brain organoid structures. Similarly, invasion can also be followed directly in genetically-engineered organoids as GBM-like cells develop naturally within the intact cerebral organoids (61, 62). Although cerebral organoids allow for easier access to human brain structures, they miss critical structures required for invasion. In particular, it is well known that GBM cells preferentially infiltrate along vascular structures (90), which are not present in cerebral organoids. The inclusion of vascular elements into cerebral organoids (91, 92) in co-cultures with GBM organoids, as well as directly into genetically engineered GBM organoids, could therefore be a valuable tool for future studies on the dynamics of GBM invasion along blood vessels and developing invasion inhibiting treatment strategies.

Patient-Derived Orthotropic Xenografts

Patient-derived xenografts (PDXs) represent a well-established preclinical cancer model allowing for propagation and investigation of human tumors in immunodeficient rodents. Classically PDXs are derived by subcutaneous implantation of patient tumor tissue fragments, with a take rate of around 50% for GBM tumors (93). In case of specific organs, such as brain, patient-derived orthotopic xenografts (PDOXs) better recapitulate tumor histopathological features and TME. Implantation of tissue fragments directly into the brain is technically challenging and may lead to unreproducible tumor growth. Thus application of patient-derived GBM organoids for implantation ensures technical feasibility and standardization, while avoiding GBM selection and adaptation. In general, the majority of GBM organoids of different culture models give rise to tumors upon xenotransplantation in the brain and recapitulate well histopathological features of patient GBMs such as invasion and angiogenesis. To obtain consistent tumor take and growth rates, we implant six to ten intact GBM patient-derived organoids into the brain of immunodeficient mice or rats respectively (25, 27, 94, 95). We have shown that organoids derived from high grade gliomas, including IDH mutant astrocytomas and GBM, are able to grow in the brain with very high rate of tumor take (27).. Successful engraftment and PDOX propagation for > 3 *in vivo* passages was obtained for 86% of GBMs (35/41) and 25% grade III gliomas (2/8). Failure of GBM organoid engraftment was attributed to initial poor organoid quality, whereas no association between organoid quality and tumor take was seen for grade III gliomas. The *in vivo* tumor latency strongly depends on the parental tumor and can vary from several weeks to several months. Organoids from treatment naïve and treated GBMs can develop and give rise to tumors *in vivo*. We have been also able to generate paired longitudinal models from tumor samples collected at different timepoints from the same patient, thus recapitulating disease progression over time (27). Such models are invaluable tools to study tumor evolution and treatment resistance in a personalized *in vivo* setting. In case of more proliferative GBM organoids cultured in serum-free conditions, implantation of a lower number of intact organoids (down to 1 organoid/implantation) was sufficient to develop tumors *in vivo* (60). The authors reported successful engraftment of 8 organoid cultures derived from 7 patients and tumors were visible 1–3 months after implantation. Hubert et al., applied enzymatic dissociation of organoids prior to implantation (59). Although no exact tumor take rates were reported, implantation of GSC-derived organoids should be highly efficient. Interestingly, despite containing a similar number of self-renewing cells GBM organoids showed longer latency than implanted GSCs of the same patient (59). Genetically-engineered GBM organoids were also shown to give rise to intra-cranial tumors *in vivo* (no tumor take reported, mean survival 90–100 days after implantation of $3*10^5$ cells) (62) or expand in renal capsules (17/20 neoCORs, 85%) (61).

PDOXs allow for the propagation of tumor material *in vivo* (live biobanking) within an adequate brain microenvironment including structural (vasculature, blood brain barrier), cellular (neurons, glia, microglia/macrophages) and metabolic components (cerebrospinal fluid, brain interstitial fluid). This procedure allows also to avoid long-term culture and expansion of organoids *in vitro*. GBM organoids can be further obtained from established PDOXs and serially transplanted to maintain the patient tumors over multiple generations (27). We showed that organoid-derived PDOXs remain stable across generations in mice, recapitulate histopathological features of human GBM, with various level of angiogenesis, necrosis and invasiveness (25). Such PDOXs represent invaluable patient 'avatars' for downstream experimental needs and applications (**Figure 1**). Applications range from *in vivo* drug validation studies, protocol optimization for magnetic resonance imaging (MRI), the use of isotopic tracers for dynamic profiling of tumor metabolism *in vivo*, genetic and phenotypic analysis, to identification of novel biomarkers and therapeutic targets (5, 95–100). We showed that anti-angiogenic treatment in organoid-derived GBM PDOXs leads to clinically relevant responses with no survival benefit (70, 95). This is in contrast to observed GBM cell line-derived xenografts, which show strong dependence on angiogenesis to survive *in vivo* (101). Monitoring of PDOX by MRI allows to follow 'patient avatars' in a similar fashion as in the clinical setting and to complement drug testing on organoids (27, 70). This includes the visualization of an intact or disrupted blood brain barrier (BBB) in the various tumor compartments, an essential component of the GBM TME. Because of the selective permeability of the BBB regarding blood derived molecules (102), PDOXs are essential to validate the therapeutic effect of novel treatment strategies in a meaningful preclinical *in vivo* setting to avoid failure in the clinical phases.

Because human tumors need to be engrafted in immunodeficient rodents, limitations of PDOXs include the lack of a complete immune system and potential interspecies incompatibilities at the molecular level. Importantly, our previous studies showed that human tumor cells can functionally interact with cells from the TME in PDOX despite interspecies differences, e.g., rodent endothelial cells form aberrant blood vessels (25) and are affected by anti-human VEGF treatment (70, 95). Similarly, myeloid cells are present in PDOXs and

are modulated by the tumor graft (27). Since they represent the major immune cell type of the brain TME, targeting the immunosuppressive nature of myeloid cells can be tested in PDOX (17, 103). Nevertheless, while the innate immune system is largely intact in nude mice, the lack of lymphocytes prevents certain applications for modern immunotherapy. This can be overcome on the one hand by the generation of immunocompetent GBM organoids for *ex vivo* studies and on the other hand, by the establishment of PDOX models in humanized mice for *in vivo* studies.

IMMUNOCOMPETENT ORGANOID CULTURE—WHICH IMMUNE CELLS TO USE?

The interactions between immune and tumor cells critically influence the onset, progression and treatment of human malignancies. Although the brain has been for long considered as an immune privileged organ, it is clear that the immune system plays a key role in development and surveillance of brain homeostasis (104). Nevertheless, the brain remains an immunologically distinct site, which is also reflected in the TME of brain tumors (105). TME includes brain resident and infiltrating myeloid cells, natural killer cells, dendritic cells and regulatory T cells, classifying GBM as strongly lymphocyte depleted tumors (13). A major challenge of all current GBM organoid models remains the establishment of an intact TME including the immune cell compartment.

The establishment of immunocompetent cancer organoids is an active field of research and an urgent need. Such novel models fill a gap in pre-clinical research, allowing for functional and translational studies for immunotherapies and promoting the investigation of tumor-immune cell interactions (106). Considering the high demand for personalized immunotherapy, immunocompetent *ex vivo* models present a promising platform for individual patients, by advancing the development of new immunotherapeutic strategies. Here we provide an overview of protocols employing various immune cell populations for the setup of immunocompetent tumor organoids that could be applied to GBM modelling. Tumor organoids can be co-cultured with different immune cell populations depending on the origin of the immune compartment. Immune cells can be isolated from the periphery or directly from the tumor site (**Figure 2**). Opportunities and limitations of both are discussed below.

Peripheral Mononuclear Cells

To mimic the immune microenvironment, immunocompetent organoids can incorporate autologous or allogeneic immune components in the culture. In the case of autologous immune components, cells are isolated from the same patient who provided the tumor tissue to generate tumor organoids. Allogeneic immune cells imply a non-self-source, such as healthy blood donors. The main source of relevant immune cells are peripheral mononuclear cells (PBMCs), which comprise lymphocytes (T cells, B cells, and NK cells) and monocytes. Isolated PBMCs should not contain neither granulocytes (neutrophils, basophils, and eosinophils) with multi-lobulated nuclei, nor nuclei-free erythrocytes and platelets. PBMCs can be cultured as a bulk population or individual immune cell populations can be further isolated through magnetic separation or FACS, cultivated and expanded as monocultures.

Autologous Peripheral Mononuclear Cells

Patient blood presents a valuable source to obtain patient's own immune cells in the form of autologous PBMCs. PBMCs are easily accessible and can be obtained through a simple blood withdrawal prior to surgery when the tumor tissue is removed. This allows to establish matched immunocompetent organoids for individual patients. Promising results with *ex vivo* co-cultures of organoids with autologous PBMCs have been reported for non-small cell lung cancer and colorectal cancer (107, 108). A proportion of co-cultures with organoids positive for MHC class I led to the activation of T cells, which were able to eliminate tumor organoids, but left non-neoplastic organoids from the same patient unaffected. No responses were observed for MHC class I deficient tumors. In this protocol organoids were dissociated into single cells and adapted to lymphocyte medium prior to the co-culture (107, 108). This proof of concept study suggests that tumor reactive T cells can be expanded from peripheral blood and activated by matched tumor organoids. Activated T cell populations can thus be used subsequently to test cytotoxic properties *ex vivo* and/or to analyze the T cell receptor repertoire. Ultimately, effector T cells displaying immune reactivity after co-culture with tumor organoids could also be applied for adoptive cell transfer, if a sufficient number of T cells is generated.

Such systems have not yet been reported for GBM and it remains to be seen whether GBM cells will trigger an immune response and immunogenic properties in autologous PBMC-based organoids, particularly in case of MHC I deficiency. Multiple studies have shown that GBM patients' blood presents peripheral T cell lymphopenia (low T cell counts) and a high number of myeloid-derived suppressor cells (12, 15, 109). This is further exacerbated by corticosteroids (dexamethasone), a treatment often provided upfront to reduce tumor-associated edema and improve clinical symptoms. Therefore the timing of blood withdrawal is crucial and should ideally be conducted before surgery and before any other treatment is given. Additional technical issues need to be taken into account (i): pre-stimulation of tumor organoids with interferon γ (IFNγ) may be needed to enhance antigen presentation (ii), pre-stimulation of T cells with anti-CD28 and interleukin-2 (IL-2) may be required to support proliferation and expression of anti-Programmed cell death 1 (anti-PD1) thereby counteracting Programmed cell death ligand 1 (PDL1) inhibitory effects on tumor cells (107).

Allogeneic Peripheral Mononuclear Cells

Allogeneic PBMCs are isolated from the blood of healthy donors. In contrast to autologous PBMCs, they represent normal blood with appropriate cell counts and were never exposed to tumor-associated stimuli released into the peripheral system. Allogenic PBMCs have been extensively used to obtain purified immune cell populations (T cells, NK cells, monocytes), which were applied to co-cultures with conventional tumor cell lines. Although activation of immune cells in 2D cultures appears rather straightforward, patient-derived 3D systems add additional challenges linked to immunosuppressive factors such as hypoxia and high lactate levels (110) as well as

potential HLA incompatibilities. Co-cultures of allogenic blood components have not yet been reported for GBM organoids. Tang et al., developed sophisticated co-cultures of macrophages with GSCs using a bioprinting method (111). Macrophage cultures were obtained from a monocytic cell line (THP-1), human iPSCs or PBMCs from healthy donors. Co-cultures were embedded in hyaluronic acid rich hydrogels, representing a main component of GBM ECM. Additional cellular components such as astrocytes and neural stem cells, could be incorporated to the embedded co-cultures. Of note, unpolarized M0 macrophages successfully interacted with GSCs and polarized towards a protumoral M2-like macrophage phenotype.

Tumor Derived Immune Cell Populations

Tumor Infiltrating Lymphocytes

Tumor infiltrating lymphocytes (TILs) present within resected tumor fragments represent another source of lymphocytes. Isolation of TILs can be performed simultaneously during tumor tissue processing, which facilitates biobanking regulations and protocols, e.g., no additional blood withdrawal from the patient is necessary. In contrast to systems using peripheral immune cells, TILs allow for the *ex vivo* modeling of the TME-intrinsic immune responses. Cells present within the TME are enriched for populations already instructed by the tumor, hence they may not need further activation to produce the desired tumor-intrinsic phenotype. Co-cultures with TILs are particularly important for interrogating immune checkpoint expression on tumor cells and TILs and determining tumor-specific efficacy of checkpoint inhibitors. The main disadvantage lies in low number of TILs obtained from most tumors. Compared to metastatic melanoma where TILs are frequently isolated in high numbers and applied in adoptive T cell transfer, enrichment of tumor-reactive T cells in gastrointestinal cancers was more challenging (112). These limitations can be partially overcome by using organoids derived from mechanically processed tumor tissue, where TILs are naturally preserved. E.g., Neal et al. showed that patient-derived tumor organoids from different type of cancers, including melanoma, renal and non-small cell lung cancer preserve endogenous TILs and other TME components (113). Here tumor organoids were embedded in a collagen matrix and subjected to an air-liquid interface set-up. TILs and other TME components were present for up to 2 months within tumor organoids. TILs remained functional and triggered a cytotoxic response upon PD1/PDL1 checkpoint blockades. Although TIL survival was prolonged by IL-2 or anti-CD3/anti-CD28, further optimization will be needed for long-term preservation. Another study reported the maintenance of CD45+ immune cells for up to 8 days within epithelial tumor organoids (114). A protocol applying co-cultures of tumor organoids and separately isolated TILs was reported for rectal cancer, where TILs were able to interact with tumor organoids embedded in the ECM and to partially restore cytotoxic activity upon (anti-PD1) treatment (115).

Establishing a co-culture system for GBM organoids and TILs will be technically challenging due to the low number of infiltrating lymphocytes in GBM. TME components were reported to be present within patient-derived GBM organoids derived from tissue fragments including a small fraction of T cells and TAMs (60, 66). However, similar to epithelial cancer organoids, the TME compartment is progressively lost over time and separate TILs may be needed for long-term experiments. The situation in GBM is further complicated by the fact that a large fraction of infiltrative T lymphocytes represent regulatory T cells rather than tumor-directed cytotoxic T lymphocytes, promoting an immunosuppressive TME (116). Thus co-cultures and manipulation of TILs towards a different phenotype will be of particular importance for GBM-specific immunotherapies. Finally, since isolation of TILs from tumor tissue requires enzymatic

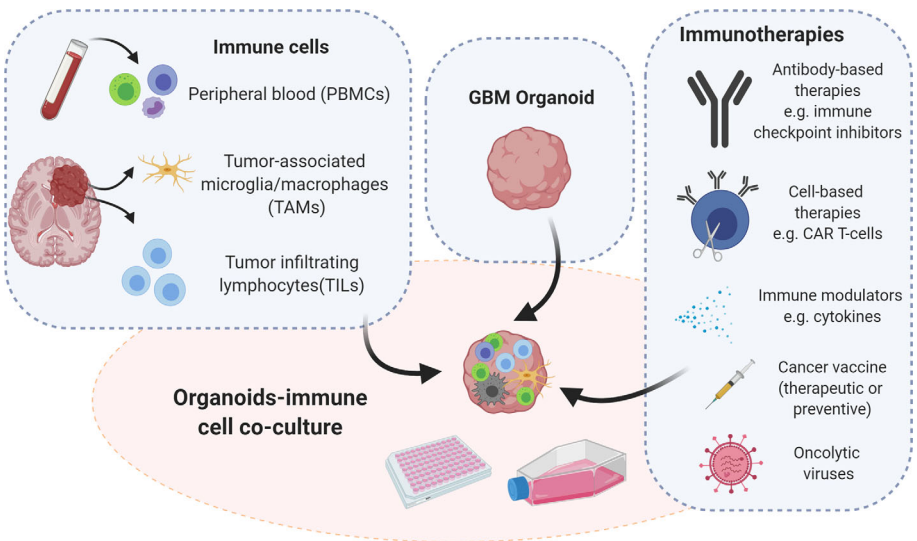

FIGURE 2 | Strategies for immunocompetent GBM organoid development. Immunocompetent organoids can be set up as co-cultures of tumor organoids with immune cells derived either from the tumor itself or from peripheral blood of patients or healthy donors. Immunocompetent organoids are applicable to functional assays and therapeutic intervention studies, which implicate assessment of tumor-immune cell interactions. Illustration created with Biorender.com.

dissociation, it interferes with the derivation of GBM organoids from mechanically cut tissue fragments. In this case GBM tissue will have to be sub-divided for TIL isolation and GMB organoid derivation, compromising the number of T cells and organoids obtained per patient.

Tumor-Associated Microglia/Macrophages

TAMs play an important role in GBM biology and are known to facilitate tumor growth and invasion. TAMs originate from both microglia and blood-derived monocytes, and acquire a strong immunosuppressive phenotype in GBM (17, 117). GBM display a prominent infiltration of TAMs which represent the majority population of non-neoplastic cells (40–50% of the non-tumor cell mass), thus they can be isolated from tumor tissue resected during surgery. This is generally based on selection of CD11b positive cells with FACS or MACS followed by subsequent cultivation. This is a laborious method which generally results in low yields, which is complicated by the fact that TAMs do not generally proliferate in culture. Culture and freezing conditions should be optimized in order to keep the viability at a high level. Similar to TILs, TAMs are also partially preserved in GBM organoids, allowing for direct investigation of tumor-TME crosstalk during early stages of organoid culture.

Modified Immune Cells (CAR-T Cells, CAR-NK Cells)

CAR-T cells are genetically modified T cells expressing a chimeric antigen receptor (CAR) on their surface, which results in the binding to specific antigens on tumor cells leading to tumor cell killing. As patient-derived tumor organoids retain well specific antigens and heterogeneity, they appear as an advantageous model for *ex vivo* testing of CAR-T cell therapies. Jacob et al. demonstrated the utility of patient-derived GBM organoids to test adoptive T cell therapy *ex vivo* (60). EGFRvIII is a constitutively activated EGF receptor mutant that is overexpressed in a large number of GBM. CAR-T cells engineered to react with EGFRvIII expressing cells were co-cultured with GBM organoids with differential EGFRvIII expression levels. CAR-T cells were able to invade GBM organoids and expansion of EGFRvIII-specific T cells was observed within organoids with high EGFRvIII levels. Specific CAR-T cell mediated toxicity was further observed towards EGFRvIII positive cells, as evidenced by an increased cleaved-caspase 3 signal and increased presence of granulated T cells in close proximity of EGFRvIII positive apoptotic cells. This proof-of-concept study demonstrated the capacity of patient-derived organoids as an *ex vivo* test bed for immunotherapy. Unfortunately the clinical situation remains more complex and a recent pilot trial with EGFR-targeting CAR-T cells did not achieve a meaningful clinical effect (118).

In addition to T cells, NK cells can also be engineered to express CARs. In a study with patient-derived colorectal cancer organoids, CAR-mediated cytotoxicity was investigated using a CAR-NK cell line (CAR-NK-92 cells), which represents a less laborious source for CAR-engineered immune cells. CAR-NK-92 mediated cytotoxicity against tumor organoids was observed at low levels of tumor associated antigen expression, whereas it was absent against healthy colon organoids (119).

Important Considerations and Optimization Steps

An increasing number of reports present protocols for derivation and maintenance of immunocompetent tumor organoids, demonstrating their utility to model the immune microenvironment and study the effects of immunotherapies (32). Although initial promising studies of immunocompetent GBM organoids were reported, further development and optimization of protocols is needed. The experimental settings for the establishment of immunocompetent GBM organoids may depend on several factors, including the research question at hand, the availability of autologous blood and the amount of available tumor tissue. Limited or unviable tumor tissue obtained from surgery is a common problem, which limits the amount of tumor organoids and TME cells that can be isolated. This is particularly challenging if tumor organoid and TIL isolation requires dedicated tissue pieces and preparation protocols. Another challenge is the timing of the co-culture set up with cells from the same patient. While establishing GBM organoids takes 1–2 weeks, blood or tumor derived immune cells are ready on the day of collection. Since the expansion of these cells is either limited (TAMs) or should be avoided (lymphocytes) and/or the cells cannot be easily maintained in culture, a proper cryopreservation and thawing process is critical for the use of viable immune cells at later time points. Furthermore, as indicated above, the recovery of T cells from GBM patients either from the tumor tissue or from PBMCs is expected to be low because of limited T cell infiltration and peripheral T cell lymphopenia, respectively, characteristic of GBM patients (12, 109).

Another challenge is to establish optimal culture conditions for all co-cultured cell types. This includes medium composition, duration of the co-culture, the immune-tumor cell ratio, and the read-out for cytotoxic responses. Co-cultures are generally performed in the immune cell-specific medium which may compromise GBM organoid viability and may not reflect brain physiology. Culture conditions need to be adapted to different GBM organoids and immune cells under investigation. The ratio between tumor and immune cells depends on the effector cells applied in the study. Generally, a target to effector ratio of 1:10 to 1:20 is reported for PBMCs (108). With specific subset of immune cells, such as CAR cells, less effector cells are required (60, 119). Whether or not the organoid is dissociated prior to co-culture also impacts tumor-immune cell interactions. Spontaneous infiltration of immune cells into intact tumor organoids may be particularly challenging if ECM is applied for organoid derivation (107). In addition, the use of a rodent-derived matrix may lead to unspecific activation of immune cells against foreign antigens. Finally, it remains to be seen whether GBM cells display sufficient immunogenicity, which requires large numbers of neo-antigens and appropriate antigen presentation capacity to induce an active immune responses. Antigen presenting cells, such as dendritic cells or TAMs are potentially needed to enhance the tumor-T cell interactions in the culture.

IMMUNOCOMPETENT *IN VIVO* TUMOR MODELS IN HUMANIZED MICE

PDOXs derived in immunodeficient rodents are gold standard preclinical models for drug efficacy *in vivo* studies in oncology (120). Yet, the lack of a fully functional immune system limits their use for testing immunotherapies. Hence, the generation of PDOXs in humanized mice appears as a promising immunocompetent *in vivo* system recapitulating patient-derived tumors and immune compartment (33). Since the first description of humanized mice in 1988, a plethora of protocols has been developed (121, 122). Generation of humanized mice requires a highly immunodeficient mouse background to obtain efficient engraftment of a hematopoietic human system. Thus, the NOD.Cg-Prkdc^{scid} Il2^{rgtm1Wjl}/SzJ (NSG) strain is frequently applied. NSG mice lack mature T, B cells and hemolytic complement, the Il2^{rgtm1Wjl} mutation prevents cell signaling through multiple cytokines leading to a lack of NK cell activity. Moreover, the polymorphism of the *signal regulatory protein* α (*sirp*α) allele in the NOD background allows a functional 'do-not-eat-me-signal' between mouse myeloid cells and human CD47, while the deficiency in Prkdc^{scid} confers sensitivity to radiation (123, 124). Currently two main approaches are in use to reconstitute the human immune system (i): HU-PBMC model applying PBMCs isolated from human adult blood or (ii) HU-CD34 model based on human CD34+ hematopoietic stem cells (HSCs).

HU-PBMC Model

The HU-PBMC model can be derived by intravenous, intraperitoneal or intrasplenic injection of human PBMCs from adult donors into adult NSG mice (>8 weeks old). This model allows a fast and efficient engraftment rate with approximately 15% of human CD45+ cells constituting blood in mice after one week and up to 50% of human CD45+ cells 4 weeks after inoculation. The human CD45+ fraction is mainly composed of mature human T cells with a higher level of CD4+ rather than CD8+ cells (125). Thus, this model is specific to T lymphocytes and is not suited for investigating monocytes, which remain mostly mouse-derived. The main advantages are the fast engraftment of human cells and the possibility to implant PBMCs and tumor cells from the same patient, avoiding HLA mismatch. Unfortunately, the model can only be applied short-term, as PBMCs undergo human thymic education and present human MHC leading to an immune reaction against mouse MHC, known as Graft versus Host Disease (GvHD), and death of the mice after approximately 4 weeks (125). Because of the short experimental window (3 weeks) the HU-PBMC model is generally difficult to adapt to *in vivo* tumor development protocols. NSG mice with a double knock out for MHC Class I and II (NOD.Cg-Prkdc^{scid} H2-Ab1^{em1Mvw} H2-K1^{tm1Bpe} H2-D1^{tm1Bpe} Il2rg^{tm1Wjl}/SzJ) can be applied to extend the experimental window. In the absence of mouse MHC, this transgenic strain allows up to 100 days for tumor development monitoring (126, 127). Ashizawa et al., took advantage of NSG MHC I/II KO mice to develop subcutaneous GBM xenografts in a HU-PBMC model with PBMCs obtained from the HLA-partially matched donor (126). One day after X-ray irradiation of mice and PBMC injection, the U87 GBM cell line was implanted subcutaneously, which allowed tumor development in the experimental time frame of the humanized model. The authors report a successful response to anti-PD1 treatment. It should be noted that MHC knock out may impact mouse microglia functionality, which was not investigated in this study. As described in this study, preconditioning irradiation can be applied in these mice to increase the percentage of human cell engraftment. This is not recommended in the NSG strain, where it will lead to a faster development of GvHD.

So far no GBM PDOX model was reported in HU-PBMC mice and it is currently not clear to what extent HU-PBMCs will translocate to the mouse brain. PDOX development in the mouse brain can take from several weeks to several months, often going far beyond the 4–10 weeks before the GvHD. To overcome this issue, PBMCs could be injected after the tumor is well established which would also avoid potential tumor cell rejection due to the brain surgery-induced inflammation (**Figure 3**). In this case, X-ray irradiation should be avoided not only because of increased GvHD, but also because of its impact on tumor growth. The implantation protocol requires 10x10^6 human PBMCs per mouse, which may be challenging to obtain from GBM patients, which display severe lymphopenia. *Ex vivo* expansion of T cells/PBMCs from patients or healthy donors with partial HLA match could overcome the T cell limitation. The application of HLA-partially matched PBMCs from healthy donors would also allow to expand humanized studies to previously established GBM PDOXs, for which patient blood is not available.

HU-CD34 Model

HU-CD34 mice are created from human CD34+ hematopoietic stem cells (HSC) isolated from umbilical cord blood, bone marrow, fetal liver or mobilized PBMCs. HSCs are injected intravenously, intrafemoraly, or intrahepatically into freshly irradiated new born or young NSG mice (<3–4 weeks old). After 12–16 weeks, up to 25% of CD45+ cells in mouse blood represent human cells and mice can be used for experiments (**Figure 3**). This provides a much wider experimental window for implantation of tumor cells. The reconstitution of the human hematopoietic system (human/mouse ratio and maturation level) differs depending on the mouse strain and the organ (128–130). HU-CD34 NSG mice reconstitute well B and T cells but a low level of myeloid lineage cells is seen in the blood. These mice are able to survive for more than a year, with a relatively stable ratio of human/mouse cells in the blood. The partial incompatibility of growth factor signaling required for hematopoiesis explains some developmental or functional defects observed in myeloid cell differentiation or maturation of T cells (128, 131, 132). Additional injection of human growth factors (133) or application of transgenic strains expressing several human growth factors can improve maturation of human immune cells (125). For example, the NSG-SGM3 (NOD.Cg-PrkdcscidIl2rgtm1WjlTg(CMV-IL3,CSF2,KITLG)1Eav/MloySzJ) triple transgenic mice expressing human Stem cell factor (SCF), Interleukin-3 (IL-3) and Granulocyte/macrophage stimulating factor (GM-CSF), enhance the number of T cells and myeloid cells (134). It is currently unclear if sublethal irradiation, necessary prior to CD34+ HSC implantation, can affect microglia functionality in the mouse brain. Interestingly, it has been reported that HU-CD34 NSG mice can present human HSC-derived microglia/macrophage-like cells integrated with mouse microglia

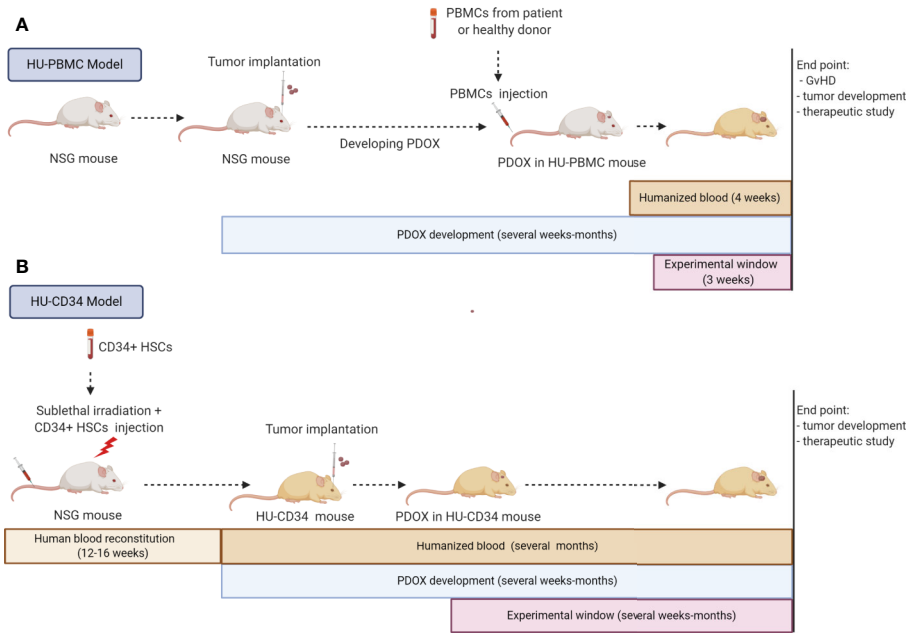

FIGURE 3 | Strategies for immunocompetent GBM PDOXs development in humanized mice. Immunocompetent GBM PDOXs can be generated in HU-PBMC or HU-CD34 mice. The experimental schedule and therapeutic window depends on the humanized model applied and tumor development time **(A)**. Due to the short survival of HU-PBMC mice, tumor implantation should precede the PBMC injection. The best time point will depend on tumor latency. The experimental window is limited due to development of Graft versus Host Disease (GvHD) within 4 weeks, depending on the genetic background of the NSG mice **(B)**. HU-CD34 model requires more time for the generation of humanized blood which is counterbalanced by the longer survival of the mice (>1 year). The tumor implantation timepoint and experimental window depend on the tumor latency and need to be synchronized according to the required readout. Illustration created with Biorender.com.

in the brain (135). A specific transgenic strain producing human IL-34 (NOG-hIL34 mice) further improved development of human microglia/macrophage-like cells in the brain (136).

The HU-CD34 model has been successfully combined with several cell line-derived xenografts and PDXs of different cancer types (137–139). Although a perfect HLA match between CD34+ HSC donor and tumor patient is impossible, a partial HLA match did not negatively affect tumor growth in recent reports on PDXs (139, 140). HLA loss is a well described escape mechanism in many tumors, including GBM, which may compensate the possible HLA mismatch (141, 142). Moreover, as human immune cells mature through the mouse thymus according to the mouse MHC I and II, human T cells are not fully functional and do not reject human tumor cells with different HLA (143). An alternative BLT (Bone marrow, Liver, Thymus) model, which applies the co-transplantation of fetal liver and thymus from autologous CD34+ HSCs donors, allows for improved development of HSCs and their positive selection through human MHC. The functionality of T cells is improved, yet in this situation the partial HLA match leads to higher incidence of GvHD (144, 145).

For GBM PDOXs the HU-CD34 model appears as a preferred model than HU-PBMC, because of the improved reconstitution of human immune cells and the longer experimental window. GBM PDOX developed in HU-CD34 mice would recreate most comprehensively a functional human immune system, allowing for *in vivo* therapeutic interventions targeting tumor-immune cell crosstalk. So far only one study described GBM orthotopic xenografts developed in HU-CD34 model. Zhai et al., have successfully implanted U87 cells and GBM cells derived from two subcutaneous PDX models into the brain of HU-CD34 BTL (146). The presence of human T and myeloid cells was confirmed in the blood, lymph nodes, spleen, as well as within the tumors developed in the brain, but not in normal adjacent brain. It remains to be seen if a similar reconstitution of the human hematopoietic system is present in GBM PDOXs that develop over longer time periods and if these humanized PDOXs recapitulate clinical features of GBM patients, such as lymphopenia, leading to decreased amount of human T cells in the blood.

CONCLUSION AND PERSPECTIVES

In recent years not much progress has been made to improve survival of GBM patients and treatment options are still very limited. The technology of tumor-treating fields is the only recent treatment modality, which provided a positive outcome in a phase III clinical trial, but has its own inherent drawbacks that are debated in the community (147). Since TMZ, no novel drug has been developed that led to prolonged patient survival (148). This failure can at least be partially attributed to inappropriate pre-clinical models, which do not fully recapitulate GBM, hence novel physiologically relevant models are urgently needed. Organoid culture models have emerged to complete the scientific toolbox. Patient-derived GBM organoids

and GBM organoids derived from genetically engineered human brain organoids have been successfully established and have been shown to better recapitulate GBM genetic and phenotypic characteristics in comparison to 2D GBM cell lines and 3D GSCs. Although technologically more challenging, GBM organoids represent a promising and exciting pre-clinical model and are a powerful tool to foster our understanding of GBM biology and an emerging platform for drug screening. If established from a patient-derived system, these organoids offer an approach for personalized medicine, prompting to better predict treatment responses for patients. Due to the relatively quick generation time of patient-derived organoids, *ex vivo* studies are being conducted in a reasonable and clinically relevant time frame and could ultimately guide clinical decisions. Technical challenges need to be addressed in future studies and further improvements to incorporate an adequate TME are warranted. Immunocompetent GBM organoids, based on co-culture with either tumor or blood-derived immune cells, will be crucial to bring forward novel immunotherapeutic approaches. We anticipate that future studies will incorporate immunocompetent organoid cultures in their experimental design to investigate not only immune-tumor interactions, but also to investigate current and novel immunotherapies, such as adoptive T cell transfer, immune checkpoint inhibitors or oncolytic viruses. Moreover, PDOX generated in humanized mice will provide another important tool essential to improve drug development and preclinical testing *in vivo*. Such developments and improvements of pre-clinical models should have a major impact on preclinical research and clinical studies and eventually on patient care.

AUTHOR CONTRIBUTIONS

EK, AG, and SN contributed to conception and design of the manuscript. EK wrote the first draft of the manuscript. AC and AO wrote sections of the manuscript. AG and SN corrected different versions and finalized the manuscript. All authors contributed to manuscript revision, read, and approved the submitted version.

FUNDING

The authors are grateful for the financial support of Télévie-FNRS (grants GBModImm no. 7.8513.18 and TETHER no. 7.4615.18).

REFERENCES

1. Louis DN, Perry A, Reifenberger G, von Deimling A, Figarella-Branger D, Cavenee WK, et al. The 2016 World Health Organization Classification of Tumors of the Central Nervous System: a summary. *Acta Neuropathol* (2016) 131(6):803–20. doi: 10.1007/s00401-016-1545-1
2. Stupp R, Mason WP, van den Bent MJ, Weller M, Fisher B, Taphoorn MJ, et al. Radiotherapy plus concomitant and adjuvant temozolomide for glioblastoma. *N Engl J Med* (2005) 352(10):987–96. doi: 10.1056/NEJMoa043330
3. Wen PY, Weller M, Lee EQ, Alexander BA, Barnholtz-Sloan JS, Barthel FP, et al. Glioblastoma in Adults: A Society for Neuro-Oncology (SNO) and European Society of Neuro-Oncology (EANO) Consensus Review on Current Management and Future Directions. *Neuro Oncol* (2020) 22 (8):1073–113. doi: 10.1093/neuonc/noaa106
4. Aldape K, Brindle KM, Chesler L, Chopra R, Gajjar A, Gilbert MR, et al. Challenges to curing primary brain tumours. *Nat Rev Clin Oncol* (2019) 16 (8):509–20. doi: 10.1038/s41571-019-0177-5
5. Dirkse A, Golebiewska A, Buder T, Nazarov PV, Muller A, Poovathingal S, et al. Stem cell-associated heterogeneity in Glioblastoma results from intrinsic tumor plasticity shaped by the microenvironment. *Nat Commun* (2019) 10(1):1787. doi: 10.1038/s41467-019-09853-z
6. Neftel C, Laffy J, Filbin MG, Hara T, Shore ME, Rahme GJ, et al. An Integrative Model of Cellular States, Plasticity, and Genetics for Glioblastoma. *Cell* (2019) 178(4):835–49.e21. doi: 10.1016/j.cell.2019.06.024
7. Waldman AD, Fritz JM, Lenardo MJ. A guide to cancer immunotherapy: from T cell basic science to clinical practice. *Nat Rev Immunol* (2020) 20:651–68. doi: 10.1038/s41577-020-0306-5
8. Lim M, Xia Y, Bettegowda C, Weller M. Current state of immunotherapy for glioblastoma. *Nat Rev Clin Oncol* (2018) 15(7):422–42. doi: 10.1038/s41571-018-0003-5
9. Reardon DA, Brandes AA, Omuro A, Mulholland P, Lim M, Wick A, et al. Effect of Nivolumab vs Bevacizumab in Patients With Recurrent Glioblastoma: The CheckMate 143 Phase 3 Randomized Clinical Trial. *JAMA Oncol* (2020) 6(7):1003–10. doi: 10.1001/jamaoncol.2020.1024
10. Weller M, Butowski N, Tran DD, Recht LD, Lim M, Hirte H, et al. Rindopepimut with temozolomide for patients with newly diagnosed, EGFRvIII-expressing glioblastoma (ACT IV): a randomised, double-blind, international phase 3 trial. *Lancet Oncol* (2017) 18(10):1373–85. doi: 10.1016/S1470-2045(17)30517-X
11. Woroniecka K, Chongsathidkiet P, Rhodin K, Kemeny H, Dechant C, Farber SH, et al. T-Cell Exhaustion Signatures Vary with Tumor Type and Are Severe in Glioblastoma. *Clin Cancer Res* (2018) 24(17):4175–86. doi: 10.1158/1078-0432.CCR-17-1846
12. Chongsathidkiet P, Jackson C, Koyama S, Loebel F, Cui X, Farber SH, et al. Sequestration of T cells in bone marrow in the setting of glioblastoma and other intracranial tumors. *Nat Med* (2018) 24(9):1459–68. doi: 10.1038/s41591-018-0135-2
13. Thorsson V, Gibbs DL, Brown SD, Wolf D, Bortone DS, Ou Yang TH, et al. The Immune Landscape of Cancer. *Immunity* (2018) 48(4):812–30.e14. doi: 10.1016/j.immuni.2018.03.023
14. Fecci PE, Mitchell DA, Whitesides JF, Xie W, Friedman AH, Archer GE, et al. Increased regulatory T-cell fraction amidst a diminished CD4 compartment explains cellular immune defects in patients with malignant glioma. *Cancer Res* (2006) 66(6):3294–302. doi: 10.1158/0008-5472.CAN-05-3773
15. Alban TJ, Alvarado AG, Sorensen MD, Bayik D, Volovetz J, Serbinowski E, et al. Global immune fingerprinting in glioblastoma patient peripheral blood reveals immune-suppression signatures associated with prognosis. *JCI Insight* (2018) 3(21):e122264. doi: 10.1172/jci.insight.122264
16. Gielen PR, Schulte BM, Kers-Rebel ED, Verrijp K, Bossman SA, Ter Laan M, et al. Elevated levels of polymorphonuclear myeloid-derived suppressor cells in patients with glioblastoma highly express S100A8/9 and arginase and suppress T cell function. *Neuro Oncol* (2016) 18(9):1253–64. doi: 10.1093/neuonc/now034
17. Pires-Afonso Y, Niclou SP, Michelucci A. Revealing and Harnessing Tumour-Associated Microglia/Macrophage Heterogeneity in Glioblastoma. *Int J Mol Sci* (2020) 21(3):689. doi: 10.3390/ijms21030689
18. White K, Connor K, Clerkin J, Murphy BM, Salvucci M, O'Farrell AC, et al. New hints towards a precision medicine strategy for IDH wild-type glioblastoma. *Ann Oncol* (2020) 31(12):1679–92. doi: 10.1016/j.annonc.2020.08.2336
19. De Witt Hamer PC, Van Tilborg AA, Eijk PP, Sminia P, Troost D, Van Noorden CJ, et al. The genomic profile of human malignant glioma is altered early in primary cell culture and preserved in spheroids. *Oncogene* (2008) 27 (14):2091–6. doi: 10.1038/sj.onc.1210850

20. Torsvik A, Stieber D, Enger PO, Golebiewska A, Molven A, Svendsen A, et al. U-251 revisited: genetic drift and phenotypic consequences of long-term cultures of glioblastoma cells. *Cancer Med* (2014) 3(4):812–24. doi: 10.1002/cam4.219
21. Clark MJ, Homer N, O'Connor BD, Chen Z, Eskin A, Lee H, et al. U87MG decoded: the genomic sequence of a cytogenetically aberrant human cancer cell line. *PloS Genet* (2010) 6(1):e1000832. doi: 10.1371/journal.pgen.1000832
22. Gomez-Roman N, Stevenson K, Gilmour L, Hamilton G, Chalmers AJ. A novel 3D human glioblastoma cell culture system for modeling drug and radiation responses. *Neuro Oncol* (2017) 19(2):229–41. doi: 10.1093/neuonc/now164
23. Balvers RK, Kleijn A, Kloezeman JJ, French PJ, Kremer A, van den Bent MJ, et al. Serum-free culture success of glial tumors is related to specific molecular profiles and expression of extracellular matrix-associated gene modules. *Neuro Oncol* (2013) 15(12):1684–95. doi: 10.1093/neuonc/not116
24. Lee J, Kotliarova S, Kotliarov Y, Li A, Su Q, Donin NM, et al. Tumor stem cells derived from glioblastomas cultured in bFGF and EGF more closely mirror the phenotype and genotype of primary tumors than do serum-cultured cell lines. *Cancer Cell* (2006) 9(5):391–403. doi: 10.1016/j.ccr.2006.03.030
25. Bougnaud S, Golebiewska A, Oudin A, Keunen O, Harter PN, Mader L, et al. Molecular crosstalk between tumour and brain parenchyma instructs histopathological features in glioblastoma. *Oncotarget* (2016) 7(22):31955–71. doi: 10.18632/oncotarget.7454
26. Huszthy PC, Daphu I, Niclou SP, Stieber D, Nigro JM, Sakariassen PO, et al. In vivo models of primary brain tumors: pitfalls and perspectives. *Neuro Oncol* (2012) 14(8):979–93. doi: 10.1093/neuonc/nos135
27. Golebiewska A, Hau AC, Oudin A, Stieber D, Yabo YA, Baus V, et al. Patient-derived organoids and orthotopic xenografts of primary and recurrent gliomas represent relevant patient avatars for precision oncology. *Acta Neuropathol* (2020) 140:919–49. doi: 10.1007/s00401-020-02226-7
28. Drost J, Clevers H. Organoids in cancer research. *Nat Rev Cancer* (2018) 18(7):407–18. doi: 10.1038/s41568-018-0007-6
29. Aslan K, Turco V, Blobner J, Sonner JK, Liuzzi AR, Nunez NG, et al. Heterogeneity of response to immune checkpoint blockade in hypermutated experimental gliomas. *Nat Commun* (2020) 11(1):931. doi: 10.1038/s41467-020-14642-0
30. Genoud V, Marinari E, Nikolaev SI, Castle JC, Bukur V, Dietrich PY, et al. Responsiveness to anti-PD-1 and anti-CTLA-4 immune checkpoint blockade in SB28 and GL261 mouse glioma models. *Oncoimmunology* (2018) 7(12):e1501137. doi: 10.1080/2162402X.2018.1501137
31. Reardon DA, Gokhale PC, Klein SR, Ligon KL, Rodig SJ, Ramkissoon SH, et al. Glioblastoma Eradication Following Immune Checkpoint Blockade in an Orthotopic, Immunocompetent Model. *Cancer Immunol Res* (2016) 4(2):124–35. doi: 10.1158/2326-6066.CIR-15-0151
32. Bar-Ephraim YE, Kretzschmar K, Clevers H. Organoids in immunological research. *Nat Rev Immunol* (2020) 20(5):279–93. doi: 10.1038/s41577-019-0248-y
33. Byrne AT, Alferez DG, Amant F, Annibali D, Arribas J, Biankin AV, et al. Interrogating open issues in cancer precision medicine with patient-derived xenografts. *Nat Rev Cancer* (2017) 17(4):254–68. doi: 10.1038/nrc.2016.140
34. Clevers H. Modeling Development and Disease with Organoids. *Cell* (2016) 165(7):1586–97. doi: 10.1016/j.cell.2016.05.082
35. Sato T, Vries RG, Snippert HJ, van de Wetering M, Barker N, Stange DE, et al. Single Lgr5 stem cells build crypt-villus structures in vitro without a mesenchymal niche. *Nature* (2009) 459(7244):262–5. doi: 10.1038/nature07935
36. Yin Y, Bijvelds M, Dang W, Xu L, van der Eijk AA, Knipping K, et al. Modeling rotavirus infection and antiviral therapy using primary intestinal organoids. *Antiviral Res* (2015) 123:120–31. doi: 10.1016/j.antiviral.2015.09.010
37. McCracken KW, Cata EM, Crawford CM, Sinagoga KL, Schumacher M, Rockich BE, et al. Modelling human development and disease in pluripotent stem-cell-derived gastric organoids. *Nature* (2014) 516(7531):400–4. doi: 10.1038/nature13863
38. Smith RC, Tabar V. Constructing and Deconstructing Cancers using Human Pluripotent Stem Cells and Organoids. *Cell Stem Cell* (2019) 24(1):12–24. doi: 10.1016/j.stem.2018.11.012
39. Lancaster MA, Renner M, Martin CA, Wenzel D, Bicknell LS, Hurles ME, et al. Cerebral organoids model human brain development and microcephaly. *Nature* (2013) 501(7467):373–9. doi: 10.1038/nature12517
40. Bhaduri A, Andrews MG, Mancia Leon W, Jung D, Shin D, Allen D, et al. Cell stress in cortical organoids impairs molecular subtype specification. *Nature* (2020) 578(7793):142–8. doi: 10.1038/s41586-020-1962-0
41. Smits LM, Reinhardt L, Reinhardt P, Glatza M, Monzel AS, Stanslowsky N, et al. Modeling Parkinson's disease in midbrain-like organoids. *NPJ Parkinsons Dis* (2019) 5:5. doi: 10.1038/s41531-019-0078-4
42. Bjerkvig R, Laerum OD, Mella O. Glioma cell interactions with fetal rat brain aggregates in vitro and with brain tissue in vivo. *Cancer Res* (1986) 46(8):4071–9.
43. Jo J, Xiao Y, Sun AX, Cukuroglu E, Tran HD, Göke J, et al. Midbrain-like Organoids from Human Pluripotent Stem Cells Contain Functional Dopaminergic and Neuromelanin-Producing Neurons. *Cell Stem Cell* (2016) 19(2):248–57. doi: 10.1016/j.stem.2016.07.005
44. Qian X, Song H, Ming GL. Brain organoids: advances, applications and challenges. *Development* (2019) 146(8):dev166074. doi: 10.1242/dev.166074
45. Bjerkvig R, Tonnesen A, Laerum OD, Backlund EO. Multicellular tumor spheroids from human gliomas maintained in organ culture. *J Neurosurg* (1990) 72(3):463–75. doi: 10.3171/jns.1990.72.3.0463
46. Jung P, Sato T, Merlos-Suárez A, Barriga FM, Iglesias M, Rossell D, et al. Isolation and in vitro expansion of human colonic stem cells. *Nat Med* (2011) 17(10):1225–7. doi: 10.1038/nm.2470
47. Sachs N, de Ligt J, Kopper O, Gogola E, Bounova G, Weeber F, et al. A Living Biobank of Breast Cancer Organoids Captures Disease Heterogeneity. *Cell* (2018) 172(1-2):373–86 e10. doi: 10.1016/j.cell.2017.11.010
48. Calandrini C, Schutgens F, Oka R, Margaritis T, Candelli T, Mathijsen L, et al. An organoid biobank for childhood kidney cancers that captures disease and tissue heterogeneity. *Nat Commun* (2020) 11(1):1310. doi: 10.1038/s41467-020-15155-6
49. Broutier L, Mastrogiovanni G, Verstegen MM, Francies HE, Gavarro LM, Bradshaw CR, et al. Human primary liver cancer-derived organoid cultures for disease modeling and drug screening. *Nat Med* (2017) 23(12):1424–35. doi: 10.1038/nm.4438
50. Gao D, Vela I, Sboner A, Iaquinta PJ, Karthaus WR, Gopalan A, et al. Organoid cultures derived from patients with advanced prostate cancer. *Cell* (2014) 159(1):176–87. doi: 10.1016/j.cell.2014.08.016
51. Boj SF, Hwang CI, Baker LA, Chio II, Engle DD, Corbo V, et al. Organoid models of human and mouse ductal pancreatic cancer. *Cell* (2015) 160(1-2):324–38. doi: 10.1016/j.cell.2014.12.021
52. Weeber F, van de Wetering M, Hoogstraat M, Dijkstra KK, Krijgsman O, Kuilman T, et al. Preserved genetic diversity in organoids cultured from biopsies of human colorectal cancer metastases. *Proc Natl Acad Sci U.S.A.* (2015) 112(43):13308–11. doi: 10.1073/pnas.1516689112
53. Schutte M, Risch T, Abdavi-Azar N, Boehnke K, Schumacher D, Keil M, et al. Molecular dissection of colorectal cancer in pre-clinical models identifies biomarkers predicting sensitivity to EGFR inhibitors. *Nat Commun* (2017) 8:14262. doi: 10.1038/ncomms14262
54. Bolhaqueiro ACF, Ponsioen B, Bakker B, Klaasen SJ, Kucukkose E, van Jaarsveld RH, et al. Ongoing chromosomal instability and karyotype evolution in human colorectal cancer organoids. *Nat Genet* (2019) 51(5):824–34. doi: 10.1038/s41588-019-0399-6
55. van de Wetering M, Francies HE, Francis JM, Bounova G, Iorio F, Pronk A, et al. Prospective derivation of a living organoid biobank of colorectal cancer patients. *Cell* (2015) 161(4):933–45. doi: 10.1016/j.cell.2015.03.053
56. Backlund EO, Bjerkvig R. Stereotactic biopsies as a model for studying the interaction between gliomas and normal brain tissue in vitro. *J Neurosurg Sci* (1989) 33(1):31–3.
57. Allen M, Bjerke M, Edlund H, Nelander S, Westermark B. Origin of the U87MG glioma cell line: Good news and bad news. *Sci Transl Med* (2016) 8(354):354re3. doi: 10.1126/scitranslmed.aaf6853
58. Campos B, Wan F, Farhadi M, Ernst A, Zeppernick F, Tagscherer KE, et al. Differentiation therapy exerts antitumor effects on stem-like glioma cells.

Clin Cancer Res (2010) 16(10):2715–28. doi: 10.1158/1078-0432.CCR-09-1800
59. Hubert CG, Rivera M, Spangler LC, Wu Q, Mack SC, Prager BC, et al. A Three-Dimensional Organoid Culture System Derived from Human Glioblastomas Recapitulates the Hypoxic Gradients and Cancer Stem Cell Heterogeneity of Tumors Found In Vivo. *Cancer Res* (2016) 76(8):2465–77. doi: 10.1158/0008-5472.CAN-15-2402
60. Jacob F, Salinas RD, Zhang DY, Nguyen PTT, Schnoll JG, Wong SZH, et al. A Patient-Derived Glioblastoma Organoid Model and Biobank Recapitulates Inter- and Intra-tumoral Heterogeneity. *Cell* (2020) 180(1):188–204 e22. doi: 10.1016/j.cell.2019.11.036
61. Bian S, Repic M, Guo Z, Kavirayani A, Burkard T, Bagley JA, et al. Genetically engineered cerebral organoids model brain tumor formation. *Nat Methods* (2018) 15(8):631–9. doi: 10.1038/s41592-018-0070-7
62. Ogawa J, Pao GM, Shokhirev MN, Verma IM. Glioblastoma Model Using Human Cerebral Organoids. *Cell Rep* (2018) 23(4):1220–9. doi: 10.1016/j.celrep.2018.03.105
63. Sakariassen P, Prestegarden L, Wang J, Skaftnesmo KO, Mahesparan R, Molthoff C, et al. Angiogenesis-independent tumor growth mediated by stem-like cancer cells. *Proc Natl Acad Sci USA* (2006) 103(44):16466–71. doi: 10.1073/pnas.0607668103
64. Talasila KM, Soentgerath A, Euskirchen P, Rosland GV, Wang J, Huszthy PC, et al. EGFR wild-type amplification and activation promote invasion and development of glioblastoma independent of angiogenesis. *Acta Neuropathol* (2013) 125(5):683–98. doi: 10.1007/s00401-013-1101-1
65. Han M, Wang S, Fritah S, Wang X, Zhou W, Yang N, et al. Interfering with long non-coding RNA MIR22HG processing inhibits glioblastoma progression through suppression of Wnt/beta-catenin signalling. *Brain* (2020) 143(2):512–30. doi: 10.1093/brain/awz406
66. Christensen K, Aaberg-Jessen C, Andersen C, Goplen D, Bjerkvig R, Kristensen BW. Immunohistochemical expression of stem cell, endothelial cell, and chemosensitivity markers in primary glioma spheroids cultured in serum-containing and serum-free medium. *Neurosurgery* (2010) 66(5):933–47. doi: 10.1227/01.NEU.0000368393.45935.46
67. Daubon T, Leon C, Clarke K, Andrique L, Salabert L, Darbo E, et al. Deciphering the complex role of thrombospondin-1 in glioblastoma development. *Nat Commun* (2019) 10(1):1146. doi: 10.1038/s41467-019-08480-y
68. Wang J, Daphu I, Pedersen PH, Miletic H, Hovland R, Mork S, et al. A novel brain metastases model developed in immunodeficient rats closely mimics the growth of metastatic brain tumours in patients. *Neuropathol Appl Neurobiol* (2011) 37(2):189–205. doi: 10.1111/j.1365-2990.2010.01119.x
69. Stieber D, Golebiewska A, Evers L, Lenkiewicz E, Brons NH, Nicot N, et al. Glioblastomas are composed of genetically divergent clones with distinct tumourigenic potential and variable stem cell-associated phenotypes. *Acta Neuropathol* (2014) 127(2):203–19. doi: 10.1007/s00401-013-1196-4
70. Abdul Rahim SA, Dirkse A, Oudin A, Schuster A, Bohler J, Barthelemy V, et al. Regulation of hypoxia-induced autophagy in glioblastoma involves ATG9A. *Br J Cancer* (2017) 117(6):813–25. doi: 10.1038/bjc.2017.263
71. Golebiewska A, Bougnaud S, Stieber D, Brons NH, Vallar L, Hertel F, et al. Side population in human glioblastoma is non-tumorigenic and characterizes brain endothelial cells. *Brain* (2013) 136(Pt 5):1462–75. doi: 10.1093/brain/awt025
72. Sanzey M, Abdul Rahim SA, Oudin A, Dirkse A, Kaoma T, Vallar L, et al. Comprehensive analysis of glycolytic enzymes as therapeutic targets in the treatment of glioblastoma. *PloS One* (2015) 10(5):e0123544. doi: 10.1371/journal.pone.0123544
73. Steele NG, Chakrabarti J, Wang J, Biesiada J, Holokai L, Chang J, et al. An Organoid-Based Preclinical Model of Human Gastric Cancer. *Cell Mol Gastroenterol Hepatol* (2019) 7(1):161–84. doi: 10.1016/j.jcmgh.2018.09.008
74. Linkous A, Balamatsias D, Snuderl M, Edwards L, Miyaguchi K, Milner T, et al. Modeling Patient-Derived Glioblastoma with Cerebral Organoids. *Cell Rep* (2019) 26(12):3203–11 e5. doi: 10.1016/j.celrep.2019.02.063
75. Kim S, Choung S, Sun RX, Ung N, Hashemi N, Fong EJ, et al. Comparison of Cell and Organoid-Level Analysis of Patient-Derived 3D Organoids to Evaluate Tumor Cell Growth Dynamics and Drug Response. *SLAS Discovery* (2020) 25(7):744–54. doi: 10.1177/2472555220915827
76. Ghandi M, Huang FW, Jane-Valbuena J, Kryukov GV, Lo CC, McDonald ER,3, et al. Next-generation characterization of the Cancer Cell Line Encyclopedia. *Nature* (2019) 569(7757):503–8. doi: 10.1038/s41586-019-1186-3
77. Lee JK, Liu Z, Sa JK, Shin S, Wang J, Bordyuh M, et al. Pharmacogenomic landscape of patient-derived tumor cells informs precision oncology therapy. *Nat Genet* (2018) 50(10):1399–411. doi: 10.1038/s41588-018-0209-6
78. Francies HE, Barthorpe A, McLaren-Douglas A, Barendt WJ, Garnett MJ. Drug Sensitivity Assays of Human Cancer Organoid Cultures. *Methods Mol Biol* (2019) 1576:339–51. doi: 10.1007/7651_2016_10
79. Qiu ZK, Shen D, Chen YS, Yang QY, Guo CC, Feng BH, et al. Enhanced MGMT expression contributes to temozolomide resistance in glioma stem-like cells. *Chin J Cancer* (2014) 33(2):115–22. doi: 10.5732/cjc.012.10236
80. Lee SH, Hu W, Matulay JT, Silva MV, Owczarek TB, Kim K, et al. Tumor Evolution and Drug Response in Patient-Derived Organoid Models of Bladder Cancer. *Cell* (2018) 173(2):515–28 e17. doi: 10.1016/j.cell.2018.03.017
81. Liffers K, Lamszus K, Schulte A. EGFR Amplification and Glioblastoma Stem-Like Cells. *Stem Cells Int* (2015) 2015:427518. doi: 10.1155/2015/427518
82. Doh I, Kwon YJ, Ku B, Lee DW. Drug Efficacy Comparison of 3D Forming and Preforming Sphere Models with a Micropillar and Microwell Chip Platform. *SLAS Discovery* (2019) 24(4):476–83. doi: 10.1177/2472555218821292
83. Pasch CA, Favreau PF, Yueh AE, Babiarz CP, Gillette AA, Sharick JT, et al. Patient-Derived Cancer Organoid Cultures to Predict Sensitivity to Chemotherapy and Radiation. *Clin Cancer Res* (2019) 25(17):5376–87. doi: 10.1158/1078-0432.CCR-18-3590
84. Fabian C, Han M, Bjerkvig R, Niclou SP. Novel facets of glioma invasion International Review of Cell and Molecular Biology. *Int Rev Cell Mol Biol* (2021). doi: 10.1016/bs.ircmb.2020.08.001
85. Marques-Torrejon MA, Gangoso E, Pollard SM. Modelling glioblastoma tumour-host cell interactions using adult brain organotypic slice co-culture. *Dis Model Mech* (2018) 11(2):dmm031435. doi: 10.1242/dmm.031435
86. Eisemann T, Costa B, Strelau J, Mittelbronn M, Angel P, Peterziel H. An advanced glioma cell invasion assay based on organotypic brain slice cultures. *BMC Cancer* (2018) 18(1):103. doi: 10.1186/s12885-018-4007-4
87. Krieger TG, Tirier SM, Park J, Jechow K, Eisemann T, Peterziel H, et al. Modeling glioblastoma invasion using human brain organoids and single-cell transcriptomics. *Neuro Oncol* (2020) 22(8):1138–114. doi: 10.1093/neuonc/noaa091
88. da Silva B, Mathew RK, Polson ES, Williams J, Wurdak H. Spontaneous Glioblastoma Spheroid Infiltration of Early-Stage Cerebral Organoids Models Brain Tumor Invasion. *SLAS Discovery* (2018) 23(8):862–8. doi: 10.1177/2472555218764623
89. Engebraaten O, Bjerkvig R, Lund-Johansen M, Wester K, Pedersen PH, Mørk S, et al. Interaction between human brain tumour biopsies and fetal rat brain tissue in vitro. *Acta Neuropathol* (1990) 81(2):130–40. doi: 10.1007/BF00334501
90. Cuddapah VA, Robel S, Watkins S, Sontheimer H. A neurocentric perspective on glioma invasion. *Nat Rev Neurosci* (2014) 15(7):455–65. doi: 10.1038/nrn3765
91. Cakir B, Xiang Y, Tanaka Y, Kural MH, Parent M, Kang YJ, et al. Engineering of human brain organoids with a functional vascular-like system. *Nat Methods* (2019) 16(11):1169–75. doi: 10.1038/s41592-019-0586-5
92. Pham MT, Pollock KM, Rose MD, Cary WA, Stewart HR, Zhou P, et al. Generation of human vascularized brain organoids. *Neuroreport* (2018) 29(7):588–93. doi: 10.1097/WNR.0000000000001014
93. Vaubel RA, Tian S, Remonde D. Genomic and Phenotypic Characterization of a Broad Panel of Patient-Derived Xenografts Reflects the Diversity of Glioblastoma. *Clin Cancer Res* (2020) 26: (5):1094–104. doi: 10.1158/1078-0432.CCR-19-0909
94. Wang J, Miletic H, Sakariassen P, Huszthy PC, Jacobsen H, Brekkå N, et al. A reproducible brain tumour model established from human glioblastoma biopsies. *BMC Cancer* (2009) 9:465. doi: 10.1186/1471-2407-9-465
95. Keunen O, Johansson M, Oudin A, Sanzey M, Rahim SA, Fack F, et al. Anti-VEGF treatment reduces blood supply and increases tumor cell invasion in glioblastoma. *Proc Natl Acad Sci U.S.A.* (2011) 108(9):3749–54. doi: 10.1073/pnas.1014480108
96. Fack F, Tardito S, Hochart G, Oudin A, Zheng L, Fritah S, et al. Altered metabolic landscape in IDH-mutant gliomas affects phospholipid, energy, and oxidative stress pathways. *EMBO Mol Med* (2017) 9(12):1681–95. doi: 10.15252/emmm.201707729

97. Tardito S, Oudin A, Ahmed SU, Fack F, Keunen O, Zheng L, et al. Glutamine synthetase activity fuels nucleotide biosynthesis and supports growth of glutamine-restricted glioblastoma. *Nat Cell Biol* (2015) 17(12):1556–68. doi: 10.1038/ncb3272
98. Demeure K, Fack F, Duriez E, Tiemann K, Bernard A, Golebiewska A, et al. Targeted Proteomics to Assess the Response to Anti-Angiogenic Treatment in Human Glioblastoma (GBM). *Mol Cell Proteomics* (2016) 15(2):481–92. doi: 10.1074/mcp.M115.052423
99. Johansson M, Oudin A, Tiemann K, Bernard A, Golebiewska A, Keunen O, et al. The soluble form of the tumor suppressor Lrig1 potently inhibits in vivo glioma growth irrespective of EGF receptor status. *Neuro Oncol* (2013) 15(9):1200–11. doi: 10.1093/neuonc/not054
100. Fack F, Espedal H, Keunen O, Golebiewska A, Obad N, Harter PN, et al. Bevacizumab treatment induces metabolic adaptation toward anaerobic metabolism in glioblastomas. *Acta Neuropathol* (2015) 129(1):115–31. doi: 10.1007/s00401-014-1352-5
101. Miletic H, Niclou SP, Johansson M, Bjerkvig R. Anti-VEGF therapies for malignant glioma: treatment effects and escape mechanisms. *Expert Opin Ther Targets* (2009) 13(4):455–68. doi: 10.1517/14728220902806444
102. Pardridge WM. The blood-brain barrier: bottleneck in brain drug development. *NeuroRx J Am Soc Exp Neurother* (2005) 2(1):3–14. doi: 10.1602/neurorx.2.1.3
103. Hutter G, Theruvath J, Graef CM, Zhang M. Microglia are effector cells of CD47-SIRPα antiphagocytic axis disruption against glioblastoma. *Proc Natl Acad Sci USA* (2019) 116: (3):997–1006. doi: 10.1073/pnas.1721434116
104. Negi N, Das BK. CNS: Not an immunoprivilaged site anymore but a virtual secondary lymphoid organ. *Int Rev Immunol* (2018) 37(1):57–68. doi: 10.1080/08830185.2017.1357719
105. Quail DF, Joyce JA. The Microenvironmental Landscape of Brain Tumors. *Cancer Cell* (2017) 31(3):326–41. doi: 10.1016/j.ccell.2017.02.009
106. Ye W, Luo C, Li C, Huang J, Liu F. Organoids to study immune functions, immunological diseases and immunotherapy. *Cancer Lett* (2020) 477:31–40. doi: 10.1016/j.canlet.2020.02.027
107. Dijkstra KK, Cattaneo CM, Weeber F, Chalabi M, van de Haar J, Fanchi LF, et al. Generation of Tumor-Reactive T Cells by Co-culture of Peripheral Blood Lymphocytes and Tumor Organoids. *Cell* (2018) 174(6):1586–98 e12. doi: 10.1016/j.cell.2018.07.009
108. Cattaneo CM, Dijkstra KK, Fanchi LF, Kelderman S, Kaing S, van Rooij N, et al. Tumor organoid-T-cell coculture systems. *Nat Protoc* (2020) 15(1):15–39. doi: 10.1038/s41596-019-0232-9
109. Woroniecka KI, Rhodin KE, Chongsathidkiet P, Keith KA. Fecci PE. T-cell Dysfunction in Glioblastoma: Applying a New Framework. *Clin Cancer Res* (2018) 24(16):3792–802. doi: 10.1158/1078-0432.CCR-18-0047
110. Hirt C, Papadimitropoulos A, Mele V, Muraro MG, Mengus C, Iezzi G, et al. "In vitro" 3D models of tumor-immune system interaction. *Adv Drug Delivery Rev* (2014) 79-80:145–54. doi: 10.1016/j.addr.2014.05.003
111. Tang M, Xie Q, Gimple RC, Zhong Z, Tam T, Tian J, et al. Three-dimensional bioprinted glioblastoma microenvironments model cellular dependencies and immune interactions. *Cell Res* (2020) 30(10):833–53. doi: 10.1038/s41422-020-0338-1
112. Turcotte S, Gros A, Hogan K, Tran E, Hinrichs CS, Wunderlich JR, et al. Phenotype and function of T cells infiltrating visceral metastases from gastrointestinal cancers and melanoma: implications for adoptive cell transfer therapy. *J Immunol* (2013) 191(5):2217–25. doi: 10.4049/jimmunol.1300538
113. Neal JT, Li X, Zhu J, Giangarra V, Grzeskowiak CL, Ju J, et al. Organoid Modeling of the Tumor Immune Microenvironment. *Cell* (2018) 175 (7):1972–88 e16. doi: 10.1016/j.cell.2018.11.021
114. Finnberg NK, Gokare P, Lev A, Grivennikov SI, MacFarlane AWT, Campbell KS, et al. Application of 3D tumoroid systems to define immune and cytotoxic therapeutic responses based on tumoroid and tissue slice culture molecular signatures. *Oncotarget* (2017) 8(40):66747–57. doi: 10.18632/oncotarget.19965
115. Kong JCH, Guerra GR, Millen RM, Roth S, Xu H, Neeson PJ, et al. Tumor-Infiltrating Lymphocyte Function Predicts Response to Neoadjuvant Chemoradiotherapy in Locally Advanced Rectal Cancer. *JCO Precis Oncol* (2018) 2):1–15. doi: 10.1200/PO.18.00075
116. Heimberger AB, Abou-Ghazal M, Reina-Ortiz C, Yang DS, Sun W, Qiao W, et al. Incidence and prognostic impact of FoxP3+ regulatory T cells in human gliomas. *Clin Cancer Res* (2008) 14(16):5166–72. doi: 10.1158/1078-0432.CCR-08-0320
117. Klemm F, Maas RR, Bowman RL, Kornete M, Soukup K, Nassiri S, et al. Interrogation of the Microenvironmental Landscape in Brain Tumors Reveals Disease-Specific Alterations of Immune Cells. *Cell* (2020) 181 (7):1643–60 e17. doi: 10.1016/j.cell.2020.05.007
118. Goff SL, Morgan RA, Yang JC, Sherry RM, Robbins PF, Restifo NP, et al. Pilot Trial of Adoptive Transfer of Chimeric Antigen Receptor-transduced T Cells Targeting EGFRvIII in Patients With Glioblastoma. *J Immunother* (2019) 42(4):126–35. doi: 10.1097/CJI.0000000000000260
119. Schnalzger TE, de Groot MH, Zhang C, Mosa MH, Michels BE, Roder J, et al. 3D model for CAR-mediated cytotoxicity using patient-derived colorectal cancer organoids. *EMBO J* (2019) 38(12):e100928. doi: 10.15252/embj.2018100928
120. Gao H, Korn JM, Ferretti S, Monahan JE, Wang Y, Singh M, et al. High-throughput screening using patient-derived tumor xenografts to predict clinical trial drug response. *Nat Med* (2015) 21(11):1318–25. doi: 10.1038/nm.3954
121. Yong KSM, Her Z, Chen Q. Humanized Mice as Unique Tools for Human-Specific Studies. *Arch Immunol Ther Exp (Warsz)* (2018) 66(4):245–66. doi: 10.1007/s00005-018-0506-x
122. Mosier DE, Gulizia RJ, Baird SM, Wilson DB. Transfer of a functional human immune system to mice with severe combined immunodeficiency. *Nature* (1988) 335(6187):256–9. doi: 10.1038/335256a0
123. Takenaka K, Prasolava TK, Wang JC, Mortin-Toth SM, Khalouei S, Gan OI, et al. Polymorphism in Sirpa modulates engraftment of human hematopoietic stem cells. *Nat Immunol* (2007) 8(12):1313–23. doi: 10.1038/ni1527
124. Shultz LD, Goodwin N, Ishikawa F, Hosur V, Lyons BL, Greiner DL. Human cancer growth and therapy in immunodeficient mouse models. *Cold Spring Harb Protoc* (2014) 2014(7):694–708. doi: 10.1101/pdb.top073585
125. De La Rochere P, Guil-Luna S, Decaudin D, Azar G, Sidhu SS, Piaggio E. Humanized Mice for the Study of Immuno-Oncology. *Trends Immunol* (2018) 39(9):748–63. doi: 10.1016/j.it.2018.07.001
126. Ashizawa T, Iizuka A, Nonomura C, Kondou R, Maeda C, Miyata H, et al. Antitumor Effect of Programmed Death-1 (PD-1) Blockade in Humanized the NOG-MHC Double Knockout Mouse. *Clin Cancer Res* (2017) 23(1):149–58. doi: 10.1158/1078-0432.CCR-16-0122
127. Brehm MA, Kenney LL, Wiles MV, Low BE, Tisch RM, Burzenski L, et al. Lack of acute xenogeneic graft- versus-host disease, but retention of T-cell function following engraftment of human peripheral blood mononuclear cells in NSG mice deficient in MHC class I and II expression. *FASEB J* (2019) 33(3):3137–51. doi: 10.1096/fj.201800636R
128. Tanaka S, Saito Y, Kunisawa J, Kurashima Y, Wake T, Suzuki N, et al. Development of mature and functional human myeloid subsets in hematopoietic stem cell-engrafted NOD/SCID/IL2rγKO mice. *J Immunol* (2012) 188(12):6145–55. doi: 10.4049/jimmunol.1103660
129. Wunderlich M, Chou FS, Sexton C, Presicce P, Chougnet CA, Aliberti J, et al. Improved multilineage human hematopoietic reconstitution and function in NSGS mice. *PloS One* (2018) 13(12):e0209034. doi: 10.1371/journal.pone.0209034
130. Yao LC, Aryee KE, Cheng M, Kaur P, Keck JG, Brehm MA. Creation of PDX-Bearing Humanized Mice to Study Immuno-oncology. *Methods Mol Biol* (2019) 1953:241–52. doi: 10.1007/978-1-4939-9145-7_15
131. Gille C, Orlikowsky TW, Spring B, Hartwig UF, Wilhelm A, Wirth A, et al. Monocytes derived from humanized neonatal NOD/SCID/IL2Rγ(null) mice are phenotypically immature and exhibit functional impairments. *Hum Immunol* (2012) 73(4):346–54. doi: 10.1016/j.humimm.2012.01.006
132. Lee JY, Han AR, Lee DR. T Lymphocyte Development and Activation in Humanized Mouse Model. *Dev Reprod* (2019) 23(2):79–92. doi: 10.12717/DR.2019.23.2.079
133. Coughlan AM, Harmon C, Whelan S, O'Brien EC, O'Reilly VP, Crotty P, et al. Myeloid Engraftment in Humanized Mice: Impact of Granulocyte-Colony Stimulating Factor Treatment and Transgenic Mouse Strain. *Stem Cells Dev* (2016) 25(7):530–41. doi: 10.1089/scd.2015.0289
134. Billerbeck E, Barry WT, Mu K, Dorner M, Rice CM, Ploss A. Development of human CD4+FoxP3+ regulatory T cells in human stem cell factor-, granulocyte-macrophage colony-stimulating factor-, and interleukin-3-expressing NOD-SCID IL2Rgamma(null) humanized mice. *Blood* (2011) 117(11):3076–86. doi: 10.1182/blood-2010-08-301507
135. Llewellyn GN, Alvarez-Carbonell D, Chateau M, Karn J, Cannon PM. HIV-1 infection of microglial cells in a reconstituted humanized mouse model and

identification of compounds that selectively reverse HIV latency. *J Neurovirol* (2018) 24(2):192–203. doi: 10.1007/s13365-017-0604-2

136. Mathews S, Branch Woods A, Katano I, Makarov E, Thomas MB, Gendelman HE, et al. Human Interleukin-34 facilitates microglia-like cell differentiation and persistent HIV-1 infection in humanized mice. *Mol Neurodegener* (2019) 14: (1):12. doi: 10.1186/s13024-019-0311-y
137. Meraz IM, Majidi M, Meng F, Shao R, Ha MJ. An Improved Patient-Derived Xenograft Humanized Mouse Model for Evaluation of Lung Cancer Immune Responses. *Cancer Immunol Res* (2019) 7:1267–79.
138. Rios-Doria J, Stevens C, Maddage C, Lasky K, Koblish HK. Characterization of human cancer xenografts in humanized mice. *J Immunother Cancer* (2020) 8.
139. Zhao Y, Shuen TWH, Toh TB, Chan XY, Liu M, Tan SY, et al. Development of a new patient-derived xenograft humanised mouse model to study human-specific tumour microenvironment and immunotherapy. *Gut* (2018) 67(10):1845–54. doi: 10.1136/gutjnl-2017-315201
140. Wang M, Yao LC, Cheng M, Cai D, Martinek J, Pan CX, et al. Humanized mice in studying efficacy and mechanisms of PD-1-targeted cancer immunotherapy. *FASEB J* (2018) 32(3):1537–49. doi: 10.1096/fj.201700740R
141. Garrido F. MHC/HLA Class I Loss in Cancer Cells. *Adv Exp Med Biol* (2019) 1151:15–78. doi: 10.1007/978-3-030-17864-2_2
142. Boegel S, Lower M, Bukur T, Sorn P, Castle JC, Sahin U. HLA and proteasome expression body map. *BMC Med Genomics* (2018) 11(1):36. doi: 10.1186/s12920-018-0354-x
143. Han S, Fink J, Jorg DJ, Lee E, Yum MK, Chatzeli L, et al. Defining the Identity and Dynamics of Adult Gastric Isthmus Stem Cells. *Cell Stem Cell* (2019) 25 (3):342–56 e7. doi: 10.1016/j.stem.2019.07.008
144. Greenblatt MB, Vrbanac V, Tivey T, Tsang K, Tager AM, Aliprantis AO. Graft versus host disease in the bone marrow, liver and thymus humanized mouse model. *PloS One* (2012) 7(9):e44664. doi: 10.1371/journal.pone.0044664
145. Jangalwe S, Shultz LD, Mathew A, Brehm MA. Improved B cell development in humanized NOD-scid IL2Rγ(null) mice transgenically expressing human stem cell factor, granulocyte-macrophage colony-stimulating factor and interleukin-3. *Immun Inflammation Dis* (2016) 4(4):427–40. doi: 10.1002/iid3.124
146. Zhai L, Ladomersky E, Lauing KL, Wu M, Genet M, Gritsina G, et al. Infiltrating T Cells Increase IDO1 Expression in Glioblastoma and Contribute to Decreased Patient Survival. *Clin Cancer Res* (2017) 23 (21):6650–60. doi: 10.1158/1078-0432.CCR-17-0120
147. Stupp R, Taillibert S, Kanner A, Read W, Steinberg D, Lhermitte B, et al. Effect of Tumor-Treating Fields Plus Maintenance Temozolomide vs Maintenance Temozolomide Alone on Survival in Patients With Glioblastoma: A Randomized Clinical Trial. *Jama* (2017) 318(23):2306–16. doi: 10.1001/jama.2017.18718
148. Tan AC, Ashley DM, López GY, Malinzak M, Friedman HS, Khasraw M. Management of glioblastoma: State of the art and future directions. *CA Cancer J Clin* (2020) 70(4):299–312. doi: 10.3322/caac.21613

Conflict of Interest: The authors declare that the research was conducted in the absence of any commercial or financial relationships that could be construed as a potential conflict of interest.

frontiers in Immunology

REVIEW
published: 10 December 2020
doi: 10.3389/fimmu.2020.603640

3D Tumor Models and Their Use for the Testing of Immunotherapies

Nicolas Boucherit, Laurent Gorvel[*†] *and Daniel Olive*[†]

Cancer Research Center in Marseille, CRCM, Paoli Calmette Institute, Marseille, France

Over the past decade, immunotherapy has become a powerful and evident tool in the fight against cancers. Notably, the rise of checkpoint blockade using monoclonal antibodies (anti-CTLA4, anti-PD1) to avoid interaction between inhibitory molecules allowed the betterment of patient care. Indeed, immunotherapies led to increased overall survival in forms of cutaneous melanoma or lung cancer. However, the percentage of patients responding varies from 20 to 40% depending on the type of cancer and on the expression of the target molecules by the tumor. This is due to the tumor microenvironment which allows the acquisition of resistance mechanisms to immunotherapies by tumor cells. These are closely linked to the architecture and cellular composition of the tumor microenvironment. This one acts on different parameters such as the immune cells infiltrate its composition and therefore, favors the recruitment of immunosuppressive cells as well as the tumor expression of checkpoint inhibitors such as Programmed Death Ligand-1 (PD-L1). Therefore, the analysis and modeling of the complexity of the microenvironment is an important parameter to consider, not only in the search for new therapies but also for the identification and stratification of patients likely to respond to immunotherapy. This is why the use of 3D culture models, reflecting the architecture and cellular composition of a tumor, is essential in immuno-oncology studies. Nowadays, there are several 3-D culture methods such as spheroids and organoids, which are applicable to immuno-oncology. In this review we evaluate 3D culture models as tools for the development of treatments in the field of immuno-oncology.

Keywords: spheroid, organoid, immunotherapy, tumor on a chip, tumor microenvironment, immune infiltrate, patient derived organoids, 3D culture

OPEN ACCESS

Edited by:
Roberta Castriconi, Università di Genova, Italy

Reviewed by:
María Paula Roberti, German Cancer Research Center (DKFZ), Germany
Tiziana Schioppa, University of Brescia, Italy

***Correspondence:**
Laurent Gorvel
laurent.gorvel@inserm.fr

[†]These authors have contributed equally to this work

Specialty section:
This article was submitted to Cancer Immunity and Immunotherapy, a section of the journal Frontiers in Immunology

Received: *07 September 2020*
Accepted: *10 November 2020*
Published: *10 December 2020*

Citation:
Boucherit N, Gorvel L and Olive D (2020) 3D Tumor Models and Their Use for the Testing of Immunotherapies. Front. Immunol. 11:603640. doi: 10.3389/fimmu.2020.603640

INTRODUCTION: TUMOR MICROENVIRONMENT AND IMMUNOTHERAPIES

The tumor microenvironment (TME) represents tissue, cellular, and soluble factors which are being affected by the development or the evolution of a tumor. The TME affects the main function of the tissue such as its metabolism and vascularization as well as the immune system (1). The immune system in the TME proved to be a keystone of the tumor development. Indeed, the immune system is affected by the tumor at two levels. First, tissue resident immune cells are affected and see their phenotype and function modified toward tumor promoting profile. Second, recruited immune cells are either affected by the TME when they reach the tumor invaded tissue or at a distant site such as tumor-cell invaded draining lymph nodes. This will profoundly influence the becoming of the tumor, as it might be eradicated or

might progress and metastasize (2). In the TME, immune cells are polarized to promote tumor growth according diverse mechanisms. TME metabolic constraints are known to increase myeloid-derived suppressive cells (3) (MDSCs) and regulatory T cells (Tregs) recruitment (4), as well as increasing inhibitory checkpoint molecule expression on immune cells such as PD-1, Programmed Death ligand-1 (PD-L1) (5) and CD47 a receptor part of the "don't eat me signal" which avoids phagocytosis of tumor cells (6). Tumor cells such as CAFs (cancer associated fibroblasts) are known to limit the entry of anti-tumoral T cells (7) and to promote Tumor associated M2 Macrophages (M2) (8). Therefore, the TME affects every aspects of tissue homeostasis which explains why conventional treatments such as chemotherapy, radiotherapy or surgical resection (when possible) often leads to relapse in most aggressive forms of cancer (9). Recently the study of the immune system within the TME allowed to develop new treatments based on the targeting of inhibitory receptors present on tumor infiltrating leukocytes (CTLA-4, PD-1), and later on their ligands which are expressed by other immune cells as well as tumor cells (PD-L1) (10). Nowadays, more and more targets are being tested using mAbs, such as ICOS and TIGIT (11, 12). Also, asides of immune checkpoint receptors, soluble molecules are being targeted by mAbs. Indeed, cytokines such as TNF-α, IL-17, or IL-6 (13–15) or chemokines such as CCR5 and CXCR2 (16, 17) are being tested using several approaches and often in combination with checkpoint inhibitors or conventional treatments. Another approach of immunotherapies is to stimulate immune cells with tumor antigens, or carcinogenic antigens to induce a repertoire of immune cells which will only target the tumor. Indeed, the cancer vaccination approach uses peptide-based approaches and select synthetic long peptides, neoantigens, and tumor lysates to stimulate antigen presentation and therefore expend tumor reactive clones of T cells. In viro-induced cancer (hepatocellular carcinomas, cervical cancer) viral peptides can be used to prime the immune system to avoid infection and therefore the development of tumors (Gardasil, Cervarix). Cell based immunotherapy relies on the selection, activation, and/or genetic modification of immune cell types to direct them against the tumor cells. Indeed, dendritic cells can be activated *in vitro* or pulsed with tumor antigens to be activated and specifically present the antigen to cytotoxic T cells and polarize them to kill tumor cells (18, 19). More recently, Chimeric-Antigen-Receptor T cells have been designed by genetic editing of T cell receptor and co-receptors to be aggressive against the tumor (20). The migration and survival of CAR T-cells can be improved by the addition of cytokines and chemokines such as IL-7 and CCL19 (21, 22). However, as efficient as some of these treatments might be, the resistance of patients to immunotherapy remains an issue. Therefore, the prediction of a situation where the patient will not respond to the treatment is a keystone to improve Immunotherapies. On one hand, predictive murine models often intertwine human tumors and a mix of human transferred immunity and murine innate immunity. this occurs in patient derived xenografts (PDX) where a patient tumor or tumor cells are transferred to an NGS mouse model which still possess components of the innate immune system of the host (mainly tissue resident myeloid cells). On the other hand, the testing on human tumors remain difficult because 2D cell culture/co-culture do not represent the whole TME. This is why the emerging use of 3D cell culture models for the testing of immunotherapies represent an elegant alternative.

3D MODELS

Two-dimensional culture models, which are based on the growth and proliferation of a monolayer of cells, do not allow to fully understand cell-cell and cell-extracellular matrix interactions. 3D culture models generate a polarization of cells with a basal and an apical pole, which induces genomic and protein alterations (23–27). The tissue microenvironment and the extracellular matrix are altered in the presence of a tumor. This translates by an alteration of oxygen, nutrients, metabolites distribution as well as cell proliferation and interactions. However, none of the 2D models are able to assess all these important parameters at once, and therefore fail to fully represent *in vivo* interactions. 3D models, such as melanoma-derived spheroids exhibit better immuno-modulatory, proliferation, and activation abilities than 2D cultures (28).

The expression of immune checkpoint molecules *in vivo* differs from their expression in 2D culture models. This why it becomes critical to use 3D cell culture models that reproduce the TME in a more accurate way. Among 3D cell culture models, two terminologies are used, spheroids and organoids. In both of these models, technical advances allowed to complexify cocultures to better the TME representation. Indeed, Tumors-on-ship and bioprinting associate technology and 3D culture, to mime fluidics or tumor cell architecture. However, the difference between spheroid and organoids is blurry in terms of semantics and seem to be based on the author preference. The organoid term is often applied to healthy primary cells and tissue biopsy cultures, when tumor-organoid or spheroid are applied to cancer studies. Spheroid is used for simple 3D structures when tumor organoids is used for complex structures involving multiple cell types and miming tissue architecture. The border between the two terms still remains ambiguous especially when biopsies are used without any digestion step. Here, the term tumor-spheroid can be used when cell lines, digested biopsies, and non-digested biopsies cultured in non-adherent condition to generate 3D models. Tumor organoids should be used when tissue lysates or undigested tissue are cultured in an extracellular matrix to conserve the tissue architecture as well as the tissue diversity. According to this, we classified 3D models as a complexity gradient where cellular composition is at the center as shown in **Figure 1**.

Cell-Lines Spheroids

The spherical model or spheroid model has been considered as the gold standard among the 3D *in vitro* models for the past 40–50 years. Spheroids are cells aggregates growing in suspension in three dimensions with or without an extracellular matrix. They have the ability to reproduce the architecture and metabolism of their tissue of origin to a certain extent. Indeed, they reproduce

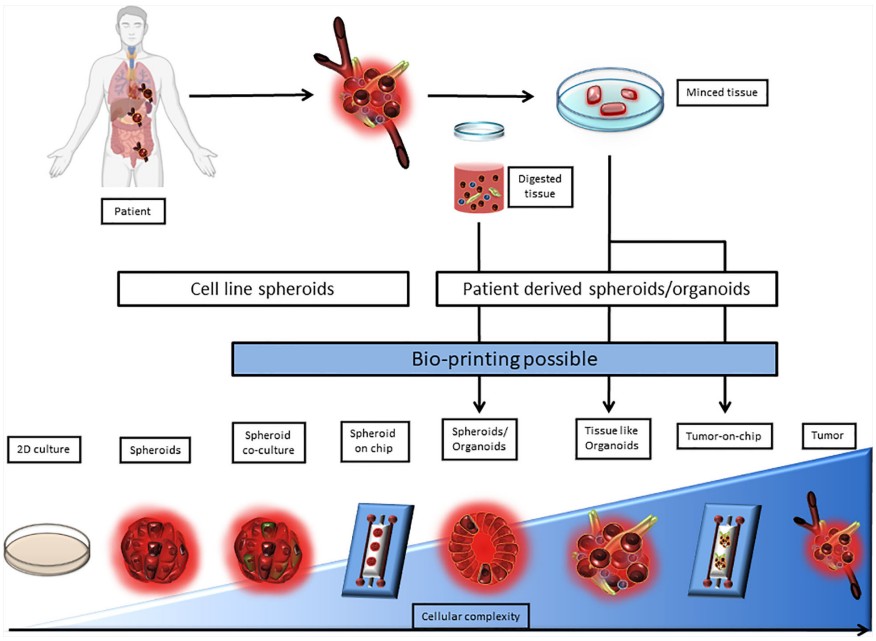

FIGURE 1 | Representation of 3D culture models according to their complexity. 3D culture models are depicted as a range from spheroids derived from a single cell line to a very complex model derived from patient tissue or tumor upgraded with a microfluidic chip. 2D culture and tumor biopsy are used as complexity references. 3D cultures can be separated between cell line derived and patient derived models. Patient derived 3D models require either tissue mincing or both tissue mincing and enzymatic digestion prior to the culture. Noteworthy, Bioprinting can be used to generate most models that require multiple cell type-dependent structures, and can be applied directly on microfluidic chips.

hypoxia (oxygen accumulation), nutrient gradient (glucose distribution), a necrotic/apoptotic core, lactate accumulation, and ATP distribution which the classical 2D culture failed to do (29). Several spheroids can be distinguished, based on cell origin and the culture methods: the multicellular tumor spheroid model (MTCS) using cells line and non-adherent support, tumorosphere using cells obtained from solid tumor dissociation, tissue-derived tumor spheres (TDTS) which comes from cells obtained by a partial dissociation of the solid tumor, and finally, organotypic multicellular spheroids (OMS), which differ of TDTS by the absence of tissue dissociation. Therefore, the methods to generate different type of spheroid vary (30). However, this classification remains blurry between the terms "spheroid" and "organoid," especially when it comes to TDTS and OMS. Nevertheless, the term "spheroid" is commonly used to refer to cell line derived 3D cell cultures. The MTCS model, often derived from primary cell or cell line suspension is the most used and well characterized. Indeed, the MTCS model allows a good representation of oxygen, nutrient, and other soluble factor diffusion and exchange (31). However, to depict these parameters properly, the size of the spheroid needs to be comprised between 0.5 mm^3 and 1 mm^3 (29). A spheroid (>500um) is divided according to three areas from its core to its periphery. First, there is the necrotic/apoptotic core, then a quiescent cell layer, and, at the periphery, proliferative cells (32, 33) which mime tumor growth (30). It is nowadays the most used model for the assessment of immunotherapeutic strategies, thanks to its relatively low cost and high reproducibility (31).

Spheroid models may be used for the testing of immunotherapies, especially to assess the efficiency of therapeutic antibodies and drug screening for the enhancement of immune cell infiltration and anti-tumoral effects against the spheroid targets. Indeed, Courau et al. showed an NKG2D T cell and NK cell infiltrate with a colorectal cancer model of MTCS (HT29 cell line). The targeting of the NKG2D axis, and more precisely MICA/B molecules, highlighted an increase in NK cell infiltrate as well as a greater cytotoxicity. They also demonstrated that a combination of anti-MICA/B and anti NKG2A resulted in a synergistic effect against primary colorectal cancer-derived spheroids (34). Varesano et al. measured the anti-tumoral effect of Vd2 γδ-Tcells against colorectal carcinoma spheroids. Indeed, the authors showed the susceptibility to lysis of colorectal carcinoma spheroid subtypes by Vd2 γδ-Tcells, stimulated with zoledronate or cetuximab, by measuring physical characteristics of spheroids such as volume and area as well as their viability (35). MTCS models can be used to test the efficiency of CAR Tcells. Zhang et al. tested their mesothelin-targeting CAR T cells and found this treatment enhanced the anti-tumoral response in gastric and ovarian MTCS models (36).

Besides the generation of tumor-derived spheroids, another approach consists in the development of immune cell-derived spheroids. In an article where they generate J774.1 macrophage-derived spheroids in polydimethyl soloxane (PDMS) wells, Tanaka et al. could demonstrate that macrophage tend to polarize toward a tumoricidal M1 phenotype, by opposition to M2 pro-tumoral phenotype, in the spheroid condition (37). This seemed to be due to the hypoxia and the increasing production of reactive oxygen

species, parameters which are generated by the structural properties of the macrophage spheroid. The authors proceeded to inject these M1 macrophage spheroids in insulinoma NIT-1 models, or colon adenocarcinoma, and they could demonstrate that spheroid injection led to greater biological activities compared to cell suspension spheroids (37). These models can also be improved and complexified by the technology and the systems being used. Indeed, in the MTCS scaffold-free monocellular model, Sherman et al. added a permeable layer on 96-well plates and could develop a 3D cell culture model which allows the screening of cell migration in a A549 lung carcinoma spheroid model (38). The authors highlight the fact that these models are limited by the absence of stromal cells, which are usually present in the tumor and are critical in the biology of the tumor as well as therapeutic resistance (38). Therefore, the possibility of increasing the diversity of cell types in MTCS cultures is enticing. Jeong et al. improved their colorectal carcinoma spheroid model by adding Cancer Associated Fibroblasts (CAFs). By doing so, they demonstrated that their spheroids became resistant to paclitaxel and modified protein expression, such as CD26 involved in the control of signal transduction for apoptosis and immune regulation (39). Hence, incrementing a monocellular model with another cell type seems necessary to strengthen the representation of the tumor microenvironment. However, to be accurate and mime the tumor composition, the new cell-type(s) should be introduced in the spheroid in a quantitatively accurate manner, meaning that cell ratios in the model should respect what is displayed by the tumor. This, requires an extensive study of tumor cellular composition before the creation of the model. In their scaffold-free MTCS model of pancreatic cancer, Lazzari et al. used the PANC-1 tumor cell line, along with MRC5 fibroblasts and the endothelial HUVEC cell line (40). In another example, Herter et al. demonstrated that the use of IgG-IL2v (an Immunocytokine) combined with the use of a tumor fibroblast-targeted T cell bispecific antibody (TCB) increased the immune infiltrate as well as their cytolytic function in their spheroid model (41). The presence of fibroblasts in the tumor cell culture allows and can even be necessary to allow the formation of spheroids. In our hands, it was the case for MIAPACA and LNCaP pancreatic cancer cell line. The coculture of MIAPACA-derived spheroids with monocytes led to an increase in immunosuppressive cytokines and the polarization of monocytes into monocyte-derived suppressor cells (MDSCs) or M2 polarized macrophages (42).

Patient Derived 3D Models

Organoids are mini-organs reconstituted and embedded in an extracellular matrix. They are obtained from mechanically dissociated or enzymatically digested primary tissue, and arise from stem or slightly differentiated cells. Organoids reproduce the architecture as well as the cellular compartment diversity and organization of the parent tissue, which allows a better modeling of the tissue functions (43). Organoid culture appeared recently in the field of cancer research as the culture of tumor-organoids/Patient-derived organoids (PDOs) only started a decade ago. PDOs allow the 3D culture of cancerous cells isolated from primary tissue digestion, which leads to the loss of stromal and immune compartments. After growing the PDO, which is time consuming (2 to 3 weeks) (43), peripheral blood mononuclear cells (PBMCs) or other immune cell subsets can be added as a coculture. Among patient-derived 3D models can be found multiple models such as, but not limited to:

Tumorospheres: They are spheroid/organoid models, which are generated from cell suspensions after digestion of the original tissue of the tumor. These tumorospheres usually arise from cancer stem cells (CSC), where one isolated CSC should create a spheroid simply by proliferating. Therefore, tumorospheres are clonal models of spheroids/organoids. However, this spheroid model is limited to CSC study as it fails to reproduce the multiplicity of cell types in the TME, and is poorly reproducible as some CSC remain undifferentiated (44).

Tissue derived tumor spheres (TDTSs): They are obtained from enzymatic digestion of the original tumor tissue. This model is therefore composed of tumor cells only and allows to preserve tumoral cell interactions. Indeed, tumor cell interaction are rather strong and resist to enzymatic dissociation while stromal-to-tumor cell interaction are cleaved. TDTSs reproduce small versions of unvascularized tumor areas (30). Among TDTSs, there are spheroids and organoids models. Unfortunately, these denominations also vary with authors and therefore makes it harder to stratify the different models. TDTSs are often use in the study of colorectal tumors, and gave birth to different models such as colospheres. Colospheres are derived from colorectal cancer tumors, which were implanted as PDX in nude female mice and expanded. Tumors were then extracted from mice and cultured to form spheroids (45, 46). Other TDTS models are derived from breast tumors such as MARY-X. MARY-X is a model of TDTS, which was derived from a single breast tumor minced and engrafted as a PDX (patient-derived xenograft) on nude mice. These PDXs were dissociated and mice components removed (99% human cells, "MARY-X shake"). These cells spontaneously form spheroids which are used for experiments (47). Di Liello et al. could demonstrate a reproduction of patient tumor response to chemotherapy by using a spheroid model derived from a non-small cell lung cancer biopsy. This model of spheroid was generated from the cell suspension from the tumor digestion culture on an extracellular matrix (Matrigel) (48). Although tissue digestion preserves tumor cell interaction, the architecture of the tissue is lost and the loss of stromal cells. To palliate to this effect, James et al. developed an organoid model where tumor tissues are digested and cultured in a dome of Matrigel, in a growth factor-enriched media. Simultaneously, CAFs are cultured to generate fibroblasts. These fibroblasts were phenotyped for the expression of Vimentin and were devoided of KRAS mutations (carried by tumor cells). The coculture between the organoids and the fibroblast led to an increased resistance to gemcitabine, therefore showing the importance of the association of stromal and tumor compartments. Furthermore, the authors showed that the addition of lymphocytes in the coculture led them to migrate towards organoids through the Matrigel (49).

Organotypic multicellular spheroid/organoid (OMS): They are simply derived from minced tumor explants cultured media without enzymatic or mechanical digestion, the latter being

required only for longer cultures and passages. OMS are often referred to as tumor explants, tumor slices, PDE (patient derived explant) or organotypic tumor slice culture (TSC). OMS certainly represent the closest models to the parental tumor as they conserve the origin tissue architecture as well as its cellular heterogeneity (30, 50). OMS can usually be cultured for a week according to different methods. Indeed, they can be submerged in culture medium, or with an Air-Liquid Interface. Air-liquid interfaces can be created by putting the OMS in contact with the culture media through a matrix (Geltrex, Matrigel, collagen) or membrane, by entrapping the OMS within gelatin or collagen, which is then put in the culture medium ("sponge method"). OMS can be used for drug testing (51) and biomarker discovery (52) as they represent valid patient pre-clinical models (53, 54). Interestingly, PDEs can be implemented within a microfluidic platform (55) (please see the *Organ-on-Chip* section). Breast cancer tumor explants have been maintained during 7 days in standard culture conditions, and could be used to determine resistance or susceptibility to FAC treatment, which consists in a combination of 5-FU, Adriamicyn, and Cyclophosphamide. However the authors did not describe the immune compartment in their study (51). The immune system component of OMS was investigated in a pancreatic ductal adenocarcinoma culture slice model were the authors observed the presence of $CD8^+$ T cells ($CD3^+$ $CD8^+$), Tregs ($CD3^+$, $FoxP3^+$), and macrophages ($CD68^+$, $CD163^+$, HLA-DR^+) (56). Noteworthy, the pancreatic tumor slice model could be kept in culture for 6 days (56). Powley et al. showed encouraging results for the testing of Immunotherapies using OMS (called PDE). Indeed, they showed that the treatment of melanoma PDE with Nivolumab increased the distance between $CD8^+$ effector T cells and Tregs, avoiding Treg mediated suppression of $CD8^+$ T cells (52). This study is not the sole example of the use of OMS for Immunotherapy testing. OMS derived from pancreatic ductal carcinomas, endometrial cancer, and prostate cancer were used to study new approaches for checkpoint inhibitors and cytotoxic cell recruitment (54, 57, 58). Using models of colospheres generated from the HT29 and DLD-1 cell lines as well as a patient-derived CTO (colorectal tumor organoids) model, Liu et al. evaluated the diffusion and distribution of Cetuximab, a monoclonal antibody targeting the extracellular model of the epidermal growth factor (EGFR) by MALDI-MSI. CTOs are organoids derived from colorectal tumors. Briefly, tumor fragments are embedded in gelatin to keep tissue integrity and cultured in stem cell media. CTOs poorly retain immune cells usually and often require cocultures with immune cells (59). They could show that the diffusion and distribution of Cetuximab in 3D tumor models was similar to those occurring *in vivo* in previous studies (60). Organoids can be cultured in the presence of immune cells to assess their anti-tumoral activity as well as to test methods to stimulate them. Therefore, the adoptive transfer of autologous lymphocytes becomes an attractive strategy (61). Colorectal cancer (CRC)-derived and Non-small cell lung carcinoma (NSCLC)-derived organoids can be cultured in the presence of autologous circulating lymphocytes and IFN-γ to increase antigen presentation. They combined this approach with the use of an anti-PD-L1 mAb to avoid any suppressive effect of IFN-γ derived PD-L1 expression. Among class I MHC expressing CRC-derived organoids, half exhibited an increase of IFN-γ secretion along with an increase in CD107a expression (a surrogate marker for degranulation) in $CD8^+$ T cells. Interestingly, among the responders, 50% did not show tumor specific $CD8^+$ T cells in the blood. In four over five cases, $CD8^+$ T cells activity against organoids was specific, as illustrated by the expression of CD137. Indeed, CD137 was expressed by T cells cultured with organoids in the presence or absence of IFN-γ, and was not expressed when cultured with healthy tissue organoids or in resting conditions. The cell product ($CD137^+$ or expended) showed cytotoxicity against tumor organoids compared to healthy tissue organoids. This effect could be reversed, by adding an anti-MHC class I mAb in the co-culture (62–64).

Patient-derived organoids (PDOs): PDOs and OMS are both tumor or tissue fragments which are cultured in a dish. The difference between OMS and PDOs mainly relies the fact that OMS are a one-step enzyme-free culture while PDO culture requires two steps. Indeed, the first step is similar to OMS culture and preserves tissue integrity. The second step is the organoid expansion, which requires enzymatic dissociation and allows long-term culture but affects tissue integrity. PDOs reflect protein and gene expression from the biopsies they originated from. Multiple models can be found such as non-small cell lung cancer (NSCLC)-derived organoids, CCRC-derived organoids and melanoma-derived organoids, glioblastoma organoids (GBOs). NSCLC-derived organoids, CCRC-derived organoids, and melanoma-derived organoids are minced human tumors, which were cultured on an Air-Liquid Interface cell culture dish, fed with media routinely, and passaged every 2–4 weeks by dissociating PDOs with collagenase IV (65). GBOs are generated by simply culturing tumor slices without enzymatic nor mechanical digestion on an orbital shaker. They can be kept for 2 weeks in these conditions. For extended culture times (>1 month) GBOs are cut to smaller pieces and divided in different subcultures (66). Neal et al. demonstrated that the PD-1/PD-L1 axis was conserved in NSCLC-derived organoids. Noteworthily, their PDO was generated without enzymatic digestion at the first step, whereas different passages to allow longer culture times required enzymatic digestion (65). This protocol allowed the culture of 14 different types of tissue and mimed 28 diseases, with a high culture success rate (73% after a month). The conservation of architectural and cellular features was assessed by microscopy and the presence of the stroma was done by Vimentin and SMA expression. The immune compartment was also observed in these PDO models as $CD3^+CD8^+$ and $CD3^+CD4^+$ T lymphocytes as well as B cells, Natural killer cells and macrophages could be observed (65). More precisely, some of the organoid infiltrating T cells harbored an exhausted phenotype ($LAG3^+TIGIT^+PD\text{-}1^+TIM3^+$) which also could be observed in tumor biopsies. Furthermore, the lymphocyte infiltrate in PDOs conserves its diversity as the TCR clonal diversity was assessed in a comparison between seven different organoid cultures and a biopsy of human clear cell renal carcinoma. The most expanded

clones in tumors were the same in the organoid cultures. However, the immune compartment tends to decrease overtime, and seems to disappear after a month of culture. This effect can be slowed by the addition of cytokines such as IL-2 in the culture media. Therefore, the resemblance of PDOs with their tumor of origin is critical as organoids can therefore be used as tools for the study of response to immunotherapies. Targeting the PD-1/PD-L1 axis in immune-oncology was already proven to be efficient. However, the prediction of the patient response to its treatment is a keystone in the process of improving immunotherapies and PDO cultures might be of help. Neal et al. also tested the response to nivolumab in nine NSCLC, eight CCRC, and three melanomas PDOs. They found that six over 20 PDOs responded to the treatment as T cells expressed higher levels of IFNG, PRF1, and/or GZMB transcripts, and $CD8^+$ T cells proliferated. Among the six organoids that responded to nivolumab, three were from NSCLC, two were from ccRC, and one melanoma. Ten PDO were tested with nivolumab, anti-CD3, and anti-CD28 to allow T cell proliferation and activation. Two PDOs cultured responded to these conditions as tumor infiltrating lymphocytes increased their cytolytic function against tumor cells (65). In another study, Scognamiglio et al. used chordoma-derived organoids to assess the response to nivolumab (anti-PD-1 mAb). Chordoma tissue from each patient were digested and cultured on a Matrigel matrix to form the organoid, then anti-PD-1 or anti-PD-L1 mAbs were added for 24 h. They could observe that PD-L1 expressing PDOs were disrupted and lysed after treatment with Nivolumab, which allows to theoretically predict the response to this immunotherapy in patients (67). Immunotherapies are not limited to antagonistic or agonistic mAbs directed against checkpoint markers such as CTLA-4, PD-1, or PD-L1. Indeed, CAR-T cells are being developed for hematological malignancies and start to be tested against solid tumors. Therefore, Jacob et al. created a model of glioblastoma organoid against which they tested CAR-T cell function. These organoids (GBOs) have the same histological and transcriptomic properties as the tissue the originated from. Also, the cell heterogeneity in GBOs is similar to that of parental tissues and allow to maintain the microenvironment up to 2 weeks after the beginning of the culture. However, the main differences between parental tissue and GBOs are the transcripts related to blood and vasculature functions as well as immune related genes. Among the aspects that are conserved in GBOs, EGFRvIII (epidermal growth factor receptor vIII) is an important marker for glioblastoma progression. Thus, the authors designed EGFRvIII-specific CAR-T cells and performed a co-culture with GBOs. They observed that CAR-T cells were infiltrating and expending in GBOs. This was happening concomitantly to a reduction of EGFRvIII/EGFR ratio intensity and an increase of cleaved-Caspase 3 levels, showing the killing of $EGFRvIII^+$ cells. However, $EGFR^+EGFRvIII^-$ cells remained in the culture after 3 days of co-culture with CAR-T cells, showing the specificity of the CAR-T cells, but also that they may not be sufficient to eradicate the tumor (66). Considering the complexity of the immune-evasion mechanisms by tumors, the prediction of patient response to a specific immunotherapy is key. Noteworthily, there are two registered clinical trials involving cancer organoids for immunotherapy (NCT03778814, NCT02718235). Overall, these results indicate that cancer organoid culture is a promising system to generate tumor-reactive T cells, to predict immunotherapy sensitivity, and to examine combination. Taken together, PDOs represent valid preclinical models in the era of personalized medicine (68).

As complex as these models are, they still lack one or multiple compartments to allow the best representation of the *in vivo* system. Indeed, the vascular system, and therefore the diffusion of drugs, cellular products, and their penetration inside the tumor, is missing in these models. This is being studied and the use of microfluidic systems and/or microchips for the improvement of organoid models is being assessed.

Organ-on-Chip

The three-dimensional spheroid/organoid culture models offer the possibility of approaching the architecture and functionalities of the tissue from which they originate, and despite the advances which make it possible to consider part of the micro-environment such as stroma cells and the TILs (Tumor Infiltrating Leukocytes), it still lacks the dynamics of the environment found *in-vivo*. The strength of the recently applied microfluidic technology in the field of oncology is to combine the advantages of 3D culture in a controllable and dynamic environment. Microfluidics add to the production of spheroids/organoids makes it possible to overcome this default and to position 3D models in a physiologically dynamic environment, making it possible to investigate several parameters of carcinogenesis and to carry out drug screening and predict the response therapies. In a simple manner, the spheroid/organoid formed is placed in a microfluidic chip, the medium being perfused with the addition or not of therapeutic agents (69, 70). This technology can be used for classical cell line-derived spheroids, but also PDOs. Nguyen et al. reconstituted a $HER2^+$ breast tumor from four cell lines, along with its microenvironment. They combined breast cancer, CAF, endothelial cell, and fibroblastic cell lines and cultured them on a micro-fluidic chip. Indeed, they cultured breast tumor cell line and PBMCs in both lateral chambers of the chip, when CAFs where only present in one of the chambers endothelial cells were cultured as a monolayer in the central chamber. Although this model does not use a reperfusion system, this created a flow of media from the lateral chambers through the central one, and mimed a circulation in the tissue. They used their model to evaluate the effect of Trastuzumab, an anti-HER2 mAb and could show that the ADCC effect of trastuzumab was highly reduced in the chamber containing the CAF. The authors concluded that CAFs were modulating the immune cell functions by reducing their contact time with tumor cell lines. This model allowed the testing of a therapeutic agent in a complex 3D system, which allows perfusion of soluble molecules (71).

PDOs can also be placed on fluidic microchips. In a study using the 40 to 100 μm fractions of the digested tissue, the authors could generate organoids which contained the TME as well as the immune cell populations (B cells, $CD4^+$ and $CD8^+$ T cells, myeloid cell subsets). They could also demonstrate that

some T cells expressed immune checkpoint markers such as PD-1, CTLA-4, and TIM3. These organoids were place on a microfluidic chip to test an anti-PD-1 treatment and the eventuality of a resistance to this treatment. The authors could show that CCL19 and CXCL13, two chemokines involved in the recruitment of immune cells, were produced in the anti-PD-1 treated organoids. The cytokine secretion profile was assessed and revealed that the organoids which were treated by anti-PD-1 expressed the IPRES (innate PD-1 resistance) signature. This signature is a cocktail of cytokines which are expressed by patient with a shorter progression free survival. Therefore, this microchip organoid model allows to assess the resistance to checkpoint blockade resistance, and maybe allow a better distribution of these treatments to patients (72–74). Different models of microchip exist and all are adaptable to the need of studies. Initially, these chips were used to study tumor cells migration as well as macrophages (75), dendritic cells (76), PBMCs in general (77), and TILs (78). Indeed, Moore et al. used a model of multiplexed microfluidic perfusion named EVIDENT (*Ex-Vivo* Immuno-oncology Dynamic Environment for tumor biopsies). This model can hold up to 12 tumor tissue samples which can interact with their autologous perfused TILs. They could test multiple immune checkpoint inhibitors simultaneously and observe immune cell infiltration and cytotoxicity. In these conditions the organoids can be cultured for 5 days. To test the effect of anti-PD-1 blockade, the authors used murine tumors generated by subcutaneous injection of MC38 cell line. TILs were isolated and expended, and incubated with an anti-PD-1 overnight before the experiment in the microfluidic system. Here, they could demonstrate that TIL infiltration of organoids as well as cytotoxicity was increased in anti-PD-1 treatment conditions. They could replicate this result by using a human biopsy of NSCLC after treatment of the TILs with anti-PD-1 (78). The microfluidic technology is therefore a tool in the study of 3D culture models and immunotherapies. Indeed, as we discussed above, Immune checkpoint blockade and CAR-T cells can be investigated at the level of infiltration, immune checkpoint expression and cytotoxicity (72). Although this model is not standardized, and that the design is dependent on each team, microfluidic are promising and allow to make another step towards *in vitro*-preclinical models (39, 68).

3D Bioprinting

Bio-printing allows the reconstruction of 3D tissue by organizing drops on a cell culture treated surface. These drops contain both extracellular matrix as well as tumor cells. The advantage of this model is that the organization of the tissue can be fully designed, and drops can be hardened chemically or mechanically to obtain the desired tissue resistance. Bio-printing therefore allows a very precise in terms of tissue architecture and cellular placements. There are three types of bio-printers, droplet bio-printing, extrusion bio-printing, and laser bio-printing. Droplet bio-printing, is the most used technique in the pharmaceutical industry thanks to its high throughput yield (79–81). As an example, bioprinting was used to generate a breast cancer model using MDAMB-231 cells and RAW264.7 macrophages. Here, the aim was to study the two cell type interactions in an accurate representation of the TME (82). Although bioprinting is a very recent and still little used technology in the field of tumor immunology, it remains a promising candidate in the testing of immunotherapy strategies (83).

DISCUSSION

As we described, 3D cell culture is constantly evolving and offers more and more opportunities to use these models as pre-clinical tests for the screening of therapies, as well as personalized medicine with PDOs. It is important to keep in mind that the evolution of 3D culture models evolves toward a better representation of human or murine tissues and tumors *in vitro*. The TME, CAFs, and TILs play a critical role in the evolution of a tumor and its resistance to diverse treatments (38, 84, 85), such as CAFs which reduce the ADCC effect of Trastuzumab (70). Therefore, 3D models provide a mean to study the TME by incorporating it in spheroids and organoids.

Cell line-derived spheroids coculture with fibroblasts and immune cells is relatively cheap, reproducible, and might be used as a high throughput technology to test therapeutic mAbs or drugs and even cell therapies such as CAR-T cells (86). The effect of therapies on spheroids is measured by microscopy, mainly by assessing sphere volume, circularity, and cell viability. However, not all cell lines spontaneously form spheroids. Indeed, to be a valid model, spheroids should reach a sufficient size to form a central apoptotic or necrotic core and therefore a gradient of oxygen, nutrient and lactate accumulation (29, 32, 33). Another limitation of the extracellular matrix embedded-MCTS is the effect of Matrigel or Geltrex on immune cells. Both matrixes are generated from murine sarcoma and therefore are compose of great murine antigen amounts, which can activate immune cell subtypes such as $CD4^+$ T cells (87). These limitations can be avoided by using synthetic or collagen extracellular matrix (88). Recently, the culture of tumoral tissue digestion products in an extracellular matrix and a growth factor enriched culture media allowed the creation of patient derived spheroids or organoids. This model gets more and more attention and is extensively being studied because they accurately represent the origin tissue properties, even at the genetic level where mutations are conserved (64, 67). Immune cell coculture with PDOs represent a valid model to evaluate the effect of immune checkpoint blockade, CAR-T cell infusion, to educate T cells to recognize tumor antigens and to predict patient response to these therapies. Although PDO represent another step toward a complete imitation of *in vivo* tissues, these models also have inconvenient. Indeed, their culture requires the bio banking of samples, which can be expensive, and the time of these cultures can be long, up to 2 months to obtain a stable culture. Furthermore, the culture of PDO also requires a non-synthetic or collagen extracellular matrix (89).

Noteworthy, the possibility to transfer 3D culture back to 2D culture exists. This was performed on canine bladder cancer organoids. The culture medium was modified so that cell from the organoid would migrate to the bottom of the flask and create what the authors called a 2.5 organoid. This culture method is less restrictive and expensive than that of the 3D models, and still shares the major compartments of the original tumor tissue (90).

However, this model does not seem suitable to study immunology or immunotherapy as the immune compartment is lost. This highlight the fact that the conservation or incorporation of the immune system remains challenging (90). In the organoid or spheroid models that require tissue digestion, the incorporation of PBMCs at the time of the culture is possible but do not represent the profile of the TILs. On the contrary, PDOs, which are not or only partially digested, conserve the original TILs but do not represent the part of immune cell which are recruited from the blood. Another issue in the PDOs is the survival of immune cell which can be boosted (up to a month) by adding IL-2 in the culture media. This ALI model allows the testing of Immune checkpoint blockade mAbs since the PD-1/PD-L1 axis is conserved. Furthermore, these PDOs can be bio-banked to allow further testing patient per patient. The major drawback of this model is that the first organoid culture has to be performed on a high-quality fresh tissue sample, which means that the time between surgery and the beginning of the culture as to be as short as possible. This impacts the reproducibility as the quality of the sample decreases quickly over time in terms of architecture and cell population viability.

To complete these already complex models, technologies such as microfluidics or microchips allow to culture organoids or spheroids into dynamic models. Indeed, they mime vascularization, cell and soluble molecules such as antibodies diffusion (49). The EVIDENT technology from Bornstein et al. pushed the use of microfluidics forward as it allows the testing of multiple conditions at the same time on a single chip. Although this method requires the freezing of both TILs and tissues, it open the way to pre-clinical models of organoids where the testing of multiple conditions or drugs are required at the same time. Furthermore, the fact that the experiment is performed on the same microchip avoid batch effects between conditions (78). The EVIDENT approach is rather fast (2 weeks compared to 1–2 months) and is still able to mime the vascularization that to the microfluidics. The notions of time and speed are critical here, especially when this model might be used for the testing of therapies and/or the assessment of patient response to the treatments. They also provide a time advantage against patient derived xenografts (PDX, patient tumor engrafted on NGS mice), which take 3 to 5 months to be used.

PDX, on their side, possess the advantages of *in vivo* models with vascularization and allow the testing of virtually any drugs or treatment. However, these models are transient as the engrafted tumor and its TME are slowly being replaced by that of the murine (91). Also, the patient immune system is not engrafted on the host and therefore would require the use of humanized hosts. PDX remain long and requires constant care and an animal facility. However, it remains possible to engraft organoids to mice, resect them the organoids to put them back in culture. Interestingly, PDX can also be resected from mice to be used as basis for organoids or spheroids.

Overall, 3D models are a crucial tool in the development of new immunotherapy strategies (92). Indeed, evolved models such as PDOs, coupled with microfluidics or not, represent promising pre-clinical models to test patient response to therapies.

AUTHOR CONTRIBUTIONS

NB designed and wrote the manuscript. LG designed, wrote, and proofread the manuscript. DO funded and proofread the manuscript. All authors contributed to the article and approved the submitted version.

FUNDING

DO team was labeled "Equipe FRM DEQ20180339209." DO is Senior Scholar of the Institut Universitaire de France. LG is supported by a Fondation ARC experienced post-doc/young researcher fellowship (Aides individuelles—session de printemps 2018- Post-doctorat en France).

REFERENCES

1. Hui L, Chen Y. Tumor microenvironment: Sanctuary of the devil. *Cancer Lett* (2015) 368:7–13. doi: 10.1016/j.canlet.2015.07.039
2. Locy H, de Mey S, de Mey W, De Ridder M, Thielemans K, Maenhout SK. Immunomodulation of the Tumor Microenvironment: Turn Foe Into Friend. *Front Immunol* (2018) 9:2909. doi: 10.3389/fimmu.2018.02909
3. Dysthe M, Parihar R. Myeloid-Derived Suppressor Cells in the Tumor Microenvironment. *Adv Exp Med Biol* (2020) 1224:117–40. doi: 10.1007/978-3-030-35723-8_8
4. Wolf D, Sopper S, Pircher A, Gast G, Wolf AM. Treg(s) in Cancer: Friends or Foe? *J Cell Physiol* (2015) 230:2598–605. doi: 10.1002/jcp.25016
5. Alsaab HO, Sau S, Alzhrani R, Tatiparti K, Bhise K, Kashaw SK, et al. PD-1 and PD-L1 Checkpoint Signaling Inhibition for Cancer Immunotherapy: Mechanism, Combinations, and Clinical Outcome. *Front Pharmacol* (2017) 8:561. doi: 10.3389/fphar.2017.00561
6. Feng R, Zhao H, Xu J, Shen C. CD47: the next checkpoint target for cancer immunotherapy. *Crit Rev Oncol Hematol* (2020) 152:103014. doi: 10.1016/j.critrevonc.2020.103014
7. Chen X, Song E. Turning foes to friends: targeting cancer-associated fibroblasts. *Nat Rev Drug Discov* (2019) 18:99–115. doi: 10.1038/s41573-018-0004-1
8. Noy R, Pollard JW. Tumor-associated macrophages: from mechanisms to therapy. *Immunity* (2014) 41:49–61. doi: 10.1016/j.immuni.2014.06.010
9. Wu T, Dai Y. Tumor microenvironment and therapeutic response. *Cancer Lett* (2017) 387:61–8. doi: 10.1016/j.canlet.2016.01.043
10. Wei SC, Duffy CR, Allison JP. Fundamental Mechanisms of Immune Checkpoint Blockade Therapy. *Cancer Discov* (2018) 8:1069–86. doi: 10.1158/2159-8290.CD-18-0367
11. Amatore F, Gorvel L, Olive D. Role of Inducible Co-Stimulator (ICOS) in cancer immunotherapy. *Expert Opin Biol Ther* (2020) 20:141–50. doi: 10.1080/14712598.2020.1693540
12. Gorvel L, Olive D. Targeting the "PVR-TIGIT axis" with immune checkpoint therapies. *F1000Res* (2020) 9(F1000 Faculty Rev):354. doi: 10.12688/f1000research.22877.1
13. Mercogliano MF, Bruni S, Elizalde PV, Schillaci R. Tumor Necrosis Factor alpha Blockade: An Opportunity to Tackle Breast Cancer. *Front Oncol* (2020) 10:584. doi: 10.3389/fonc.2020.00584
14. Gorczynski RM. IL-17 Signaling in the Tumor Microenvironment. *Adv Exp Med Biol* (2020) 1240:47–58. doi: 10.1007/978-3-030-38315-2_4
15. Kang S, Tanaka T, Narazaki M, Kishimoto T. Targeting Interleukin-6 Signaling in Clinic. *Immunity* (2019) 50:1007–23. doi: 10.1016/j.immuni.2019.03.026
16. Wente MN, Keane MP, Burdick MD, Friess H, Buchler MW, Ceyhan GO, et al. Blockade of the chemokine receptor CXCR2 inhibits pancreatic cancer

cell-induced angiogenesis. *Cancer Lett* (2006) 241:221–7. doi: 10.1016/j.canlet.2005.10.041
17. Tanabe Y, Sasaki S, Mukaida N, Baba T. Blockade of the chemokine receptor, CCR5, reduces the growth of orthotopically injected colon cancer cells via limiting cancer-associated fibroblast accumulation. *Oncotarget* (2016) 7 (30):48335–45. doi: 10.18632/oncotarget.10227
18. Harari A, Graciotti M, Bassani-Sternberg M, Kandalaft LE. Antitumour dendritic cell vaccination in a priming and boosting approach. *Nat Rev Drug Discov* (2020) 19(9):635–52. doi: 10.1038/s41573-020-0074-8
19. Palucka K, Banchereau J. Dendritic-cell-based therapeutic cancer vaccines. *Immunity* (2013) 39:38–48. doi: 10.1016/j.immuni.2013.07.004
20. Labanieh L, Majzner RG, Mackall CL. Programming CAR-T cells to kill cancer. *Nat BioMed Eng* (2018) 2:377–91. doi: 10.1038/s41551-018-0235-9
21. Adachi K, Kano Y, Nagai T, Okuyama N, Sakoda Y, Tamada K. IL-7 and CCL19 expression in CAR-T cells improves immune cell infiltration and CAR-T cell survival in the tumor. *Nat Biotechnol* (2018) 36:346–51. doi: 10.1038/nbt.4086
22. Martinez M, Moon EK. CAR T Cells for Solid Tumors: New Strategies for Finding, Infiltrating, and Surviving in the Tumor Microenvironment. *Front Immunol* (2019) 10:128. doi: 10.3389/fimmu.2019.00128
23. Kelm JM, Timmins NE, Brown CJ, Fussenegger M, Nielsen LK. Method for generation of homogeneous multicellular tumor spheroids applicable to a wide variety of cell types. *Biotechnol Bioeng* (2003) 83:173–80. doi: 10.1002/bit.10655
24. Nickerson P, Jeffery J, Rush D. Long-term allograft surveillance: the role of protocol biopsies. *Curr Opin Urol* (2001) 11:133–7. doi: 10.1097/00042307-200103000-00002
25. Cukierman E, Pankov R, Stevens DR, Yamada KM. Taking cell-matrix adhesions to the third dimension. *Science* (2001) 294:1708–12. doi: 10.1126/science.1064829
26. Delarue M, Montel F, Vignjevic D, Prost J, Joanny JF, Cappello G. Compressive stress inhibits proliferation in tumor spheroids through a volume limitation. *Biophys J* (2014) 107:1821–8. doi: 10.1016/j.bpj.2014.08.031
27. Delarue M, Joanny JF, Julicher F, Prost J. Stress distributions and cell flows in a growing cell aggregate. *Interface Focus* (2014) 4:20140033. doi: 10.1098/rsfs.2014.0033
28. Ramgolam K, Lauriol J, Lalou C, Lauden L, Michel L, de la Grange P, et al. Melanoma spheroids grown under neural crest cell conditions are highly plastic migratory/invasive tumor cells endowed with immunomodulator function. *PLoS One* (2011) 6:e18784. doi: 10.1371/journal.pone.0018784
29. Groebe K, Mueller-Klieser W. Distributions of oxygen, nutrient, and metabolic waste concentrations in multicellular spheroids and their dependence on spheroid parameters. *Eur Biophys J* (1991) 19:169–81. doi: 10.1007/BF00196343
30. Weiswald LB, Bellet D, Dangles-Marie V. Spherical cancer models in tumor biology. *Neoplasia* (2015) 17:1–15. doi: 10.1016/j.neo.2014.12.004
31. Nunes AS, Barros AS, Costa EC, Moreira AF, Correia IJ. 3D tumor spheroids as in vitro models to mimic in vivo human solid tumors resistance to therapeutic drugs. *Biotechnol Bioeng* (2019) 116:206–26. doi: 10.1002/bit.26845
32. Hirschhaeuser F, Menne H, Dittfeld C, West J, Mueller-Klieser W, Kunz-Schughart LA. Multicellular tumor spheroids: an underestimated tool is catching up again. *J Biotechnol* (2010) 148:3–15. doi: 10.1016/j.jbiotec.2010.01.012
33. Bell HS, Whittle IR, Walker M, Leaver HA, Wharton SB. The development of necrosis and apoptosis in glioma: experimental findings using spheroid culture systems. *Neuropathol Appl Neurobiol* (2001) 27:291–304. doi: 10.1046/j.0305-1846.2001.00319.x
34. Courau T, Bonnereau J, Chicoteau J, Bottois H, Remark R, Assante Miranda L, et al. Cocultures of human colorectal tumor spheroids with immune cells reveal the therapeutic potential of MICA/B and NKG2A targeting for cancer treatment. *J Immunother Cancer* (2019) 7:74. doi: 10.1186/s40425-019-0553-9
35. Varesano S, Zocchi MR, Poggi A. Zoledronate Triggers Vdelta2 T Cells to Destroy and Kill Spheroids of Colon Carcinoma: Quantitative Image Analysis of Three-Dimensional Cultures. *Front Immunol* (2018) 9:998. doi: 10.3389/fimmu.2018.01343
36. Zhang Z, Jiang D, Yang H, He Z, Liu X, Qin W, et al. Modified CAR T cells targeting membrane-proximal epitope of mesothelin enhances the antitumor function against large solid tumor. *Cell Death Dis* (2019) 10:476. doi: 10.1038/s41419-019-1711-1
37. Tanaka Y, Nishikawa M, Mizukami Y, Kusamori K, Ogino Y, Nishimura S, et al. Control of polarization and tumoricidal activity of macrophages by multicellular spheroid formation. *J Control Release* (2018) 270:177–83. doi: 10.1016/j.jconrel.2017.12.006
38. Sherman H, Gitschier HJ, Rossi AE. A Novel Three-Dimensional Immune Oncology Model for High-Throughput Testing of Tumoricidal Activity. *Front Immunol* (2018) 9:857. doi: 10.3389/fimmu.2018.00857
39. Jeong SY, Lee JH, Shin Y, Chung S, Kuh HJ. Co-Culture of Tumor Spheroids and Fibroblasts in a Collagen Matrix-Incorporated Microfluidic Chip Mimics Reciprocal Activation in Solid Tumor Microenvironment. *PLoS One* (2016) 11:e0159013. doi: 10.1371/journal.pone.0159013
40. Lazzari G, Nicolas V, Matsusaki M, Akashi M, Couvreur P, Mura S. Multicellular spheroid based on a triple co-culture: A novel 3D model to mimic pancreatic tumor complexity. *Acta Biomater* (2018) 78:296–307. doi: 10.1016/j.actbio.2018.08.008
41. Herter S, Morra L, Schlenker R, Sulcova J, Fahrni L, Waldhauer I, et al. A novel three-dimensional heterotypic spheroid model for the assessment of the activity of cancer immunotherapy agents. *Cancer Immunol Immunother* (2017) 66:129–40. doi: 10.1007/s00262-016-1927-1
42. Kuen J, Darowski D, Kluge T, Majety M. Pancreatic cancer cell/fibroblast co-culture induces M2 like macrophages that influence therapeutic response in a 3D model. *PLoS One* (2017) 12:e0182039. doi: 10.1371/journal.pone.0182039
43. Lou YR, Leung AW. Next generation organoids for biomedical research and applications. *Biotechnol Adv* (2018) 36:132–49. doi: 10.1016/j.biotechadv.2017.10.005
44. Valent P, Bonnet D, De Maria R, Lapidot T, Copland M, Melo JV, et al. Cancer stem cell definitions and terminology: the devil is in the details. *Nat Rev Cancer* (2012) 12:767–75. doi: 10.1038/nrc3368
45. Weiswald LB, Richon S, Validire P, Briffod M, Lai-Kuen R, Cordelieres FP, et al. Newly characterised ex vivo colospheres as a three-dimensional colon cancer cell model of tumour aggressiveness. *Br J Cancer* (2009) 101:473–82. doi: 10.1038/sj.bjc.6605173
46. Weiswald LB, Richon S, Massonnet G, Guinebretiere JM, Vacher S, Laurendeau I, et al. A short-term colorectal cancer sphere culture as a relevant tool for human cancer biology investigation. *Br J Cancer* (2013) 108:1720–31. doi: 10.1038/bjc.2013.132
47. Alpaugh ML, Tomlinson JS, Shao ZM, Barsky SH. A novel human xenograft model of inflammatory breast cancer. *Cancer Res* (1999) 59:5079–84
48. Di Liello R, Ciaramella V, Barra G, Venditti M, Della Corte CM, Papaccio F, et al. Ex vivo lung cancer spheroids resemble treatment response of a patient with NSCLC to chemotherapy and immunotherapy: case report and translational study. *ESMO Open* (2019) 4:e000536. doi: 10.1136/esmoopen-2019-000536
49. Tsai S, McOlash L, Palen K, Johnson B, Duris C, Yang Q, et al. Development of primary human pancreatic cancer organoids, matched stromal and immune cells and 3D tumor microenvironment models. *BMC Cancer* (2018) 18:335. doi: 10.1186/s12885-018-4238-4
50. Kenerson HL, Sullivan KM, Seo YD, Stadeli KM, Ussakli C, Yan X, et al. Tumor slice culture as a biologic surrogate of human cancer. *Ann Transl Med* (2020) 8:114. doi: 10.21037/atm.2019.12.88
51. Dhandapani M, Goldman A. Preclinical Cancer Models and Biomarkers for Drug Development: New Technologies and Emerging Tools. *J Mol Biomark Diagn* (2017) 8(5):356. doi: 10.4172/2155-9929.1000356
52. Powley IR, Patel M, Miles G, Pringle H, Howells L, Thomas A, et al. Patient-derived explants (PDEs) as a powerful preclinical platform for anti-cancer drug and biomarker discovery. *Br J Cancer* (2020) 122:735–44. doi: 10.1038/s41416-019-0672-6
53. Majumder B, Baraneedharan U, Thiyagarajan S, Radhakrishnan P, Narasimhan H, Dhandapani M, et al. Predicting clinical response to anticancer drugs using an ex vivo platform that captures tumour heterogeneity. *Nat Commun* (2015) 6:6169. doi: 10.1038/ncomms7169
54. Collins A, Miles GJ, Wood J, MacFarlane M, Pritchard C, Moss E. Patient-derived explants, xenografts and organoids: 3-dimensional patient-relevant pre-clinical models in endometrial cancer. *Gynecol Oncol* (2020) 156:251–9. doi: 10.1016/j.ygyno.2019.11.020
55. Horowitz LF, Rodriguez AD, Dereli-Korkut Z, Lin R, Castro K, Mikheev AM, et al. Multiplexed drug testing of tumor slices using a microfluidic platform. *NPJ Precis Oncol* (2020) 4:12. doi: 10.1038/s41698-020-0117-y
56. Jiang X, Seo YD, Chang JH, Coveler A, Nigjeh EN, Pan S, et al. Long-lived pancreatic ductal adenocarcinoma slice cultures enable precise study of the

immune microenvironment. *Oncoimmunology* (2017) 6:e1333210. doi: 10.1080/2162402X.2017.1333210
57. Seo YD, Jiang X, Sullivan KM, Jalikis FG, Smythe KS, Abbasi A, et al. Mobilization of CD8(+) T Cells via CXCR4 Blockade Facilitates PD-1 Checkpoint Therapy in Human Pancreatic Cancer. *Clin Cancer Res* (2019) 25:3934–45. doi: 10.1158/1078-0432.CCR-19-0081
58. Muthuswamy R, Corman JM, Dahl K, Chatta GS, Kalinski P. Functional reprogramming of human prostate cancer to promote local attraction of effector CD8(+) T cells. *Prostate* (2016) 76:1095–105. doi: 10.1002/pros.23194
59. Kondo J, Endo H, Okuyama H, Ishikawa O, Iishi H, Tsujii M, et al. Retaining cell-cell contact enables preparation and culture of spheroids composed of pure primary cancer cells from colorectal cancer. *Proc Natl Acad Sci U S A* (2011) 108:6235–40. doi: 10.1073/pnas.1015938108
60. Liu X, Lukowski JK, Flinders C, Kim S, Georgiadis RA, Mumenthaler SM, et al. MALDI-MSI of Immunotherapy: Mapping the EGFR-Targeting Antibody Cetuximab in 3D Colon-Cancer Cell Cultures. *Anal Chem* (2018) 90:14156–64. doi: 10.1021/acs.analchem.8b02151
61. Rosenberg SA, Restifo NP. Adoptive cell transfer as personalized immunotherapy for human cancer. *Science* (2015) 348:62–8. doi: 10.1126/science.aaa4967
62. Sachs N, de Ligt J, Kopper O, Gogola E, Bounova G, Weeber F, et al. A Living Biobank of Breast Cancer Organoids Captures Disease Heterogeneity. *Cell* (2018) 172:373–86.e10. doi: 10.1016/j.cell.2017.11.010
63. Cattaneo CM, Dijkstra KK, Fanchi LF, Kelderman S, Kaing S, van Rooij N, et al. Tumor organoid-T-cell coculture systems. *Nat Protoc* (2020) 15:15–39. doi: 10.1038/s41596-019-0232-9
64. Sahin U. Studying Tumor-ReacTive T Cells: A Personalized Organoid Model. *Cell Stem Cell* (2018) 23:318–9. doi: 10.1016/j.stem.2018.08.015
65. Neal JT, Li X, Zhu J, Giangarra V, Grzeskowiak CL, Ju J, et al. Organoid Modeling of the Tumor Immune Microenvironment. *Cell* (2018) 175:1972–88.e16. doi: 10.1016/j.cell.2018.11.021
66. Jacob F, Salinas RD, Zhang DY, Nguyen PTT, Schnoll JG, Wong SZH, et al. A Patient-Derived Glioblastoma Organoid Model and Biobank Recapitulates Inter- and Intra-tumoral Heterogeneity. *Cell* (2020) 180:188–204.e22. doi: 10.1016/j.cell.2019.11.036
67. Scognamiglio G, De Chiara A, Parafioriti A, Armiraglio E, Fazioli F, Gallo M, et al. Patient-derived organoids as a potential model to predict response to PD-1/PD-L1 checkpoint inhibitors. *Br J Cancer* (2019) 121:979–82. doi: 10.1038/s41416-019-0616-1
68. Aboulkheyr Es H, Montazeri L, Aref AR, Vosough M, Baharvand H. Personalized Cancer Medicine: An Organoid Approach. *Trends Biotechnol* (2018) 36:358–71. doi: 10.1016/j.tibtech.2017.12.005
69. Bhatia SN, Ingber DE. Microfluidic organs-on-chips. *Nat Biotechnol* (2014) 32:760–72. doi: 10.1038/nbt.2989
70. Sontheimer-Phelps A, Hassell BA, Ingber DE. Modelling cancer in microfluidic human organs-on-chips. *Nat Rev Cancer* (2019) 19:65–81. doi: 10.1038/s41568-018-0104-6
71. Nguyen M, De Ninno A, Mencattini A, Mermet-Meillon F, Fornabaio G, Evans SS, et al. Dissecting Effects of Anti-cancer Drugs and Cancer-Associated Fibroblasts by On-Chip Reconstitution of Immunocompetent Tumor Microenvironments. *Cell Rep* (2018) 25:3884–93.e3. doi: 10.1016/j.celrep.2018.12.015
72. Aung A, Kumar V, Theprungsirikul J, Davey SK, Varghese S. An Engineered Tumor-on-a-Chip Device with Breast Cancer-Immune Cell Interactions for Assessing T-cell Recruitment. *Cancer Res* (2020) 80:263–75. doi: 10.1158/0008-5472.CAN-19-0342
73. Jenkins RW, Aref AR, Lizotte PH, Ivanova E, Stinson S, Zhou CW, et al. Ex Vivo Profiling of PD-1 Blockade Using Organotypic Tumor Spheroids. *Cancer Discov* (2018) 8(2):196–215. doi: 10.1158/2159-8290.CD-17-0833
74. Aref AR, Campisi M, Ivanova E, Portell A, Larios D, Piel BP, et al. 3D microfluidic ex vivo culture of organotypic tumor spheroids to model immune checkpoint blockade. *Lab Chip* (2018) 18:3129–43. doi: 10.1039/C8LC00322J
75. Zervantonakis IK, Hughes-Alford SK, Charest JL, Condeelis JS, Gertler FB, Kamm RD. Three-dimensional microfluidic model for tumor cell intravasation and endothelial barrier function. *Proc Natl Acad Sci U S A* (2012) 109:13515–20. doi: 10.1073/pnas.1210182109
76. Agliari E, Biselli E, De Ninno A, Schiavoni G, Gabriele L, Gerardino A, et al. Cancer-driven dynamics of immune cells in a microfluidic environment. *Sci Rep* (2014) 4:6639. doi: 10.1038/srep06639
77. Biselli E, Agliari E, Barra A, Bertani FR, Gerardino A, De Ninno A, et al. Organs on chip approach: a tool to evaluate cancer -immune cells interactions. *Sci Rep* (2017) 7:12737. doi: 10.1038/s41598-017-13070-3
78. Moore N, Doty D, Zielstorff M, Kariv I, Moy LY, Gimbel A, et al. A multiplexed microfluidic system for evaluation of dynamics of immune-tumor interactions. *Lab Chip* (2018) 18:1844–58. doi: 10.1039/C8LC00256H
79. Knowlton S, Onal S, Yu CH, Zhao JJ, Tasoglu S. Bioprinting for cancer research. *Trends Biotechnol* (2015) 33:504–13. doi: 10.1016/j.tibtech.2015.06.007
80. Belgodere JA, King CT, Bursavich JB, Burow ME, Martin EC, Jung JP. Engineering Breast Cancer Microenvironments and 3D Bioprinting. *Front Bioeng Biotechnol* (2018) 6:66. doi: 10.3389/fbioe.2018.00066
81. Langer EM, Allen-Petersen BL, King SM, Kendsersky ND, Turnidge MA, Kuziel GM, et al. Modeling Tumor Phenotypes In Vitro with Three-Dimensional Bioprinting. *Cell Rep* (2019) 26:608–23.e6. doi: 10.1016/j.celrep.2018.12.090
82. Grolman JM, Zhang D, Smith AM, Moore JS, Kilian KA. Rapid 3D Extrusion of Synthetic Tumor Microenvironments. *Adv Mater* (2015) 27:5512–7. doi: 10.1002/adma.201501729
83. Zhang YS, Duchamp M, Oklu R, Ellisen LW, Langer R, Khademhosseini A. Bioprinting the Cancer Microenvironment. *ACS Biomater Sci Eng* (2016) 2:1710–21. doi: 10.1021/acsbiomaterials.6b00246
84. Belli C, Trapani D, Viale G, D'Amico P, Duso BA, Della Vigna P, et al. Targeting the microenvironment in solid tumors. *Cancer Treat Rev* (2018) 65:22–32. doi: 10.1016/j.ctrv.2018.02.004
85. Alvarez R, Musteanu M, Garcia-Garcia E, Lopez-Casas PP, Megias D, Guerra C, et al. Stromal disrupting effects of nab-paclitaxel in pancreatic cancer. *Br J Cancer* (2013) 109:926–33. doi: 10.1038/bjc.2013.415
86. Friedrich J, Seidel C, Ebner R, Kunz-Schughart LA. Spheroid-based drug screen: considerations and practical approach. *Nat Protoc* (2009) 4:309–24. doi: 10.1038/nprot.2008.226
87. Dijkstra KK, Cattaneo CM, Weeber F, Chalabi M, van de Haar J, Fanchi LF, et al. Generation of Tumor-Reactive T Cells by Co-culture of Peripheral Blood Lymphocytes and Tumor Organoids. *Cell* (2018) 174:1586–98.e12. doi: 10.1016/j.cell.2018.07.009
88. Gjorevski N, Sachs N, Manfrin A, Giger S, Bragina ME, Ordonez-Moran P, et al. Designer matrices for intestinal stem cell and organoid culture. *Nature* (2016) 539:560–4. doi: 10.1038/nature20168
89. Jee JH, Lee DH, Ko J, Hahn S, Jeong SY, Kim HK, et al. Development of Collagen-Based 3D Matrix for Gastrointestinal Tract-Derived Organoid Culture. *Stem Cells Int* (2019) 2019:8472712. doi: 10.1155/2019/8472712
90. Abugomaa A, Elbadawy M, Yamanaka M, Goto Y, Hayashi K, Mori T, et al. Establishment of 2.5D organoid culture model using 3D bladder cancer organoid culture. *Sci Rep* (2020) 10:9393. doi: 10.1038/s41598-020-66229-w
91. Chao C, Widen SG, Wood TG, Zatarain JR, Johnson P, Gajjar A, et al. Patient-derived Xenografts from Colorectal Carcinoma: A Temporal and Hierarchical Study of Murine Stromal Cell Replacement. *Anticancer Res* (2017) 37:3405–12. doi: 10.21873/anticanres.11707
92. Karolak A, Markov DA, McCawley LJ, Rejniak KA. Towards personalized computational oncology: from spatial models of tumour spheroids, to organoids, to tissues. *J R Soc Interface* (2018) 15(138):20170703. doi: 10.1098/rsif.2017.0703

Conflict of Interest: DO is a cofounder and shareholder of Imcheck Therapeutics, Emergence Therapeutics, and Alderaan Biotechnology.

The remaining authors declare that the research was conducted in the absence of any commercial or financial relationships that could be construed as a potential conflict of interest.

The handling editor declared a past co-authorship with one of the authors DO.

frontiers in Immunology

METHODS
published: 23 December 2020
doi: 10.3389/fimmu.2020.564887

Physical Characterization of Colorectal Cancer Spheroids and Evaluation of NK Cell Infiltration Through a Flow-Based Analysis

*Azzurra Sargenti[1], Francesco Musmeci[1], Francesco Bacchi[1], Cecilia Delprete[2], Domenico Andrea Cristaldi[1], Federica Cannas[1], Simone Bonetti[1], Simone Pasqua[1], Daniele Gazzola[1], Delfina Costa[3], Federico Villa[3], Maria Raffaella Zocchi[4] and Alessandro Poggi[3]**

[1] CellDynamics isrl, Bologna, Italy, [2] Laboratory of Human and General Physiology, Department of Pharmacy and Biotechnology (FaBiT), University of Bologna, Bologna, Italy, [3] Molecular Oncology and Angiogenesis Unit, Istituto di Ricovero e Cura a Carattere Scientifico (IRCCS) Ospedale Policlinico San Martino, Genoa, Italy, [4] Division of Immunology, Transplants and Infectious Diseases, Istituto di Ricovero e Cura a Carattere Scientifico (IRCCS) San Raffaele Scientific Institute, Milan, Italy

OPEN ACCESS

Edited by:
Jacques Zimmer, Luxembourg Institute of Health, Luxembourg

Reviewed by:
Sylvie Lesage, Université de Montréal, Canada
Michael C. Burger, Goethe University Frankfurt, Germany
Maria Vinci, Bambino Gesù Children Hospital (IRCCS), Italy

***Correspondence:**
Alessandro Poggi
alessandro.poggi@hsanmartino.it

Specialty section:
This article was submitted to Cancer Immunity and Immunotherapy, a section of the journal Frontiers in Immunology

Received: *22 May 2020*
Accepted: *16 November 2020*
Published: *23 December 2020*

Citation:
Sargenti A, Musmeci F, Bacchi F, Delprete C, Cristaldi DA, Cannas F, Bonetti S, Pasqua S, Gazzola D, Costa D, Villa F, Zocchi MR and Poggi A (2020) Physical Characterization of Colorectal Cancer Spheroids and Evaluation of NK Cell Infiltration Through a Flow-Based Analysis. Front. Immunol. 11:564887. doi: 10.3389/fimmu.2020.564887

To improve pathogenetic studies in cancer development and reliable preclinical testing of anti-cancer treatments, three-dimensional (3D) cultures, including spheroids, have been widely recognized as more physiologically relevant *in vitro* models of in *vivo* tumor behavior. Currently, the generation of uniformly sized spheroids is still challenging: different 3D cell culture methods produce heterogeneous populations in dimensions and morphology, that may strongly influence readouts reliability correlated to tumor growth rate or antitumor natural killer (NK) cell-mediated cytotoxicity. In this context, an increasing consensus claims the integration of microfluidic technologies within 3D cell culture, as the physical characterization of tumor spheroids is unavoidably demanded to standardize protocols and assays for *in vitro* testing. In this paper, we employed a flow-based method specifically conceived to measure weight, size and focused onto mass density values of tumor spheroids. These measurements are combined with confocal and digital imaging of such samples. We tested the spheroids of four colorectal cancer (CRC) cell lines that exhibit statistically relevant differences in their physical characteristics, even though starting from the same cell seeding density. These variations are seemingly cell line-dependent and associated with the number of growing cells and the degree of spheroid compaction as well, supported by different adenosine-triphosphate contents. We also showed that this technology can estimate the NK cell killing efficacy by measuring the weight loss and diameter shrinkage of tumor spheroids, alongside with the commonly used cell viability *in vitro* test. As the activity of NK cells relies on their infiltration rate, the *in vitro* sensitivity of CRC spheroids proved to be exposure time- and cell line-dependent with direct correlation to the cell viability reduction. All these functional aspects can be measured by the system and are documented by digital image analysis. In conclusion, this flow-based method potentially paves the way towards standardization of 3D cell cultures

and its early adoption in cancer research to test antitumor immune response and set up new immunotherapy strategies.

Keywords: colorectal cancer, spheroid, natural killer cells, mass density, microfluidics, weight, 3D cell culture

INTRODUCTION

In the last years, growing interest has developed in creating and evolving three-dimensional (3D) culture systems to allow more detailed studies of cancer biology and response to therapy (1–4). Indeed, 2D cultures cannot reproduce all the complex features and cell-to-cell interactions occurring at the site of lesion. On the other hand, animal models do not always reproduce the pathophysiology of human cancers, besides being very expensive and showing a negative environmental impact (5–8). Several 3D culture systems, including spheroids, have been validated by the European Union Reference Laboratories for Alternatives to Animal Testing (EURL ECVAM) as preclinical models (9–11). These systems possess many advantages over 2D cultures or animal models, such as reproducibility, the high number of replicates, systematic evaluation of multiple parameters and the possibility to set up standardized co-cultures with different cell types (12–14). In this context, we used the spheroid culture system to evaluate some aspects of the antitumor immune response exerted by a subset of T lymphocytes against colorectal cancer (CRC) cells (15). Thus, spheroids can be a reliable 3D culture system that allows the co-culture of cancer cells and effector immunocompetent cells. However, static culture conditions do not allow the evaluation of all the dynamic events occurring during tumor growth, moreover, such systems cannot fully overcome the limited distribution of oxygen or nutrients and waste removal operating *in vivo*. As a consequence, there is a growing interest for the combination of microfluidic technologies within 3D cultures, including tumor spheroids, to reproduce more faithfully the real tissue microenvironment that undergoes multiple chemical and mechanical challenges, eventually leading to changes in physical parameters (16–19).

Physical features of a tumor include spatial cell organization, external mechanical stimuli, extracellular matrix architecture and stiffness. Mechanobiological modifications, such as active stretch and tension, are other important functional aspects that may condition tumor cell growth and drug response (18, 19). Such microenvironmental aspects should be considered when using 3D culture methods, including multicellular spheroids that take advantage of the natural disposition of several epithelial tumor cells to aggregate (16, 19). Thus, the measurement of physical variations of growing tumors in vitro represents a useful tool in cancer biology, both for elucidation of the mechanisms underlying tumor development and spreading and for testing anti-cancer drugs.

In a recent paper, a linear relationship between impedance and cell number was found for some tumor cell lines and referred to proliferation rates (17). Also, cell size can be measured as volume or mass, as an indicator of cell integrity and state; more precisely, the ratio between mass and volume (i.e. mass density) can be used to distinguish between cell populations even when volume and mass do not vary (20). From this viewpoint, mass density may evidence early modifications in cellular composition that precede size and weight changes, such as organelle enlargement underlying the high metabolic rate of neoplastic cells or nuclear segmentation that occurs at the beginning of apoptotic process due, for example, to anti-cancer drugs (21). In more advanced phases of cell proliferation, mass density might also be influenced by cell number, especially during the first cellular duplications that conceivably do not alter weight and volume yet. In principle, since variations in mass density and volume occur during cell growth and are connected to changes in the cell cycle, the measurement of cell weight and mass density can provide a direct evaluation of the biological processes, underlying tumor progression and environmental changes (20, 21).

Mass density is usually indirectly monitored by software elaboration (22) of bi-dimensional images to assess the compaction degree of cells inside the spheroids, even if 2D projection might alter the real 3D structure. Some papers report mass density as "tightness" (23) "solidity" (24), "optical density" (25) and "compactness index" (26), each one presenting some measurement variations due to different chosen parameters or image quantification software. Therefore, these parameters are used to assess the effects of a specific treatment in the spheroids, such as a toxicity test, efficacy study, tumor cell resistance, and others (24).

Several methods for determining weight and mass density of cells were established with the development of nanomechanical resonator or electrokinetic microfluidic chip (20, 27–30). However, these techniques are not intended, nor proven, for reaching the average size of spheroids and organoids. Indeed, the above-mentioned systems are suitable for corpuscles ranging between nanometers to a few micrometers scale, as single cells or small samples. Moreover, data are often collected in one step, limiting sample replication and analysis repetition essential for accurate biometric studies. We have recently developed a precise and rapid technique, that enables the simultaneous determination of weight, size and mass density of sphere-like samples (31).

In the present paper, we adopted this method to further describe the physical intrinsic differences of spheroids generated from four human CRC cell lines. Furthermore, by this system, we analyzed possible variations induced by spheroid interaction with anti-cancer effector lymphocytes: natural killer (NK) cells were chosen due to their reported role in anti-tumor immunity against CRC. As effectors of natural immunity, they work without the need of recognizing tumor associated antigen by specific receptors, such as the T cell receptor, in the HLA-class I

context. Thus, their action is efficient, although broadly directed towards a large panel of cancers (32–34). In this experimental setting, we recorded variations of these parameters depending on interactions between CRC spheroids and antitumor natural killer (NK) cells during the killing process. These changes are dependent on CRC infiltration by NK cells, followed by the elimination of tumor targets.

MATERIALS AND EQUIPMENT AND METHODS

Cell Cultures and Tumor Spheroid Generation

The human certified CRC cell lines HT-29 (Duke's type B stage), HCT-15, SW620 and DLD-1, all Duke's type C stage, were obtained from the cell bank of the Policlinico San Martino (kind gift of Blood Transfusion Centre, Dr Barbara Parodi). HCT-15 and DLD1 were derived from the same patient but present a different karyotype (35). In particular HCT-15 is quasidiploid and DLD-1 pseudiploid; SW620 derives from a metastatic site in a lymph node and is hyperdiploid, while HT-29 is hypertriploid. A detailed description of karyotype and marker designations for each cell line is available on the American Type Culture Collection website. CRC cell lines in adherent cultures were maintained in RPMI-1640 (Gibco, Life Technologies Italy, Monza) medium supplemented with 10% fetal serum (FBS, Gibco™ One Shot™ Fetal Bovine Serum, ThermoFisher Scientific Italy, Monza, Italy), penicillin/streptomycin and L-Glutamine (BioWhittaker® Reagents, Lonza, Basel, Switzerland) in a humidified incubator at 37 °C with 5% CO_2. HT-29, HCT-15, SW620, and DLD-1 were analyzed by indirect immunofluorescence and flow cytometry for the expression of the epithelial-specific antigen (ESA) and HLA-I with the specific monoclonal antibodies (mAbs) TROP1 (R&D System, Minneapolis, MN, USA) and W6/32 (American Type Culture Collection, Manassas, WA, USA) respectively, followed by Alexafluor647-goat anti-mouse anti-isotype antibody (GAM, ThermoFisher Scientific,) and cytofluorimetric analysis as reported (15). As shown in **Supplementary Figure S1**, all the cell lines were ESA positive, but only HT-29 and SW620 expressed HLA-I. CRC spheroids were generated as described (15) in flat-bottom 96-well plates (Ultra-Low attachment multiwell plates, Corning®Costar®, NY, USA) with DMEM-F12 (BioWhittaker®Reagents, Lonza) in serum-free medium (SFM), supplemented with EGF (Peprotech Europe, London UK) at 10ng/ml final concentration($\geq 1*10^6$ units/mg). Spheroids were monitored along time and dimension (perimeter, area and volume) measured on images taken with the Olympus IX70 bright field inverted microscope equipped with a CCD camera (ORCA-ER, C4742-80-12AG, Hamamatsu, Japan) by the analysis of regions of interest, defining each spheroid, with the CellSens software (version 1.12, Olympus, Tokyo, Japan) (15). Experiments were performed on day 6 of spheroids formation as at this time point all cells in culture were alive, as assessed by culturing a sample under adherent conventional conditions for 12h and subsequent identification of living cells with propidium iodide (PI, Sigma) staining (15), and the diameter of spheroids was about 100 to 200 μm. Some spheroid samples were disrupted in $Ca^{2+}Mg^{2+}$ free PBS and cells stained with the anti-ICAM1 14D12D2 (15) or the anti-PVR (DNAM1 ligand mAb MA5-13490, Invitrogen Thermo Fisher), the anti-MIC-A mAb M2032B5 (clone 12, Sino Biologicals Inc., Beijing, China) and the anti-ULPBs mAbs (anti-huULBP1 M295, anti-huULBP2 M311 and anti-huULBP3 M551) kindly provided by Amgen (Seattle, WA, M.T.A. n.200309766-001). The expression of these molecules on the CRC cell lines is shown in **Supplementary Figure S2A**. The Fc chimeras (soluble receptors fused with the Fc of human immunoglobulins): Fc-NKG2D and Fc-DNAM1 were purchased from R&D System (Minneapolis, MN, USA) and used on CRC cell lines in immunofluorescence assay followed by Alexafluor647 goat anti-human antiserum (Life Technologies). At least 5,000 cells/sample were run on a CyAn ADP cytofluorimeter (Beckman-Coulter Italia, Milan, Italy) and results analyzed with the Summit 4.3 software. The reactivity of Fc-NKG2D and Fc-DNAM1chimeras is depicted in **Supplementary Figure S2B**.

Measurement of Weight, Diameter, and Mass Density of Spheroids

The adopted method is based on tracking the sample's motion, when free-falling into a vertical flow-channel while the flow is at rest, to calculate its terminal velocity. This is achieved by using customized software that relies on a specific physical method, combined with detailed statistical analyses (31). Briefly, as shown in **Supplementary Figure S3**, the device is composed of a fluidic-core chip, equipped with a bright-field imaging setup, a peristaltic pump, a temperature sensor and a flow-circuit for the introduction and elimination of samples. Furthermore, the software assigns a circular reference to each image of the falling sample, allowing the extrapolation of the final radius from the physical calculation, as the average of the maximum radii obtained from each repetition. The terminal velocity is whereas calculated from the vertical position of the falling sample, and for each repetition a linear regression plot is derived. During the entire analysis different internal data control are performed: (i) initial visual screening of the operator; (ii) circular reference assignment; (iii) measurements repetition; (iv) calculation of the average radius; (v) linear regression plot analysis; and (vi) statistical validation with outliers elimination. All these check points insure the conformity of the analyzed samples in term of shape and size. CRC spheroids were fixed with PFA 4% overnight at 4°C, resuspended in 3.5mL of Dulbecco's phosphate-buffered saline (DPBS), 1X w/o Ca^{2+}& Mg^{2+}(Corning® Life Sciences) at low concentration (<200 spheroids/mL), transferred in a centrifuge conical tube and then analyzed according to the previous protocol performed by Cristaldi et al. for biological samples (31). A minimum of 10 single spheroids was analyzed for every test condition and values were extrapolated from at least 10 repetitions. The same procedure was applied to CRC spheroids exposed to NK cells.The fixation protocol had no effect on mass density, as no statistical difference was observed in live and fixed spheroids of the 4 CRC cell lines (not shown). In particular, no statistical differences were found in weight and

diameter variations in fixed or unfixed HT-29 and HCT-15 spheroids, while weight changes in SW620 (+53%) and DLD-1 (−49%), as well as diameter (+21% in SW620 and −14% in DLD-1). Since variations are concordant (a spheroid with a big diameter, also has a big weight, while a small spheroid in size also presents a little weight), mass density is not influenced: in fact, these spheroids show the same mass density values, as mass density normalizes the values of diameter and weight.

Cell Viability and Cytolytic Assay by Crystal Violet Staining

NK cells were obtained from peripheral blood mononuclear cells by negative depletion using RosetteSep NK negative selection kit (StemCell Biotechnology, Vancouver, Canada) as described and cultured for 15 days with interleukin-2 (IL-2, 30IU/ml, Miltenyi Biotech, Milan, Italy) (34). NK cell population used in functional assays was >97% CD3 negative CD56 positive (34) (not shown in this paper). The number of CRC cells in a culture well was determined measuring the ATP spheroid content in that well, referred to the ATP content of the same cell line at a known cell concentration in suspension. The optimal amount of NK cells to detect the cytotoxic effect, determined by crystal violet assay or by image analysis, was $0.75x10^5$ cells/well and it corresponded approximately to a 1:1 effector to target (E:T) ratio (15). Spheroids were incubated at 37°C with NK cells, for 6h or 24h; then cytolytic activity was evaluated with the Crystal Violet Cell Cytotoxicity Assay Kit (Biovision, Milpitas, CA 95035 USA). CRC spheroids, alone or co-cultured with NK cells, at the indicated time points (6h or 24h), were transferred in conventional adherent plates and after further 24h were washed to remove NK cells.,The presence of residual NK cells was verified by bright field microscopy, based on dimension and morphology, before staining adherent CRC cells with crystal violet following manufacturer's instructions. In further experiments, suspensions or adherent or CRC cell lines were challenged with NK cells at 1:1, 3:1 or 10:1 E:T ratios for 24h; under these conditions only living CRC cells remain adherent. Then, non-adherent cells were washed out, crystal violet staining was performed according to the manufacturer's instructions and adherent cells were solubilized. The amount of crystal violet proportional to the number of living cells was measured with the VICTORX5 multilabel plate reader (Perkin Elmer, Milan, Italy) at the optical density (O.D.) of 595nm and referred to $O.D._{595}$ of CRC cell samples without NK cells (15). Results are expressed as the percentage of living cells compared to CRC spheroids without NK cells.

Measurement of Adenosine-Triphosphate (ATP)

Intracellular ATP was determined using the CellTiter-Glo® Luminescent Cell Viability Kit (Promega Italia Srl, Milan, Italy), following manufacturer's instruction, using the luciferase reaction consisting in mono-oxygenation of luciferin catalyzed by luciferase in the presence of Mg^{2+}, ATP and molecular oxygen. Luminescence was detected with the VICTORX5 multilabel plate reader (Perkin Elmer) expressed as relative light units (RLU) (15). Results are the mean±SD of 16 wells/spheroid cell line or samples of $20x10^3$ CRC cells in suspension for each cell line.

Confocal Microscopy and Imaging of Spheroid Composition and Invasion

CRC spheroids were fixed with 4% PFA 5 min at 4°C, permeabilized with 1% NP40, washed with PBS and stained with 1μM Syto16 Green Fluorescent Nucleic Acid Stain (ThermoFisher). After washing, samples were seeded into a 96w Cell Imaging plate (Eppendorf AG, Hamburg, Germany) and run under the FV500 laser scanning confocal microscope. Images were taken with a 20x objective 0.40 NA, at Z points set every 8 to 10 μm, with FluoView 4.3b software (Olympus GmbH, Hamburg, Germany). In a first set of experiments, a z-stack analysis (12 sections of 8 μm for 80 to 96 μm total thickness) was performed for spheroids of each cell line in order to check their shape. Orthogonal cross-section of x-y focal planes were reconstructed and shown as x-z or y-z planes. In other experiments, spheroids were identified with the Threshold tool of the Image J software and nuclei were counted with the Multipoint Analyze Particle tool; at least 30 spheroids/cell line were analyzed on 6 Z points/spheroid; results are expressed as cell number/area. In other experiments, NK cells were stained with CFSE ($1μg/ml/10^6$ cells) for 1h at 37°C; then they were washed, added to CRC spheroids at the E:T ratio of 1:1 and incubated at 37°C with NK cells for 24h. Samples were included in a Matrigel dome, seeded into a 96w Cell Imaging plate (Eppendorf AG) and run under the FV500 laser scanning confocal microscope. Other samples were fixed with 4%PFA, washed to remove NK cells adherent to the external spheroid layer and counterstained with the anti-ESA mAb TROP-1, followed by Alexafluor647-GAM (ThermoFisher Scientific). Images were taken at different Z points, set every 10μm, with a 20x objective 0.40 NA, analyzed with FluoView 4.3b software (Olympus GmbH) and shown in pseudocolor. Region of interest (ROI) designed on the inner perimeter of spheroids, were selected for cell count calculated with the Multipoint Analyze Particle tool of the Image J software on the ROI of 6 to 20 spheroids evaluated at 10 different Z positions.

Cytofluorimetric Analysis of Spheroid Invasion

Spheroids incubated with NK cells as described in paragraph 1.5, were washed to remove free-floating NK cells. Staining with the anti-CD56 mAb C218, followed by Alexafluor488 anti-isotype-specific GAM (34) was then performed to label external NK cells, taking into consideration that mAbs can penetrate some peripheral layers of the spheroid (not shown), thus labeling also NK cells infiltrating spheroid periphery. The spheroids were then dissociated in phosphate buffer without Ca^{++}/Mg^{++} and the resulting cell suspension was labeled with the anti-CD45 mAb 9.4, followed by Alexafluor647 anti-isotype-specific GAM (34) to identify all NK cells. Samples were run on a MACSQuant cytofluorimeter (Miltenyi Biotech, Gladbach, Germany) and results analyzed with the FlowJo software (Ashland, Oregon, USA), are expressed as Log green fluorescence intensity (a.u.) vs Log far-red fluorescence intensity (a.u.).

Immunohistochemistry (IHC) and Digital Imaging

Samples of spheroids incubated with NK cells were centrifuged in 1.5ml tubes at 1000 rpm 1 min at RT, fixed with 4% PFA 1h at RT, washed with PBS and suspended in 50µl of melted agarose (2% in distilled water). After agarose polymerization, samples were dehydrated in a progressive series of ethanol, clarified in xylene and paraffin embedded. Then, 4µm thick serial sections were cut (3 sections every 15µm) and dried o.n. at 37°C. Using the Leica Bond Rx Automated Stainer (Leica Biosystems), the slides were dewaxed with Leica Bond Dewax solution. After treatment with Bond Epitope Retrieval, sections were stained with the anti-CD45 LCA mAb (2µg/mL, Ventana), or an isotypic unrelated antibody as negative control (Dako Cytomation) and reactions visualized using Leica Bond Refine Detection kit (DS9800) with diaminobenzidine (DAB) chromogen and a hematoxylin counterstain. Digital images were acquired using the Aperio ScanScope Slide program of the Aperio AT2 Scanner (Leica Biosystem, Aperio Technologies) at 20 to 40×. The number of infiltrating cells was calculated with the Image J Multipoint Analyze Particle tool on the ROI designed on the spheroid perimeter. Six spheroids/cell line were analyzed on 10 serial sections.

Statistical Analysis

The Shapiro–Wilk test was performed on the measured outputs obtained from the biological experiments to analyze the distribution of the dataset based on skewness and/or kurtosis (36). For all the cases that resulted in a non-normal distribution, descriptive statistics box plots (Tukey method plots) were carried out for determining outliers' values. Outliers were identified as individual points for the terminal velocity, mass density, diameter, and weight box plots. The presence of at least one outlier in one of the categories was considered sufficient to remove the related sample from the dataset. For these cases, the Shapiro–Wilk approach was reused to confirm the normal distribution. Data are presented as mean ± SEM or ±SD. Statistical analysis was performed using two-tailed unpaired Student's *t*-test. The cutoff value of significance is indicated in each figure legend.

RESULTS

Characterization of the Physical Properties of CRC Spheroids

We analyzed tumor spheroids obtained culturing the representative CRC cells lines HT-29, SW620, HCT-15, and DLD-1 in ultra-low attachment plates, as reported (15). Ten single spheroids for each cell line were analyzed, and each spheroid values of mass density, diameter and weight, and the related standard deviation, are extrapolated from 10 repetitions. Experiments were performed on a heterogeneous population of spheroids in terms of dimension, to test the feasibility of our methods in cell aggregates having the different size ranging from 100 to 200µm diameter, as shown in **Figure 1A**. HCT-15, DLD-1, and SW620 spheroids displayed round shape with a smooth surface, while HT-29 spheroids showed irregular shape with a rough surface (**Figure 1A**). CRC spheroid samples were fixed with 4% PFA and analyzed with the flow-based system: as shown in **Figure 1B**, SW620 and DLD-1 spheroids' weights (ng, left graph) were higher than that of HT-29. Also, their diameter (µm, central graph), calculated automatically from the images acquired during the free-fall motion, were larger than those of HT-29 spheroids. Noteworthy, the measured mass density of the sample was consistently higher in SW620 and DLD-1 than HT-29 spheroids (fg/µm^3, right graph). As mass density represents a

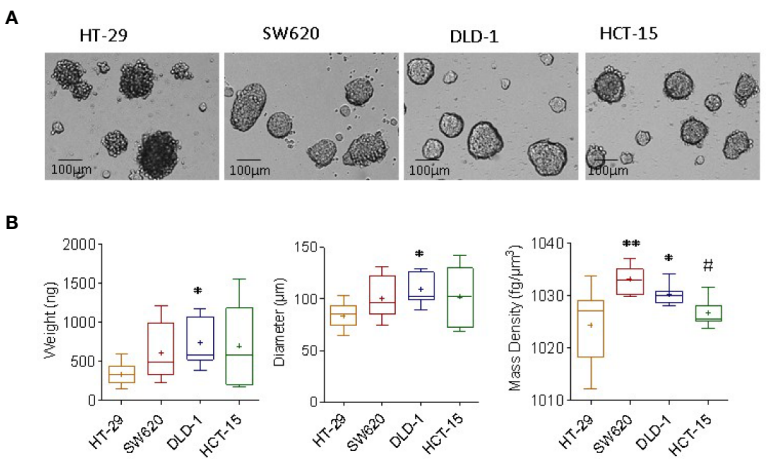

FIGURE 1 | Measurement of mass density, weight and diameter of CRC spheroids. **(A)** CRC spheroids were generated with HT-29, SW620, DLD-1, and HCT-15 CRC cell lines cultured in ultra-low adherent flat-bottomed microplates and analyzed on day 6 by inverted IX70 microscope (Olympus); images were taken with 20x objective NA 0.40 (200x magnification). Bar in each panel: 100µm. **(B)** CRC spheroid samples were fixed with 4% PFA and analyzed with the flow-based system. Data are graphically depicted in box-and-whisker plots and the lines, extending from the boxes, indicate variability outside the upper and lower quartiles. Results are expressed as the weight (ng, left graph), diameter (µm, central graph) and mass density (fg/µm^3, right graph). *p< 0.05 and **p< 0.001 vs HT-29. #p<0.05 vs DLD-1.

direct parameter to evaluate the degree of aggregate compaction, data agreed with the preliminary microscopic investigation, where HT-29 cells formed loose aggregates, instead of compact 3D tumor spheres. Weight and diameter of HCT-15 spheroids were comparable to that of SW620 and DLD-1 ones, although much more dispersed due to sample intrinsic heterogeneity (**Figure 1B**, left and central graphs); however, their mass density was similar to that of HT-29 and significantly different from that of DLD-1 (**Figure 1B**, right graph).

Quantification of Cell Number and ATP Content Within the CRC Spheroids

To better clarify the biophysics of mass density heterogeneity, spheroids of HT-29, SW620, DLD-1, or HCT-15 cell lines underwent nuclear staining with the green Syto16 probe followed by laser scanning confocal microscope analysis. Images were taken at different Z points set every 10μm (**Figure 2A**), spheroids were identified with the threshold tool of the Image J software in red pseudocolor, while nuclei were evidenced in blue pseudocolor (**Figure 2B**) and counted with the multipoint analyze particle tool (30 spheroid/cell line counted on 6 Z points/spheroid). **Figure 2C** shows in SW620 spheroids a striking higher cell number/mm^2 than in HT-29, DLD-1, and HCT-15 spheroids: the latter two, in turn, contain many more cells than HT-29. Intracellular ATP content was detectable in all spheroids, documenting cell viability (**Figure 2D**). The higher ATP content in SW620, and to a lesser extent in DLD-1, than in HT-29 or HCT-15 spheroids, can be referred to the higher cell number, mainly evident in SW620 spheroids (**Figure 2D** vs **Figure 2C**). Since DLD-1 and HCT-15 spheroids contained approximately the same number of cells, differences in ATP content may depend on a different metabolic state. This is also suggested by the finding that ATP values measured in cell suspensions of each cell line display differences among the four cell lines, as shown in **Figure 2E**.

Cytotoxic Activity of NK Cells on CRC Spheroids Evaluated by Weight, Diameter, and Mass Density Measurement

We further planned to test the variations of physical parameters caused by the antitumor effect of NK cells and occurring during the killing process. Then, SW620, HCT-15, and DLD-1 spheroids were chosen due to their comparable weights,

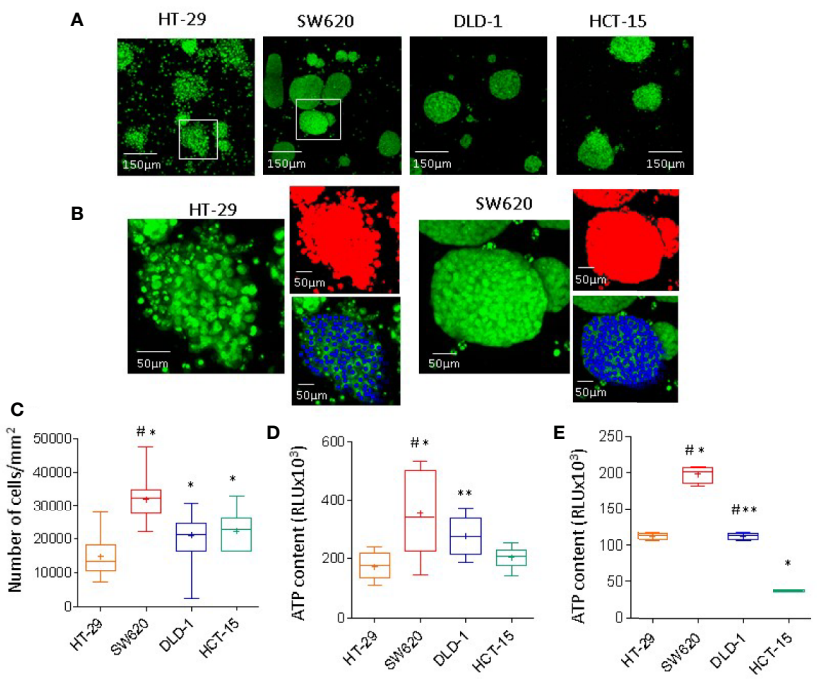

FIGURE 2 | CRC spheroids cell composition and viability. **(A)** CRC spheroids of HT-29, SW620, DLD-1, or HCT-15 were stained with 1μM Syto16 Green, seeded into a 96w Cell Imaging plate (Eppendorf) and run under the FV500 laser scanning confocal microscope (200x). Images were taken at different Z points set every 10μm (one representative is shown), with FluoView 4.3b software (Olympus GmbH). **(B)** Image analysis (Image J software) of a spheroid of HT-29 (left) or SW620 (right); enlargement of the white squares in A. Spheroids identified in red pseudocolor, nuclei evidenced in blue pseudocolor. **(C)** Nuclei were counted with the multipoint and analyze particle tool; results are expressed as cell number/area (mm^2) and are the mean±SD of 30 spheroid/cell line counted on 6 Z points/spheroid. ANOVA was performed to evaluate the differences between groups, followed by the Tukey-HSD posthoc test. *p<0.0001 vs HT-29, #p<0.0001 vs DLD-1 and HCT-15. **(D)** Intracellular ATP content measured using the CellTiter-Glo® Luminescent Cell Viability Kit (Promega). Results are expressed as relative light units (RLU) and are the mean±SD of 16 wells/spheroid cell line. Two-tailed unpaired Student's *t*-test was performed to calculate statistical significance. *p<0.0001 vs HT-29, **p<0.001 vs HT-29, #p<0.0001 vs HCT-15. **(E)** Intracellular ATP content in 20x10^3 cells for each cell line, rescued from subconfluent (70%) cultures and kept in suspension. Results are expressed as in **(D)** and are the mean±SD of 4 wells/cell line. Two-tailed unpaired Student's *t*-test was performed to calculate statistical significance. *p<0.0001 vs HT-29, **p<0.0001 vs SW620, #p<0.0001 vs HCT-15.

diameters and shape, although with different mass density. On the contrary, HT29 aggregates exhibited significantly less weight and lower, dispersed values of mass density. Confocal analysis, followed by orthogonal cross-section reconstruction from a set of a z-stack scans, showed that HT-29 spheroids were far from being spherical (example shown in **Figure 3A**) so that the flow-based system struggled to properly assign them a circular reference and, as a consequence, also the final calculated radius was affected by the samples' irregularity. Conversely, SW620, HCT-15, and DLD-1 3D structures predominantly displayed a round shape in the orthogonal views of the z planes analyzed (z3, z6, and z9 shown in **Figures 3B–D**), indicating that they can be considered spheroids. HT29 were thereby considered less suitable models for the reliable testing of infiltrating NK cells.

CRC tumor spheroids were co-incubated with NK cells at E:T ratio of 1:1 and parallel samples were analyzed for weight, diameter and mass density at 6h and 24h, while cell viability was measured with crystal violet assay. In SW620 and DLD-1 CRC spheroids, co-culture with NK cells led to a statistically significant decrease in weight (**Figures 4Aa, Ba**) and diameter (**Figures 4Ab, Bb**). In particular, SW620 weight loss was about 47% at 6h and 23% at 24h, with a decrease in the diameter of 18% and 13% respectively (**Figures 4Aa, Ab**), while DLD-1 and HCT-15 weight and diameter decreased at 24h by 34% and 13% for DLD-1 (**Figures 4Ba, Bb**) versus 23% and 7% for HCT-15 (**Figures 4Ca, Cb**). Notably, these changes were already evident at 6h, when cytotoxicity with the crystal violet assay, that is determined after 6h or 24h followed by further 24h of cell adhesion, was still undetectable or negligible (**Figures 4Ad, Bd**). Furthermore, a tendency for an increase in the mass density of SW620 and DLD-1 spheroids was observed upon co-incubation with NK cells, with different kinetics, as depicted in **Figure 4**. The tendency for an increase in SW620 mass density was already evident at 6h (**Figure 4Ac**, brown boxes and whiskers); conversely, in DLD-1 (**Figure 4Bc**, light blue boxes and whiskers) spheroids mass density significantly raised at 24h, immediately before the detection of cytotoxicity by crystal violet assay (**Figure 4Bd**). Weight and diameter of HCT-15 showed a tendency for a decrease only after 24h of co-incubation with NK cells (**Figures 4Ca and Cb**), although cytotoxicity was already evident at 6h (**Figure 4Cd**); mass density did not vary significantly, conceivably due to the small decrease in weight and diameter (**Figure 4Cc** vs **Figures 4Ca and Cb**). Thus, weight measurement can precisely reveal spheroid variations, due to NK cell cytotoxic activity, even earlier than crystal violet assay and in addition to other information such as diameter modifications and mass density changes.

When the cytolytic assay was performed with CRC cells in suspension, we observed that DLD-1 was less susceptible than SW620 and HCT-15 cell lines to NK cell-mediated lysis (**Supplementary Figure S4A**); however, this difference was not evident using the three cell lines as adherent targets (**Supplementary Figure S4B**), suggesting that cancer cell shape might influence the outcome of NK cell anti-tumor activity.

NK Cell Infiltration of CRC Spheroids

We further investigated whether mass density variations in SW620 and DLD-1 spheroids were associated with NK cell infiltration. To this aim, NK cells were labeled with CFSE probe (green) and NK cell entry into the spheroids was

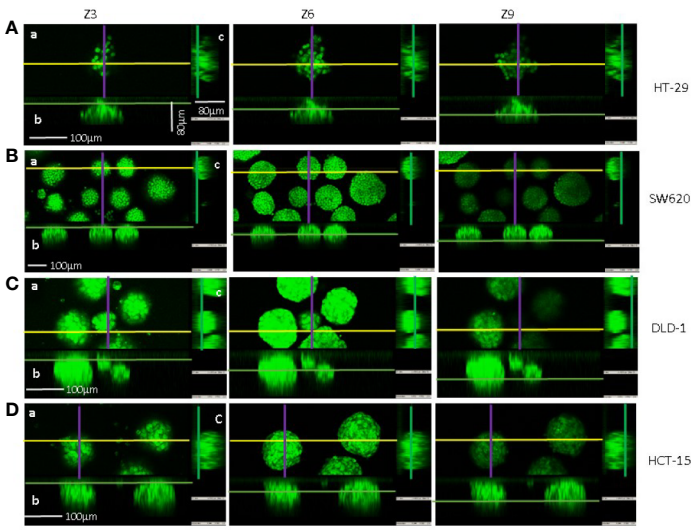

FIGURE 3 | Confocal microscopy and imaging of CRC spheroid shape. Spheroids of HT-29 **(A)**, SW620 **(B)**, DLD-1 **(C)**, or HCT-15 **(D)** cell lines were stained with 1µM Syto16 Green Fluorescent Nucleic Acid Stain and run under the FV500 laser scanning confocal microscope. Images were taken with a 20x objective 0.40 NA, at Z points set every 8µm, with FluoView 4.3b software (Olympus). Orthogonal cross-section (indicated as follows: yellow for x axis, purple for y axis and green for z axis) were reconstructed from a set of a z-stack scans (12 sections for 80–96 µm total thickness: z3, z6, z9 are shown for each cell line). For each panel **(A–C)**: a) an example of x-y focal plane of the z reported in the subpanel a; b) side view of the z-stack (orthogonal x-z plane) for subpanel a); c) view in the orthogonal y-z plane for subpanel a. Bar: 100µm are indicated in panels **(A–D)** of z3.

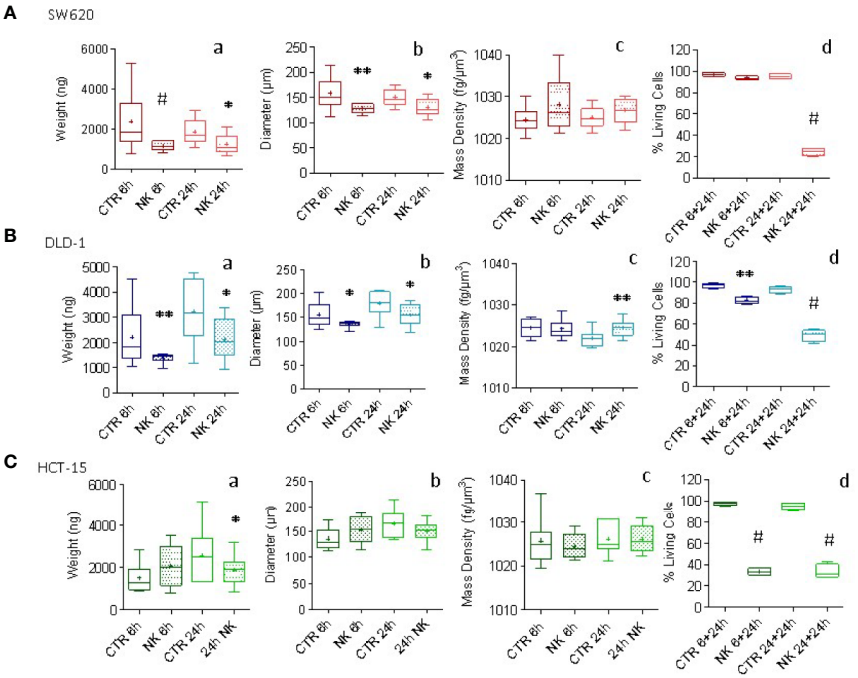

FIGURE 4 | Evaluation of NK cell killing of CRC spheroids. CRC spheroids generated with SW620 **(A)**, DLD-1 **(B)** and HCT-15 **(C)** cell lines were incubated at 37°C with NK cells at the effector:target (E:T) ratio of 1:1 for 6h or 24h. Then, samples were fixed with 4% PFA and analyzed with the flow-based system. Data are graphically depicted in boxes-and-whisker plots and the lines extending from the boxes indicate variability outside the upper and lower quartiles. Results are expressed as weight (ng, a), diameter (µm, b) and mass density (fg/µm^3, c). (graph d of **A, B, C**) Cytolytic activity evaluated in parallel samples at 6h or 24h (+additional 24h to allow living cell attachment) with the Crystal Violet Cell Cytotoxicity Assay Kit (Biovision). The amount of crystal violet proportional to the amount of living cells was measured with the VICTORX5 multilabel plate reader (Perkin Elmer) at the optical density (O.D.) of 595nm. Results are expressed as the percentage of living cells compared to CRC spheroids without NK cells. A-C: *p<0.05; **p<0.001, #p<0.0005.

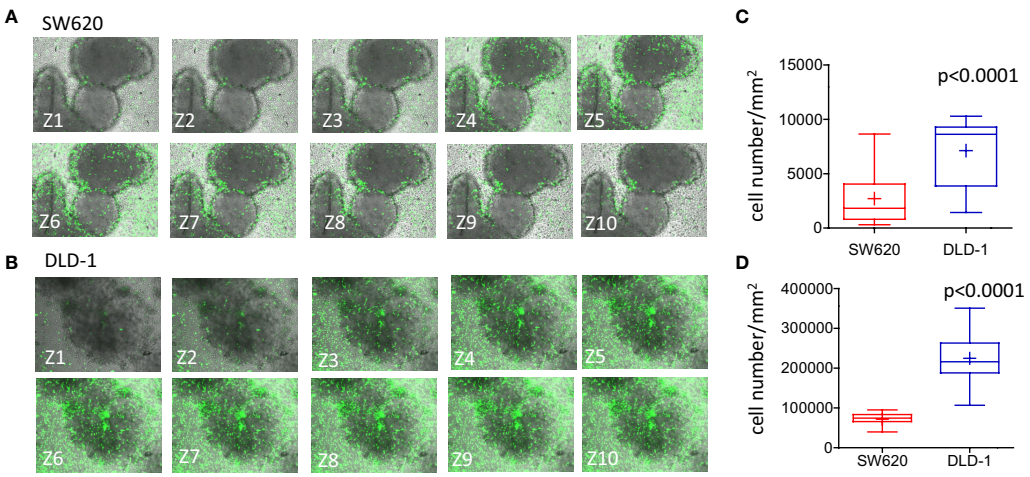

FIGURE 5 | Infiltration of CRC spheroids by NK cells.I. **(A, B)**: SW620 **(A)** or DLD-1 **(B)** spheroids were seeded into a Matrigel dome in Cell Imaging plates (Eppendorf) and incubated with CFSE-labeled NK cells (E:T ratio of 1:1) for 24h. Samples were run under the FV500 confocal microscope and analyzed with FluoView 4.3b software (Olympus). Images were taken at different Z planes (Z1-Z10) every 10µm with a 20x objective NA 0.40 and shown as green CFSE$^+$ NK cells merged with bright field spheroids. **(C, D)**: NK cells present in each Z plane were counted with the Multipoint Analyze Particle tool of the Image J software and plotted as the number of NK cells/mm^2 infiltrating SW620 (red boxes and whiskers) or DLD-1 (blue boxes and whiskers) and the mean±SD of 10 Z plans of a single spheroid **(C)** or mean±SD of NK cells/mm^2 infiltrating 20 spheroids evaluated each at 10 different Z positions **(D)**.

evaluated after 24h of co-culture. These two CRC spheroids were chosen since they underwent significant variations in their mass density upon 24h of interaction with NK cells. The method used for cell count applied the Multipoint and Analyze Particle tool of the Image J software to the ROI defined as single spheroids, as described in **Supplementary Figure S2**. Data were plotted as the number of infiltrating NK cells/mm^2. **Figure 5A** shows SW620 spheroids, surrounded and progressively infiltrated by NK cells (green CFSE$^+$), documented by the representative images taken at 10 different Z planes. In **Figure 5B**, NK cells invading DLD-1 spheroids are depicted, displaying an elongated shape that indicates their position inside the spheroid. A significantly higher number of NK cells could infiltrate DLD-1 (**Figures 5C, D**, blue boxes and whiskers) compared to SW620 (**Figures 5C, D**, red boxes and whiskers) spheroids, where NK cells accumulated at the periphery (**Figure 5C**: mean±SD of NK cells/mm^2 in a single spheroid evaluated at 10 different Z positions; **Figure 5D**: mean±SD of NK cells/mm^2 infiltrating 20 spheroids evaluated each at 10 different Z positions). These data might explain the differences in mass density detected with the flow-based system and reveal a different mode of action of NK cells to attack tumors, depending on the biological features of tumor spheroids associated with their physical properties.

Parallel specimens of spheroids incubated with NK cells were extensively washed, to remove unbound NK cells, and counterstained with the anti-ESA mAb, followed by Alexafluor647-GAM. Samples were analyzed by confocal microscopy with the FluoView 4.3b software. **Figure 6** shows three representative z-stack images, out of 10 set every 10µm, of SW620 (A) vs DLD-1 (B) spheroid (CRC cells identified in red as ESA-positive) infiltrated by NK cells (green CFSE$^+$). DLD-1 or SW620 incubated with NK cells were also included in melted agarose and paraffin embedded for IHC; serial sections were cut and stained with the anti-CD45 mAb to detect NK cells (C and D). Immunofluorescence was analyzed by Image J software on the ROI designed on the inner spheroid perimeter, to exclude NK cells confined in the external spheroid layer, defined on the basis of ESA staining; 6 spheroids/cell line were analyzed at 10 different Z positions and the number of NK cells calculated with the Image J Multipoint Analyze Particle tool. **Figure 6E** shows that the number

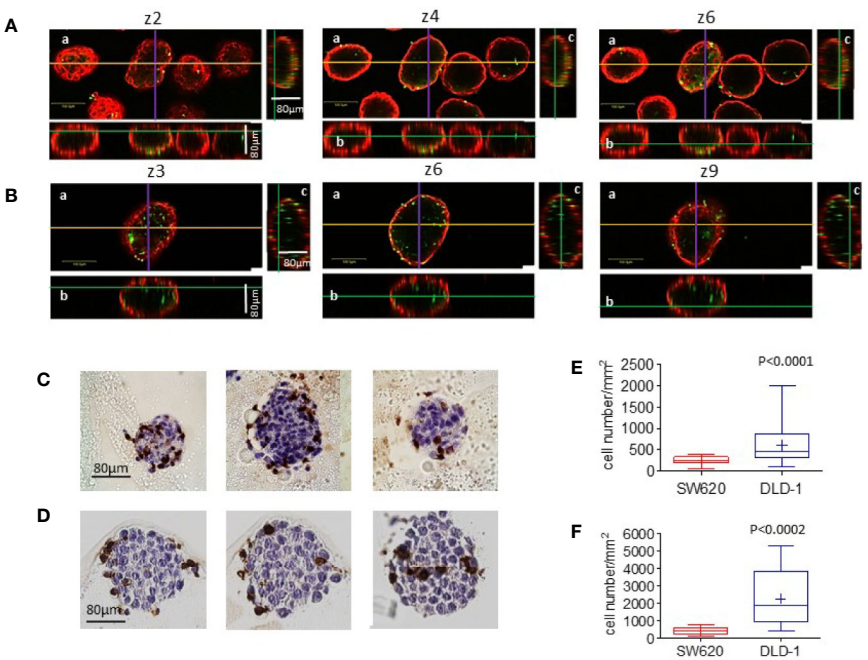

FIGURE 6 | Infiltration of CRC spheroids by NK cells II. (A-B): SW620 **(A)** or DLD-1 **(B)** spheroids were seeded as in **Figure 5**, incubated with CFSE-labeled NK cells (green, E:T ratio of 1:1) for 24h, washed and counterstained with the anti-ESA mAb TROP-1, followed by Alexafluor647-GAM (red). Samples were run under the FV500 confocal microscope and analyzed with FluoView 4.3b software (Olympus). Images were taken at different Z planes (Z1-Z10) with a 20x objective NA 0.40: three representative z stack sections are shown. Orthogonal cross-section (indicated as yellow line for x axis, purple for y axis and green for z axis) were reconstructed from z-stack scans (80 µm total thickness). For each panel: a) an example of x-y focal plane of the z reported in the subpanel a; b) side view of the z-stack (orthogonal x-z plane) for subpanel a); c) view in the orthogonal y-z plane for subpanel a. Bar in subpanels a: 100µm. **(C, D)**: Other samples of SW620 **(C)** or DLD-1 **(D)** spheroids incubated with NK cells were fixed, suspended in melted agarose and paraffin embedded. Four µm thick serial sections were cut (3 sections every 15 µm) and stained with the anti-CD45 LCA mAb, visualized with DAB chromogen (brown) and a hematoxylin counterstain. Digital images were acquired using the Aperio ScanScope Slide program of the Aperio AT2 Scanner with a 40X objective. **(E, F)**: The number of infiltrating cells was calculated with the Image J Multipoint Analyze Particle tool on the ROI designed on the inner spheroid perimeter (graph E), defined on the basis of ESA staining showed in A and B, or on the visible spheroid perimeter (graph F) in the IHC stained specimens depicted in C and D. This is the main reason for the different NK cell number counted in E vs F. Six spheroids/cell line were analyzed at 10 different Z positions in **(E)** or on 10 serial sections in **(F)** Results are expressed as cell number/mm^2. p<0.0001 **(E)** or p<0.0002 **(F)** vs SW620.

of NK cells inside DLD-1 spheroids was significantly higher than that of NK cells infiltrating SW620 spheroids ($p<0.0001$). That NK cell infiltration of DLD-1 was more efficient than that of SW620 spheroids was also documented by IHC and digital imaging (**Figure 6C** vs **Figure 6D**). Image J Multipoint Analyse Particle tool was applied on the ROI defined on the visible spheroid perimeter on 10 serial sections. Also in this case, the number of infiltrating NK cells was significantly greater in DLD-1 than in SW620 spheroids (**Figure 6F**, $p<0.0002$).

To further verify the degree of NK cell infiltration of DLD-1 vs SW620 spheroids, staining with the anti-CD56 mAb, followed by Alexafluor488 anti-isotype-specific GAM was performed to label external NK cells. The spheroids were then dissociated and the resulting cell suspension was labeled with the anti-CD45 mAb, followed by Alexafluor647 anti-isotype-specific GAM to identify all NK cells, including those derived from the inner part of tumor spheroids. Thus, CD45 single-positive cells should identify bona fide deeply infiltrating NK cells. Samples were then analyzed by flow cytometry, gating on lymphocytes based on FSC/SSC physical parameters (**Figure 7A**, left plots). Of note, the percentage of $CD45^{+}CD56^{-}$NK cells was much higher in cell suspensions derived from DLD-1 than from SW620 spheroids (39.1% vs 12.2% NK1, **Figure 7A** right plots; 26.6% vs 16% NK2, **Figure 7B**). These findings are in line with those obtained by confocal microscopy and digital imaging analysis.

DISCUSSION

Alongside with the optimization of 3D cell culture methods, many efforts have been made to develop new technologies for the full characterization of these complex spherical aggregates (3, 37, 38). As regards the biophysical characterization of size and mass density, although few technical solutions have been presented for single-cell analysis, literature does not cover this aspect for 3D models of hundreds of micrometers in diameter, such as spheroids (30).

To overcome this shortage, microfluidics provides a promising technique due to its peculiar properties, including liquid handling automation, small volumes of reagents/sample required, and cost-effective fabrication. In this work, we have described a flow-based technology and the associated method for the non-invasive and accurate measure of size, weight and mass density. Although both mass and volume are important parameters for a comprehensive physical overview of the samples, mass (i.e. weight) is more fundamentally related to cell growth than is volume, thereby altering the density (39). Volume can change disproportionately to mass, thereby altering a cell's density (39). As previously shown, this system relies on software-driven process automation that remarkably increases the ease of use of the device (30).

Tumor spheroids composed of four different CRC cell lines (HT-29, SW620, DLD-1, and HCT-15) were analyzed with this flow-based method. Interestingly, not all the CRC cell lines tested give rise to spheroids of the same shape and size, under the same experimental conditions, starting from the same number of cells seeded. Indeed, HT-29 cell spheroids appeared like loose cell aggregates where single cells can be still distinguishable. In turn, SW620 and DLD-1 spheroids displayed a smooth surface and oval (SW620) or round (DLD-1 and HCT-15) shape. This might represent a limitation, since physical measures and functional assays were performed on heterogeneous spheroids populations; nevertheless, the standardized culture conditions used allow the formation of spheroids mostly included in the range of 60 to 140 μm for all the CRC cell lines. Of note, these different characteristics can be captured, measured and evaluated by the flow-based system that can evidence distinct weight, diameter and mass density, according to the cell composition of the

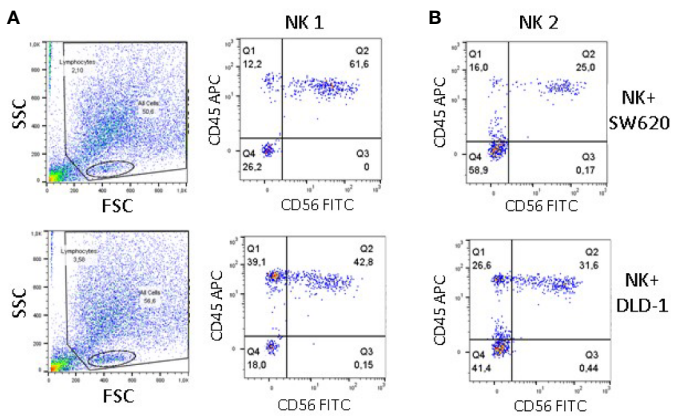

FIGURE 7 | Infiltration of CRC spheroids by NK cells evaluated by cytofluorimetry. SW620 (upper panels) or DLD-1 (lower panels) spheroids were incubated with NK cells from two donors (NK1, panel **A** and NK2, panel **B**), as in **Figure 4**, washed and stained with the anti-CD56 mAb C218, followed by Alexafluor488 anti-isotype-specific GAM. After dissociation in phosphate buffer without Ca^{++}/Mg^{++}, the resulting cell suspension was labeled with the anti-CD45 mAb 9.4, followed by Alexafluor647 anti-isotype-specific GAM. Samples were run on a MACS Quant cytofluorimeter, 10,000 events were recorded and gating was performed on lymphocytes (panel A, left plots) Results, analyzed with the Flow Jo software, are expressed as Log green fluorescence intensity (a.u.) vs Log far-red fluorescence intensity (a.u.).In each quadrant are reported the percentage of single-positive (upper left and lower right) double-negative (lower left) or double-positive (upper right) cells.

tumor-spheres. Although fixation, that allows sample recruitment in multicenter studies, may modify weight and diameter of spheroids in some instances, both parameters vary in the same direction so that mass density is not influenced. These findings disclose that mass density is a more reliable parameter than diameter and weight. Of note, the higher mass density detected in DLD-1 compared with HCT-15, both derived from the same patient but displaying a different karyotype (35), might indicate that the heterogeneity of clones inside the same tumor can be distinguished also on the basis of mass density measurement. In addition, the differences in spheroid mass density can be referred to the spheroid cell number. Indeed, computerized imaging, showed in SW620 spheroids a significantly higher cell number/mm^2 than in HT-29, DLD-1, and HCT-15 spheroid: the latter two, in turn, contain a higher cell number compared to HT-29. Likewise, intracellular ATP content was not only detectable in all spheroids, as a parameter of cell viability and metabolism, but also related to cell number and mass density, determined with the flow-based system.

We could also measure the results of effector lymphocyte activity on CRC spheroids. Although controversial for many years, the role of NK cells in anti-tumor immune response is documented (31, 32, 40, 41). In CRC, the contemporary infiltration of T and NK cells is apparently linked to a better prognosis and an anti-cancer response mediated by NK cell activation has been reported in a metastatic CRC patient (42, 43). In the present flow-based system, co-culture with NK cells led to a decrease in weight and diameter of CRC spheroids, with different kinetics depending on the cell line. Indeed, SW620 and DLD-1 changes were already evident at 6 h, much earlier than cytotoxicity detection with the crystal violet assay, whereas changes in HCT-15 spheroids were evident only after 24h of co-incubation of NK cells. This might depend, at least in part, on the size, being small spheroids more susceptible to NK cell infiltration than large ones. However, the CRC spheroid populations exposed to NK cells displayed similar size variations (diameter of 80–130 μm for SW620, 90–130 μm for DLD-1 and 70–140 μm for HCT-15). Furthermore, the tendency for an increase in mass density observed at first in SW620 and later in DLD-1 spheroids, upon co-incubation with NK cells, conceivably reflects the different kinetics and degree of spheroid infiltration by NK cells. As demonstrated by confocal analysis and computerized imaging, DLD-1 spheroids are invaded by NK cells that reach in great number the inner layers and the center of the tumor by 24 h; conversely, NK lymphocytes remain in the periphery of SW620 spheroids and a few cells reach the center of the tumor mass. This behavior in invasion might explain the differences in mass density detected with the flow-based system in DLD-1 and SW620 spheroids during interaction with NK cells and evidences a different mode of action of NK cells, depending, at least in part, on the physical properties of the tumor. Also in the case of SW620 spheroids, however, the antitumor cytotoxic activity is operating, as revealed by the reduction in weight and diameter. In addition, differences in the expression of molecules involved in tumor cell killing could contribute to cancer cell sensitivity. We reported that all these CRC cell lines expressed adhesion molecules, such as ICAM1, and the ligands of NKG2D and DNAM-1 NK cell-activating receptors (35). The expression of these ligands, and the consequent reactivity of the Fc-NKG2D and Fc-DNAM1 chimeras, is maintained in CRC cell lines involved in tumor spheroid formation; this would indicate that NK cells can use most of their classic receptor-ligand systems to invade CRC spheroids and exert their anti-tumor function. On the other hand, the expression of HLA-I may be relevant to favour NK cell spheroid invasion and killing: indeed at variance with SW620, DLD-1 does not express HLA-I, that can deliver inhibitory signals to NK cells [reviewed in (33)], thus reducing their infiltrating and killing potential. Nevertheless, cancer cell shape and tumor architectural organization seem to be crucial for the outcome of NK cell anti-tumor activity; indeed the degree of cytolytic activity exerted by NK cells varies using the same tumor targets as single-cell suspensions, as adherent cells or as spheroids.

Since the 3D spheroid system is evocative of the small tumor cell clusters that may occur in the first cancer stages, a precise measurement of weight, size and density variations provide substantial information on disease progression. This is particularly relevant in CRC, where a reliable animal model is still to be defined. Moreover, with this innovative flow-based system we can measure the size and physical properties of a large number of spheroids in several replicates and different experimental conditions; this experimental setting can be useful to test new drugs or therapeutic schemes for their antitumor efficiency. Not only CRC cell lines but also primary tumor cells obtained from bioptic specimens can be used in this system, allowing the assembling of personalized precision medicine.

In conclusion, 3D spheroid models represent a reliable, reproducible and cost-effective solution that allows the evaluation and measurement of the first steps of cancer growth, taking into account the heterogeneity of tumor cells. This experimental setting also allows the evaluation of the degree and kinetics of antitumor effects exerted by immunocompetent cells; also, the system reveals any difference in the sensitivity of CRC cell types to lymphocyte effects. Potentially, the fine-tuning of the physical parameter recording could be useful in the evaluation of anti-cancer drug efficacy, including that of therapeutic antibodies and immunotherapy.

DATA AVAILABILITY STATEMENT

The raw data supporting the conclusions of this article will be made available by the authors, without undue reservation.

ETHICS STATEMENT

The studies involving human participants were reviewed and approved by Peripheral blood mononuclear cells (PBMC) were obtained from healthy adult donor's buffy coat upon institutional informed consent signed at the time of donation and EC approval PR163- REG2014 of the Ligurian Regional Ethics Committee. This Committee is placed at the IRCCS Ospedale Policlinico San

Martino, 16132, Genoa, Italy. The patients/participants provided their written informed consent to participate in this study.

AUTHOR CONTRIBUTIONS

AP, MZ, and FB designed the rationale behind the work. SB, DG, DC, and SP designed and fabricated the flow-based technology. FV, AP, and MZ carried out cell culture, generation of spheroids, and performed functional assays, immunofluorescence, FACS analysis and confocal imaging. AS, FM, CD, and FC performed all the measurements with the flow-based device and statistical analysis. DC performed IHC and digital imaging analysis. AP, MZ, AS, and FB wrote sections of the manuscript. All authors contributed to the article and approved the submitted version. AP and MZ take primary responsibilities for the paper content.

FUNDING

This work has been partially supported by grants from AIRC (IG-21648), Compagnia di San Paolo (ROL 32567), Ministero della Salute 5x1000 2014 and 2015 and Ricerca Corrente 2018 to AP and by the Ministry of Economic Development-AGRIFOOD PON I&C 204-2020 "Development of a technological platform for the functional testing of nutraceutical molecules". Project Nr F/200110/01-03/X45-CUP B61B19000580008 to Cell Dynamics isrl.

ACKNOWLEDGMENTS

We are also grateful to Dr. Paolo Canevali for technical assistance in FACS analysis and to Prof. Marco Caprini from FABIT Department of the University of Bologna, who supported the research grant of Cecilia Delprete by Progetto Alte Competenze 2016-8426-Regione Emilia Romagna—ONCOPENTA.

SUPPLEMENTARY MATERIAL

The Supplementary Material for this article can be found online at: https://www.frontiersin.org/articles/10.3389/fimmu.2020.564887/full#supplementary-material

SUPPLEMENTARY FIGURE 1 | ESA and HLA-I expression on CRC cell lines. HT-29, HCT-15, SW620, and DLD-1 cell lines were analyzed by indirect immunofluorescence and flow cytometry for the expression of the epithelial-specific antigen (ESA) with the specific monoclonal antibody (mAb) TROP-1 and for and HLA-I, with the W632 mAb followed by Alexafluor647-goat anti-mouse anti-isotype antibody (GAM) (light grey histograms) (15). Samples were run on a CyAN ADP cytofluorimeter. At least ten thousand events were run and results are expressed as Log far-red fluorescence intensity (arbitrary units, a.u.) vs cell number. Dark grey histograms: negative control with Alexafluor647-GAM alone.

SUPPLEMENTARY FIGURE 2 | ICAM1, NKG2DL, DNAM1L expression on CRC cell lines. **(A)** spheroid samples of the indicated CRC cell lines were disrupted in $Ca^{2+}Mg^{2+}$ free PBS and cells stained with the anti-ICAM1 14D12D2 or the anti-PVR (DNAM1 ligand, MA5-13490), the anti-MIC-A mAb M2032B5 or the anti-ULPBs mAbs (anti-huULBP1 M295, anti-huULBP2 M311 and anti-huULBP3 M551), followed by Alexafluor647 GAM. Samples were run on a CyAn ADP cytofluorimeter, results analyzed with the Summit 4.3 software and expressed as Log far red fluorescence intensity (arbitrary units, a.u.) vs number of cells. **(B)** spheroid-derived CRC cells were incubated with Fc-DNAM1 or Fc-NKG2D chimeras followed by Alexafluor647 goat anti-hu antiserum and run on the CyAn ADP cytofluorimeter. Results were analyzed and expressed as in panel **(A)**.

SUPPLEMENTARY FIGURE 3 | Flow-based technology for the multiparametric physical analysis of three-dimensional biological samples. **(A)** Schematic representation of the technology system. **(B)** Front view of the field of view within the analysis channel containing the analysis medium and the 3D spheroid. Representation of the forces involved and the terminal velocity.

SUPPLEMENTARY FIGURE 4 | Evaluation of NK cell killing of CRC cell lines. The SW620, DLD-1, and HCT-15 cell lines were incubated, either in suspension **(A)** or as adherent cells **(B)**, at 37°C with NK cells at the effector:target (E:T) ratio of 1:1, 3:1 or 10:1 as indicated. Cytolytic activity was evaluated at 24h with the Crystal Violet Cell Cytotoxicity Assay Kit (Biovision). The amount of crystal violet proportional to the amount of living cells was measured with the VICTORX5 multilabel plate reader (Perkin Elmer) at $O.D._{595}$. Results are expressed as the percentage of living cells compared to CRC cells without NK cells and are the mean±SD from 8 wells with NK cells of two donors (4 wells counted for each donor). A-C: $^{*}p<0.001$ vs E:T 1:1; $^{**}p<0.0001$ vs E:T 1:1; #$p<0.0001$ vs SW620 and HCT-15.

SUPPLEMENTARY FIGURE 5 | Measurement of the infiltration of CRC spheroids by NK cells. **(A)** DLD-1 spheroids were seeded into a Matrigel dome in Cell Imaging plates (Eppendorf) and incubated with CFSE-labeled NK cells (E:T ratio of 1:1) for 24h. Samples were run under the FV500 confocal microscope and analyzed with FluoView 4.3b software (Olympus). Left picture: green $CFSE^{+}$ NK cells, with an elongated shape, indicating spheroid infiltration, merged with the bright field. White lane: ROI definition for cell count as indicated in the enlarged images of the white square (central and right). Blue points indicate infiltrating lymphocytes inside the ROI. **(B)** Images taken at different Z planes (Z1-Z10) taken every 10μm with a 20x objective. Blue points: infiltrating lymphocytes inside the ROI. The number of NK cells present in each Z plane were counted with the Multipoint Analyze Particle tool of the Image J software and plotted in the right graph as cell number/mm^2 for each section.

REFERENCES

1. Breslin S, O'Driscoll L. Three-dimensional cell culture: the missing link in drug discovery. *Drug Discov Today* (2013) 18(5–6):240–9. doi: 10.1016/j.drudis.2012.10.003
2. Lovitt CJ, Shelper TB, Avery VM. Advanced Cell Culture Techniques for Cancer Drug Discovery. *Biology* (2014) 3(2):345–67. doi: 10.3390/biology3020345
3. Costa EC, Moreira AF, de Melo-Diogo D, Gaspar VM, Carvalho MP, Correia IJ. 3D tumor spheroids: an overview on the tools and techniques used for their analysis,". *Biotechnol Adv* (2016) 34(8):1427–41. doi: 10.1016/j.biotechadv.2016.11.002
4. Verjans ET, Doijen J, Luyten W, Landuyt B, Schoofs L. Three-dimensional cell culture models for anticancer drug screening: Worth the effort? *J Cell Physiol* (2018) 233:2993–3003. doi: 10.1002/jcp.26052
5. Zimmermann M, Box C, Eccles SA. Two-dimensional vs. three-dimensional in vitro tumor migration and invasion assays. *Methods Mol Biol* (2013) 986:227–52. doi: 10.1007/978-1-62703-311-4_15
6. Enna SJ, Williams M. Defining the role of pharmacology in the emerging world of translational research. *Adv Pharmacol* (2009) 57:1–30. doi: 10.1016/S1054-3589(08)57001-3
7. Ellis LM, Fidler IJ. Finding the tumor copycat. *Ther fails patients don't Nat Med* (2010) 16:974–5. doi: 10.1038/nm0910-974
8. Akhtar A. The flaws and human harms of animal experimentation. *Camb Q Health Ethics* (2015) 24(4):407–19. doi: 10.1017/S0963180115000079
9. Fennema E, Rivron N, Rouwkema J, van Blitterswijk C, de Boer J. Spheroid culture as a tool for creating 3D complex tissues. *Trends Biotechnol* (2013) 31(2):108–15. doi: 10.1016/j.tibtech.2012.12.003

10. Rodrigues T, Kundu B, Silva-Correia J, Kundu SC, Oliveira JM, Reis RL, et al. Emerging tumor spheroids technologies for 3D in vitro cancer modeling. *Pharmacol Ther* (2017) 184:201–11. doi: 10.1016/j.pharmthera.2017.10.018
11. Zanoni M, Piccinini F, Arienti C, Zamagni A, Santi S, Polico R, et al. 3D tumor spheroid models for in vitro therapeutic screening: a systematic approach to enhance the biological relevance of data obtained. *Sci Rep* (2016) 6(1):19103. doi: 10.1038/srep19103
12. Cox MC, Reese LM, Bickford LR, Verbridge SS. Toward the Broad Adoption of 3D Tumor Models in the Cancer Drug Pipeline. *ACS Biomater Sci &Engineering* (2015) 1(10):877–94. doi: 10.1021/acsbiomaterials.5b00172
13. Sant S, Johnston PA. The production of 3D tumor spheroids for cancer drug discovery. *Drug Discov Today Technol* (2017) 23:27–36. doi: 10.1016/j.ddtec.2017.03.002
14. Zanoni M, Pignatta S, Arienti C, Bonafè M, Tesei A. Anticancer drug discovery using multicellular tumor spheroid models. *Expert Opin Drug Discov* (2019) 14(3):289–301. doi: 10.1080/17460441.2019.1570129
15. Varesano S, Zocchi MR, Poggi A. Zoledronate Triggers Vδ2 T Cells to Destroy and Kill Spheroids of Colon Carcinoma: Quantitative Image Analysis of Three-Dimensional Cultures. *Front Immunol* (2018) 9:998. doi: 10.3389/fimmu.2018.00998
16. Li XJ, Valadez AV, Zuo P, Nie Z. Microfluidic 3D cell culture: potential application for tissue-based bioassays. *Bioanalysis* (2012) 4(12):1509–25. doi: 10.4155/bio.12.133
17. Shih SC, Barbulovic-Nad I, Yang X, Fobel R, Wheeler AR. Digital microfluidics with impedance sensing for integrated cell culture and analysis. *Biosensors Bioelectronics* (2013) 42:314–20. doi: 10.1016/j.bios.2012.10.035
18. van Duinen V, Trietsch SJ, Joore J, Vulto P, Hankemeier T. Microfluidic 3D cell culture: from tools to tissue models. *Curr Opin Biotechnol* (2015) 35:118–26. doi: 10.1016/j.copbio.2015.05.002
19. Liu Y, Gill E, Shery Huang YY. Microfluidic on-chip biomimicry for 3D cell culture: a fit-for-purpose investigation from the end user standpoint. *Future Sci OA* (2017) 3(2):FSO173. doi: 10.4155/fsoa-2016-0084
20. Bryan AK, Hecht VC, Shen W, Payer K, Grover WH, Manalis SR, et al. Measuring single cell mass, volume, and density with dual suspended microchannel resonators. *Lab Chip* (2013) 14(3):569–76. doi: 10.1039/c3lc51022k
21. Neurohr G, Amon A. Relevance and regulation of cell density. *Trends Cell Biol* (2020) 30(3):213–25. doi: 10.1016/j.tcb.2019.12.006
22. Moraes G, de S, Wink MR, Klamt F, Silva AO, da Cruz Fernandes M. Simplified low-cost methodology to establish, histologically process and analyze three-dimensional cancer cell spheroid arrays. *Eur J Cell Biol* (2020) 99(5):151095. doi: 10.1016/j.ejcb.2020.151095
23. Schmidt M, Scholz C-J, Polednik C, Roller J. Spheroid-based 3-dimensional culture models: Gene expression and functionality in head and neck cancer. *Oncol Rep* (2016) 35(4):2431–40. doi: 10.3892/or.2016.4581
24. Eilenberger C, Rothbauer M, Ehmoser E-K, Ertl P, Küpcü S. Effect of Spheroidal Age on Sorafenib Diffusivity and Toxicity in a 3D HepG2 Spheroid Model. *Sci Rep* (2019) 9(1):4863. doi: 10.1038/s41598-019-41273-3
25. Ware MJ, Colbert K, Keshishian V, Ho J, Corr SJ, Curley SA, et al. Generation of Homogenous Three-Dimensional Pancreatic Cancer Cell Spheroids Using an Improved Hanging Drop Technique. *Tissue Eng Part C Methods* (2016) 22(4):312–21. doi: 10.1089/ten.TEC.2015.0280
26. Lin R-Z, Chou L-F, Chien C-CM, Chang H-Y. Dynamic analysis of hepatoma spheroid formation: roles of E-cadherin and beta1-integrin. *Cell Tissue Res* (2006) 324(3):411–22. doi: 10.1007/s00441-005-0148-2
27. Burg TP, Godin M, Knudsen SM, Shen W, Carlson G, Foster JS, et al. Weighing of biomolecules, single cells and single nanoparticles in fluid. *Nature* (2007) 446(7139):1066–9. doi: 10.1038/nature05741
28. Wang Z, Belovich J. A Simple Apparatus for Measuring Cell Settling Velocity. *Biotechnol Progress* (2010) 26(5):1361–6. doi: 10.1002/btpr.432
29. Zhao Y, Lai HS, Zhang G, Lee GB, Li WJ. Rapid determination of cell mass and density using digitally controlled electric field in a microfluidic chip. *Lab Chip* (2014) 14(22):4426–34. doi: 10.1039/c4lc00795f
30. Xie J, Zhang C, Gu F, Wang Y, Fu J, Zhao P, et al. An accurate and versatile density measurement device: Magnetic levitation. *Sensors Actuators B: Chem* (2019) 295:204–14. doi: 10.1016/j.snb.2019.05.071
31. Cristaldi DA, Sargenti A, Bonetti S, Musmeci F, Delprete C, Bacchi F, et al. A reliable flow-based method for the accurate measure of mass density, size and weight of live 3D tumor spheroids. *Micromachines* (2020) 11:465. doi: 10.3390/mi11050465
32. Morvan MG, Lanier LL. NK cells and cancer: you can teach innate cells new tricks. *Nat Rev Cancer* (2016) 16(1):7–19. doi: 10.1038/nrc.2015.5
33. Pahl J, Cerwenka A. Tricking the balance: NK cells in anti-cancer immunity. *Immunobiology* (2017) 222(1):11–20. doi: 10.1016/j.imbio.2015.07.012
34. Costa D, Venè R, Benelli R, Romairone E, Scabini S, Catellani S, et al. Targeting the Epidermal Growth Factor Receptor Can Counteract the Inhibition of Natural Killer Cell Function Exerted by Colorectal Tumor-Associated Fibroblasts. *Front Immunol* (2018) 29;9:1150. doi: 10.3389/fimmu.2018.01150
35. Chen TR, Dorotinsky CS, Mc Guire LJ, Macy ML, Hay RJ. DLD-1 and HCT-15 cell lines derived separately from colorectal carcinomas have totally different chromosome changes but the same genetic origin. *Cancer Genet Cytogenet* (1995) 81(2):103–8. doi: 10.1016/0165-4608(94)00225-z
36. Althouse LA, Ware WB, Ferron JM. *Detecting Departures from Normality: A Monte Carlo Simulation of a New Omnibus Test Based on Moments*. ERIC Institute for Education Sciences (1998). Available at: https://eric.ed.gov/?id=ED422385.
37. Desmaison A, Guillaume L, Triclin S, Weiss P, Ducommun B, Lobjois V, et al. Impact of physical confinement on nuclei geometry and cell division dynamics in 3D spheroids. *Sci Rep* (2018) 8:8785. doi: 10.1038/s41598-018-27060-6
38. Gomes A, Guillaume L, Grimes DR, Fehrenbach J, Lobjois V, Ducommun B. Oxygen Partial Pressure Is a Rate-Limiting Parameter for Cell Proliferation in 3D Spheroids Grown in Physioxic Culture Condition. *PLoS One* (2016) 11:e0161239. doi: 10.1371/journal.pone.0161239
39. Godin M, Delgado FF, Son S, Grover WH, Bryan AK, Tzur A, et al. Using buoyant mass to measure the growth of single cells. *Nat Methods* (2010) 7(5):387–90. doi: 10.1038/nmeth.1452
40. López-Soto A, Gonzalez S, Smyth MJ, Galluzzi L. Control of Metastasis by NK Cells. *Cancer Cell* (2017) 14;32(2):135–54. doi: 10.1016/j.ccell.2017.06.009
41. Poggi A, Benelli R, Venè R, Costa D, Ferrari N, Tosetti F, et al. Human Gut-Associated Natural Killer Cells in Health and Disease. *Front Immunol* (2019) 10:961. doi: 10.3389/fimmu.2019.00961
42. Sconocchia G, Eppenberger S, Spagnoli GC, Tornillo L, Droeser R, Caratelli S, et al. NK cells and T cells cooperate during the clinical course of colorectal cancer. *Oncoimmunology* (2014) 3(8):e952197. doi: 10.4161/21624011.2014.952197
43. Ottaiano A, Napolitano M, Capozzi M, Tafuto S, Avallone A, Scala S, et al. Natural killer cells activity in a metastatic colorectal cancer patient with complete and long lasting response to therapy. *World J Clin Cases* (2017) 5(11):390–6. doi: 10.12998/wjcc.v5.i11.390

Conflict of Interest: The authors of Affiliation 1 (AS, FM, FB, DC, FC, SB, SP, and DG) are employed by Cell Dynamics isrl company. The authors declare that a Patent Application (No. 102020000006031) incorporating parts of this work has been filed. DG, SB, DC, AS, and FM are the inventors of patent No. 102020000006031.

The remaining authors declare that the research was conducted in the absence of any commercial or financial relationships that could be construed as a potential conflict of interest.

frontiers in Immunology

ORIGINAL RESEARCH
published: 03 May 2021
doi: 10.3389/fimmu.2021.639572

3D Bioprinting Allows the Establishment of Long-Term 3D Culture Model for Chronic Lymphocytic Leukemia Cells

*Francesca Vittoria Sbrana[1], Riccardo Pinos[1,2], Federica Barbaglio[1], Davide Ribezzi[1,3], Fiorella Scagnoli[1], Lydia Scarfò[2,4], Itedale Namro Redwan[5], Hector Martinez[5], Silvia Farè[3], Paolo Ghia[2,4] and Cristina Scielzo[1]**

[1] Malignant B Cells Biology and 3D Modelling Unit, Division of Experimental Oncology, IRCCS Ospedale San Raffaele, Milano, Italy, [2] School of Medicine, Università Vita-Salute San Raffaele, Milano, Italy, [3] Department of Chemistry, Materials and Chemical Engineering, Politecnico di Milano, Milano, Italy, [4] B-Cell Neoplasia Unit and Strategic Research Program on CLL, Division of Experimental Oncology, IRCCS Ospedale San Raffaele, Milano, Italy, [5] CELLINK AB, Gothenburg, Sweden

OPEN ACCESS

Edited by:
Silvia Scaglione,
National Research Council (CNR), Italy

Reviewed by:
Marek Mraz,
Central European Institute of Technology (CEITEC), Czechia
Zoltan Janos Vereb,
University of Szeged, Hungary

***Correspondence:**
Cristina Scielzo
scielzo.cristina@hsr.it

Specialty section:
This article was submitted to Cancer Immunity and Immunotherapy, a section of the journal Frontiers in Immunology

Received: 09 December 2020
Accepted: 01 April 2021
Published: 03 May 2021

Citation:
Sbrana FV, Pinos R, Barbaglio F, Ribezzi D, Scagnoli F, Scarfò L, Redwan IN, Martinez H, Farè S, Ghia P and Scielzo C (2021) 3D Bioprinting Allows the Establishment of Long-Term 3D Culture Model for Chronic Lymphocytic Leukemia Cells. Front. Immunol. 12:639572. doi: 10.3389/fimmu.2021.639572

Chronic Lymphocytic Leukemia (CLL) represents the most common leukemia in the western world and remains incurable. Leukemic cells organize and interact in the lymphoid tissues, however what actually occurs in these sites has not been fully elucidated yet. Studying primary CLL cells *in vitro* is very challenging due to their short survival in culture and also to the fact that traditional two-dimensional *in vitro* models lack cellular and spatial complexity present *in vivo*. Based on these considerations, we exploited for the first time three-dimensional (3D) bioprinting to advance *in vitro* models for CLL. This technology allowed us to print CLL cells (both primary cells and cell lines) mixed with the appropriate, deeply characterized, hydrogel to generate a scaffold containing the cells, thus avoiding the direct cell seeding onto a precast 3D scaffold and paving the way to more complex models. Using this system, we were able to efficiently 3D bioprint leukemic cells and improve their viability *in vitro* that could be maintained up to 28 days. We monitored over time CLL cells viability, phenotype and gene expression, thus establishing a reproducible long-term 3D culture model for leukemia. Through RNA sequencing (RNAseq) analysis, we observed a consistent difference in gene expression profile between 2D and 3D samples, indicating a different behavior of the cells in the two different culture settings. In particular, we identified pathways upregulated in 3D, at both day 7 and 14, associated with immunoglobulins production, pro-inflammatory molecules expression, activation of cytokines/chemokines and cell-cell adhesion pathways, paralleled by a decreased production of proteins involved in DNA replication and cell division, suggesting a strong adaptation of the cells in the 3D culture. Thanks to this innovative approach, we developed

a new tool that may help to better mimic the physiological 3D *in vivo* settings of leukemic cells as well as of immune cells in broader terms. This will allow for a more reliable study of the molecular and cellular interactions occurring in normal and neoplastic conditions *in vivo*, and could also be exploited for clinical purposes to test individual responses to different drugs.

Keywords: chronic lymphocytic leukemia, 3D culture, bioprinting, B cell, leukemia

INTRODUCTION

Chronic Lymphocytic Leukemia (CLL) is the most common leukemia among adults in the Western World and it is characterized by the relentless accumulation of mature monoclonal B lymphocytes with a specific immunophenotype, positive for CD19 and CD5, along with CD23 (1). CLL is considered a dynamic and heterogeneous disease, where leukemic cells traffic and home in the peripheral blood (PB), bone marrow (BM) and secondary lymphoid tissues, such as lymph nodes (LNs) and spleen (SP) (2–5). Despite the contribution of an increasing number of studies, not only CLL is still incurable but also the underlying pathogenic mechanisms still need to be fully elucidated. In particular, mechanisms orchestrating the trafficking of the leukemic cells between the PB and the lymphoid tissues, where they organize and interact with a supportive microenvironment, have not been fully explained yet (6). Leukemic cells in the tissues establish a crosstalk with the cells from the microenvironment, which strongly support their survival and proliferation through direct contact and the secretion of specific stimuli (7, 8). Recently, Primo et al. (9) demonstrated that primary CLL B cells increase their survival and proliferation rate *in vitro* when co-cultured with stromal cells and in the presence of specific factors, such as CpG and IL2, thereby resembling the extracellular tissue microenvironment. Indeed, one of the biggest challenges in studying primary CLL cells alone *in vitro* originates from the inability to maintain their viability for a long time without the addition of exogenous stimuli that inevitably affect the function and behavior of the cells (10). A reason could be that traditional two-dimensional (2D) cultures, commonly utilized for *in vitro* studies, lack the complexity of the spatial cellular organization taking place in the tissues, providing a simplified overview of tumor biology. In addition, animal models show many limitations in particular being expensive, time consuming and not adequately reproducing all features of human tumors (11). As a consequence, it has become evident that innovative approaches are necessary to potentially overcome 2D culture-systems limitations, thus providing a better way to mimic *in vitro* what actually occurs *in vivo* (12, 13). Interestingly, over the last few years, three-dimensional (3D) culture systems have been largely implemented. The term "3D culture" refers to a 3D system in which cells can survive, proliferate, migrate, communicate and behave in a more realistic environment from a spatial point of view, and are no longer cultured on a 2D plastic or glass surface (14). In the most recent years, *in vitro* 3D models have been developed to recapitulate specialized microenvironments, such as lymphoid tissues, by integrating advanced biomaterials and microfluidics. This allowed elucidating new regulatory mechanisms and potential therapeutic targets that could have not otherwise been studied in conventional 2D cultures (15). Several 3D systems have also been applied to the study of different B cell malignancies; however, this has only recently been used for CLL and with rather limited attempts (13). In particular, we recently demonstrated the advantages of co-culturing CLL cells with bone-marrow stromal cells seeded on a 3D scaffold to study their response to targeted therapy *in vitro* (16) and, in parallel, we realized the need for exploring additional 3D culture systems to allow the growth of primary CLL cells alone as well as to improve the reproducibility of the cell seeding. Lately, relevant technological advancements have been achieved and have started being applied in biomedicine. One of the most striking is the implementation of 3D bioprinting in biomedical research, which, to date, is considered a very promising approach to generate complex and advanced 3D *in vitro* models (17, 18). Specifically, 3D bioprinting is an additive manufacturing technique in which cells are encapsulated (avoiding cell seeding limitations) within a "bioink" that ideally mimics the native extracellular matrix (ECM), and are subsequently deposited in a layer-by-layer process to a previously defined geometry (19).

In the present work, we tested for the first time whether 3D bioprinting could be applied in our system and could therefore advance *in vitro* models for CLL. We successfully evaluated CLL cells for printability, optimized the printing strategy and set-up the protocols to perform the analysis. Our results demonstrate that we can efficiently 3D bioprint primary CLL cells and improve their viability without the addition of exogenous stimuli and/or stromal cells. We can maintain and study in-culture 3D bioprinted CLL cells for up to 28 days, thus establishing an innovative and reproducible long-term 3D culture model for leukemia cells.

MATERIALS AND METHODS

Human Ethics Statement

Patients with CLL were diagnosed according to the updated National Cancer Institute Working Group (NCIWG) guidelines (20). Peripheral blood (PB) samples were obtained after informed consent from patients who were untreated or off treatment for at least 6 months. The study was approved by the Ospedale San Raffaele (OSR) ethics committee under the protocol VIVI-CLL entitled: "*In vivo* and *in vitro* characterization on CLL". Clinical and biological characteristics of patients with CLL who provided samples for the experiments are reported in **Supplementary Table 1**.

Cell Culture and Human Primary Samples Purification

MEC1 cell line (21) was obtained from Deutsche Sammlung von Mikroorganismen und Zellkulturen GmbH (DSMZ, Braunschweig, Germany) and was recently genotyped as following: 10 ng of DNA from MEC1 cells was purified with QiAmp DNA Mini Kit (Qiagen, Düsseldorf, Germany) and amplified through PCR with GenePrint ® 10 System (Qiagen, Düsseldorf, Germany) and sold Eurofins Genomics Standard FLA Service to perform genotyping. Data was analyzed with DSMZ Online STR Analysis. We confirmed the identity of the cell line analyzed. MEC1 cells were cultured in RPMI 1640 medium (EuroClone, Pero, Italy) supplemented with 10% (v/v) Fetal Bovine Serum (FBS) and 15 mg/ml Gentamicin (complete RPMI) at 37°C and 5% CO_2. Leukemic CD19 cells were negatively selected from fresh peripheral blood using the RosetteSep B-lymphocyte enrichment kit according to the manufacturer protocol (StemCellTechnologies, Vancouver, Canada). Then, the Lymphoprep™ reagent (StemCellTechnologies, Vancouver, Canada) is added to the sample and centrifuged at 2000RPM, 20 minutes. After washing twice with PBS 1500RPM, 5 minutes, the cells are ready to use.

The purity of all preparations was always higher than 99%, and the cells co-expressed CD19 and CD5 on their surfaces as assayed by flow cytometry (Navios Flow Cytometer; Beckman Coulter); preparations were virtually devoid of natural killer (NK) cells, T lymphocytes, and monocytes.

Bioink Preparation and 3D Hydrogel Scaffold Fabrication

MEC1 (21), MEC-GFP (22) or leukemic primary cells were counted, centrifuged at 1500RPM for 5 minutes, resuspended in 1:10 medium:hydrogel ratio, then gently mixed with CELLINK Bioink, CELLINK RGD10, CELLINK Laminink111, CELLINK Laminink411 or CELLINK Laminink521 hydrogels (CELLINK AB, Gothenburg, Sweden) using two luer lock syringes. We virtually calculated the number of cells potentially present in a tissue with the dimension of the printed scaffold ($5x5x1mm^3$). We calculated the theoretical volume of a lymphoid cell, considering it as a sphere ($\frac{4}{3}\pi r^3$, *median cell radius* $\simeq 5\mu m$) and the volume of the scaffold, considering it as a rectangular parallelepiped (LxLxH). We approximately estimated that to entirely fill the scaffold we should need about $\simeq 50x10^6$ cells for scaffold, alias $\simeq$50µl hydrogel, (n°cells=scaffold volume/cell volume). Following an experiment in which we used decreasing concentration of cells, we established a final optimal concentration ranging from 5 to $10x10^6$cells/100µl for the cell lines, and from 15 to $20x10^6$ cells/100µl for primary cells (data not shown).

The bioink mixed with the cells was then loaded in a cartridge and placed in the Bio X 3D bioprinter (CELLINK AB, Gothenburg, Sweden). The 3D scaffolds ($5x5x1mm^3$) were designed with Fusion360 (Autodesk). The slicing process was directly made exploiting the Bio X slicer software, using a rectilinear pattern with 30% infill density. The Bio X was equipped with a 25G (250µm) nozzle and the layer height was set at 0.25mm. The pressure applied to the 3D bioprinting process is hydrogel/cells-dependent, a range of values around 11-14 kPa was used. All the settings of the printing process were uploaded on Bioverse (https://bioverse.com/). Printing of 3D scaffolds was directly performed in 12-well plates at 7mm/s deposition speed. The constructs were crosslinked with 50mM $CaCl_2$ (CELLINK AB, Gothenburg, Sweden) for 4 minutes at room temperature and washed once with Hank's Balanced Salt Solution (HBSS, EuroClone, Pero, Italy), according to the manufacturer protocol (CELLINK AB, Gothenburg, Sweden). RPMI complete medium (EuroClone, Pero, Italy) was added to MEC1 and MEC-GFP-laden scaffolds while CLL primary cells-laden scaffolds were added with DMEM high glucose (EuroClone, Pero, Italy) supplemented with 10% Human Serum (EuroClone, Pero, Italy) and 1% Penicillin/Streptomycin (Lonza, Basel, Switzerland), since CLL primary cells viability was found to be improved in the just-mentioned conditions from previous *in vitro* tests (data not shown). The medium was changed within 30 minutes after the printing, before the culture was placed in an incubator at 37°C, 5% CO_2.

Compressive Mechanical Properties

The compressive mechanical properties of 3D printed hydrogels under investigation was tested by Dynamic Mechanical Analyzer (DMA Q800, TA Instruments) with or without loaded cells. Scaffold hydrogels (n = 5) were prepared by printing of Cellink Bioink and Cellink Laminink 411 with an air pressure ranging from 11 to 14 kPa, with a deposition speed of 7 mm/s. All scaffolds were plotted with cylindrical geometry (2:3 height: diameter ratio) and crosslinked in 50mM $CaCl_2$ (CELLINK AB, Gothenburg, Sweden) for 4 minutes. Tests were performed at room temperature, applying a 0,001 N preload. Each test consisted of a loading run (strain ramp = - 2,5% min^{-1} down to -30%) followed by the unloading run (strain ramp = + 5% min^{-1} up to + 1%). The stress-strain curves were elaborated and the following mechanical parameters were considered: elastic modulus (E, considered as the slope of the regression curve in the 0-5% strain range), stiffness (K, as the slope of the regression curve in the 25-30% strain range), the maximum stress σ_{max} (corresponding to the maximum strain, i.e. ϵ = 30%), and the residual strain ϵ_{res} (corresponding to the unrecovered strain at the end of the unloading run). Rheology data of the hydrogels used (CELLINK AB, Gothenburg, Sweden) are shown in **Supplementary Figure 1**.

Live/Dead Assay

3D bioprinted cells viability was assessed overtime by using the LIVE/DEAD® Cell Imaging Kit (Thermo Fisher Scientific, Massachusetts, USA), which allows for the visualization of live (green) and dead (red) cells. The scaffolds were washed one time (30 min) with DMEM without serum (Thermo Fisher Scientific, Massachusetts, USA) and Live/Dead reagent was added in a 1:3 ratio. After 1 hour of incubation at 37°C, 5% CO_2 the constructs were washed one time with DMEM without serum and observed with the AXIO Observer Z1 fluorescent microscope using FITC and TRITC filters, through Volocity Acquisition software, and then processed using FIJI (ImageJ) software. A grid was drawn on both the fitc-live and tritc-dead images, and live and dead

cells, respectively, lying in the same fields were manually counted. Then, the percentage of live and dead cells on the total count was performed as follows: living and dead cells, respectively, were divided by the total number (live + dead) of counted cells and multiplied by 100.

Alamar Blue Assay

The Alamar blue® assay (Thermo Fisher Scientific, Massachusetts, USA) was performed on the same 3D scaffolds over time (up to 28 days of culture), in order to minimize intra-experiment replicate variability. The reagent was mixed with the appropriate medium (RPMI 1640 or DMEM complete medium) in a 1:10 ratio, respectively; then 1mL of the mix was added to each well. As assay blank, RPMI or DMEM complete medium with a 3D bioprinted scaffold without cells was used. After 4h 30' of incubation at 37°C, 5% CO_2, 100µl of the mix were collected and transferred to a 96-well white plate and the fluorescence values were read using the Victor spectrophotometer. The scaffolds were then washed once and placed in the proper medium for subsequent analyses.

For 2D cultures, the manufacturer's instructions were followed. Briefly, the amount of medium per well was measured and mixed in a 1:10 ratio with the Alamar blue® reagent. After 4h 30' of incubation at 37°C, 5% CO_2, the cells were centrifuged at 2000RPM, 5 minutes and then 100µl of the supernatant were collected and transferred to a 96-well white plate to measure fluorescence values using the Victor spectrophotometer.

RNA Extraction and Real-Time PCR

RNA extraction was performed overtime (day 0-7-14-21-28 for 3D samples, n=16; day 0-3-7-10-14 for 2D samples, n = 16), according to the manufacturer's instructions, using TRIzol reagent (Ambion) for 3D bioprinted scaffolds and ReliaPrep RNA Cell Miniprep System® (Promega, Madison, USA) for 2D cell lines and primary samples. In general, 3D bioprinted constructs were smashed and chloroform added. The RNA is then collected after consecutive centrifugation steps and isopropanol/ethanol washes and resuspended in a variable amount of nuclease-free water. RNA from 2D cell lines and primary samples is obtained by isopropanol/DNAse solution washes and centrifugation steps. Lastly, the RNA is resuspended in nuclease-free water. cDNA was synthesized according to the manufacturer's protocol using the RevertAid® H Minus First Strand DNA Synthesis kit (Thermo Fisher Scientific, Massachusetts, USA). RT-qPCR analysis was performed using Titan HotTaq Probe qPCR mix (BioAtlas) in an ABI7900 Thermal Cycler instrument (Applied Biosystem, Foster City, USA). The analysis was performed in triplicate. Quantification of *BAX*, *BCL2, AICDA, SELL, CXCR3, CCL22, HCLS1, PIM3, MYC* transcripts (Applied Biosystem probes) was performed according to the Ct method (23), using *GAPDH/YWHAZ* as the housekeeping gene.

RNAseq Analysis

After performing RNA extraction as described above, 3D bioprinted cells were further treated with DNase I (Thermo Fisher Scientific, Massachusetts, USA) and Ambion™ RNase Inhibitor (Thermo Fisher Scientific, Massachusetts, USA) for 15 minutes at 37°C, and eventually a second RNA extraction was performed by using ReliaPrep RNA Cell Miniprep System® (Promega, Madison, USA). RNA quality was confirmed with a 2100 Bioanalyzer (Agilent), and all samples had RIN (RNA Integrity Number) greater than 7. We exploited the SMQRT-Seq® v4 Ultra® Low Input RNA (TaKaRa) protocol, to generate the next-generation sequencing (NGS) libraries starting from 2ng of RNA. Libraries were barcoded, pooled and sequenced on an Illumina Nova-Seq 6000 sequencing system (Illumina, San Diego, USA), in SR (single read) mode, with reads 100nt long. We estimated to obtain 80 million single-end reads per sample on average.

Reads were trimmed using Trimmomatic, version 0.39, in order to remove adapters and to exclude low-quality reads from the analysis. The remaining reads were then aligned to the reference genome GRCh38, GENCODE release 31, using STAR aligner, version 2.5.3a. FeatureCounts (v 1.6.4) was used to assign reads to the corresponding genes. Only genes with a CPM (Counts per million) value higher than 1 in at least three samples were retained. Gene expression read counts were exported and analyzed in R environment (v. 3.6.2) to identify differentially expressed genes (DEGs), using the DESeq Bioconductor library (24). p-values were adjusted using a threshold for false discovery rate (FDR) ≤ 0.05 (25). Using the 500 most variable genes in terms of RPKM (counts per million reads normalized on library sizes and gene lengths), we performed Principal Component Analysis (prcomp function in R) and clustering analysis *via* heatmap (pheatmap R library). The RNAseq data, including raw sequence files, have been submitted to NCBI's Gene Expression Omnibus and are accessible through the GEO series accession number GSE163977.

Go to: https://www.ncbi.nlm.nih.gov/geo/query/acc.cgi?acc=GSE163977.

Flow Cytometry

3D bioprinted scaffolds were smashed with 500µl of dissolution buffer (26), passed through a 30µm CellTrics filter (Sysmex, Kobe, Japan) to flow cytometer tubes, and eventually stained for 25 minutes RT for the following antibodies: CD5 PC5 (Beckman Coulter, Brea, USA), CD19 PC7 (Beckman Coulter, Brea, USA), and IgM PE (Miltenyi, Bergisch Gladbach, Germany). After washing with PBS 1500RPM, 5 minutes, cells were analyzed on Navios Flow Cytometer (Beckman Coulter, Brea, USA). Analyses were performed with the FCS Express software (DeNovo Software). Representative density plots were normalized on equal numbers of events occurring in the gates of interest. 3D bioprinted scaffold without cells was stained with the antibodies we used, in order to exclude nonspecific binding.

Immunohistochemistry and Fluorescent Images

3D bioprinted scaffolds containing CLL primary cells after 7 days of culture were washed twice with HBSS with 50mM of $CaCl_2$ for 8 minutes at 37°C, and then fixed with 4% PFA containing 50mM of $CaCl_2$ o/n at 4C. After fixation, scaffolds were washed twice with HBSS with 50mM of $CaCl_2$ for 10 minutes RT and eventually

incubated, first, for 45 minutes at 4°C in HBSS with 50mM, then for another 45 minutes RT in sucrose 30% in PBS. The scaffolds were then embedded in OCT matrix and placed at -80°C until cryosectioning. Frozen samples were sectioned (5-7μm) on Superfrost-plus microscope slides (Thermo Fisher Scientific, Massachusetts, USA), washed one time with PBS, and then stained with Mayer's Hematoxylin (Bio-Optica, Milan, Italy) for 1 minute, washed with tap water and stained with Eosin G (Bio-Optica, Milan, Italy) for 2 minutes. Images were taken with Zeiss Axio Imager M2m microscope with AxioVision (Rel. 4.9.1) software, and then processed using FIJI (ImageJ) software. Images of MEC-GFP cells inside and outside the 3D bioprinted scaffolds were obtained by using JuLI^{TM} Stage fluorescent microscope.

Statistical Analysis

Student's t-test was performed for statistical analysis (GraphPad Prism v.8.0a). Mann-Whitney unpaired t test was used for non-parametric comparisons of data sets (*$p < 0.05$; **$p < 0.01$; *** $p < 0.001$; ****$p < 0.0001$).

RESULTS

3D Bioprinting Supports CLL Cells Viability

We initially used the CLL cell line MEC1 (21) to set up the 3D bioprinting strategy and the analytic protocols, considering that there were no previous studies showing the printability of lymphocytes and their behavior in these settings of 3D culture.

First of all, we had to define the optimal number of lymphoid cells to be 3D bioprinted proportionally to the hydrogel quantity. Following a theoretical calculation (see *Materials and Methods* section for details) and based on cells dilution experiments (data not shown), we defined that the ratio of 10 x 10^6 MEC1 cells per 100μl of hydrogel was the optimal cell density, to adequately fill the scaffold but also to leave enough space for subsequent cell proliferation and eventually for the deposition of the extracellular matrix. To print MEC1 cells, we used CELLINK Bioink hydrogel, which is specifically designed to support cellular adhesion and functions, as it has high printability and biocompatibility (**Supplementary Table 2**). The cells were premixed with the hydrogel; we designed the geometry of the 3D bioprinted scaffold with Fusion 360 software and, eventually, we bioprinted the cells encapsulated in the hydrogel matrix. The pressure applied to the 3D bioprinting process is hydrogel/cells-dependent and a range of values around 11-14 kPa was used for our setting (see *Materials and Methods* section). The resulting scaffold was then cross-linked with $CaCl_2$ in order to give the needed stiffness and it was placed in a traditional culture plate (**Figure 1**). We measured the stiffness of the CELLINK Bioink hydrogel with and without cells (n = 4); stiffness values were found ranging around 16 and 7 kPa for cell-free and cellularized scaffolds, respectively, and lower maximum stress at 30% strain (**Figure 2**), showing a significant difference comparing 3D printed scaffold without cells and after 7 days of culture. In particular, the stiffness values matched the expected ones for the lymphoid tissues of our interests (26).

Soon after printing (after 7 days), we performed a Live/Dead assay that allowed us to discriminate viable and dead MEC1 cells quantified by drawing a grid on the images acquired by fluorescent microscope, and counting the cells manually (**Figure 3A**). About 75% of the cells in the printed scaffolds were alive (**Figure 3B**), thus demonstrating that CLL cells can be efficiently 3D bioprinted and that the printing process has only limited effects on their viability.

In order to visualize the spatial organization of the cells inside the 3D bioprinted hydrogel matrix, we used GFP-labelled MEC1 cell line (MEC-GFP) (22): we detected MEC-GFP cells homogeneously distributed throughout the 3D structure (**Figure 3C**).

Furthermore, we tested the ability of 3D bioprinted cells (MEC-GFP cells) (n=5) to move throughout the hydrogel scaffold after the print, up to 3 weeks of culture. Specifically, starting from day 0 to day 21 after printing, MEC-GFP were still found inside the scaffold (**Figure 3C**) but also outside, floating in the medium (0; $1{,}5x10^5$; $7x10^5$; $14{,}8x10^5$ cells at day 0, 7, 14, 21, respectively) (**Figure 3D**). MEC-GFP cells might be found outside the scaffold, by actively moving throughout the hydrogel as a consequence of the expansion due to their proliferation or by passively diffusing outside the hydrogel matrices because of its spontaneous degradation after a few days in culture (27–30).

Moreover, once MEC-GFP cells leave the scaffold, they maintain the characteristic phenotype of the cell line as demonstrated by their typical growth in clusters when cultured in suspension (**Supplementary Figure 2A**).

3D Bioprinted and 2D Cultured MEC1 Cells Show Differences in Gene Expression

We performed RNAseq analysis to compare 3D bioprinted to 2D cultured MEC1 cells, in order to evaluate genes and pathways affected by the 3D printing strategy. The Principal Component Analysis (PCA) was performed, and the two principal components were identified (PC1 and PC2) by using the 500 most variable genes in terms of RPKM (reads per kilobase of transcript per million reads mapped) (31). Specifically, we observed a clear segregation of the samples according to the different conditions: 2D and 3D samples substantially separated along PC1, expressing 54,4% of the total variance, while the effect of the considered 3D time points (day 7 vs day 14) is evident along PC2, representing 22,1% of the total variance (**Figure 4A**). Similarly, we observed a visible different effect of the analyzed conditions in the heatmap (**Figure 4B**), showing a strong separation between 2D and 3D bioprinted samples in terms of gene expression.

By performing the differential expression analysis with the package DESeq2 (24) using FDR (False Discovery Rate) as the cut-off to determine the significance of the differential genes (32), we detected a high number of modulated genes in the 2D vs 3D conditions, some up-regulated and some down-regulated (**Figure 4C**). Among the first 100 most modulated genes, we identified genes with particular interest for CLL pathophysiology (**Figures 4D, E**), which we successfully validated by RT-qPCR (**Figure 4F**). In detail, we observed upregulation in 3D culture of the following genes: *CXCR3*, chemokine receptor that is involved in cellular responses, leukocyte trafficking, integrin activation, cytoskeletal remodeling

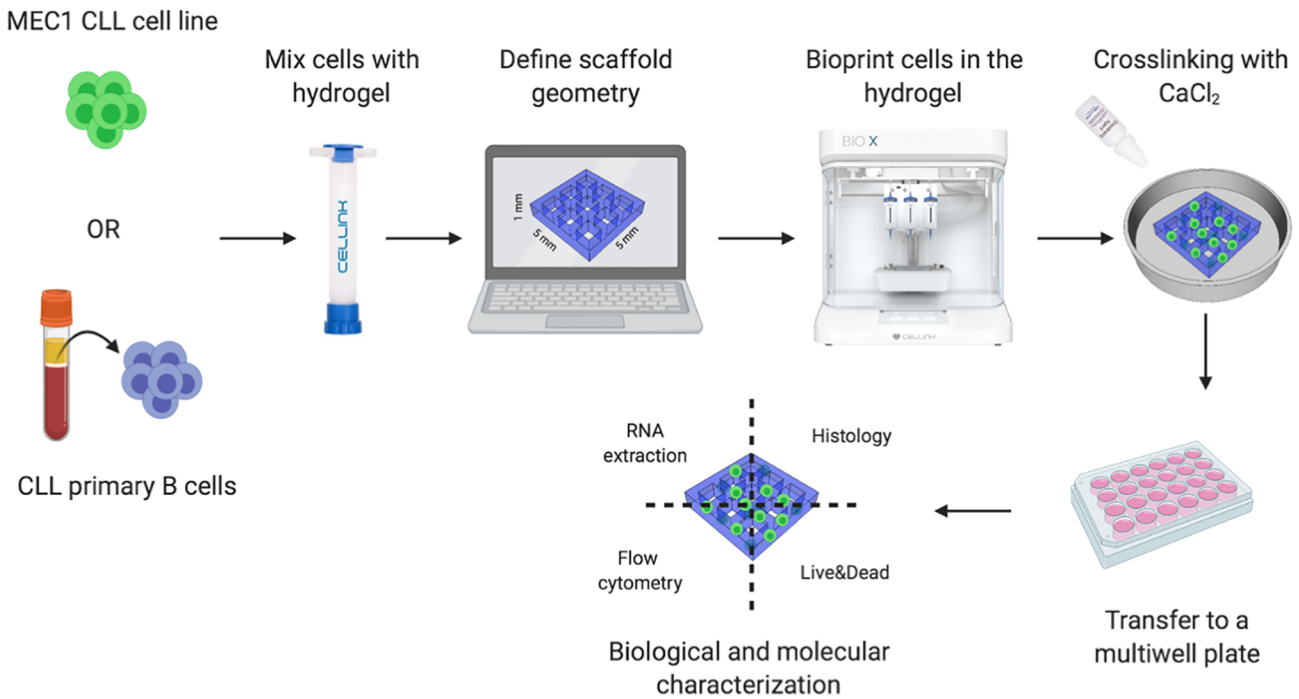

FIGURE 1 | 3D bioprinting strategy. Schematic representation of our 3D bioprinting strategy: CLL cell line MEC1 or CLL primary B cells were used. The cells are pre-mixed with hydrogels specifically designed to support cellular adhesion and functions, as well as high printability and biocompatibility. Once the geometry of the 3D bioprinted scaffolds is defined, the cells are printed, encapsulated in the hydrogel matrix, crosslinked with $CaCl_2$ and placed in a culture plate. The constructs are then processed to extract the RNA, perform histological analyses, assess cell surface markers and cell viability.

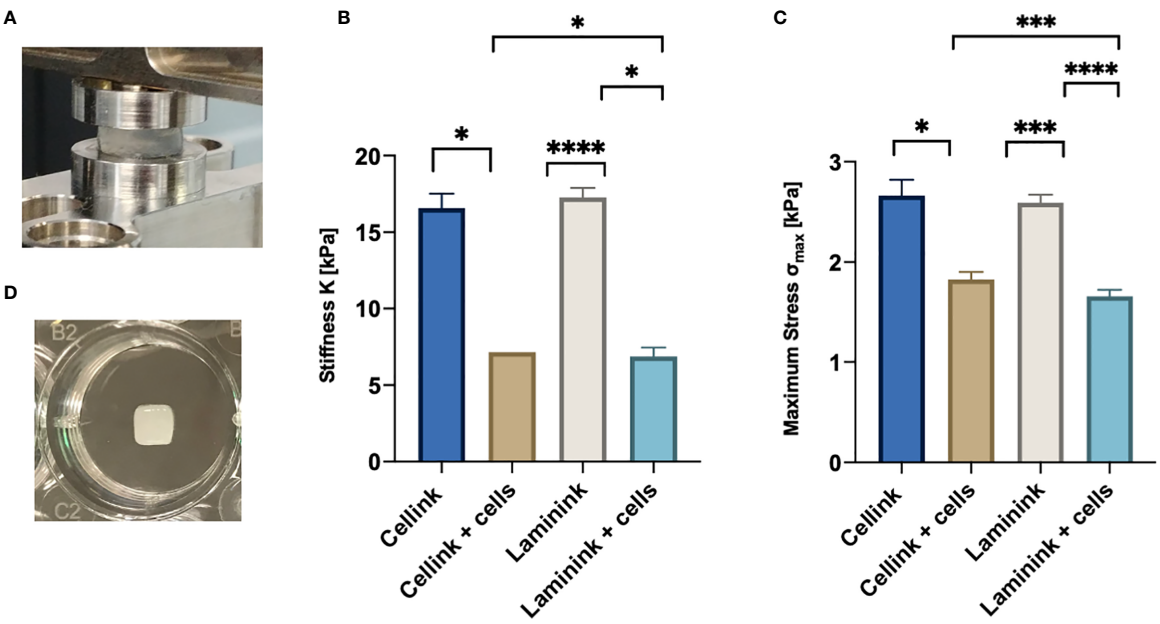

FIGURE 2 | Compressive mechanical properties of hydrogel scaffolds with and without embedded cells. **(A)** Hydrogel scaffold specimen in the compression mode clamps. **(B)** Average and standard deviation values of stiffness, K, for the scaffolds (n=4). **(C)** Average and standard deviation values of maximum stress, σ_{max} (n=4). **(D)** Representative picture of a 5x5x1mm^3 3D-bioprinted scaffold in a well of a 24-well plate. *p < 0.05, ***p < 0.001, ****p < 0.0001.

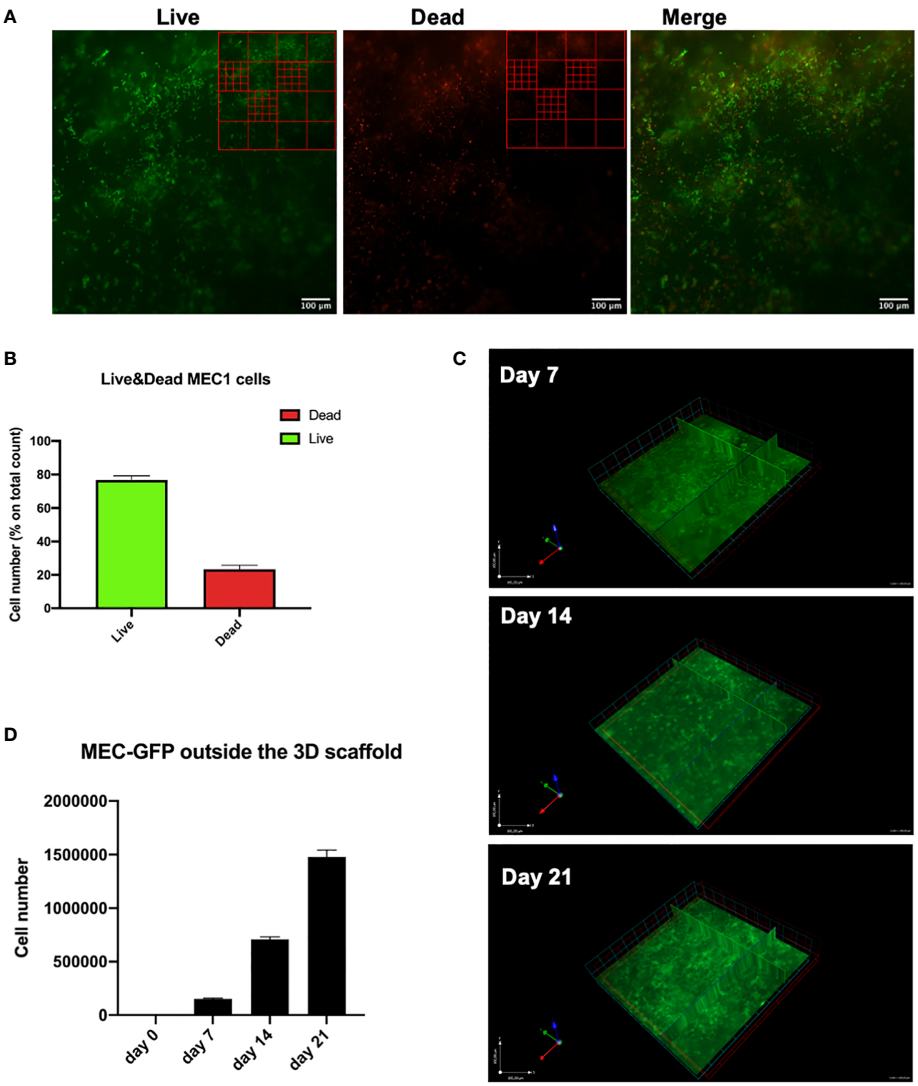

FIGURE 3 | CLL cells are viable and homogeneously distributed in the hydrogel matrix. MEC1 and/or MEC-GFP cell lines were used to define the optimal number of cells and hydrogel quantity to be printed. **(A)** Representative images of Live/Dead assay of 3D bioprinted MEC1 cell line acquired with Axio Observer Zeiss fluorescent microscope. Green cells are alive cells; red cells are dead cells. An example of a grid scheme used to quantify alive and dead cells is shown on the top right of each image. **(B)** The graph shows quantification of alive (green column portion) and dead (red column portion) 3D bioprinted MEC1 cells. **(C)** Representative z-stack images of 3D bioprinted MEC-GFP cells in the scaffold overtime showing their distribution. Images were obtained with Axio Observer Zeiss fluorescent microscope. **(D)** The graph shows quantification by cell count, at different time points (day 0-7-14-21), of viable MEC-GFP cells found outside the 3D bioprinted scaffold. Data are represented as mean ± SEM, n=3 **(B)** and n=5 **(D)**.

(33), and its expression has been demonstrated to play a prognostic role in CLL (34); *CCL22*, cytokine that has been demonstrated to be produced by CLL cells to chemo attract T lymphocytes (35, 36); *SELL*, gene that encodes for a Calcium-dependent lectin that mediates the adherence of lymphocytes to endothelial cells in peripheral lymph nodes and promotes the initial tethering and the rolling of leukocytes in endothelium and has been recently demonstrated to be involved in CLL transformation to high-grade B-cell lymphoma (37, 38); *HCLS1*, gene that we demonstrated in the past being involved in cytoskeletal remodeling, migration, trafficking and homing of CLL cells (16, 22); *AICDA*, gene that is involved in somatic hypermutation, gene conversion, and class-switch recombination in B-lymphocytes, and it is required for several crucial steps of B-cell terminal differentiation necessary for efficient antibody responses (39, 40). Interestingly, we also observed downregulation of: *MYC*, proto-oncogene that plays a central role in cell cycle progression, apoptosis and cellular transformation and promotes VEGFA production and subsequent sprouting angiogenesis, its role has been recognized in the transformation in aggressiveness of indolent B cell malignancies (41, 42); *PIM3*, proto-oncogene overexpressed in hematological and epithelial tumors and associated with MYC, their coexpression has a role in the regulation

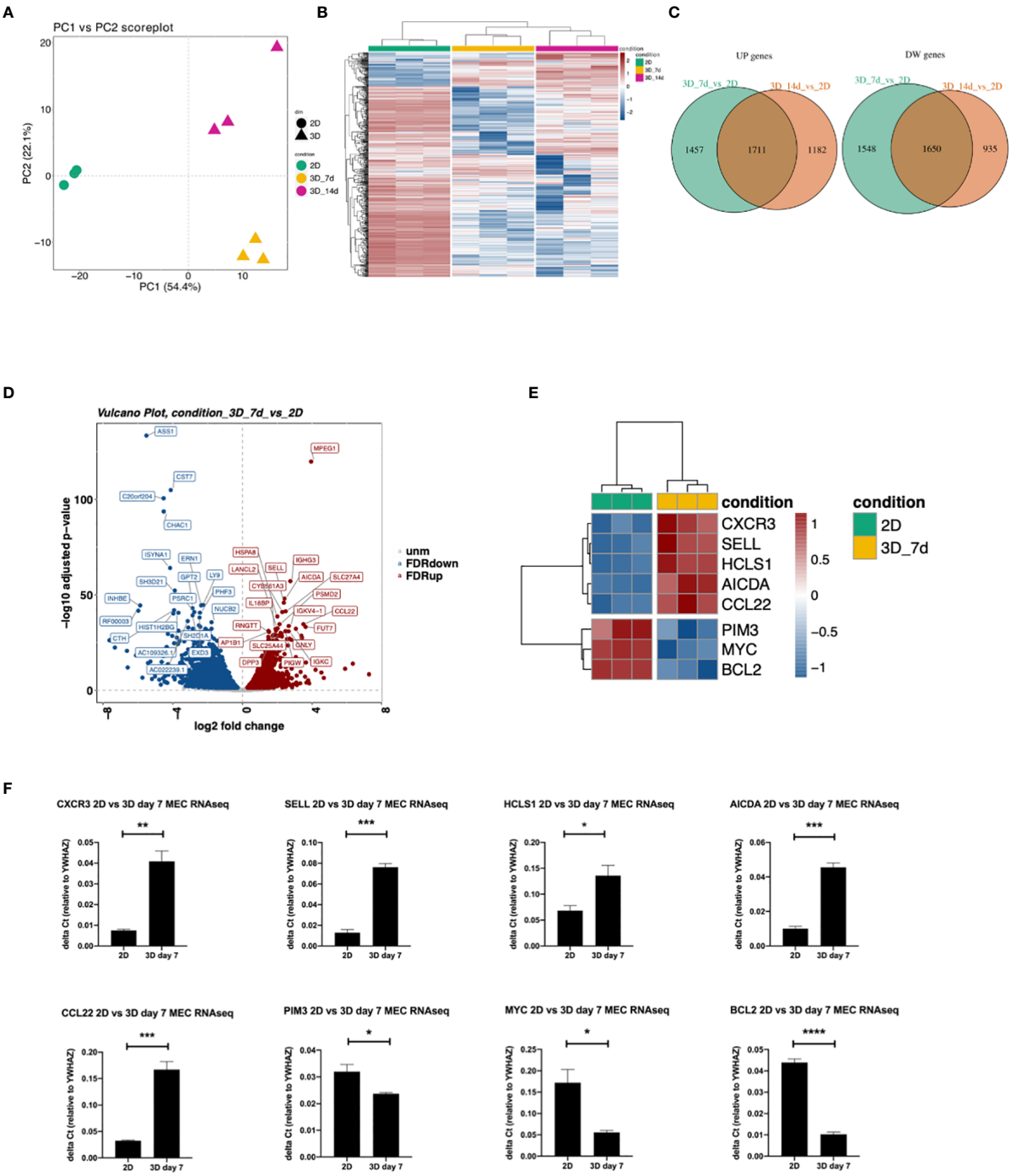

FIGURE 4 | Differences in gene expression between 3D bioprinted and 2D cultured MEC1 cells: clustering analysis and top genes validation. **(A)** PCA plot built using the 500 most variable genes (in RPKM). **(B)** Heatmap of the 500 most variable genes (in RPKM), clustering row (genes) and columns (samples). Expression is scaled. **(C)** Intersection between up-regulated (left) and down-regulated (right) genes between the comparisons 3D_7d_vs_2D and 3D_14d_vs_2D. **(D)** Vulcano plot for the comparison 3D_7d_vs_2D highlighting the 20 most significantly up-regulated (red) and down-regulated (blue) features for the FDR filter. **(E)** Heatmap summarizing genes among the first 100 most modulated in the comparison 3D_7d_vs_2D. **(F)** The graphs show mRNA levels of n=8 genes selected among the first 100 most modulated in the comparison 3D_7d_vs_2D which have been validated by RT-qPCR (*AICDA, SELL, CXCR3, CCL22, HCLS1, PIM3, MYC, BCL2*). *p < 0.05, **p < 0.01, ***p < 0.001, ****p < 0.0001. Data are represented as mean ± SEM, n=3 MEC1 cell line samples. Student's t-test was performed for statistical analysis.

of signal transduction cascades, contributing to both cell proliferation and survival, and provides a selective advantage in tumorigenesis (43). The last gene that we validated for its importance in CLL is *BCL2* gene that is downregulated in 3D cultured MEC1 cells and encodes for a protein that suppresses apoptosis in a variety of cellular systems including factor-dependent lymphohematopoietic and neural cells, thus it is used as a therapeutic target for B-cells malignancies in particular in CLL (44).

By Gene Ontology analysis, we further investigated pathways potentially affected by the different culture conditions. We observed that 3D cultured cells at both day 7 and 14 show increased production of immunoglobulins, a key feature for CLL pathobiology and current therapeutic target (45–47) (**Figure 5A** and **Supplementary Figure 3A**) pro-inflammatory molecules (e.g. IFN alpha and beta), immune response activation and cellular stress markers with respect to 2D ones (**Figure 5B** and **Supplementary Figure 3B**), paralleled by a decreased production of proteins involved in protein targeting the Endoplasmic Reticulum (ER) and cell membrane, DNA replication, organelle fission, protein translation and cell division respect to 2D ones (**Figure 5C** and **Supplementary Figure 3C**). Interestingly, we found upregulated genes enriching for pathways involved in the formation of focal adhesion, as well as in the production and activation of cytokines/chemokines, and cell-cell adhesion at both day 7 (**Figure 5D** and **Supplementary Figure 3D)** and day 14 in 3D compared to 2D (**Figure 5D** and **Supplementary Figure 4**), suggesting a strong adaptation of the cell line MEC1 in the 3D culture.

3D Bioprinted Primary CLL Cells Show a Long-Term Viability

Once we set up the 3D bioprinting strategy for the MEC1 cell line, we transitioned to primary B lymphocytes isolated from the peripheral blood (PB) of patients affected by CLL and healthy donors.

First, we evaluated primary CLL cells printability by testing different hydrogels (CELLINK AB) that could favor CLL cells survival, namely: RGD10, Lam111, Lam411 and Lam521; we embedded $20x10^6$ primary CLL cells in 100µl of hydrogel. The Alamar blue viability assay showed that leukemic cells may survive for up to 7 days in all considered matrices (**Supplementary Figures 5A–D**), showing higher and thus more promising viability values [expressed in Fluorescence mean value (FM)] in the hydrogel matrix containing laminin 411, after 7 days of culture (FM Lam411 = 876103 vs FMs RGD10 = 388774, Lam111 = 492252, Lam521 = 394100) (**Supplementary Figure 5E**). Taken together, these results led us to conclude that CELLINK Laminink411 hydrogel was the most suitable for our study on primary CLL cells. Indeed, we also tested MEC1 cells printability in the laminin hydrogel series but we didn't observe an improvement in cell survival in comparison with CELLINK Bioink (data not shown).

Stiffness of CELLINK Laminink411 hydrogel was found in the range of 7 and 17 kPa for scaffolds printed with and without cells, respectively (**Figure 2**). Values measured on cellularized scaffolds were similar to what expected in the lymphoid tissues of our interests (19).

To study a larger cohort of patients (n = 26), we selected them based on the mutational status of the IGHV gene (IGHV<98%=mutated=good prognosis (mCLL) n = 16; IGHV≥98%=unmutated=bad prognosis (uCLL) n = 9) (48), in order to evaluate possible differences in the outcomes of their PB-derived cells behavior *in vitro* (**Supplementary Table 1**).

Primary CLL cells were 3D bioprinted in the CELLINK Laminink411 hydrogel, placed in standard culture conditions without the addition of any stimuli, and their viability was evaluated over time (up to 28 days). First, we confirmed a homogeneous distribution of 3D bioprinted primary CLL cells by performing H&E staining on a 5µm frozen section (**Figure 6A**). Then, by performing Live/Dead assay, we observed viability up to 28 days for 3D bioprinted primary CLL cells (n = 8), independently of their clinical/biological features (**Figure 6B**). In detail, using the Live/Dead assay, we observed 93%, 66%, 69%, 47% of viable cells at 7, 14, 21, 28 days after the print, respectively (**Figure 6C**). This data was confirmed by Alamar blue viability assay (n = 11) that showed 90%, 63%, 62%, 58% of live cells at the same Live/Dead assay time points (**Figure 6E**).

Notably, we also performed a Live/Dead assay on the scaffolds (n = 3 patients) that we cut in half and then images were acquired at all the time points (0-7-14-21-28 days), and we observed that cells are viable in the entire scaffold (**Supplementary Figure 6**).

In contrast, when we evaluated the viability over time (up to 14 days) of traditionally 2D cultured primary CLL cells (n = 16), grown on Laminin411 coated tissue culture plates without the addition of exogenous factors, we observed a dramatic decrease in cells viability after a few days in culture: 68%, 37%, 14%, 4% of viable cells by Alamar blue assay at 3, 7, 10, 14 days after the print, respectively (**Figure 6D**).

When we compared 2D cultured with 3D bioprinted primary CLL cells viability after 7 days of culture (n = 16), a time point when a proportion of 2D cultured cells is still viable, 3D bioprinted primary CLL cells showed a significantly higher viability by Alamar blue assay compared to 2D cultured ones ($p < 0.0001$) (**Figure 6F**). Interestingly, primary CLL cells derived from mCLL were found to be significantly more viable ($p = 0.0006$) than those obtained from uCLL ($p = 0.0115$) (**Supplementary Figures 7A, B**).

In parallel, we tested the ability of 3D bioprinted CLL cells (n = 3) to move throughout the hydrogel scaffold after the print, up to 4 weeks of culture. We noted that CLL cells were virtually absent outside the scaffold, thus supporting the hypothesis that matrix degradation is not the main cause for the presence of cells in the supernatant, which can be explained by active movement through the matrix in response to the increased number of proliferating cells that is not taking place in the case of primary resting CLL cells.

Notably, we tested the possibility of 3D bioprint Peripheral Blood Mononuclear Cells (PBMCs) from healthy donors in the Cellink Laminink411 hydrogel, and we observed also in this case a sustained viability over time (up to 28 days) (**Supplementary Figure 8**), thus paving the way to the use of this approach in the study of both healthy and malignant lymphocytes.

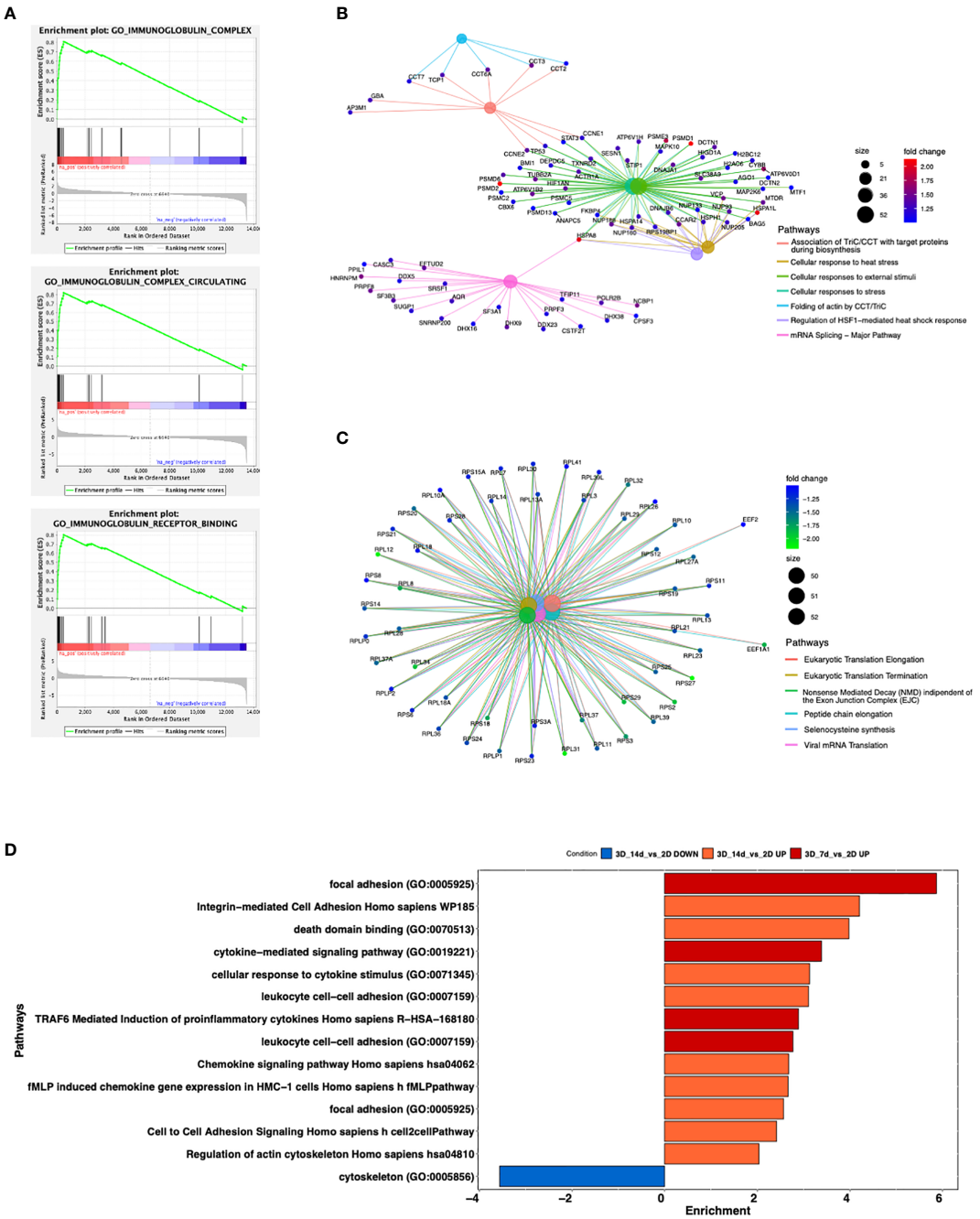

FIGURE 5 | Enrichment analysis of significantly modulated genes enriching different pathways. **(A)** GSEA curves for the first most significantly up-regulated pathways for Gene Ontology database in the comparison 3D_7d_vs_2D. **(B, C)** Cnetplots highlighting up-regulated **(B)** and down-regulated **(C)** pathways between the comparisons 3D_7d_vs_2D. **(D)** Bar plot showing most modulated pathways in both comparisons 3D_7d_vs_2D and 3D_14d_vs_2D.

The CLL Cells Phenotype Is Preserved Throughout the 3D Culture

To further validate our 3D model of leukemic B cells, we evaluated, by flow cytometry, the ability of 3D bioprinted primary CLL cells to maintain the characteristic surface phenotype throughout the whole culture period. We observed that the CLL clone maintained CD19 and CD5 expression during the whole culture period, with mean values of 93%, 89%, 89%, 87%, 95% for day 0-7-14-21-28, respectively (**Figures 7A, B** and **Supplementary Figures 9A, B**) (n = 15). The same observation can be done for surface IgM expression (**Figures 7A, C** and **Supplementary Figures 9A, C**) (n = 18), whose levels showed a trend toward an increase in 15 patients (7

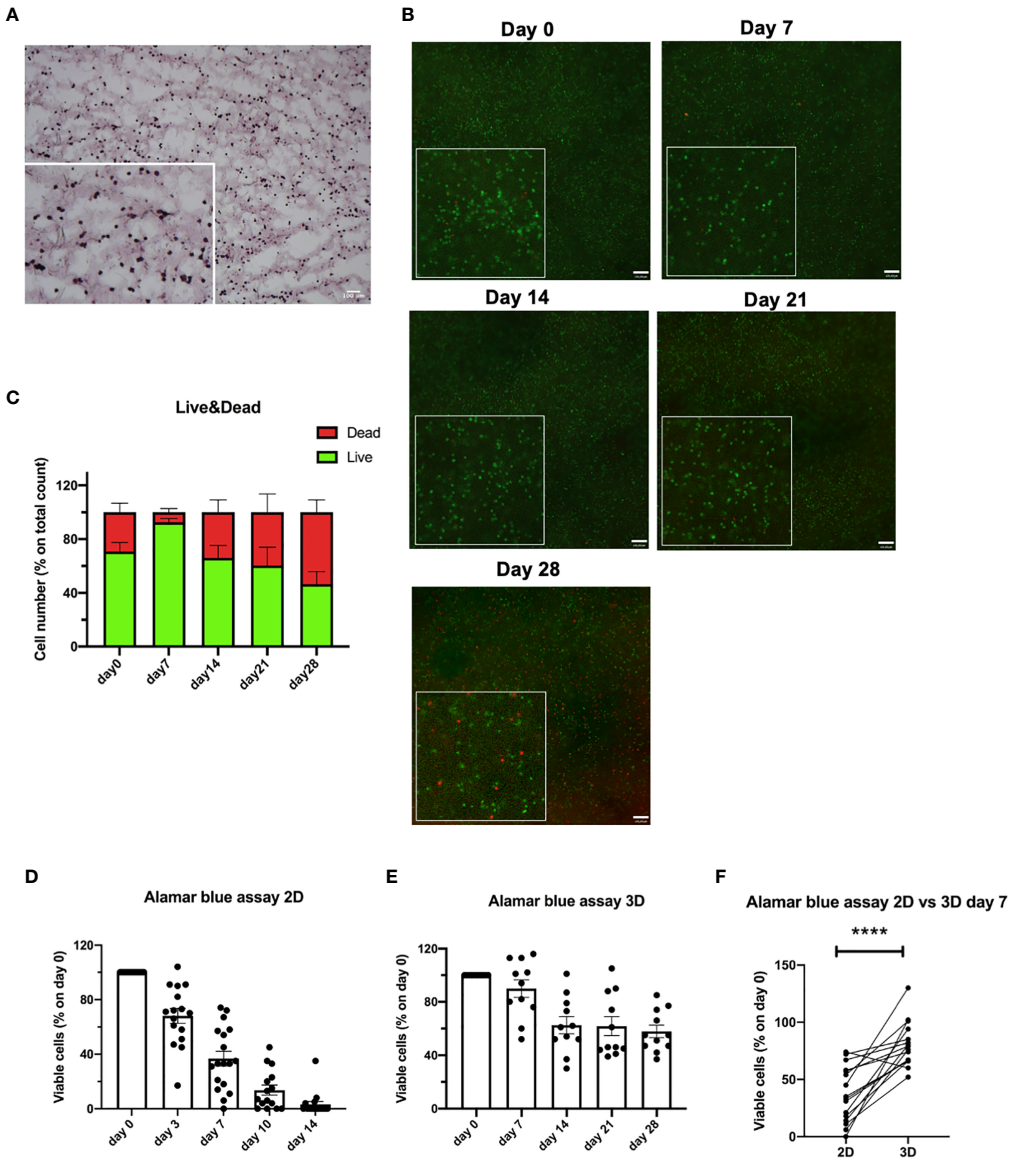

FIGURE 6 | 3D bioprinted CLL primary cells show a long-term viability in the scaffolds. **(A)** Representative H&E staining on 5 µm frozen sections of 3D bioprinted CLL primary cells showing their distribution in the scaffold. Images were obtained with Zeiss Axio Imager M2m microscope. A magnification of the image is shown. **(B)** Representative images of Live/Dead assay of 3D bioprinted CLL primary cells at different time points (day 0-7-14-21-28) acquired with Axio Observer Zeiss fluorescent microscope. Green cells are live cells; red cells are dead cells. A magnification for each image is shown. **(C)** The graph shows quantification, at different time points (day 0-7-14-21-28), of alive (green column portion) and dead (red column portion) 3D bioprinted CLL primary cells. **(D)** The graph shows Alamar blue assay fluorescence values of 2D cultured CLL primary cells at different time points (day 0-3-7-10-14). **(E)** The graph shows Alamar blue assay fluorescence values of 3D bioprinted CLL primary cells at different time points (day 0-7-14-21-28). **(F)** The graph shows the percentages of viable 3D bioprinted CLL primary cells compared to CLL primary cells cultured in the traditional 2D system. Cell viability was measured by Alamar blue assay after 7 days of culture and normalized to day 0. ****$p < 0.0001$. Data are represented as mean ± SEM, n=16 **(D, F)** and n = 11 **(E)** patient samples. Paired t-test was performed for statistical analysis.

uCLL and 8 mCLL) out of 18 cases analyzed (10 uCLL and 8 mCLL). The increment observed on the percentage of IgM+ cells was about 10-20% from day 0 to the following time points visualized in **Figure 7C** (mean % of IgM+ cells weekly increase from day 0 to day 28, respectively: 34%, 16%, 5%, 4%). We didn't observe any statistical differences between mutated and unmutated cases.

3D Bioprinted Primary CLL Cells Show *BAX* and *BCL2* Regulation in Culture

To further elucidate the biological mechanisms at the basis of the improved viability shown in the 3D system, we decided to evaluate possible changes in the levels of expression of genes known to be involved in the apoptotic process, such as *BAX* and *BCL2* (49)

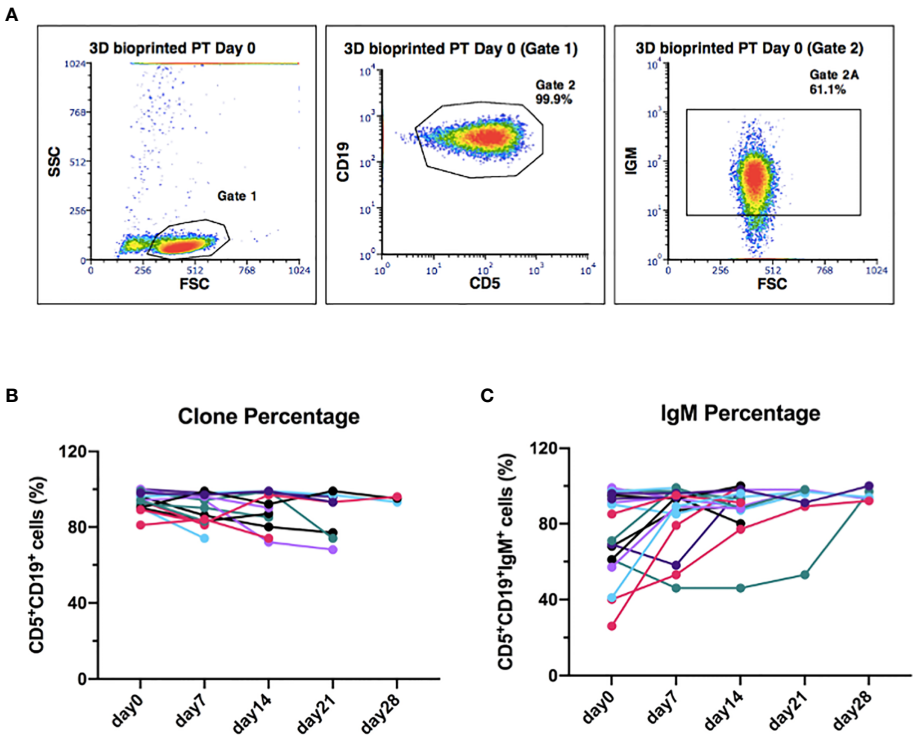

FIGURE 7 | The original CLL clone phenotype CD19/CD5 is maintained throughout the 3D culture, including the levels of IgM. **(A)** Representative flow cytometry plots of 3D-bioprinted CLL primary cells (day 0) showing the presence of the leukemic clone and the surface marker IgM, based on the expression of CD19/CD5 and IgM surface markers. Physical parameters of 3D bioprinted hydrogel alone are shown as well. **(B)** The graph shows the leukemic clone percentage of all samples analyzed overtime (n = 15). **(C)** The graph shows IgM surface marker percentage of all samples analyzed overtime (n = 18).

(**Supplementary Figures 10A, B**) (n = 10). Interestingly, we observed significantly lower values of the pro-apoptotic gene *BAX* and significantly higher values of the anti-apoptotic gene *BCL2* in 3D bioprinted CLL primary cells as compared to 2D cultured ones, analyzed after 7 days, independently of their clinical/biological features (**Figures 8A, B**) (n = 16).

DISCUSSION

In the present work, we tested for the first time whether 3D bioprinting strategy could be applied to immune cells and in particular to leukemic B cells.

This strategy is currently successfully explored for other cancers such as breast, brain, skin and pancreatic (18). In solid tumors, researching the need to develop *in vitro* models with a 3D structure recapitulating *in vivo* tumor growth was more obvious, while this need was appreciated much later in hematological cancer, due to the circulating nature of most diseases (2, 3). It is now evident that leukemia cells in the peripheral blood do not represent entirely the disease, that is composed by the cells accumulating and proliferating in lymphoid tissues (4).

Several 3D systems have been recently applied to the study of different B cell malignancies in order to recapitulate the tissue environment, including spheroids (50), organoids and microfluidic devices (51). In particular, the BM microenvironment niche has been more frequently investigated as in the case of acute myeloid leukemia and multiple myeloma in order to study the resistance to chemotherapeutics. For CLL rather limited attempts have been made by using co-culture with stromal cells in both spheroids (52) or gelatin scaffolds, the latter kept in dynamic growth in bioreactor (16).

However, all these systems have their intrinsic limitations such as the need of cell seeding. Indeed, the main difference between 3D printing and other 3D culture systems is that multiple cell types can be deposited with a microscale precision (53). We believe that before exploring the possibility to print different cell types in the hydrogel to generate complex 3D scaffolds to study CLL, we need to understand how CLL cells behave in this context.

To this aim we directly printed CLL cells embedded in hydrogels specifically designed to support cellular adhesion and functions, as well as high printability and biocompatibility. We successfully tested CLL cells for printability, optimized the printing strategy and set-up the protocols to perform the analysis (cell viability assays, protein/gene expression, imaging among others). The CLL cell line MEC1 was used to define the optimal number of cells and cell/hydrogel ratio to be printed,

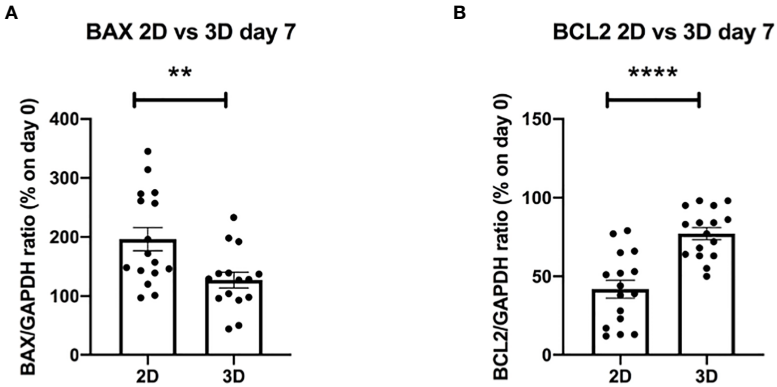

FIGURE 8 | The evaluation of apoptotic genes shows better survival of 3D bioprinted primary cells compared to 2D cultured ones at the same time of culture. **(A, B)** The graphs show mRNA levels of pro-apoptotic gene *BAX* and anti-apoptotic gene *BCL2*, after 7 days of culture, of 3D bioprinted CLL primary cells compared to CLL primary cells cultured in the traditional 2D system. **$p < 0.01$, ****$p < 0.0001$. Data are represented as mean ± SEM, n = 16 patient samples. Mann-Whitney t-test was used for statistical analysis.

followed by validation of the derived settings using primary cells obtained from the PB of patients affected by CLL, which we selected based on the mutational status of the IGHV gene (IGHV<98%=mutated=good prognosis (mCLL); IGHV≥98%= unmutated=bad prognosis (uCLL); **Supplementary Table 2**).

We observed a different printability of the cell line with respect to primary cells: in particular, MEC1 cells showed better behavior in the hydrogel without the addition of external factors (Laminins), while CLL cells prefer hydrogels with the addition of laminins. This result suggests and confirms that primary cells are still highly dependent on the microenvironment, including extracellular matrix (7).

In general, CLL cells, both cell line and primary cells, were found to be homogeneously distributed in the hydrogel scaffolds and, specifically, we observed a long-term viability (up to 28 days) for primary CLL cells cultured in the 3D bioprinted hydrogel, independently on their clinical/biological features, result that is not achievable when CLL cells are cultured in 2D alone.

Of note, CLL cells appear to be indeed affected by the 3D culture in the presence of a sort of extracellular matrix, as indicated by the strikingly different expression profile shown by RNAseq analysis when we compared cells cultured in 2D and 3D cultures. In particular, the upregulation of Immunoglobulin complexes (45–47), the activation of integrins (54), inflammation and cytoskeletal (55) related pathways suggest that the cells possibly lay in a more physiological environment. It is clear that the traditional 2D culture system does not represent the proper control for our 3D model, and it will be interesting to see how leukemic cells mirror e.g. cells obtained *ex vivo* from BM or LN from patients in terms of expression profile and functional behavior, and to understand which pathways might be more affected than others in the presence of extracellular matrix alone.

To this aim, we measured the stiffness of the hydrogel used in our experiments as we believe that this will be a fundamental parameter to be studied in the tissues of origin, since it could influence the maintenance/promotion of CLL cells viability. In the future, this could lead to the development of smart materials with tuned stiffness to be used for 3D bioprinting cells of different origin(s).

Focusing on primary CLL cells, we observed that the well-being of the 3D bioprinted cells is also suggested by their phenotype (expression of surface CD19 and CD5) that remains unaffected through the culture period. Inspired by the RNAseq results, we measured the levels of the B cell receptor IgM that increases in 15/18 patients analyzed. This is intriguing considering that Coulter et al. (56) recently reported that the B cell receptors of LN and PB derived CLL cells might be functionally distinct, in particular LN-CLL cells express higher levels of surface IgM thus suggesting that the 3D environment may more reliably reproduce this particular *in vivo* environment. Similarly, cells showed higher levels of *BCL2* expression in 3D vs 2D after 7 days of culture, with lower levels of *BAX* indicating a higher viability and less priming toward apoptosis. The overall higher fitness of the cells is crucial, especially when considering the potential application of this technique to study the response of CLL cells *ex vivo* to different drugs and immunotherapeutic approaches. Keeping in mind that *BCL2* is a therapeutic target in CLL (57), this system might potentially be more reliable in predicting responses in patients and also to understand how cells may adapt to the presence of the drug with time, when cultured in a more protective microenvironment.

In summary, our results demonstrate that we can efficiently 3D bioprint primary CLL cells and healthy lymphocytes, and improve their viability, which can be maintained for up to 28 days, thus establishing the first long-term 3D culture model for leukemia cells. Considering that no similar approach has been so far established also for normal B lymphocytes, this is an innovative tool that may help better mimic the physiological *in vivo* settings

not only of leukemic lymphocytes but also of immune cells in general. In the future, the system can be further improved by increasing the complexity of the cellular and molecular components to be included in the 3D bioprinted models in order to even better recapitulate a tumor microenvironment. This could allow to recreate the molecular and cellular interactions that occur in normal and neoplastic conditions *in vivo*, and most importantly could be exploited to test individual response(s) to different drugs such as target therapies or immunotherapy.

DATA AVAILABILITY STATEMENT

The RNAseq data, including raw sequence files, have been submitted to NCBI's Gene Expression Omnibus and are accessible through the GEO series accession number GSE163977.

ETHICS STATEMENT

The studies involving human participants were reviewed and approved by the Ospedale San Raffaele (OSR) ethics committee under the protocol VIVI-CLL entitled: "In vivo and *in vitro* characterization on CLL." The patients/participants provided their written informed consent to participate in this study.

AUTHOR CONTRIBUTIONS

CS, FVS, and RP wrote the manuscript. CS, FVS, RP, FB, DR, and SF performed the experiments and analyzed the data. LS and PG provided patients' and clinical information. FS, INR, HM, SF, and PG revised the manuscript. All authors contributed to the article and approved the submitted version.

ACKNOWLEDGMENTS

The research leading to these results has received funding from: Associazione Italiana per la Ricerca sul Cancro - AIRC under IG 2018 - ID. 21332 project – P.I. CS; Leukemia research foundation grant 2018 P.I. CS; EHA advances research grant 2020 P.I. CS. And AIRC, Special Program on Metastatic Disease – 5 per mille #2119, P.I. Robin Foà, to PG. We thank Alembic and CORS facilities (in particular Anna Sofia Tascini) for helpful suggestions and technical support. **Figure 1** was created with BioRender.com (https://biorender.com).

SUPPLEMENTARY MATERIAL

The Supplementary Material for this article can be found online at: https://www.frontiersin.org/articles/10.3389/fimmu.2021.639572/full#supplementary-material

REFERENCES

1. Hallek M, Fürstenau M. How to Approach CLL in Clinical Practice. *Hematol Oncol* (2019) 37(Suppl 1):38–42. doi: 10.1002/hon.2583
2. Calissano C, Damle RN, Hayes G, Murphy EJ, Hellerstein C, Moreno C, et al. In Vivo Intraclonal and Interclonal Kinetic Heterogeneity in B-cell Chronic Lymphocytic Leukemia. *Blood* (2009) 114(23):4832–42. doi: 10.1182/blood-2009-05-219634
3. Scarfò L, Ferreri AJ, Ghia P. Chronic Lymphocytic Leukaemia. *Crit Rev Oncol Hematol* (2016) 104:169–82. doi: 10.1016/j.critrevonc.2016.06.003
4. Calissano C, Damle RN, Marsilio S, Yan XJ, Yancopoulos S, Hayes G, et al. Intraclonal Complexity in Chronic Lymphocytic Leukemia: Fractions Enriched in Recently Born/Divided and Older/Quiescent Cells. *Mol Med* (2011) 17(11-12):1374–82. doi: 10.2119/molmed.2011.00360
5. Pavlasova G, Borsky M, Seda V, Cerna K, Osickova J, Doubek M, et al. Ibrutinib Inhibits Cd20 Upregulation on CLL B Cells Mediated by the CXCR4/SDF-1 Axis. *Blood* (2016) 128(12):1609–13. doi: 10.1182/blood-2016-04-709519
6. Haselager MV, Kater AP, Eldering E. Proliferative Signals in Chronic Lymphocytic Leukemia; What Are We Missing? *Front Oncol* (2020) 10:592205. doi: 10.3389/fonc.2020.592205
7. Caligaris-Cappio F, Bertilaccio MT, Scielzo C. How the Microenvironment Wires the Natural History of Chronic Lymphocytic Leukemia. *Semin Cancer Biol* (2014) 24:43–8. doi: 10.1016/j.semcancer.2013.06.010
8. Herndon TM, Chen SS, Saba NS, Valdez J, Emson C, Gatmaitan M, et al. Direct In Vivo Evidence for Increased Proliferation of CLL Cells in Lymph Nodes Compared to Bone Marrow and Peripheral Blood. *Leukemia* (2017) 31(6):1340–7. doi: 10.1038/leu.2017.11
9. Primo D, Scarfò L, Xochelli A, Mattsson M, Ranghetti P, Esponosa AB, et al. A Novel Ex Vivo High-Throughut Assay Revels Antiproliferative Effects of Idelalisib and Ibrutinib in Chronic Lymphocytic Leukemia. *Oncotarget* (2018) 9(40):26019–31. doi: 10.18632/oncotarget.25419
10. Herman SE, Wiestner A. Preclinical Modeling of Novel Therapeutics in Chronic Lymphocytic Leukemia: The Tools of the Trade. *Semin Oncol* (2016) 43(2):222–32. doi: 10.1053/j.seminoncol.2016.02.007
11. Pampaloni F, Reynaud EG, Stelzer EH. The Third Dimension Bridges the Gap Between Cell Culture and Live Tissue. *Nat Rev Mol Cell Biol* (2007) 8(10):839–45. doi: 10.1038/nrm2236
12. Jensen C, Teng Y. Is It Time to StqRT Transitioning From 2D to 3D Cell Culture? *Front Mol Biosci* (2020) 7:33. doi: 10.3389/fmolb.2020.00033
13. Scielzo C, Ghia P. Modeling the Leukemia Microenviroment. *Front Oncol* (2020) 10:607608. doi: 10.3389/fonc.2020.607608
14. Edmondson R, Broglie JJ, Adcock AF, Yang L. Three-Dimensional Cell Culture Systems and Their Applications in Drug Discovery and Cell-Based Biosensors. *Assay Drug Dev Technol* (2014) 12(4):207–18. doi: 10.1089/adt.2014.573
15. Shah SB, Singh A. Creating QRTificial Lymphoid Tissues to Study Immunity and Hematological Malignancies. *Curr Opin Hematol* (2017) 24(4):377–83. doi: 10.1097/MOH.0000000000000356
16. Barbaglio F, Belloni D, Scarfò L, Sbrana FV, Ponzoni M, Bongiovanni L, et al. 3d Co-Culture Model of Chronic Lymphocytic Leukemia Bone Marrow Microenvironment Predicts Patient-Specific Response to Mobilizing Agents. *Haematologica* (2020). doi: 10.3324/haematol.2020.248112
17. Derakhshanfar S, Mbeleck R, Xu K, Zhang X, Zhong W, Xing M. 3d Bioprinting for Biomedical Devices and Tissue Engineering: A Review of Recent Trends and Advances. *Bioact Mater* (2018) 3(2):144–56. doi: 10.1016/j.bioactmat.2017.11.008
18. Augustine R, Kalva SN, Ahmad R, Zahid AA, Hasan S, Nayeem A, et al. 3d Bioprinted Cancer Models: Revolutionizing Personalized Cancer Therapy. *Transl Oncol* (2021) 14(4):101015. doi: 10.1016/j.tranon.2021.101015
19. Sommer AC, Blumenthal EZ. Implementations of 3D Printing in Ophthalmology. *Graefes Arch Clin Exp Ophthalmol* (2019) 257(9):1815–22. doi: 10.1007/s00417-019-04312-3
20. Hallek M, Cheson BD, Catovsky D, Caligaris-Cappio F, Dighiero G, Döhner H, et al. Guidelines for the Diagnosis and Treatment of Chronic Lymphocytic

Leukemia: A Report From the International Workshop on Chronic Lymphocytic Leukemia Updating the National Cancer Institute-Working Group 1996 Guidelines. *Blood* (2008) 111(12):5446–56. doi: 10.1182/blood-2007-06-093906
21. Stacchini A, Aragno M, Vallario A, Alfarano A, Circosta P, Gottardi D, et al. MEC1 and MEC2: Two New Cell Lines Derived From B-Chronic Lymphocytic Leukaemia in Prolymphocytoid Transformation. *Leuk Res* (1999) 23(2):127–36. doi: 10.1016/S0145-2126(98)00154-4
22. Scielzo C, Bertilaccio MT, Simonetti G, Dagklis A, ten Hacken E, Fazi C, et al. HS1 has a Central Role in the Trafficking and Homing of Leukemic B Cells. *Blood* (2010) 116(18):3537–46. doi: 10.1182/blood-2009-12-258814
23. Livak KJ, Schmittgen TD. Analysis of Relative Gene Expression Data Using Real-Time Quantitative PCR and the 2(T)(-Delta Delta C) Method. *Methods* (2001) 25(4):402–8. doi: 10.1006/meth.2001.1262
24. Love MI, Huber W, Anders S. Moderated Estimation of Fold Change and Dispersion for RNA-seq Data With Deseq2. *Genome Biol* (2014) 15(12):550. doi: 10.1186/s13059-014-0550-8
25. Benjamini Y, Drai D, Elmer G, Kafkafi N, Golani I. Controlling the False Discovery Rate in Behavior Genetics Research. *Behav Brain Res* (2001) 125(1-2):279–84. doi: 10.1016/S0166-4328(01)00297-2
26. Vu TT, Lim C, Lim M. Characterization of Leukemic Cell Behaviors in a Soft Marrow Mimetic Alginate Hydrogel. *J Biomed Mater Res B Appl Biomater* (2012) 100(7):1980–8. doi: 10.1002/jbm.b.32765
27. Caliari SR, Burdick JA. A Practical Guide to Hydrogels for Cell Culture. *Nat Methods* (2016) 13(5):405–14. doi: 10.1038/nmeth.3839
28. Kong HJ, Alberg E, Kaigler D, Lee KY, Mooney DJ. Controlling Degradation of Hydrogels Via the Size of Cross-Linked Junctions. *Adv Mater* (2004) 16 (21):1917–21. doi: 10.1002/adma.200400014
29. Kharkar PM, Kiick KL, Kloxin AM. Designing Degradable Hydrogels for Orthogonal Control of Cell Microenvironments. *Chem Soc Rev* (2013) 42 (17):7335–72. doi: 10.1039/C3CS60040H
30. Draghi L, Brunelli D, Farè S, Tanzi MC. Programmed Cell Delivery From Biodegradable Microcapsules for Tissue Repair. *J Biomater Sci Polym Ed* (2015) 26(15):1002–12. doi: 10.1080/09205063.2015.1070706
31. Mortazavi A, Williams BA, McCue K, Schaeffer L, Wold B. Mapping and Quantifying Mammalian Transcriptomes by RNA-Seq. *Nat Methods* (2008) 5 (7):621–8. doi: 10.1038/nmeth.1226
32. Glickman ME, Rao SR, Schultz MR. False Discovery Rate Control is a Recommended Alternative To Bonferroni-Type Adjustments in Health Studies. *J Clin Epidemiol* (2014) 67(8):850–7. doi: 10.1016/j.jclinepi.2014.03.012
33. Susek KH, Karvouni M, Alici E, Lundqvist A. The Role of CXC Chemokine Receptors 1-4 on Immune Cells in the Tumor Microenvironment. *Front Immunol* (2018) 9:2159. doi: 10.3389/fimmu.2018.02159
34. Ocaña E, Delgado-Pérez L, Campos-Caro A, Muñóz J, Paz A, Franco R, et al. The Prognostic Role of CXCR3 Expression by Chronic Lymphocytic Leukemia B Cells. *Haematologica* (2007) 92(3):349–56. doi: 10.3324/haematol.10649
35. Ghia P, Strola G, Granziero L, Geuna M, Guida G, Allusto F, et al. Chronic Lymphocytic Leukemia B Cells are Endowed With the Capacity to Attract Cd4+, Cd40l+ T Cells by Producing Ccl22. *Eur J Immunol* (2002) 32(5):1403–13. doi: 10.1002/1521-4141(200205)32:5<1403::AID-IMMU1403>3.0.CO;2-Y
36. Rapp M, Wintergerst MWM, Kunz WG, Vetter VK, Knott MML, Lisowski D, et al. Ccl22 Controls Immunity by Promoting Regulatory T Cell Communication With Dendritic Cells in Lymph Nodes. *J Exp Med* (2019) 216(5):1170–81. doi: 10.1084/jem.20170277
37. Bernimoulin MP, Xeng XL, Abbal C, Giraud S, MqRTinez M, Michielin O, et al. Molecular Basis of Leukocyte Rolling on PSGL-1. Predominant Role of Core-2 O-Glycans and of Tyrosine Sulfate Residue 51. *J Biol Chem* (2003) 278 (1):37–47. doi: 10.1074/jbc.M204360200
38. Mehta-D'souza P, Klopocki G, Oganesyan V, Terzyan S, Mather T, Li Z, et al. Glycan Bound to the Selectin Low Affinity State Engages Glu-88 to Stabilize the High Affinity State Under Force. *J Biol Chem* (2017) 292(6):2510–8. doi: 10.1074/jbc.M116.767186
39. Chaudhuri J, Tian M, Khuong C, Chua K, Pinaud E, Alt FW. Transcription-Targeted DNA Deamination by the AID Antibody Diversification Enzyme. *Nature* (2003) 422(6933):726–30. doi: 10.1038/nature01574
40. Caratão N, Cortesão CS, Reis PH, Freitas RF, Jacob CMA, Pastorino AC, et al. A Novel Activation-Induced Cytidine Deaminase (Aid) Mutation in Brazilian Patients With Hyper-Igm Type 2 Syndrome. *Clin Immunol* (2013) 148 (2):279–86. doi: 10.1016/j.clim.2013.05.017
41. Filip D, Mraz M. The Role of MYC in the Transformation and Aggressiveness of 'Indolent' B-cell Malignancies. *Leuk Lymphoma* (2020) 61(3):510–24. doi: 10.1080/10428194.2019.1675877
42. Duffy MJ, O'Grady S, Tang M, Crown J. MYC as a Target for Cancer Treatment. *Cancer Treat Rev* (2021) 94:102154. doi: 10.1016/j.ctrv.2021.102154
43. Forshell LP, Li Y, Forshell TZP, Rudelius M, Nilsson L, Keller U, et al. The Direct Myc Target Pim3 Cooperates With Other Pim Kinases in Supporting Viability of Myc-induced B-Cell Lymphomas. *Oncotarget* (2011) 2(6):448–60. doi: 10.18632/oncotarget.283
44. Kapoor I, Bodo J, Hill BT, His ED, Almasan A. Targeting BCL-2 in B-cell Malignancies and Overcoming Therapeutic Resistance. *Cell Death Dis* (2020) 11(11):941. doi: 10.1038/s41419-020-03144-y
45. Agathangelidis A, Chatzidimitriou A, Gemenetzi K, Giudicelli V, Karypidou M, Plevova K, et al. Higher-Order Connections Between Stereotyped Subsets: Implications for Improved Patient Classification in CLL. *Blood* (2021) 137 (10):1365–76. doi: 10.1182/blood.2020007039
46. Gemenetzi K, Agathangelidis A, Zaragoza-Infante L, Sofou E, Papaioannou M, Chatzidimitriou A, et al. B Cell Receptor Immunogenetics in B Cell Lymphomas: Immunoglobulin Genes as Key to Ontogeny and Clinical Decision Making. *Front Oncol* (2020) 10:67. doi: 10.3389/fonc.2020.00067
47. Kipps TJ, Choi MY. Targeted Therapy in Chronic Lymphocytic Leukemia. *Cancer J* (2019) 25(6):378–85. doi: 10.1097/PPO.0000000000000416
48. Condoluci A, Terzi di Bergamo L, Langerbeins P, Hoechstetter MA, Herling CD, De Paoli L, et al. International Prognostic Score for Asymptomatic Early-Stage Chronic Lymphocytic Leukemia. *Blood* (2020) 135(21):1859–69. doi: 10.1182/blood.2019003453
49. Cory S. Regulation of Lymphocyte Survival by the Bcl-2 Gene Family. *Annu Rev Immunol* (1995) 13:513–43. doi: 10.1146/annurev.iy.13.040195.002501
50. Colella G, Fazioli F, Gallo M, De Chiara A, Apice G, Ruosi C, et al. Sarcoma Spheroids and Organoids-Promising Tools in the Era of Personalized Medicine. *Int J Mol Sci* (2018) 19(2):615. doi: 10.3390/ijms19020615
51. Bruce A, Evans R, Mezan R, Shi L, Moses BS, MqRTin KH, et al. Three-Dimensional Microfluidic Tri-Culture Model of the Bone Marrow Microenvironment for Study of Acute Lymphoblastic Leukemia. *PloS One* (2015) 10(10):e0140506. doi: 10.1371/journal.pone.0140506
52. Farinello D, Wozinska M, Lenti E, Genovese L, Bianchessi S, Migliori E, et al. A Retinoic Acid-Dependent Stroma-Leukemia Crosstalk Promotes Chronic Lymphocytic Leukemia Progression. *Nat Commun* (2018) 9(1):1787. doi: 10.1038/s41467-018-04150-7
53. Magin CM, Alge DL, Anseth KS. Bio-Inspired 3d Microenvironments: A New Dimension in Tissue Engineering. *BioMed Mater* (2016) 11(2):022001. doi: 10.1088/1748-6041/11/2/022001
54. Redondo-Muñoz J, García-Pardo A, Teixidó J. Molecular Players in Hematologic Tumor Cell Trafficking. *Front Immunol* (2019) 10:156. doi: 10.3389/fimmu.2019.00156
55. Jewell AP, Worman CP, Lydyard PM, Yong KL, Giles FJ, Goldstone AH. Interferon-Alpha Up-Regulates Bcl-2 Expression and Protects B-Cll Cells From Apoptosis in Vitro and In Vivo. *Br J Haematol* (1994) 88(2):268–74. doi: 10.1111/j.1365-2141.1994.tb05017.x
56. Coulter EM, Pepper A, Mele S, Folarin N, Townsend W, Cuthill K, et al. In Vitro and In Vivo Evidence for Uncoupling of B-cell Receptor Internalization and Signaling in Chronic Lymphocytic Leukemia. *Haematologica* (2018) 103 (3):497–505. doi: 10.3324/haematol.2017.176164
57. Jain N, Gandhi V, Wierda W. Ibrutinib and Venetoclax for First-Line Treatment of CLL. Reply. *N Engl J Med* (2019) 381(8):789. doi: 10.1056/NEJMc1908754

Conflict of Interest: Authors INR and HM were employed by CELLINK AB.

The remaining authors declare that the research was conducted in the absence of any commercial or financial relationships that could be construed as a potential conflict of interest.

frontiers in Immunology

ORIGINAL RESEARCH
published: 29 June 2021
doi: 10.3389/fimmu.2021.689697

A Reproducible Bioprinted 3D Tumor Model Serves as a Preselection Tool for CAR T Cell Therapy Optimization

*Laura Grunewald[1,2†], Tobias Lam[3,4†], Lena Andersch[1], Anika Klaus[1], Silke Schwiebert[1], Annika Winkler[1], Anton Gauert[1], Anja I. Heeren-Hagemann[1], Kathy Astrahantseff[1], Filippos Klironomos[1], Alexander Thomas[3,4], Hedwig E. Deubzer[1,5,6,7], Anton G. Henssen[1,8], Angelika Eggert[1,6,7,8], Johannes H. Schulte[1,6,7], Kathleen Anders[1,7], Lutz Kloke[3,4] and Annette Künkele[1,6,7,8]**

[1] Charité – Universitätsmedizin Berlin, Corporate Member of Freie Universität Berlin and Humboldt-Universität zu Berlin, Department of Pediatric Oncology and Hematology, Berlin, Germany, [2] Freie Universität Berlin, Berlin, Germany, [3] Technische Universität Berlin, Berlin, Germany, [4] Cellbricks GmbH Berlin, Berlin, Germany, [5] Neuroblastoma Research Group, Experimental and Clinical Research Center (ECRC) of the Charité and the Max-Delbrück-Center for Molecular Medicine (MDC) in the Helmholtz Association, Berlin, Germany, [6] German Cancer Consortium (DKTK), Heidelberg, Germany, [7] German Cancer Research Center (DKFZ), Heidelberg, Germany, [8] Berlin Institute of Health at Charité – Universitätsmedizin Berlin, Berlin, Germany

Chimeric antigen receptor (CAR) T cell performance against solid tumors in mouse models and clinical trials is often less effective than predicted by CAR construct selection in two-dimensional (2D) cocultures. Three-dimensional (3D) solid tumor architecture is likely to be crucial for CAR T cell efficacy. We used a three-dimensional (3D) bioprinting approach for large-scale generation of highly reproducible 3D human tumor models for the test case, neuroblastoma, and compared these to 2D cocultures for evaluation of CAR T cells targeting the L1 cell adhesion molecule, L1CAM. CAR T cells infiltrated the model, and both CAR T and tumor cells were viable for long-term experiments and could be isolated as single-cell suspensions for whole-cell assays quantifying CAR T cell activation, effector function and tumor cell cytotoxicity. L1CAM-specific CAR T cell activation by neuroblastoma cells was stronger in the 3D model than in 2D cocultures, but neuroblastoma cell lysis was lower. The bioprinted 3D neuroblastoma model is highly reproducible and allows detection and quantification of CAR T cell tumor infiltration, representing a superior *in vitro* analysis tool for preclinical CAR T cell characterization likely to better select CAR T cells for *in vivo* performance than 2D cocultures.

Keywords: CAR T cells, neuroblastoma, T cell infiltration, 3D tumor model, bioprint technology

OPEN ACCESS

Edited by:
Katy Rezvani, University of Texas MD Anderson Cancer Center, United States

Reviewed by:
Bipulendu Jena, Independent Researcher, San Diego, CA, United States

***Correspondence:**
Annette Künkele
Annette.kuenkele@charite.de

†These authors have contributed equally to this work

Specialty section:
This article was submitted to Cancer Immunity and Immunotherapy, a section of the journal Frontiers in Immunology

Received: *01 April 2021*
Accepted: *02 June 2021*
Published: *29 June 2021*

Citation:
Grunewald L, Lam T, Andersch L, Klaus A, Schwiebert S, Winkler A, Gauert A, Heeren-Hagemann AI, Astrahantseff K, Klironomos F, Thomas A, Deubzer HE, Henssen AG, Eggert A, Schulte JH, Anders K, Kloke L and Künkele A (2021) A Reproducible Bioprinted 3D Tumor Model Serves as a Preselection Tool for CAR T Cell Therapy Optimization. Front. Immunol. 12:689697. doi: 10.3389/fimmu.2021.689697

HIGHLIGHTS

We present a highly reproducible bioprinted three-dimensional tumor model for preclinical *in vitro* CAR T cell evaluation allowing tumor and T cell characterization following experiments.

INTRODUCTION

Genetically engineering a patient's own primary T cells holds great immunotherapeutic promise. Chimeric antigen receptor (CAR) T cell therapy is currently receiving attention since treatments for various hematological malignancies in children and adults are showing remarkable clinical success (1, 2). Success has been limited for treating solid tumors with CAR T cell approaches, since CAR T cells need to find, enter and survive in a hostile tumor microenvironment (3), which require further improvement and preclinical testing. Here, we use CAR T cells targeting the glycosylated CE7 epitope of the L1 cell adhesion molecule, L1CAM (formerly CD171), which is specifically expressed on tumor cells and a promising target for neuroblastoma and ovarian carcinoma (4–6). Neuroblastoma is the most common extracranial solid tumor in childhood, and remains the third leading cause of pediatric cancer death despite multimodal therapies (7). Recently, children suffering from refractory neuroblastoma were treated with L1CAM-targeting CAR T cells in a clinical phase I trial (NCT02311621, https: clinicaltrials.gov) (4, 6).

The CAR construct expressed in T cells provides an extracellular single-chain variable fragment (scFv) derived from an antibody for specific antigen recognition, fused to a variably long spacer domain and transmembrane domain. The transmembrane domain connects to the CD3 zeta (ζ) signaling domain of the T cell receptor (1st generation) and is embellished with one (2nd generation) or two (3rd generation) intracellular costimulatory domains. The most commonly used costimulatory domains are 4-1BB and CD28. Costimulus with 4-1BB is associated with a slower, more continuous anti-tumor response comparable to a memory T cell response, whereas a strong fast, effector-like T cell response is induced by CD28 costimulation (8). Minor differences in CAR design, such as spacer length, can significantly impact CAR T cell functionality (9, 10). Excessive *in vitro* testing followed by labor-intensive and time-consuming preclinical evaluation in mouse models are currently necessary to select the most suitable CAR construct for a given antigen.

CAR T cell effector functions are currently most often evaluated in two-dimensional (2D) cocultures where T cells encounter a tumor cell monolayer growing adherently on culture plastic. Three-dimensional (3D) connections to cells and matrix components in the tumor environment can influence cancer cell phenotype, including gene expression, cell signaling and nutrient supply (11). These influences are lacking in a cancer cell monolayer, in which tumor cells are also easily accessible to T cells, poorly reflecting cellular and matrix obstructions that T cells face in the *in vivo* tumor environment. CAR T cell efficacy achieved in cocultures often cannot be achieved in preclinical mouse models, extending the animal testing necessary to select CAR T cell candidates. The dramatic evolution of 3D printing technology over the past decades [reviewed in (12) and (13)] enables an innovative approach to *in vitro* testing, surpassing the environment created in 2D cocultures. Stereolithography combines high resolution and speed with the ability to simultaneously print large numbers of objects with high reproducibility (14). This technology uses photopolymerization to sequentially solidify layers of bio-ink printed on top of each other to build a 3D structure mimicking native tissues and demonstrating significant improvements to 2D cocultures (15).

Our aim was to build on data from our previous comparisons of a L1CAM-specific CAR T cell constructs harboring either long or short spacers and the 4-1BB costimulatory domain, which showed functional discrepancies between preclinical evaluations *in vitro* and in mouse models, and are used in the ongoing clinical phase I trial for children with neuroblastoma (ClinicalTrials.gov Identifier: NCT02311621) (6). Here we repeated the functional evaluation of L1CAM-specific CAR T cells with different spacer lengths in 2D cocultures and directly compared functionality with that in bioprinted 3D neuroblastoma models.

MATERIALS AND METHODS

Neuroblastoma Cell Culture

SK-N-BE(2) neuroblastoma cells (passaged ≤20 times from stock cultures expanded in <10 passages from the source culture obtained from ATCC) were propagated in Dulbecco´s Modified Eagle Medium (Life Technologies, Karlsbad, CA, USA) supplemented with 10% heat-inactivated fetal calf serum (Sigma-Aldrich, St. Louis, MO, USA) to 80% density in 2D culture before 3D bioprinting or seeding for functional assays. The identity of the SK-N-BE(2) neuroblastoma cell line was confirmed by Eurofins (Luxemburg) and *Mycoplasma*-negative by a cell-based colometric HEK-Blue Detection assay (Invivogen).

Bioprinting 3D Tumor Models

Stereolithographic bioprinting using a previously described process (16) was selected to produce the 3D models. Methacrylated gelatin (GelMA) was synthesized for use in the bio-ink as previously described (17, 18) with slight changes. In short, 10 weight percent (wt%) type A gelatin from porcine skin (300 bloom, Sigma-Aldrich) was dissolved in phosphate buffered saline (PBS) at 50°C before adding methacrylic anhydride (Sigma-Aldrich) in molar excess, and allowed the reaction to proceed 2h. Resulting GelMA was dialyzed against distilled water for 4 days with frequent water changes, then sterile filtered and lyophilized several days until dry. NMR spectroscopy determined 60% methacrylation in the lyophilized product. Bio-ink was prepared using 7wt% GelMA in cell culture medium supplemented with 10% fetal calf serum and 1% penicillin/streptomycin, with 0.1wt% lithium phenyl-2,4,6-

trimethylbenzoy phosphinate as photoinitiator. SK-N-BE(2) cells were harvested, counted and viability was controlled, before resuspending in the GelMA mixture at 10^8 cells/mL to create the bio-ink. A computer-assisted design model (CAD) was created using Rhinoceros 5 software (McNeel Europe, Barcelona, Spain) for the final 3D model architecture with a diameter of 4 mm and a height of 500 µm, then computationally sliced for processing by the bioprinter. Each layer of bio-ink was printed onto the print head then photopolymerized (cured) using blue light in the wavelength range of 385 – 405nm as previously described (16). The individual 3D tumor models were printed in a layer-by-layer fashion therefore achieving a homogeneous distribution of cells throughout the 3D tumor model. After printing, the models were washed in PBS to remove excess liquid bio-ink and cultivated in cell culture medium in a multi-well plate at 37°C and 5% CO_2 atmosphere.

Assaying Viability in Bioprinted 3D Tumor Models

Cell viability was determined using an NC-200™ NucleoCounter® (Chemometec). Prior to their suspension in the bio-ink for printing, neuroblastoma cells were stained with CellTracker™ Red CMTPX dye (Thermo Fisher Scientific, Waltham, MA, USA) according to the manufacturer's protocol with prolonged incubation times, then washed in PBS and counter-stained with CellTox™ Green dye (Promega, Madison, WI, USA) according to the manufacturer's protocol. The stained 3D tumor models were analyzed using a 2-photon microscope (LaVision Biotec GmbH, Bielefeld, Germany). A region of interest comprising 2.5 x 2.5 x 0.3mm from 5 models was imaged two and eleven days after printing. Imaris Software 7.6.5 (Oxford Instruments, Oxford, UK) was used to count red cells (total cell number) and green cell cores (dead cells) were counted. Live/dead cell ratios in percent were calculated using the simple formula:

$$Cell\quad viability\quad [\%] = \frac{total\quad cell\quad count - green\quad cell\quad count}{total\quad cell\quad count} * 100$$

CAR Construct and CAR T Cell Generation

The previously described L1CAM-specific CE7-CAR (19) was cloned into the SIN epHIV7 lentiviral vector then propagated in 293T cells and isolated as previously described (20). The single-chain variable Fragment (scFv) in the CAR construct was codon optimized and subsequently linked to a 12 (short) or 229 (long) amino acid spacer domain from the human IgG4-Fc hinge. The long spacer domain was modified by substituting L235D and N297Q to reduce binding to the IgG Fc gamma receptor (on natural killer cells and monocytes), which causes unintended CAR T cell activation *via* innate immune cell activation (21). The spacer domain connects the antigen-binding domain to CD28 transmembrane domain followed by the signaling module containing the CD3zeta (ζ) cytoplasmic domain and the 4-1BB (second generation CAR) costimulatory domain. CAR constructs were linked downstream to a T2A self-cleaving peptide and a truncated epidermal growth factor receptor (EGFRt) allowing CAR T cell detection and enrichment (22). CAR T cells were generated from healthy donors (Charité ethics committee approval EA2/216/18) as previously described (19). T cells used as controls alongside CAR T cells in experiments were not lentivirally transduced. CAR and control T cells were cryopreserved until further use. Cryopreserved cells were thawed and stimulated with irradiated peripheral blood mononuclear cells, irradiated $CD19^+$ EBV-transformed lymphoblastoid cell line (TM-LCL), and 30ng/mL antibody activating the CD3 complex (OKT3 clone, Miltenyi Biotec, Bergisch Gladbach, Germany). For rapid expansion, T cells were maintained in RPMI 1640 media supplemented with 10% fetal calf serum, 0.5ng/mL IL15 (Miltenyi Biotec) and 50U/mL IL2 (Novartis, Basel, Switzerland) according to a rapid expansion protocol (23). Functional *in vitro* assays were conducted between days 11 and 16 of culture adding fresh IL2 and IL15 to the coculture experiments.

Immunofluorescent Marker Detection in Bioprinted 3D Tumor Models

To visualize cells in their orientations in the bioprinted 3D model, models were fixed in 4% paraformaldehyde, embedded in paraffin and sectioned into 5µm slices using a microtome (HM 340E, Thermo Fisher Scientific). Immunofluorescence staining was performed with fluorochrome-conjugated antibodies diluted in blocking buffer directed against mouse monoclonal anti-human L1CAM (clone UJ127.11; Thermo Fisher Scientific) 1:500, rabbit monoclonal anti-human CD3 (clone SP7; Abcam, Cambridge, UK) 1:100 on sections overnight at 4°C. Recommended secondary antibodies were diluted in 1:500 and incubated for 1 hour. Nuclei were counterstained with Hoechst (B2261 Sigma Aldrich) diluted in 1:5,000-1:10,000 stain. Another staining approach for the bioprinted 3D tumor model was conducted by prestaining tumor cells with CellTracker™ Red CMTPX dye (Thermo Fisher Scientific) prior bioprinting. T cells were prestained with CellTracker™ Green CMFDA dye (Thermo Fisher Scientific) before coculture and following live-cell imaging. Images were acquired using a Nikon eclipse Ti-A1 microscope (Nikon, Tokyo, Japan) or a Leica M165 FC (LAS X software, Leica, Wetzlar, Germany) microscope. Cross sections of immunofluorescently stained samples were analyzed using Fiji ImageJ and MorpholibJ software. T cell infiltration was assessed from vertical scans conducted at 3 arbitrary locations in each bioprinted 3D model. Vertical scans were conducted in 1µm partitions in which T cells were identified by the mean red fluorescence, and mean fluorescence intensity was normalized to between 0 and 1 for combination of the vertical partitions and calculation of the depth of overall T cell infiltration (µm from the model surface).

Enzymatic Digestion of Bioprinted 3D Tumor Models

Bioprinted 3D tumor models could be processed into a single-cell suspension by digestion of non-cellular material using an enzymatic cocktail of 0.1% dispase II, 0.01% DNase I, 0.01% papain and 12.4 mM $MgSO_4$ in Hank´s balanced salt solution as described (24). Briefly, individual bioprinted 3D tumor models were washed with

PBS and then each mechanically minced into small pieces using a scalpel in a culture dish. Minced pieces were digested in the enzymatic cocktail for 20-30 minutes at room temperature directly in the culture dish. To assist matrix dissolution and release of single cells, tumor model pieces were gently triturated through a 1000 µL pipette tip every 5 minutes. The resulting cell suspension was centrifuged at 300 x g for 5 minutes, before discarding supernatant and washing twice in PBS.

Flow Cytometric Marker and Antigen Detection

Cell surface expression of L1CAM (clone REA163, Miltenyi Biotec), GD2 (clone 14.G2a; BD), CD3 (clone Hit3a, BioLegend, San Diego, CA, USA) and CD8 (clone SK1; BioLegend) was detected by fluorophore-conjugated monoclonal antibodies on a Fortessa X-20 (BD Biosciences, Franklin Lakes, NJ, USA) 4-laser flow cytometer. EGFRt expression was detected using biotinylated cetuximab (Bristol-Myers Squibb, New York, NY, USA) and a phycoerythrin (PE)-conjugated streptavidin antibody (cat #12-4317-87, BioLegend). Activation was assessed by fluorophore-conjugated monoclonal antibodies detecting TNFRSF9 (formerly CD137, clone 4B4-1; BioLegend) and IL2RA (formerly CD25, clone BC96; BioLegend). The Annexin V/7-AAD detection kit (BioLegend) was used to assess apoptosis. Dead cells were excluded from analyses using the LIVE/DEAD™ Fixable Green Dead Cell Stain Kit (cat#L23101, Life Technologies). Precision count beads (BioLegend) were used to quantify T cell infiltration according to the manufacturer's instructions. Flow cytometry data was processed using FlowJo_V10 Software (Tree Star Inc., Ashland, OR, USA).

Cytokine Release Assays

For cytokine release assays, $3x10^6$ T cells were seeded into wells (24-well plates) together with stimulator cells at a 5:1 effector: target ratio. All data points were performed as technical triplicates. After 12, 24, 36, 72 and 120 hours, supernatants were collected and stored at -80°C until analysis of IFNG using the OptEIA™ Set (BD Biosciences) ELISA kits in accordance with the manufacturer's instructions.

Statistical Analysis

Differences in cytotoxic activity, cell surface marker expression and cytokine release between treatment groups and controls were analyzed using the paired or unpaired Student's T test in GraphPad prism 8 software (GraphPad Software, La Jolla, CA, USA). All experiments were independently repeated (n = 3 or 4). P values <0.05 were considered statistically significant.

RESULTS

Neuroblastoma Cells Can Be Stereolithographically Bioprinted Into a 3D Tumor Model

Two major challenges for CAR T cell therapies used against solid tumors, are tumor infiltration and preservation of functionality upon massive antigen encounter (25, 26). Currently used 2D *in vitro* models cannot address these challenges. We developed a 3D tumor model that allows analysis of CAR T cell infiltration and phenotype. A digital, computer-assisted design (CAD) file was generated for the desired design. The 3D tumor model design used a disk with channel-like features that increased the surface area for CAR T cell interaction with tumor components (**Figure 1A**). Since channel-like features were located along the top surface (open to culture medium) of the bioprinted 3D tumor model, this structured surface also preserved orientation of the 3D model during cultivation, manipulation and post-experiment analyses including the preparation of slices for microscopic visualization. The physical 3D tumor model was then created by stereolithographically bioprinting a bio-ink composed of the established human SK-N-BE(2) neuroblastoma cell line suspended in 7% methacrylated gelatin with a photoinitiator (**Figure 1B**). Methacrylated gelatin forms an extracellular matrix allowing the cell migration necessary to study CAR T cell invasion in the models. As our technology is not dependent on extruders, but only on the size of the build space, 3D models can be produced in parallel in one production step. Our light projection-based bioprinting technology enabled the simultaneous printing of 16 neuroblastoma tumor models in parallel in this study, creating a high degree of comparability within each experiment (**Figure 1C**). These data demonstrate that stereolithographic bioprinting can be used to produce multiple bioprinted 3D neuroblastoma models at a time.

Bioprinted 3D Neuroblastoma Models Remain Viable Over Time

Model usefulness for preclinical testing requires that tumor cells living in the 3D models retain their viability for several days. Most experiments to test CAR T cell efficacy and activity require 3-5 days, but we purposely chose to assess an extreme experimental window to explore maximal experimental support with this novel 3D tumor model. We assessed the viability of neuroblastoma cells in the bio-ink before printing and the bioprinted 3D models after 2 and 11 days of cultivation using 2-photon image analysis. SK-N-BE(2) cells were labeled with CellTracker™ and CellTox™ before printing, to distinguish viable (red) from dead (green) cells in the 2-photon image analysis (**Figures 2A–C**). Cell viability in the bio-ink suspension was 94.8%. Viability in cell suspensions isolated from 5 bioprinted 3D models averaged 93.0% (range 88.2-97.2%) two days after printing and 76.0% (range 68.2-87.8%) eleven days after printing (**Figures 2D, E**). These data demonstrate that on average 76.0% of neuroblastoma cells in the model remain viable even after 11 days of cultivation in the bioprinted 3D model, supporting preclinical analyses of CAR T cell infiltration and T cell status even in extended experimental designs testing multiple antigen encounters.

CAR T Cells Can Infiltrate the Bioprinted 3D Tumor Model

Conventional coculture of CAR T cells with an adherent tumor cell monolayer has been extensively used to preclinically evaluate

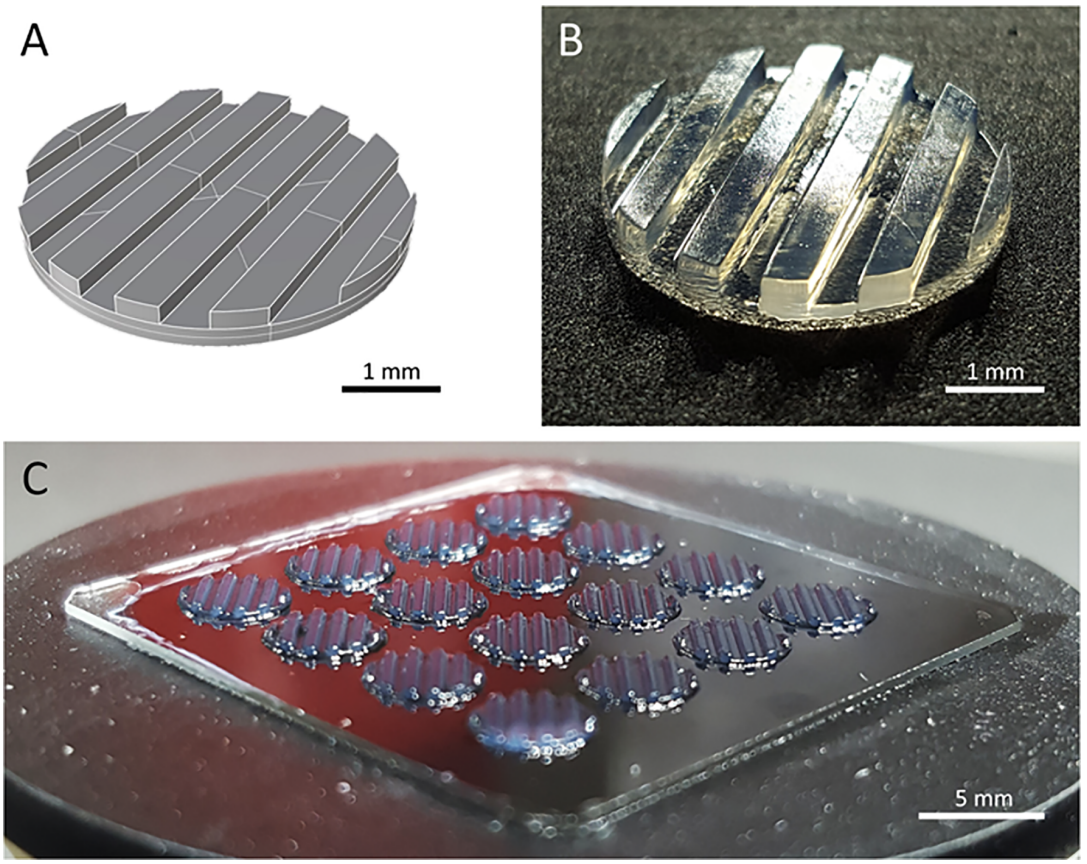

FIGURE 1 | The bioprinted 3D neuroblastoma tumor model. **(A)** Computer-assisted design file (CAD) used for printing the 4 mm diameter and 500 µm depth model. **(B)** Macroscopic photograph of bioprinted 3D tumor model. Scale bar = 1 mm. **(C)** An array of 16 multiple tumor models directly after printing. Scale bar = 5 mm.

CAR T cell efficacy, mainly utilizing cytokine production, tumor cell lysis and T cell exhaustion as endpoints in short-time experiments (27, 28). These models, however, do not support assessment of the ability of CAR T cells to infiltrate the solid tumor structure, an ability necessary for tumor eradication. Here, we test whether $CD8^+$ L1CAM-specific CAR T cell infiltration can be assessed using a bioprinted 3D neuroblastoma model, in which the embedded neuroblastoma cells express the target antigen, L1CAM. We engineered T cells to express a second-generation L1CAM-specific CAR with 4-1BB as costimulatory domain harboring either a short (SS-BB/ζ) or a long (LS-BB/ζ) spacer (**Figure 3A**). Following immunomagnetic selection for EGFRt, >90% of T cells expressed either CAR construct used (**Figure 3B**). Untransduced T cells served as a negative control. We microscopically investigated whether we see L1CAM-CAR T cells within the bioprinted 3D tumor models. For detailed analysis, live-cell confocal microscopy was used to analyze prestained CAR T cells (green) in coculture with prestained neuroblastoma cells (red) in the bioprinted 3D tumor model. Live-cell imaging revealed T cell proximity to tumor cells and infiltration of untransduced and L1CAM-CAR T cells into the bioprinted 3D models (**Figure 3C**). We also applied immunofluorescence staining to determine whether CAR T cells infiltrated the bioprinted 3D tumor model. Samples were formalin-fixed and paraffin-embedded (FFPE) 24 hours after introducing CAR T cells to the bioprinted 3D model, then sectioned before detecting L1CAM and CD3 with Hoechst counterstaining to detect nuclei (**Figure 3D**). T cell infiltration into the bioprinted 3D tumor model was determined by analyzing three distinct areas of three individually stained T cell-treated 3D tumor models (**Supplementary Figure 1A**). CAR T cell infiltration depth was investigated by normalizing $CD3^+$ (red) immunofluorescence (**Figure 3E**). Interestingly, both L1CAM-specific CAR T cell subsets infiltrated into the top (indicated by the peaks between channels) and bottom of the bioprinted 3D tumor models. A region within the sections from the bioprinted 3D tumor model was viewed under higher magnification to observe T cell proximity to tumor cells (**Supplementary Figure 1B**). These results demonstrate that our bioprinted 3D neuroblastoma model is suitable for visualizing and quantifying target-specific CAR T cell infiltration either by live-cell imaging using prelabeled (Celltracker™) cell populations or using immunofluorescence staining of cryopreserved or FFPE specimens.

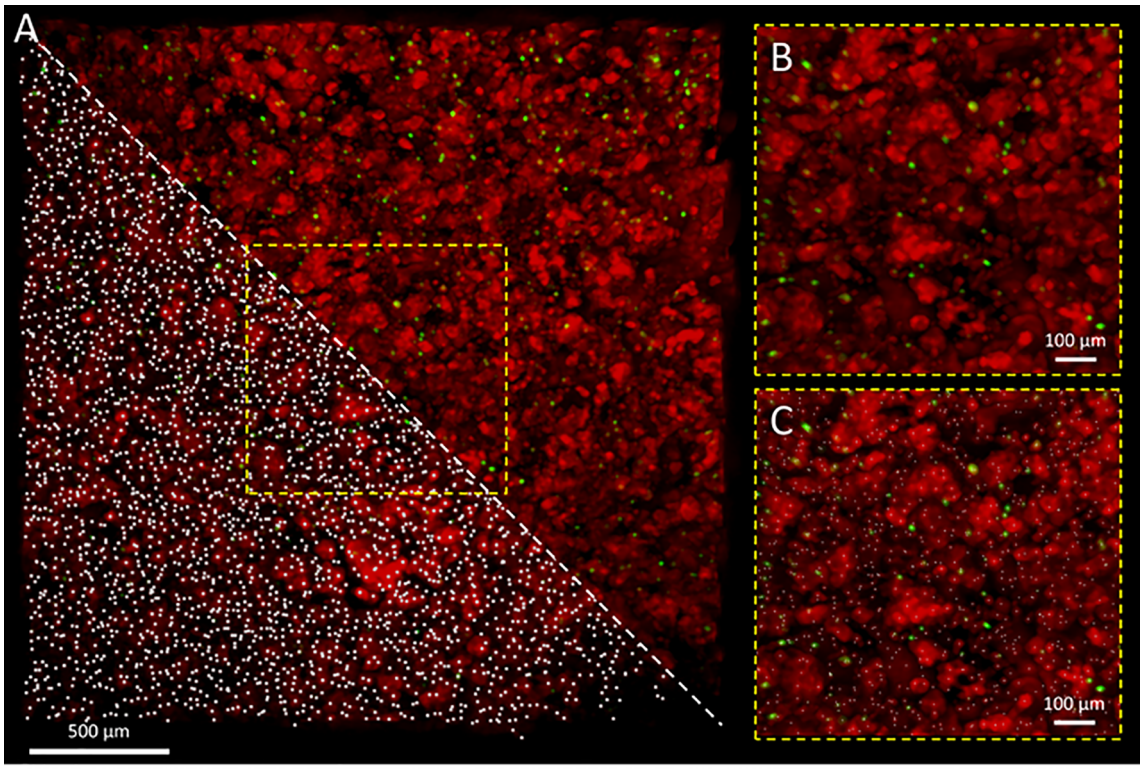

D

cell suspension (before printing)	sample no.	tumor day 02	tumor day 11
94.8	1	94.5	87.8
	2	88.2	77.7
	3	97.2	75.5
	4	94.5	72.8
	5	93.0	68.2

Table 01. Viability of printed 3D tumors determined by 2-photon-microscopy image analysis in percent of total cell number.

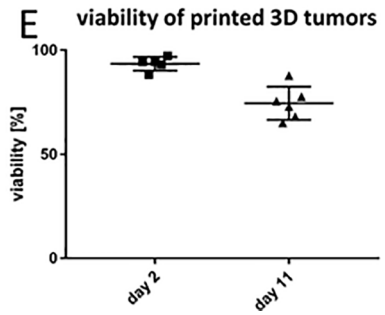

FIGURE 2 | Neuroblastoma cells remain viable over 11 days in bioprinted 3D tumor model. **(A)** Image shows 0.75mm³ cut-out of bioprinted 3D tumor model, which was visualized by 2-photon image analysis. Viable cells are stained by CellTracker™ red and dead cells by CellTox™ green. A region of interest is enlarged without marking cells (upper triangle and **B**) and by computationally counting cells visualized by white dots (lower triangle and **C**) Scale bar = 100 µm. Neuroblastoma cell viability both before and after printing is presented in the table **(D)** and graph **(E)**. Viability of printed cells after 2 days and 11 days in culture was determined by 2-photon image analysis.

Single-Cell Suspensions Can Be Harvested From Bioprinted 3D Models for Functional Assays

We have shown that infiltrated L1CAM-CAR T cells can be visualized with different microscopic approaches. Next, we tested whether CAR T cell-treated bioprinted 3D tumor models could be processed into a single-cell suspension allowing flow cytometric analysis of both tumor and CAR T cells from treatment groups. This would present a highly useful protocol for experimental analyses or endpoint measurements requiring single cells or multiple cells freed from their interacting components and enhance bioprinted 3D tumor model experimental applications. Different mechanical (not shown) and enzymatic treatment methods for dissociation were tested. The method of choice was to digest non-cellular material in the bioprinted 3D models using an enzymatic cocktail (see *Materials and Methods* section; **Figure 4A**). To check if enzymatic digestion reduced cell viability, 2D tumor and T cell monocultures were digested with the same enzymatic cocktail alongside the bioprinted 3D models, then cell viability was flow cytometrically determined using a fluorescent dye labeling dead cells. The digested 3D neuroblastoma models, as well as SK-N-BE(2) and L1CAM-CAR T cells enzymatically digested from 2D monocultures were as viable as their undigested controls (**Figure 4B**). Maintenance of protein expression during sample preparation is highly relevant for immunological research. We flow cytometrically analyzed

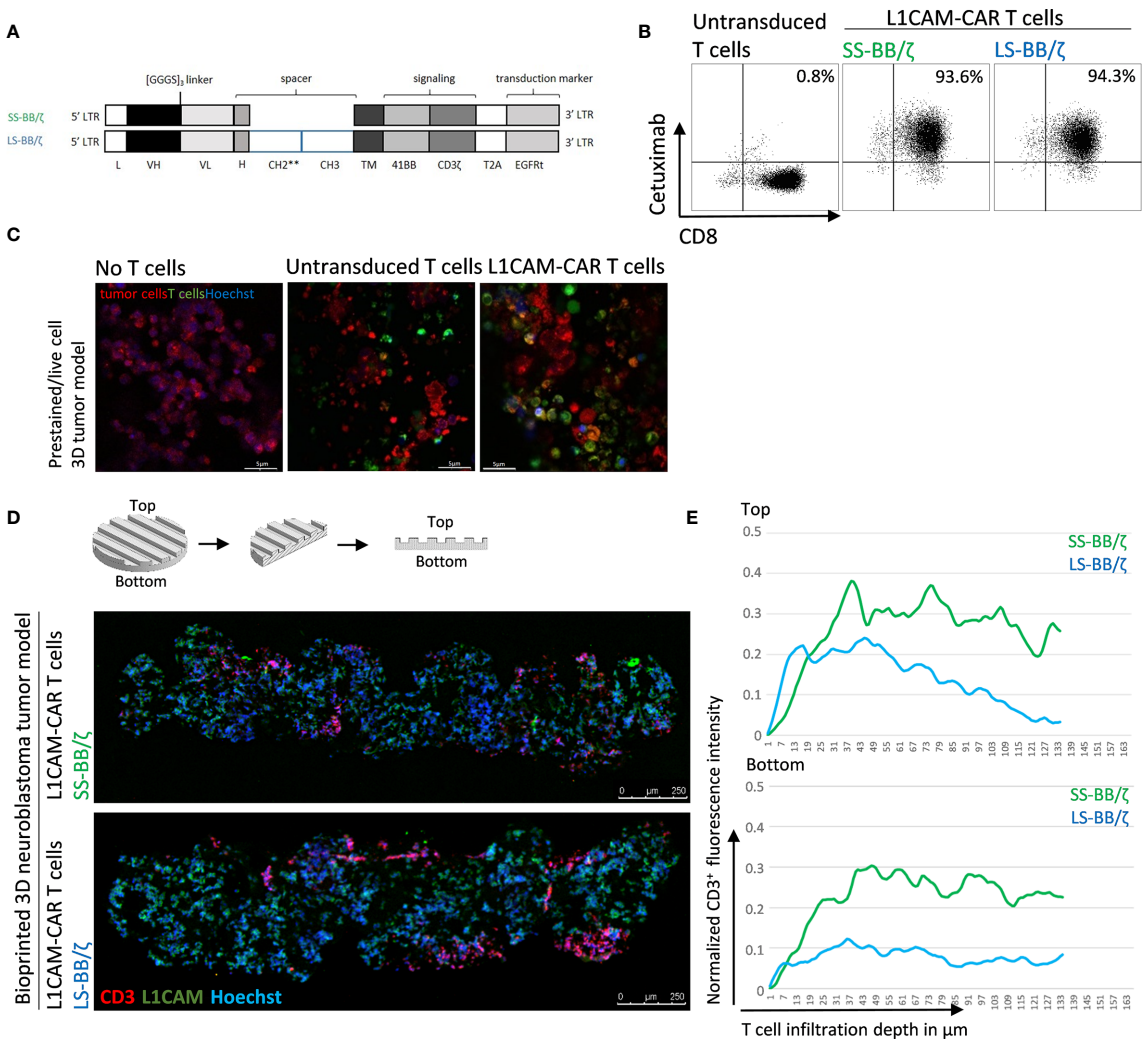

FIGURE 3 | L1CAM-specific CAR T cells in coculture with bioprinted 3D neuroblastoma tumor model. **(A)** Schematic representation of lentiviral constructs used to generate L1CAM-specific second-generation CAR T cells. L, long-terminal repeat; VH, variable region of the heavy chain; VL, variable region of the light chain; H, hinge region with either short (IgG4) or long (CH2**-CH3) spacer; CH2**, CH2 harboring both L235D and N297Q point mutations; TM, transmembrane domain; T2A, virus 2A self-cleaving sequence. **(B)** Representative flow cytometry plots showing EGFRt transduction marker expression on CD8+ T cells transduced with L1CAM-specific short spacer 4-1BB zeta (SS-BB/ζ) and long spacer 4-1BB zeta (LS-BB/ζ) constructs after enrichment. Untransduced T cells served as negative control. **(C)** Live-cell imaging of prestained bioprinted 3D tumor models (lower panel) alone (prestained with CellTracker™ Red CMTPX, red and Hoechst, blue) or in coculture with untransduced or LS-BB/ζ T cells (prestained with CellTracker™ Green CMFDA, green, and Hoechst, blue) using confocal microscopy (E:T = 5:1) Scale bar = 5 µm. **(D)** Schematic depiction of 3D print and FFPE sample processing and orientation. Immunofluorescence staining of formalin-fixed paraffin-embedded (FFPE) 3D tumor models treated with L1CAM-CAR T cells for CD3 (red), L1CAM (green) and Hoechst (blue). Schematic 3D print serves for orientation; Scale bar = 250 µm. **(E)** T cell infiltration depth quantified by red fluorescence channel profiling. Staining intensity is depicted as normalization of CD3+ T cells fluorescence intensity on the y-axis, and T cell infiltration depth into the bioprinted 3D tumor is represented on the x-axis. Top indicates the upper model surface containing the channels. Bottom indicates the flat lower model surface. Depicted is the mean of three distinct areas from biological triplicates.

expression of the L1CAM and GD2 surface antigens on neuroblastoma cells as well as $CD3^+$ and $CD8^+$ surface molecules on L1CAM-specific CAR T cells and untransduced T cells after enzymatic digestion. L1CAM expression on SK-N-BE(2) cells digested from 2D or bioprinted 3D models did not differ from undigested SK-N-BE(2) cells (digested 2D: 79.0 ± 1.1%, digested 3D: 88.3 ± 1.7%, undigested 2D: 83.2 ± 1.5%; **Figure 4C**). Similar results were obtained for GD2 expression (digested 2D: 95.4 ± 2.8%, digested 3D: 96.1 ± 0.5%, undigested 2D: 95.7 ± 3.3%; **Figure 4C**). Enzymatic digestion also did not remove $CD3^+$ and $CD8^+$ surface molecules from L1CAM-specific CAR T cells (**Supplementary Figure 2A**) or untransduced T cells ($CD3^+$: digested: 98.8 ± 0.4%, undigested: 97.9 ± 1.6%; $CD8^+$: digested: 96.2 ± 0.1%, undigested: 96.0 ± 1.7%; **Figure 4D**). These data demonstrate that bioprinted 3D tumor models and target-specific CAR T cells maintain their cell viability and, importantly, their surface molecule expression during sample preparation for single-cell suspensions following experiments conducted in the

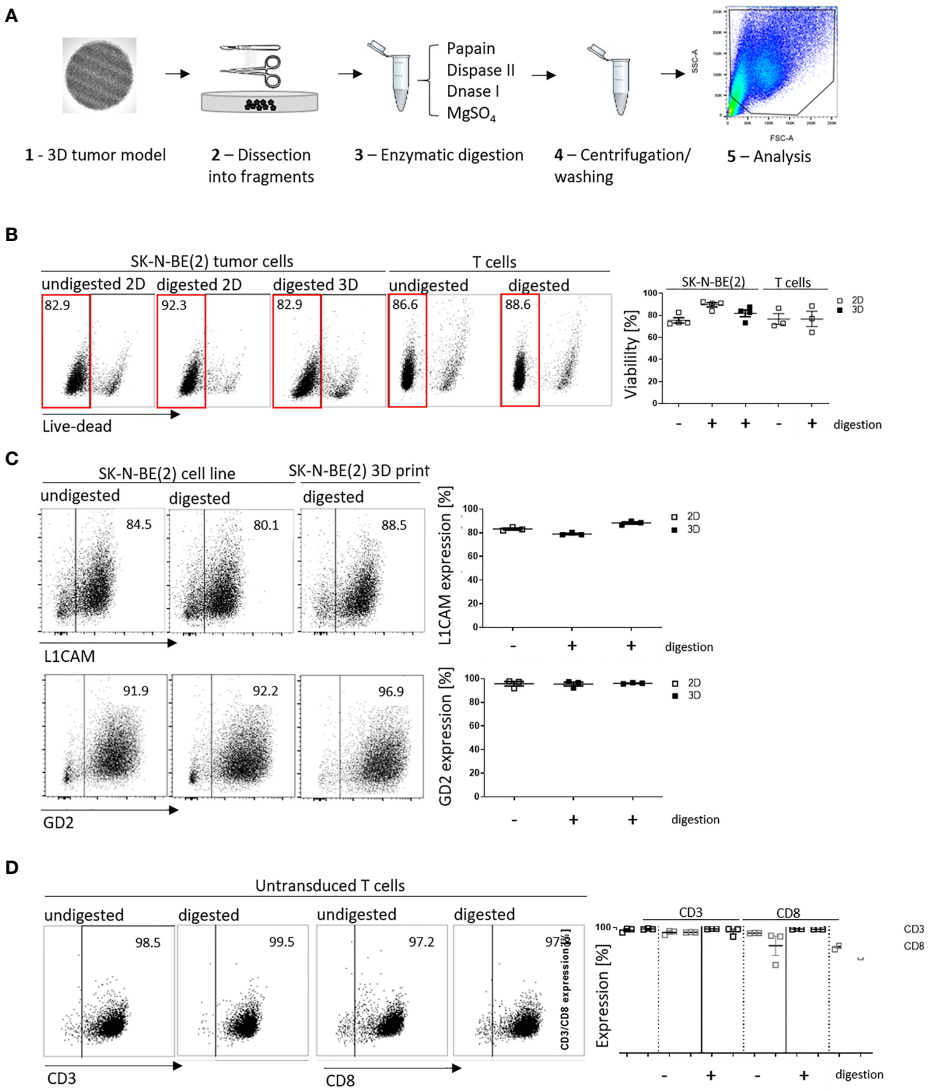

FIGURE 4 | Cell viability and cell surface molecule expression is maintained after enzymatic digestion. **(A)** Schematic depiction of enzymatic digestion protocol to produce single-cell suspensions after 3D model experiments. **(B)** Representative flow cytometry plots (left) showing live (framed in red) and dead cells that either underwent the enzymatic digestion protocol or not (from either 2D or suspension cultures) and the single-cell suspension from the 3D models. Numbers at the top of each plot indicate percent of the total cell population. SK-N-BE (2) neuroblastoma and untransduced T cells are shown in separate panels of the representative flow cytometry plots. Scatter plots on the right summarize results from 3 or 4 individual experiments. **(C)** L1CAM and GD2 antigen expression analyzed by flow cytometry (representative plots shown, left), and is summarized from 3 experiments in the scatter plot (right). **(D)** Representative $CD3^+$ and $CD8^+$ surface molecule expression on untransduced T cells without and with enzymatic digestion are shown (left) and summarized in the scatter plot (n = 3, right). All experiments were conducted after 24h of coculture.

bioprinted 3D models, enhancing bioprinted 3D tumor model usefulness for CAR T testing and experimentation.

CAR T Cell Activation Is Superior in the Bioprinted 3D Neuroblastoma Model

An important prerequisite for effective therapy is CAR T cell infiltration into tumor tissue. After confirming that T cell-treated bioprinted 3D tumor models can be enzymatically dissociated into single-cell suspensions without reducing expression of key T cell surface markers, we used $CD3^+$ cell surface staining and counting beads to flow cytometrically quantify CAR T cell infiltration. A kinetic profile of L1CAM-specific CAR T cell infiltration into the bioprinted 3D tumor model was constructed by detecting $CD3^+$ cell populations in 3D models at 12, 24, 36 and 120 hours using a flow cytometry gating strategy (**Figure 5A**) on the dissociated single-cell suspensions to quantify $CD3^+$ populations in the 3D model over time in zebra plots (**Figure 5B**). After only 12 hours, 63,604 LS-BB/ζ L1CAM-CAR T cells, 40,658 SS-BB/ζ L1CAM-CAR T cells and 33,523 untransduced T cells had infiltrated the 3D tumor model. Highest CAR T cell infiltration was detected after 24 hours,

when 198,433 SS-BB/ζ L1CAM-CAR T cells and 49,823 LS-BB/ζ L1CAM-CAR T cells had infiltrated the tumor model (**Figure 5B**). Antigen-independent infiltration of untransduced T cells remained relatively stable over the testing period (**Figure 5B**). We assessed T cell activation markers at the time of peak infiltration (24h). The proportion of T cells expressing both CD25 and CD137 activation markers was higher in bioprinted 3D tumor models, where we solely measured activation of total infiltrated T cells, compared with 2D monolayer cocultures, where all T cells were included (**Figure 5C**). CD137 and CD25 expression was higher on L1CAM-CAR T cells with the long spacer compared to their counterparts using the short spacer in assays using either 2D or 3D models. Untransduced T cells expressed minimal CD25 and no CD137, excluding unspecific T cell activation. CAR T cell activation in 2D or 3D cocultured cells was significantly higher compared to paired untransduced T cells. Tumor cell encounter in the bioprinted 3D tumor model induced release of lower levels of the cytokine, interferon gamma (IFNG), from L1CAM-CAR T cells than encounter in 2D cocultures (SS-BB/ζ: p=0.07; LS-BB/ζ: p=0.06; **Figure 5D**). CAR T cell-mediated tumor cell cytotoxicity was analyzed using a fluorescent dye labeling dead cells and a gating strategy identifying the $CD3^-$ tumor cells at the 24-hour time point (**Supplementary Figure 2B**). L1CAM-specific CAR T cells more easily killed tumor cells in 2D cocultures (SS-BB/ζ L1CAM-CAR T cells lysed: 95.9 ± 0.8% in 2D, 39.9 ± 27.1% in 3D; LS-BB/ζ L1CAM-CAR T cells lysed: 92.1 ± 3.6% in 2D and 42.4 ± 22.0% in 3D; **Figure 5E**). Control experiments induced only low-level tumor cell lysis in both 2D (no T cells: 24.6 ± 1.0%, untransduced T cells: 24.7 ± 3.0%) and 3D (no T cells: 18.0 ± 5.8%, untransduced T cells: 14.8 ± 3.6%) models (**Figure 5E**). The kinetics of neuroblastoma cytotoxicity in the bioprinted 3D tumor model was analyzed at 12, 24, 36, 72 and 120 hours, with maximal cytotoxicity being reached only after 120 hours of CAR T cell treatment and lysing 72.0 ± 23.6% (SS-BB/ζ) and 67.9 ± 18.1% (LS-BB/ζ) of neuroblastoma cells, which is significantly higher compared to untransduced T cells (**Figure 5F**). L1CAM-specific CAR T cells were more strongly activated in the bioprinted 3D tumor model, but induced less IFNG release than in 2D cocultures. The bioprinted 3D tumor model supported the detection and quantification of T cell infiltration into the tumor model, expanding *in vitro* testing possibilities.

DISCUSSION

Current strategies to analyze CAR T cell effector function heavily rely on *in vitro* analyses in 2D culture models, which only limitedly represent solid tumor physiology. CAR T cells must home to the tumor site, circumvent inhibitory effects of the tumor microenvironment and persist during multiple rounds of antigen encounter to eradicate solid tumors (25, 26). Widely used 2D coculture systems cannot investigate these hurdles. We developed a novel method to analyze CAR T cell effector function in a stereolithographically bioprinted 3D tumor model, and present proof-of-concept here using CAR T cells targeting one neuroblastoma target protein, L1CAM, and a neuroblastoma cell line. Our model is easily extensible to other tumor types and CAR T cell targets. We present live-cell and fluorescence microscopy methods to visualize interactions between second-generation L1CAM-specific CAR T cells with the 4-1BB costimulatory domain harboring the short or long spacer and tumor cells in these bioprinted 3D neuroblastoma models. We also present an optimized protocol to convert a bioprinted 3D tumor model experiment into a single-cell suspension, maintaining cell viability and surface protein markers descriptive of the cell phenotypes. This method supports analysis not only of T cell infiltration but CAR T cell activation and effector function for advanced quantitative endpoint analysis in 3D tumor model experiments.

Tumor cells clustered into spheroids from a single cell line or heterogeneous tumor cell types have been used to assess antibody (29), natural killer cell (29–31), cytotoxic T cell (32) and CAR T cell (33–35) immunotherapy *in vitro*. Highly variable spheroid size increases experimental variability if endpoints are quantified, and endpoint analysis often requires sophisticated visual monitoring (33) for quantification. The stereolithographic bioprinting of human SK-N-BE(2) neuroblastoma cells within a photoactivatable methacrylated gelatin matrix that we use here creates a group of identically viable copies with which to conduct sophisticated CAR T cell testing *in vitro*. In this way, high precision and robustness are achieved, which is essential for the comparability of the results within both small and large experimental designs and across experiments. Effector to target ratios also become more difficult to define as models become more complex. The defined structure in our bioprinted 3D model allows precise calculation, while estimation is more difficult for spheroids and almost impossible for *ex vivo* tissue slices and organoids. A closer approximation of physiological organ structure can be achieved in organoids, which can be both organ-specific and patient-specific, and *ex vivo* tissue slices [reviewed in (36)]. Jacob et al. recently described a patient-derived glioblastoma organoid model biobank used to test response to two CAR T cell therapies (37), however, results could only be immunohistochemically examined, increasing evaluation time and complexity. Wallstabe et al. recently present a microphysiological 3D lung and breast cancer model for preclinical CAR T cell evaluation that uses the porcine jejunum as a scaffold (38). An advantage of this model was that fibroblasts and other stromal cells could be included to simulate the immunosuppressive tumor environment, but it is laborious to establish and subject to donor-dependent variance. Higher model complexity reduces comparability among individual experiments, in contrast to our bioprinted 3D tumor models, and reduces accurately quantifiable endpoints that can be used to assess CAR T cell action.

We demonstrated high viability of the bioprinted 3D tumor models shortly after printing and during culture for up to 11 days, in line with results from other groups showing cell viability is preserved in bioprinted 3D tumor models for several weeks (39–44). In addition to maintaining high viability over time, incorporation of other cellular components within the bioprinted 3D tumor model will contribute to recapitulate characteristics of an *in vivo* tumor microenvironment. Langer et al. published a bioprinted 3D tumor model similar to ours, but supplemented with fibroblasts and endothelial cells (45) demonstrating that 3D bioprinting can be used to create complex and heterotypic tumor

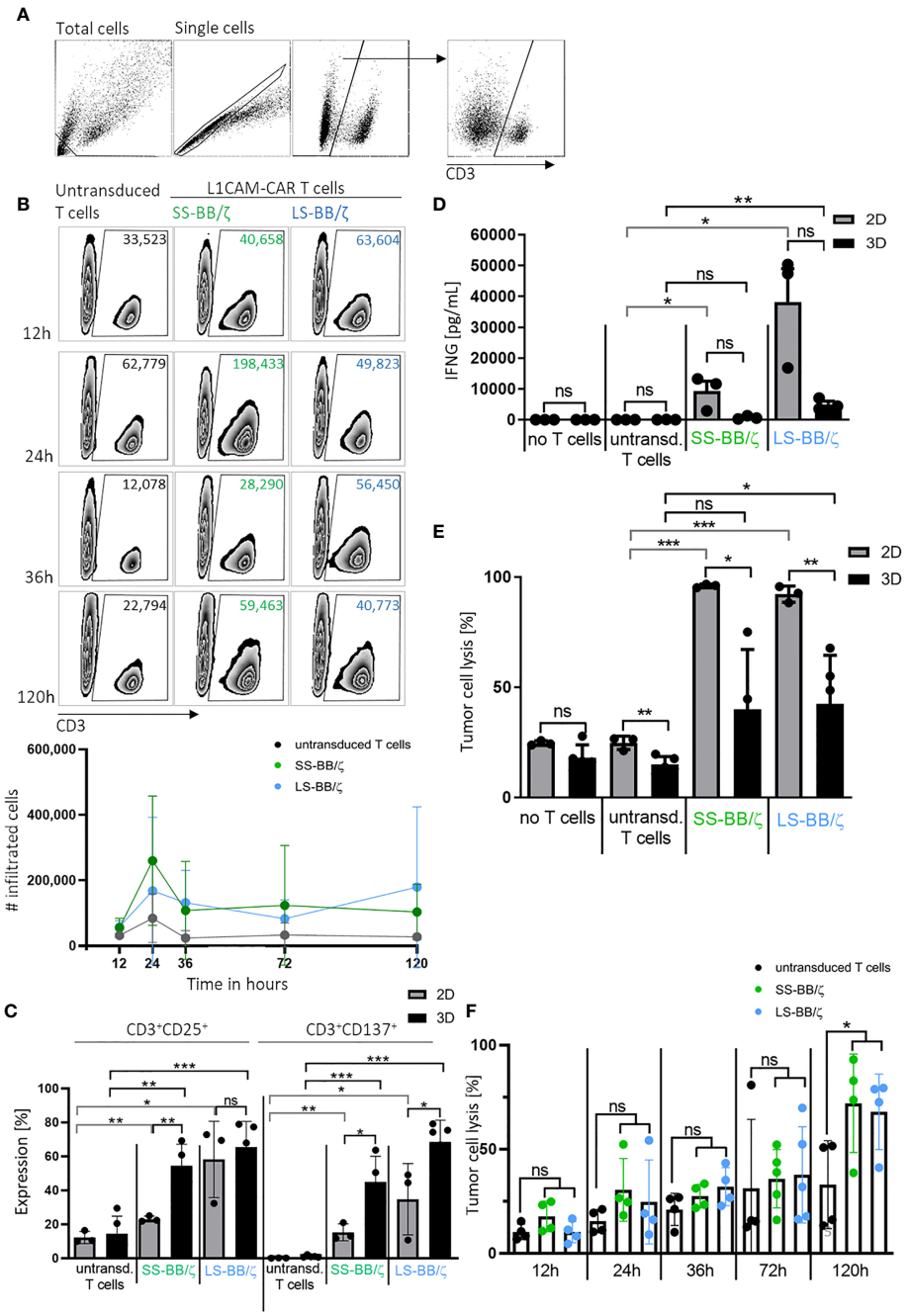

FIGURE 5 | L1CAM-CAR T cells infiltrate and are highly activated in bioprinted 3D neuroblastoma tumor models. **(A)** Gating strategy for flow cytometry (applied with FlowJo_V10) is shown. Gates are applied to distinguish single viable T ($CD3^+$) and tumor cells ($CD3^-$) within the total cells. **(B)** Representative zebra plots showing numbers of $CD3^+$ viable cells that infiltrated the 3D tumor model after the indicated time measured by flow cytometry with precision counting beads including summary of 3 biological replicates. **(C)** Surface activation markers were flow cytometrically analyzed on untransduced T cells and L1CAM-specific CAR T cells after 24h of tumor cell interaction (effector:target ratio of 5:1) in either 2D coculture or the bioprinted 3D model. Depicted are double-positive cells for $CD8^+$ and CD25 or CD137. Cells were gated from living single cells. Bars depict the mean of 3 (2D) or 4 (3D) experiments with error bars representing SD. **(D)** Interferon gamma (IFNG) released into the culture media was detected by ELISA after 24h of tumor cell interaction (effector:target ratio of 5:1) in either 2D coculture or the bioprinted 3D model. Bars depict the mean of 3 (2D) or 4 (3D) experiments with error bars representing SD. **(E)** Tumor cell cytotoxicity was analyzed (FACS) after 24h of tumor cell interaction (effector:target ratio of 5:1) in either 2D coculture or the bioprinted 3D model. Bars depict the mean of 3 (2D) or 4 (3D) experiments with error bars representing SD. **(F)** FACS-based tumor cell cytotoxicity is shown for the 5-day time course in the bioprinted 3D model after addition of untransduced T cell controls or L1CAM-specific CAR T cells, as indicated. Experiments tested L1CAM-specific CAR T cells with either the short (green) or long (blue) spacer. Bars depict the mean of 4 experiments with error bars representing SD. ns, not significant, *p ≤ 0.5, **p ≤ 0.01, ***p ≤ 0.001.

tissue that incorporate both cancer and stromal cell types. Heinrich et al. and Meng et al. have also used methacrylated gelatin for a glioblastoma cell line model containing macrophages or a metastatic lung cancer cell line model, respectively, albeit using different bioprinting techniques (40, 43). The scientific field developing 3D bioprinting possibilities is expanding with an emphasis to more closely recapitulate certain tumor microenvironment characteristics important to the scientific questions being asked and all exceeding the tumor-nearness of monolayer cultures, but 3D models for preclinical CAR T cell evaluation are still rare. We are currently developing protocols allowing inclusion of endothelial and myeloid-derived suppressor cells to create a more representative microenvironment of human tumors in the bioprinted 3D tumor models to answer questions requiring these tumor components.

L1CAM-specific CAR T cells were able to recognize and infiltrate our bioprinted 3D neuroblastoma models, with microscopic assessment verifying deep L1CAM-specific CAR T cell infiltration. Bead-based quantification of T cell infiltration demonstrated antigen-dependent T cell infiltration, since more CAR T cells, regardless of spacer length, infiltrated the bioprinted 3D neuroblastoma models than untransduced T cells. High numbers of CAR T cells had infiltrated our bioprinted 3D models after only 12 hours, peaking at 24 hours then not further increasing. This observed plateau corresponds with the time window when antigen-dependent proliferation begins and might indicate that T cell proliferation and death balanced the cell numbers, creating the observed plateau. Microscopic assessment predicts a higher infiltration of SS-BB/ζ L1CAM-specific CAR T cells compared to LS-BB/ζ CAR T cells. Tumor suppressive mechanisms that could be preventing CAR T cell proliferation can also not be ruled out. Elucidating possible mechanisms would be feasible using our bioprinted 3D models and would be of special interest to understanding the limits of CAR T cell infiltration and expansion in the solid tumor microenvironment. Ando et al. used a similar tumor cell model, where tumor cells were also embedded in methacrylated gelatin, which showed a modest infiltration of HER2-specific CAR T cells (46). In contrast to our model, where CAR T cell infiltration was already detected after 12 hours, they detected low CAR T cell infiltration after 72 hours. The shape of the bioprinted 3D tumor models, tumor entity used and/or CAR T cell architecture may contribute to differences in T cell infiltration achieved in the different models. The possibility to study CAR T cell infiltration into our bioprinted 3D model allows early and late time point comparisons among selected T cell subtypes *in vitro*.

Assessing antigen expression on tumor cells or activation marker expression on T cells is essential to evaluate novel CAR T cells. We developed a method to preserve protein expression on both tumor and T cells, after obtaining a single-cell suspension. Activation marker expression on L1CAM-CAR T cells with the long spacer was higher than on their counterparts with the short spacer after experiments in either the 2D or 3D models, while both cell types demonstrated comparable cytotoxicity *in vitro*. We have previously shown that *in vivo* function of L1CAM-CAR T cells with a long spacer element was inferior compared to L1CAM-CAR T cells harboring a short spacer in mouse models (19). The more highly activated phenotype of long-spacer L1CAM-CAR T cells observed here *in vitro* might be detrimental *in vivo* where CAR T cells are subjected to repeated antigen encounter leading to activation-induced cell death. So far, we could not predict this phenomenon with our 3D tumor model. This could be due to the relatively low E:T ratio achieved in the 3D coculture system, as only a fraction of T cells introduced to the 3D model actually entered it, resulting in delayed and reduced killing compared to the 2D coculture system. Titrating the number of CAR T cells added to the 3D tumor model to achieve comparable E:T ratios as in 2D coculture experiments are future refinements planned to improve 3D model predictability.

CAR T cells can mediate tumor-specific cytotoxicity, for example by releasing IFNG, which is necessary for complete tumor eradication (47), or by inducing the Fas/FasL axis (48). Unexpectedly, even when CAR T cells were highly activated after coculture with bioprinted 3D tumors, extremely low IFNG release was measured in comparison to 2D cultures. The lower IFNG levels in culture medium from CAR T cell-treated 3D tumors may have been caused by IFNG sequestration in the extracellular matrix of the bioprinted 3D tumors (49). However, the more likely reason for the lower levels is that only a fraction (approximately 10%) of the added CAR T cells infiltrated the 3D tumor model, reducing the amount of T cells able to produce IFNG after encountering the tumor cells, compared to the situation in monolayer co-culture. In line with this finding, L1CAM-specific CAR-mediated cytotoxicity in bioprinted 3D tumors was detected with delayed onset of 5 days and was lower than in 2D cocultures. Calculation of T cell infiltration with quantification beads shifted the effector to target ratio from, the initially added, 5:1 to 1:10 that were actually present within the 3D bioprinted model. This adjusted ratio resolves the lower tumor cell lysis and IFNG release by CAR T cells in the bioprinted 3D tumor model compared to 2D cocultures. Our initially selected 5:1 ratio was chosen only as the initial quantity of T cells to add to cocultures to initiate comparisons between the 2D and 3D models. Corroborating our results, Schnalzger et al. showed that CAR-NK92 cells induced significantly lower tumor cell lysis in 3D compared to 2D models (50). These results in our and other bioprinted 3D models indicate that cytokine release and tumor cell cytotoxicity may be overestimated by 2D coculture testing, and demonstrate that analyses in 3D models are a more effective mirror of real-life obstacles CAR T cells need to bypass in tumors.

We present a 3D tumor model produced in parallelized batch bioprinting production for use in preclinical investigations of CAR T cell effector function and as a potential preselection tool for CAR T cell constructs. CAR T cell infiltration into the bioprinted 3D tumor model proved quantifiable using two different methods, supporting comparisons of the impact of different CAR constructs on T cell infiltration. Single-cell suspensions released from completed experiments retain cell surface proteins and viable cells for quantitative and qualitative functional assessment. This highly reproducible bioprinted 3D human tumor model is a tumor-near *in vitro* environment for CAR T cell preselection based on effector functions prior to *in vivo* studies. Knowing that evaluating tumor infiltration and functionality *in vivo* is essential for CAR T cells developed to treat solid tumors, we do not mean to suggest that our 3D neuroblastoma model can replace CAR T cell evaluation in

mouse models, but make *in vitro* testing more stringent so that fewer candidates better adapted to enter solid tumors proceed to *in vivo* testing, thus increasing the speed and reducing the cost (and animal use) of thorough preclinical testing. To best illuminate the particular usefulness of the bioprinted 3D model, we selected a pair of thoroughly preclinically tested CAR constructs and repeated *in vitro* evaluation in direct comparison to the bioprinted 3D model in the experiments presented here. Human neuroblastomas contain a richer tumor tissue environment than our bioprinted 3D model, which while providing the 3D environment lacks specific matrix molecules and cellular components in human tumors. Modeling the human extracellular matrix is, however, a difficult problem also faced in mouse models. Current preclinical NSG mouse models bearing xenografts cannot completely reflect the tissue environment in human tumors due to species-specific discrepancies of chemokine and adhesion molecules resulting in limited trafficking and extravasation of CAR T cells (51, 52). Even patient-derived xenograft mouse models have shown that the tissue environment of the original tumor is rapidly replaced by a murine stroma after a few passages (53). To approach testing of individual extracellular and cellular tumor matrix components (including different patient-derived tumor cell backgrounds, target antigens and tumor entities) *in vitro*, we plan to further adapt this bioprinted 3D tumor model as a part of a future pipeline planned for standard preclinical *in vitro* evaluation of CAR constructs. A gelatin-based ECM in the bioprinted 3D model could present a more tumor-near microenvironment. Following Langer et al., the addition of fibroblasts and endothelial cell layers would benefit this model, especially to investigate the infiltration capacity of CAR T cells into the immune-suppressive environment using human-derived stroma cells (45). These potential adaptations, once standardized, could be applied to evaluate the impact of distinct parameters from tumor matrix components in experimental series. The implementation of additional cell types representing important tumor components with T cell efficacy-influencing properties, such as an immunosuppressive tumor stroma or tumor blood vasculature, will further refine our model to create an *in vitro* tool potentially capable of reducing both the time and animals necessary for preclinical testing in CAR T cell research.

DATA AVAILABILITY STATEMENT

The original contributions presented in the study are included in the article/**Supplementary Material**. Further inquiries can be directed to the corresponding author.

ETHICS STATEMENT

The studies involving human participants were reviewed and approved by Charité ethics committee approval EA2/262/20. The patients/participants provided their written informed consent to participate in this study.

AUTHOR CONTRIBUTIONS

AKü and LK conceived the project. LG performed and analyzed the CAR T cell experiments with the assistance of LA, AK, SS, and AW. TL developed the bioprinted 3D tumor model with assistance of AT. FK was consulted for statistical evaluation. AG and AH-H contributed their help with the immunofluorescence staining. HD, AH, AE and JS gave scientific advices. LG, TL, KAs, KAn, LK, and AKü wrote the manuscript. All authors contributed to the article and approved the submitted version.

FUNDING

LG is participant in, and is partly funded by, the "Berlin School of Integrative Oncology". AH and AKü are participants in the BIH-Charité Clinician-Scientist Program funded by the Charité – Universitätsmedizin Berlin and the Berlin Institute of Health. A research grant (#2017_A51) from the Else Kröner-Fresenius foundation (to AKü) and from Charité 3R| Replace - Reduce - Refine (to AKü) supported this work. AG is supported by the Deutsche José Carreras Leukämie Stiftung (R03/2016). The funders had no role in study design, data collection and analysis, decision to publish or preparation of the manuscript.

ACKNOWLEDGMENTS

The authors thank Michael C Jensen for providing the L1CAM-specific CAR T cell construct.

SUPPLEMENTARY MATERIAL

The Supplementary Material for this article can be found online at: https://www.frontiersin.org/articles/10.3389/fimmu.2021.689697/full#supplementary-material

REFERENCES

1. Smith MA, Seibel NL, Altekruse SF, Ries LA, Melbert DL, O'Leary M, et al. Outcomes for Children and Adolescents With Cancer: Challenges for the Twenty-First Century. *J Clin Oncol* (2010) 28(15):2625–34. doi: 10.1200/jco.2009.27.0421
2. Porter DL, Levine BL, Kalos M, Bagg A, June CH. Chimeric Antigen Receptor–Modified T Cells in Chronic Lymphoid Leukemia. *N Engl J Med* (2011) 365(8):725–33. doi: 10.1056/NEJMoa1103849
3. Martinez M, Moon EK. Car T Cells for Solid Tumors: New Strategies for Finding, Infiltrating, and Surviving in the Tumor Microenvironment. *Front Immunol* (2019) 10:128. doi: 10.3389/fimmu.2019.00128
4. Gonzalez S, Naranjo A, Serrano LM, Chang WC, Wright CL, Jensen MC. Genetic Engineering of Cytolytic T Lymphocytes for Adoptive T-Cell Therapy of Neuroblastoma. *J Gene Med* (2004) 6(6):704–11. doi: 10.1002/jgm.489
5. Novak-Hofer I, Amstutz HP, Morgenthaler JJ, Schubiger PA. Internalization and Degradation of Monoclonal Antibody chCE7 by Human Neuroblastoma Cells. *Int J Cancer* (1994) 57(3):427–32. doi: 10.1002/ijc.2910570322

6. Kunkele A, Taraseviciute A, Finn LS, Johnson AJ, Berger C, Finney O, et al. Preclinical Assessment of CD171-Directed Car T-Cell Adoptive Therapy for Childhood Neuroblastoma: CE7 Epitope Target Safety and Product Manufacturing Feasibility. *Clin Cancer Res* (2017) 23(2):466–77. doi: 10.1158/1078-0432.ccr-16-0354
7. Maris JM. Recent Advances in Neuroblastoma. *N Engl J Med* (2010) 362 (23):2202–11. doi: 10.1056/NEJMra0804577
8. Salter AI, Ivey RG, Kennedy JJ, Voillet V, Rajan A, Alderman EJ, et al. Phosphoproteomic Analysis of Chimeric Antigen Receptor Signaling Reveals Kinetic and Quantitative Differences That Affect Cell Function. *Sci Signaling* (2018) 11(544):eaat6753. doi: 10.1126/scisignal.aat6753
9. Watanabe N, Bajgain P, Sukumaran S, Ansari S, Heslop HE, Rooney CM, et al. Fine-Tuning the CAR Spacer Improves T-Cell Potency. *Oncoimmunology* (2016) 5(12):e1253656. doi: 10.1080/2162402x.2016.1253656
10. Hudecek M, Sommermeyer D, Kosasih PL, Silva-Benedict A, Liu L, Rader C, et al. The Nonsignaling Extracellular Spacer Domain of Chimeric Antigen Receptors Is Decisive for In Vivo Antitumor Activity. *Cancer Immunol Res* (2015) 3(2):125–35. doi: 10.1158/2326-6066.cir-14-0127
11. Luca AC, Mersch S, Deenen R, Schmidt S, Messner I, Schafer KL, et al. Impact of the 3D Microenvironment on Phenotype, Gene Expression, and EGFR Inhibition of Colorectal Cancer Cell Lines. *PLoS One* (2013) 8(3):e59689. doi: 10.1371/journal.pone.0059689
12. Kacarevic ZP, Rider PM, Alkildani S, Retnasingh S, Smeets R, Jung O, et al. An Introduction to 3D Bioprinting: Possibilities, Challenges and Future Aspects. *Mater (Basel)* (2018) 11(11):2199. doi: 10.3390/ma11112199
13. Hospodiuk M, Dey M, Sosnoski D, Ozbolat IT. The Bioink: A Comprehensive Review on Bioprintable Materials. *Biotechnol Adv* (2017) 35(2):217–39. doi: 10.1016/j.biotechadv.2016.12.006
14. Raman R, Bhaduri B, Mir M, Shkumatov A, Lee MK, Popescu G, et al. High-Resolution Projection Microstereolithography for Patterning of Neovasculature. *Adv Healthcare Mater* (2016) 5(5):610–9. doi: 10.1002/adhm.201500721
15. Knowlton S, Onal S, Yu CH, Zhao JJ, Tasoglu S. Bioprinting for Cancer Research. *Trends Biotechnol* (2015) 33(9):504–13. doi: 10.1016/j.tibtech.2015.06.007
16. Grix T, Ruppelt A, Thomas A, Amler AK, Noichl BP, Lauster R, et al. Bioprinting Perfusion-Enabled Liver Equivalents for Advanced Organ-on-a-Chip Applications. *Genes* (2018) 9(4). doi: 10.3390/genes9040176
17. Lam T, Dehne T, Kruger JP, Hondke S, Endres M, Thomas A, et al. Photopolymerizable Gelatin and Hyaluronic Acid for Stereolithographic 3D Bioprinting of Tissue-Engineered Cartilage. *J Biomed Mater Res B Appl Biomater* (2019). doi: 10.1002/jbm.b.34354
18. Van Den Bulcke AI, Bogdanov B, De Rooze N, Schacht EH, Cornelissen M, Berghmans H. Structural and Rheological Properties of Methacrylamide Modified Gelatin Hydrogels. *Biomacromolecules* (2000) 1(1):31–8. doi: 10.1021/bm990017d
19. Kunkele A, Johnson AJ, Rolczynski LS, Chang CA, Hoglund V, Kelly-Spratt KS, et al. Functional Tuning of CARs Reveals Signaling Threshold Above Which Cd8+ CTL Antitumor Potency Is Attenuated Due to Cell Fas-FasL-Dependent AICD. *Cancer Immunol Res* (2015) 3(4):368–79. doi: 10.1158/2326-6066.CIR-14-0200
20. Ausubel LJ, Hall C, Sharma A, Shakeley R, Lopez P, Quezada V, et al. Production of CGMP-Grade Lentiviral Vectors. *BioProcess Int* (2012) 10 (2):32–43.
21. Hombach A, Hombach AA, Abken H. Adoptive Immunotherapy With Genetically Engineered T Cells: Modification of the IgG1 Fc 'Spacer' Domain in the Extracellular Moiety of Chimeric Antigen Receptors Avoids 'Off-Target' Activation and Unintended Initiation of an Innate Immune Response. *Gene Ther* (2010) 17(10):1206–13. doi: 10.1038/gt.2010.91
22. Wang X, Chang WC, Wong CW, Colcher D, Sherman M, Ostberg JR, et al. A Transgene-Encoded Cell Surface Polypeptide for Selection, In Vivo Tracking, and Ablation of Engineered Cells. *Blood* (2011) 118(5):1255–63. doi: 10.1182/blood-2011-02-337360
23. Wang X, Naranjo A, Brown CE, Bautista C, Wong CW, Chang WC, et al. Phenotypic and Functional Attributes of Lentivirus-Modified CD19-Specific Human CD8+ Central Memory T Cells Manufactured at Clinical Scale. *J Immunother* (2012) 35(9):689–701. doi: 10.1097/CJI.0b013e318270dec7
24. Drachsler M, Kleber S, Mateos A, Volk K, Mohr N, Chen S, et al. CD95 Maintains Stem Cell-Like and Non-Classical EMT Programs in Primary Human Glioblastoma Cells. *Cell Death Dis* (2016) 7(4):e2209. doi: 10.1038/cddis.2016.102
25. Jensen MC, Popplewell L, Cooper LJ, DiGiusto D, Kalos M, Ostberg JR, et al. Antitransgene Rejection Responses Contribute to Attenuated Persistence of Adoptively Transferred CD20/CD19-Specific Chimeric Antigen Receptor Redirected T Cells in Humans. *Biol Blood Marrow Transplant* (2010) 16 (9):1245–56. doi: 10.1016/j.bbmt.2010.03.014
26. Scarfo I, Maus MV. Current Approaches to Increase CAR T Cell Potency in Solid Tumors: Targeting the Tumor Microenvironment. *J Immunother Cancer* (2017) 5:28. doi: 10.1186/s40425-017-0230-9
27. Gattinoni L, Klebanoff CA, Palmer DC, Wrzesinski C, Kerstann K, Yu Z, et al. Acquisition of Full Effector Function In Vitro Paradoxically Impairs the In Vivo Antitumor Efficacy of Adoptively Transferred CD8+ T Cells. *J Clin Invest* (2005) 115(6):1616–26. doi: 10.1172/jci24480
28. Long AH, Haso WM, Shern JF, Wanhainen KM, Murgai M, Ingaramo M, et al. 4-1BB Costimulation Ameliorates T Cell Exhaustion Induced by Tonic Signaling of Chimeric Antigen Receptors. *Nat Med* (2015) 21(6):581–90. doi: 10.1038/nm.3838
29. Giannattasio A, Weil S, Kloess S, Ansari N, Stelzer EHK, Cerwenka A, et al. Cytotoxicity and Infiltration of Human NK Cells in In Vivo-Like Tumor Spheroids. *BMC Cancer* (2015) 351:1–13. doi: 10.1186/s12885-015-1321-y
30. Sherman H, Gitschier HJ, Rossi AE. A Novel Three-Dimensional Immune Oncology Model for High-Throughput Testing of Tumoricidal Activity. *Front Immunol* (2018) 9:857. doi: 10.3389/fimmu.2018.00857
31. Herter S, Morra L, Schlenker R, Sulcova J, Fahrni L, Waldhauer I, et al. A Novel Three-Dimensional Heterotypic Spheroid Model for the Assessment of the Activity of Cancer Immunotherapy Agents. *Cancer Immunol Immunother* (2017) 66(1):129–40. doi: 10.1007/s00262-016-1927-1
32. Dangles-Marie V, Richon S, El-Behi M, Echchakir H, Dorothee G, Thiery J, et al. A Three-Dimensional Tumor Cell Defect in Activating Autologous CTLs Is Associated With Inefficient Antigen Presentation Correlated With Heat Shock Protein-70 Down-Regulation. *Cancer Res* (2003) 63(13):3682–7.
33. Dillard P, Koksal H, Inderberg EM, Walchli S. A Spheroid Killing Assay by CAR T Cells. *J Vis Exp* (2018) 142. doi: 10.3791/58785
34. Merker M, Pfirrmann V, Oelsner S, Fulda S, Klingebiel T, Wels WS, et al. Generation and Characterization of ErbB2-CAR-engineered Cytokine-Induced Killer Cells for the Treatment of High-Risk Soft Tissue Sarcoma in Children. *Oncotarget* (2017) 8(39):66137–53. doi: 10.18632/oncotarget.19821
35. Sureban SM, Berahovich R, Zhou H, Xu S, Wu L, Ding K, et al. Dclk1 Monoclonal Antibody-Based CAR-T Cells as a Novel Treatment Strategy Against Human Colorectal Cancers. *Cancers (Basel)* (2019) 12(1):54. doi: 10.3390/cancers12010054
36. Di Modugno F, Colosi C, Trono P, Antonacci G, Ruocco G, Nisticò PJJOE, et al. 3D Models in the New Era of Immune Oncology: Focus on T Cells. *CAF ECM* (2019) 38(1):117. doi: 10.1186/s13046-019-1086-2
37. Jacob F, Salinas RD, Zhang DY, Nguyen PTT, Schnoll JG, Wong SZH, et al. A Patient-Derived Glioblastoma Organoid Model and Biobank Recapitulates Inter- and Intra-Tumoral Heterogeneity. *Cell* (2020) 180(1):188–204. doi: 10.1016/j.cell.2019.11.036
38. Wallstabe L, Gottlich C, Nelke LC, Kuhnemundt J, Schwarz T, Nerreter T, et al. Ror1-Car T Cells Are Effective Against Lung and Breast Cancer in Advanced Microphysiologic 3D Tumor Models. *JCI Insight* (2019) 4(18). doi: 10.1172/jci.insight.126345
39. Chan V, Zorlutuna P, Jeong JH, Kong H, Bashir R. Three-Dimensional Photopatterning of Hydrogels Using Stereolithography for Long-Term Cell Encapsulation. *Lab Chip* (2010) 10(16):2062–70. doi: 10.1039/c004285d
40. Meng F, Meyer CM, Joung D, Vallera DA, McAlpine MC, Panoskaltsis-Mortari A. 3d Bioprinted in Vitro Metastatic Models Via Reconstruction of Tumor Microenvironments. *Adv Mater* (2019) 31(10):e1806899. doi: 10.1002/adma.201806899
41. van Pel DM, Harada K, Song D, Naus CC, Sin WC. Modelling Glioma Invasion Using 3D Bioprinting and Scaffold-Free 3D Culture. *J Cell Commun Signal* (2018) 12(4):723–30. doi: 10.1007/s12079-018-0469-z
42. Wang X, Zhang X, Dai X, Wang X, Li X, Diao J, et al. Tumor-Like Lung Cancer Model Based on 3D Bioprinting. *3 Biotech* (2018) 8(12):501. doi: 10.1007/s13205-018-1519-1
43. Heinrich MA, Bansal R, Lammers T, Zhang YS, Michel Schiffelers R, Prakash J. 3d-Bioprinted Mini-Brain: A Glioblastoma Model to Study Cellular

Interactions and Therapeutics. *Adv Mater* (2019) 31(14):e1806590–e. doi: 10.1002/adma.201806590
44. Fantini V, Bordoni M, Scocozza F, Conti M, Scarian E, Carelli S, et al. Bioink Composition and Printing Parameters for 3D Modeling Neural Tissue. *Cells* (2019) 8(8):830. doi: 10.3390/cells8080830
45. Langer EM, Allen-Petersen BL, King SM, Kendsersky ND, Turnidge MA, Kuziel GM, et al. Modeling Tumor Phenotypes In Vitro With Three-Dimensional Bioprinting. *Cell Rep* (2019) 26(3):608–23. doi: 10.1016/j.celrep.2018.12.090
46. Ando Y, Siegler EL, Ta HP, Cinay GE, Zhou H, Gorrell KA, et al. Evaluating CAR-T Cell Therapy in a Hypoxic 3d Tumor Model. *Adv Healthcare Mater* (2019) 8(5):e1900001. doi: 10.1002/adhm.201900001
47. Benmebarek MR, Karches CH, Cadilha BL, Lesch S, Endres S, Kobold S. Killing Mechanisms of Chimeric Antigen Receptor (CAR) T Cells. *Int J Mol Sci* (2019) 20(6):1283ff. doi: 10.3390/ijms20061283
48. O'Connell J, O'Sullivan GC, Collins JK, Shanahan F. The Fas Counterattack: Fas-Mediated T Cell Killing by Colon Cancer Cells Expressing Fas Ligand. *J Exp Med* (1996) 184(3):1075–82. doi: 10.1084/jem.184.3.1075
49. Camejo EH, Rosengren B, Camejo G, Sartipy P, Fager G, Bondjers G. Interferon Gamma Binds to Extracellular Matrix Chondroitin-Sulfate Proteoglycans, Thus Enhancing Its Cellular Response. *Arterioscler Thromb Vasc Biol* (1995) 15 (9):1456–65. doi: 10.1161/01.atv.15.9.1456
50. Schnalzger TE, de Groot MH, Zhang C, Mosa MH, Michels BE, Röder J, et al. 3D Model for CAR-Mediated Cytotoxicity Using Patient-Derived Colorectal Cancer Organoids. *EMBO J* (2019) 38(12):e100928. doi: 10.15252/embj.2018100928
51. Kato K, Koyanagi M, Okada H, Takanashi T, Wong YW, Williams AF, et al. CD48 Is a Counter-Receptor for Mouse CD2 and Is Involved in T Cell Activation. *J Exp Med* (1992) 176(5):1241–9. doi: 10.1084/jem.176.5.1241
52. Johnston SC, Dustin ML, Hibbs ML, Springer TA. On the Species Specificity of the Interaction of LFA-1 With Intercellular Adhesion Molecules. *J Immunol (Baltimore Md 1950)* (1990) 145(4):1181–7.
53. Ben-David U, Ha G, Tseng YY, Greenwald NF, Oh C, Shih J, et al. Patient-Derived Xenografts Undergo Mouse-Specific Tumor Evolution. *Nat Genet* (2017) 49(11):1567–75. doi: 10.1038/ng.3967

Conflict of Interest: TL, AT and LK were employed by Cellbricks GmbH Berlin.

The remaining authors declare that the research was conducted in the absence of any commercial or financial relationships that could be construed as a potential conflict of interest.

Advantages of publishing in Frontiers

OPEN ACCESS
Articles are free to read for greatest visibility and readership

FAST PUBLICATION
Around 90 days from submission to decision

HIGH QUALITY PEER-REVIEW
Rigorous, collaborative, and constructive peer-review

TRANSPARENT PEER-REVIEW
Editors and reviewers acknowledged by name on published articles

Frontiers
Avenue du Tribunal-Fédéral 34
1005 Lausanne | Switzerland

Visit us: www.frontiersin.org
Contact us: frontiersin.org/about/contact

REPRODUCIBILITY OF RESEARCH
Support open data and methods to enhance research reproducibility

DIGITAL PUBLISHING
Articles designed for optimal readership across devices

FOLLOW US
@frontiersin

IMPACT METRICS
Advanced article metrics track visibility across digital media

EXTENSIVE PROMOTION
Marketing and promotion of impactful research

LOOP RESEARCH NETWORK
Our network increases your article's readership